

1

AGARD-CP-462

AGARD-CP-462

AD-A225 267

AGARD

ADVISORY GROUP FOR AEROSPACE RESEARCH & DEVELOPMENT

7 RUE ANCELLE 92200 NEUILLY SUR SEINE FRANCE

AGARD CONFERENCE PROCEEDINGS No.462

Impact of Emerging NDE-NDI Methods on Aircraft Design, Manufacture and Maintenance

(L'impact des Nouvelles Méthodes d'Examen Non Destructif
et de Contrôle Non Destructif (NDE-NDI) sur la Conception,
la Fabrication et la Maintenance des Aéronefs)

This document
is published by
distribution and availability
on back cover

NORTH ATLANTIC TREATY ORGANIZATION



DISTRIBUTION AND AVAILABILITY
ON BACK COVER

1

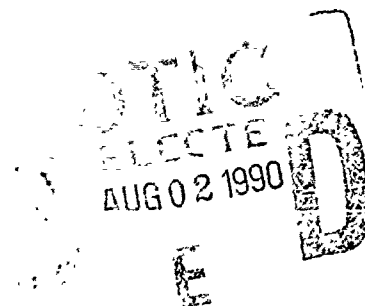
NORTH ATLANTIC TREATY ORGANIZATION
ADVISORY GROUP FOR AEROSPACE RESEARCH AND DEVELOPMENT
(ORGANISATION DU TRAITE DE L'ATLANTIQUE NORD)

AGARD Conference Proceedings No.462

Impact of Emerging NDE-NDI Methods on Aircraft Design, Manufacture and Maintenance

(L'impact des Nouvelles Méthodes d'Examen Non Destructif
et de Contrôle Non Destructif (NDE-NDI) sur la Conception,
la Fabrication et la Maintenance des Aéronefs)

Accession For	
NTIS GRA&I	<input checked="checked" type="checkbox"/>
DTIC TAB	<input type="checkbox"/>
Unannounced	<input type="checkbox"/>
Justification	
By	
Distribution/	
Availability Codes	
Dist	Avail and/or Special
A-1	



The Mission of AGARD

According to its Charter, the mission of AGARD is to bring together the leading personalities of the NATO nations in the fields of science and technology relating to aerospace for the following purposes:

- Recommending effective ways for the member nations to use their research and development capabilities for the common benefit of the NATO community;
- Providing scientific and technical advice and assistance to the Military Committee in the field of aerospace research and development (with particular regard to its military application);
- Continuously stimulating advances in the aerospace sciences relevant to strengthening the common defence posture,
- Improving the co-operation among member nations in aerospace research and development;
- Exchange of scientific and technical information;
- Providing assistance to member nations for the purpose of increasing their scientific and technical potential;
- Rendering scientific and technical assistance, as requested, to other NATO bodies and to member nations in connection with research and development problems in the aerospace field.

The highest authority within AGARD is the National Delegates Board consisting of officially appointed senior representatives from each member nation. The mission of AGARD is carried out through the Panels which are composed of experts appointed by the National Delegates, the Consultant and Exchange Programme and the Aerospace Applications Studies Programme. The results of AGARD work are reported to the member nations and the NATO Authorities through the AGARD series of publications of which this is one.

Participation in AGARD activities is by invitation only and is normally limited to citizens of the NATO nations.

The content of this publication has been reproduced
directly from material supplied by AGARD or the authors.

Published May 1990

Copyright © AGARD 1990
All Rights Reserved

ISBN 92-835-0546-8



*Printed by Specialised Printing Services Limited
40 Chigwell Lane, Loughton, Essex IG10 3TZ*

Preface

Our ability to inspect aircraft components and assemblies during manufacture and during in-service maintenance has important implications with respect to procurement and maintenance costs, as well as aircraft reliability and fleet readiness. This was recognized by the Structures and Materials Panel in the early 1970s and a Specialists' Meeting on NDI Relationships to Aircraft Design and Materials was organized and held in Voss, Norway in September 1977.

Since 1977, several NATO nations have acquired new aircraft embodying advanced design concepts, new material systems, and novel manufacturing methods. This has led to a greater appreciation by the operators of the consequence of this advanced technology on in-service inspection and maintenance. It may be expected that both positive and negative experiences have occurred. For example, while composite materials are strong, stiff, corrosion resistant and resistant to fatigue under tension, aircraft operators are now required to inspect large surface areas of composite wing and fuselage structure for internal delaminations or disbonds at metal/composite joints. Such inspections can be time consuming, difficult and expensive, particularly when access is available only through one surface or through layers of adjacent structure. Also while crack-like discontinuities in metals are invariably surface connected, flaws in composites can grow to critical dimensions while remaining hidden.

During the past ten years many aircraft companies and particularly the smaller companies have embarked upon technology enhancement programmes involving the development of new design, material or manufacturing concepts. Opportunities to exploit new concepts may be substantially influenced by the ability to inspect at a sufficient level of sensitivity and reliability to allow the requirements of the airworthiness authorities to be established.

Through the activities of the R&D community during the same ten year period, a greater understanding has developed of the capabilities and limitations of many of the newly emerging NDI techniques, and several new techniques have appeared that may be of practical value to the design, manufacturing and operator communities.

AGARD remains one of the few organizations able to effect a merging of the practical interests of the design, manufacturing and operator communities with the more fundamental interests of the R&D community. It is perhaps the foremost organization able to address this interplay on behalf of the aerospace community, and particularly with respect to military equipment.

The present meeting has been designed to review developments in non-destructive inspection applicable to the major components and assemblies used in airframes, engines and their subsystems. An attempt has been made to provide a forum through which representatives of the design, manufacturing, airworthiness and maintenance communities will be encouraged to exchange opinions and information with the research and development community. Problems associated with new design concepts, materials systems, and manufacturing methods will be highlighted and the ability of existing or emerging NDI methods to respond to these problems will be examined.

The AGARD-SMP Subcommittee responsible for this Specialists' Meeting set out with five objectives:

1. To review recent developments in the science and practice of non-destructive inspection, and to identify opportunities whereby new techniques can be used to address problems of practical importance.
2. To review practical experience gained during the design, manufacture and operation of advanced aircraft structures where non-destructive inspection technology created either an obstacle to progress or an opportunity for advancement.
3. To identify outstanding needs for, or opportunities for the development of new inspection methods.
4. To identify deficiencies with respect to available inspection equipment and the need for standardization with respect to inspection equipment and devices.
5. To review both positive and negative experiences with efforts to transition new technology to applications, and to examine efforts to expedite the implementation process.

We will leave readers to judge whether we have been successful in meeting these objectives, but certainly we have been very successful in recognizing a vigorous field of activity. The Specialists' Meeting was arranged in five sessions, and to include twenty five papers from seven nations. The papers were selected from more than fifty that were offered, and selected to provide both a reasonable national representation of the countries that wished to participate, and a reasonable cross-section of the technical matters that are being addressed by these nations. There is no doubt that many other outstanding papers were not included, and we send our apologies to the authors of those papers. We hope that they will, nevertheless, derive some value from the Conference Proceedings. More than two hundred people registered to attend the 69th Meeting of the AGARD-SMP in Brussels, when this Specialists' Meeting was held, and the majority of these people have attended at least some part of the Specialists' Meeting. The meeting has obviously dealt with a very popular topic.

As the Chairman of this AGARD-SMP activity I would like to thank the Session Chairmen (Mr P.Ward — UK, Prof. C.Roy — CA, Col. Dr-Ing J.M.Pintado — SP, Prof. L.J.Jacobs — US and Dr W.Schütz — GE) for keeping their sessions on schedule and on topic. I would like to thank all the authors for their time and effort in preparing and presenting the papers. I would like to

offer a special word of thanks to the invited Rapporteurs, Dr L.Bond of University College, London, and Mr T.Cooper of WRDC-WPAFB, Ohio, for accepting the very difficult task of summarizing the main findings of this meeting, and putting them into perspective in light of other topics and technologies not reported here. Their observations, which are published as part of the CP, will provide a basis for much further discussion within the SMP, and indeed within NATO and among its member nations.

W.Wallace, Chairman, AGARD-SMP
Subcommittee 43 on
Non-destructive Inspection

©

Préface

Nos compétences dans le domaine du contrôle des composants et des ensembles tant en cours de fabrication que lors des opérations de maintenance courantes effectuées sur des avions en ordre d'exploitation ont des conséquences importantes pour les coûts d'approvisionnement et d'entretien, ainsi que pour la fiabilité et la disponibilité de la flotte. Le Panel AGARD des Structures et Matériaux a compris l'importance de ce sujet au début des années 1970 et une réunion de spécialistes sur les essais non-destructifs a été organisée au mois de septembre 1977 à Voss, en Norvège.

Depuis 1977, plusieurs gouvernements des pays membres de l'OTAN ont acquis de nouveaux avions qui intègrent des principes de conception avancés, des nouvelles compositions des matériaux et des méthodes de fabrication novatrices. L'une des conséquences de cette démarche a été la sensibilisation des opérateurs aux conséquences de ces technologies avancées pour la maintenance et le contrôle en cours de fabrication. L'expérience s'est révélée tantôt positive, tantôt négative. A titre d'exemple, si les matériaux composites sont robustes, rigides, résistants à la corrosion et à la fatigue sous traction, il est demandé au personnel de maintenance de contrôler d'importantes surfaces de voilure et de fuselage réalisées en matériaux composites, afin de détecter d'éventuels délaminages ou désassemblages au niveau des joints métal/composite. De tels contrôles sont longs, difficiles et coûteux à réaliser, en particulier lorsque l'accès ne peut se faire que par une seule surface ou bien à la jonction entre les différentes couches d'une structure avoisinante. En outre, à la différence des discontinuités de type fissures qui se produisent dans les métaux, et qui vont jusqu'à apparaître en surface de la pièce, les failles dans les matériaux composites peuvent atteindre des dimensions critiques tout en restant cachées.

Au cours des dix dernières années, un certain nombre de constructeurs, et en particulier les plus petits, ont lancé des programmes de changement de technologie qui comprennent le développement de nouveaux concepts de construction, de matériaux et de fabrication. La possibilité d'exploiter ces nouveaux concepts pourra dépendre, dans une large mesure, de notre capacité à effectuer des contrôles qui seraient suffisamment sensibles et fiables pour permettre l'établissement des spécifications des services officiels.

Les activités de la communauté de la recherche et du développement pendant cette décennie ont permis d'établir une meilleure compréhension du potentiel et des limitations de bon nombre des nouvelles techniques d'inspection non destructive dont certaines seraient d'une grande utilité pour les concepteurs, fabricants et exploitants d'aéronefs.

AGARD reste l'une des rares organisations capable d'effectuer la synthèse de l'intérêt pratique des concepteurs, fabricants et exploitants avec celui de la communauté R&D, qui est de caractère plus fondamental. Elle est peut-être aussi la première organisation capable d'orchestrer ces effets réciproques au profit de la communauté aérospatiale, en particulier en ce qui concerne le matériel militaire.

Cette réunion a pour objet de faire le point des développements récents dans le domaine de l'inspection non destructive susceptibles d'être appliqués aux principaux composants et ensembles entrant dans la construction des cellules, des moteurs et de leurs sous-systèmes. La réunion sert de forum, où les représentants des communautés de la conception, la fabrication, la navigabilité et la maintenance peuvent échanger des idées et des informations avec la communauté R&D. Les problèmes afférents aux nouveaux concepts de construction, aux nouvelles compositions des matériaux et aux procédés de fabrication seront examinés, ainsi que la valeur des méthodes d'inspection non destructive nouvelles ou existantes pour répondre à ces difficultés.

Le sous-comité AGARD/SMP chargé de l'organisation de cette réunion s'est donné les cinq tâches suivantes:

1. Faire le point des dernières réalisations en ce qui concerne la théorie et la pratique de l'inspection non destructive et signaler des possibilités de mise en application pratique pour les nouvelles techniques.
2. Passer en revue des cas concrets d'expérience acquise lors de la conception, la fabrication et l'exploitation de structures d'aéronef avancées, où la technologie de l'inspection non destructive a soit créé un obstacle, soit permis de progresser.
3. Définir les besoins en et ou, les possibilités pour le développement des nouvelles méthodes d'inspection.
4. Constater les imperfections éventuelles du matériel d'inspection disponible à l'heure actuelle et les besoins de normalisation en ce qui concerne les divers instruments et équipements d'inspection.
5. Examiner l'expérience acquise, qui est tantôt positive, tantôt négative, en ce qui concerne la transition entre nouvelles technologies et applications, et étudier les efforts qui sont faits pour accélérer la mise en oeuvre de ces technologies.

Nous laisserons au lecteur le soin de juger si nous nous sommes bien acquittés de ces tâches, une chose est certaine, c'est que nous avons bien identifié un domaine d'activité en plein essor. Cette réunion de spécialistes a été organisée en cinq séances et comptait vingt cinq présentations données par les représentants de sept pays différents. Celles-ci avaient été sélectionnées parmi la cinquantaine offertes, sur la base d'une juste répartition entre les pays qui voulaient y participer et d'un échantillonnage représentatif des sujets techniques étudiés dans ces pays. Nous regrettons vivement de n'avoir pas pu y inclure d'autres présentations que nous avons reçues, d'une qualité remarquable. Nous présentons nos excuses aux auteurs en question. Nous

espérons que les lecteurs tireront profit du compte-rendu de la conférence. Plus de deux cent personnes se sont inscrites pour la 69ème réunion du Panel AGARD des Structures et Matériaux à Bruxelles, dont le programme incluait cette réunion de spécialistes. La majorité des participants a assisté à au moins une partie de la réunion et il est certain que le sujet a suscité beaucoup d'intérêt.

En tant que Président du sous-comité 43, je tiens à remercier les Présidents de séance (M.P.Ward, UK, Prof. C.Koy, CA, Col. Dr.Ing. J.M.Pintado, SP, Prof. L.J.Jacobs, US, et Dr W.Schütz, GE) pour avoir su faire respecter le programme tant sur le plan temporel que sur le plan de l'adaptation et la qualité des sujets traités. Je tiens également à remercier tous les auteurs pour avoir bien voulu consacrer le temps nécessaire pour la préparation et la présentation des communications. Mes plus vifs remerciements vont aux Rapporteurs, le Dr Leonard Bond de University College Londres, et M. Tom Cooper de WRDC-WPAFB Ohio, pour avoir accepté la tâche difficile de faire un résumé des principales conclusions de cette réunion et de les situer dans le contexte d'autres sujets et d'autres technologies dont il n'est pas fait mention ici. Leurs remarques, qui sont incluses dans le compte-rendu de conférence, serviront de base à de plus amples discussions au sein du SMP, voire au sein de l'OTAN et ses pays membres.

Structures and Materials Panel

Chairman: Prof. Dr-Ing. Hans Förtsch
Direktor der DLR Institut
für Aeroelastik
Bunsenstraße 10
Federal Republic of Germany

Deputy Chairman: Mr Samuel L. Venneri
Director, Materials & Structures
Division (Code RM)
Office of Aeronautics & Space Technology
NASA Hq
Washington DC 20546
United States

NON-DESTRUCTIVE INSPECTION AND EVALUATION SUB-COMMITTEE

Chairman: Dr William Wallace
Head of Structures & Materials Laboratory
National Aeronautical Establishment
National Research Council of Canada
Montreal Road
Ottawa, Ont K1A 0R6
Canada

SMP MEMBERS

E.J.Bachelet — FR	A.Gümes — SP
H.J.G.Carvalhinhos — PO	J.S.L.Leach — UK
D.P.Chappell — US	M.L.Minges — US
D.Chaumette — FR	G.Oddone — IT
D.Coutsouradis — BE	J.M.Pintado — SP
J.J.De Luccia — US	E.Redondo — SP
G.L.Denman — US	A.Salvetti — IT
A.Deruyttere — BE	M.Scolaris — IT
A.Dimarogonas — GR	S.Signoretti — IT
M.Doruk — TU	S.L.Venneri — US
W.Elber — US	J.Waldman — US
V.Giavotto — IT	A.P.Ward — UK
G.Grüninger — GE	H.Zocher — GE

HOST MEETING COORDINATOR

Major N.July
Etat-Major de la Force Aérienne (VSL/AGARD)
Quartier Reine Elizabeth
Brussels — Belgium

The Panel wishes to express its thanks to the AGARD Belgian National Delegates
for the invitation to hold this Meeting in Belgium.

PANEL EXECUTIVE

Mr Murray C.McConnell — UK

From Europe
AGARD-OTAN
7, rue Ar.celle
92200 Neuilly-sur-Seine
France

From USA and Canada
AGARD-NATO
Attr. SMP Executive
AFO New York 09777

Tel: (1) 4738 5790 & 5792
Telex: 610176F
Telefax: (1) 4738 5799

Contents

	Page
Preface	iii
Préface	iv
Structures and Materials Panel	vii
	Reference
SESSION I – USER NEEDS AND PRIORITIES	
Royal Air Force Future NDE Requirements and Priorities by K.H.Dalziel	1
The Role of NDI in the Certification of Turbine Engine Components by R.G.Taylor, Sharon I.Vukelich and T.D.Cooper	2
NDI-Concept for Composites in Future Military Aircraft by M.Stoermer	3
Assessment and Demonstration of the Capabilities of NDI Processes, Equipment and Personnel by W.D.Rummel	4
Inspection Reliability by D.A.Bruce	5
Critical Inspection of High Performance Turbine Engine Components – the Concept and Development of the Retirement for Cause (RFC) NDE System by B.Rasmussen, E.L.Pohlenz, J.Hoeffel and D.G.Williams	6
SESSION II – MATERIAL CHARACTERIZATION AND PROCESS CONTROL	
Non-Destructive Evaluation of Adhesively-Bonded Joints by A.Fahr and S.Tanary	7
Ultrasonic Inspection of Advanced CFRP Structures by Computer Controlled, Pulse-Echo Technique by B.Sainz, J.M.Bernardo, V.Cortes and C.Valdecantos	8
An Ultrasonic System for In-Service Non-Destructive Inspection of Composite Structures by F.Boschetti, F.Cipri, L.Pugliese and M.Scolaris	9
Paper 10 withdrawn	
A Technique for Rapid Inspection of Composite Aircraft Structure for Impact Damage by J.P.Komorowski, R.W.Gould and W.J.Pastorius	11
SESSION III – TECHNIQUES FOR IMPROVED RELIABILITY OF IN-SERVICE INSPECTION	
In-Service Inspection of Composite Components on Aircraft at Depot and Field Levels by N.A.Tracy, GL.Hardy and F.J.Fechek	12

* Not available at time of printing.

Development of an Automated Ultrasonic Inspection System for Composite Structure on In-Service Aircraft by W.R.Sturrock, R.W.Ramsbottom and W.J.Miller	13
Neutron Radiography — Applications and Systems by H.U.Mast and R.Schütz	14
Progress in the Detection of Cracks under Installed Fasteners Using Eddy Currents by D.J.Harrison	15
Acoustic Emission Detection of Crack Presence and Crack Advance During Flight by S.L.Mcbride, M.D.Pollard, J.D.MacPhall, P.S.Bowman and D.T.Peters	16

SESSION IV — RESEARCH STUDIES IN PROGRESS — PHYSICAL METHODS

Development and Application of Computed Tomography (CT) for Inspection of Aerospace Components by T.J.Moran	17
Application de la Thermographie Infrarouge au Contrôle Non Destructif des Matériaux Composites par H.Tretout, J.Y.Marin et R.de Mol	18
New Aspects in Aircraft Inspection Using Eddy Current Methods by M.Tietze	19
Stenopic Radiography: A Non-Destructive Test without Contact by G.Delojo, J.M.de los Rios and J.Miguel	20
Noncontact Laser Thermomechanical Nondestructive Evaluation for Advanced Coatings by H.I.Ringermacher	21
Advanced NDE Techniques for Quantitative Characterization of Aircraft by J.S.Heyman and W.P.Winfree	22

SESSION V — RESEARCH STUDIES IN PROGRESS — ANALYTICAL METHODS

Calculation of Acoustic Emission Signatures from Growing Cracks by L.J.Jacobs, W.R.Scott and Dianne M.Granata	23
Study of Failure Processes in Fiber Reinforced Composites Using Acoustic Emission Techniques by C.Roy, A.Maslouhi and M.El Ghorba	24
Inspection System for In-Situ Inspection of Aircraft Composite Structures by P.Blondet and Ines Molinero	25
Use of Acoustic Emission for Continuous Surveillance of Aircraft Structures by M.Nabil Bassim	26

SESSION VI — SPECIALIST COMMENTS FROM THE FUNDAMENTAL AND APPLIED POINTS OF VIEW

Recorders' Reports

Applied Point of View by T.D.Cooper	R-1
Impact of NDE-NDI Methods on Aircraft Design, Manufacture and Maintenance, from the Fundamental Point of View by L.J.Bond	R-2

THE ROLE OF NDI IN THE CERTIFICATION OF TURBINE ENGINE COMPONENTS

R G Taylor
Chief of NDT Technology
Rolls-Royce plc
PO Box 31, Derby, England DE2 8BJ

Sharon I Vukelich
Propulsion Systems Program Office
Aeronautical Systems Division
Wright-Patterson Air Force Base, Ohio, USA

Thomas D Cooper
Materials Laboratory
Wright Research & Development Centre
Wright-Patterson Air Force Base, Ohio, USA

ABSTRACT

During the past few years, the UK and USA have developed different approaches in the use of NDI in the certification and lifing of aircraft gas turbine engine components.

While both countries have utilized a fracture mechanics philosophy on critical rotating components, the use of NDI has been significantly different. The USA has developed NDI technology to be utilized in a quantitative role where the size of defect that must be detected to meet the lifing objectives can demonstrably be achieved to an agreed level of confidence. This approach has been defined in the USA in a Mil Standard under the acronym ENSIP (Engine Structural Integrity Program), and is now a mandatory requirement for all future USAF power plants.

In the UK, the approach has been to utilize NDI in a process monitoring role having first established, by intense NDI application together with process defect hazard reviews during the process development, that the process is under control. The paper will highlight the historical reasons for the different approaches, the current status of these activities and finally address the future developments which may have the effect of minimizing the differences which exist.

Introduction

The evolution of high performance gas turbine engines has introduced many new considerations in dealing with questions of reliability and maintainability. Foremost among these is non-destructive testing. The procedures required to insure that both initial quality and adequate depot inspection capability are satisfied, have been evolving in response to pressures from both military and commercial customers. The directions taken in the United States and Great Britain to meet these requirements have been somewhat different, but have many elements of similarity.

Crucial to insuring that the inspection operations are adequate are the procedures used to certify the equipment, the personnel and the methods involved in conducting the inspections, particularly on components that are considered to be critical for the safe operation of the engine. It is the purpose of this paper to discuss the methods that are currently being used in both the US and the UK and contrast them, while emphasizing the similarities that exist.

US Procedures

In the United States, the procedure that has had the most influence on the NDI community and the one that will be discussed in this paper, is that initiated and incorporated by the US Air Force (USAF). It is a result of the Engine Structural Integrity Program (ENSIP) as defined in MIL-STD-1783 (USAF) (Ref 1). This program was initiated to establish structural performance, design, development and verification requirements to assure structural integrity for USAF engine systems. It evolved as a result of a number of structural problems that have occurred in Air Force gas turbine engines over the last fifteen to twenty years. Many of these were safety problems causing loss of aircraft as well as significant increases in maintenance and modification costs, all of which have adversely affected fleet readiness. The ENSIP concept was developed based on specific lessons learned during that period and was intended to substantially reduce these problems. ENSIP was recommended by the Air Force Scientific Advisory Board. It is based on prior experience with the Aircraft Structural Integrity Program (ASIP), which has been very successfully applied to the design and production of much more reliable airframe structures. That program is described in MIL-STD-1530 (Ref 2). The ENSIP approach is described in more detail elsewhere (Ref 3). This discussion will be limited

to those aspects which relate to the application of NDI technology to insure that reliable component performance is achieved.

One of the most important aspects of the ENSIP approach is the concept of damage tolerance in the design of those components that are considered to be fracture critical. A fracture critical part is defined as one whose failure will result in the probable loss of the aircraft. For example, failure of a high energy rotating component, such as a disk, which will not be contained by the engine case, would probably result in the loss of the aircraft. It is, therefore, considered to be a fracture critical part. The same is true for the failure of a component that will result in a loss of power of a single engine aircraft. The ENSIP design insures that such failures will not occur by requiring that all fracture critical parts can withstand the presence of subcritical-size flaws, and that subcritical-size flaws will not grow to critical size either in the projected lifetime of the part, or at least in some predetermined safe inspection interval. The problem at hand, then, is determining what size flaw is liable to be in a new part at the time it is manufactured so that the designer, based on the known crack growth behaviour of the material under the conditions that it will be operating, can size the part accordingly. Although manufacturers insist that new parts do not contain flaws or defects that can endanger the integrity of the part, past experience has clearly shown otherwise. A similar flaw size detection capability must be established for maintenance inspection.

Significant effort in the United States has been directed toward the development of inspection equipment and procedures that will reliably detect small flaws in critical parts, and whose performance is adequately characterized so that the statistical reliability of the inspection can be clearly defined. The two methods which have been extensively developed and evaluated for such applications are eddy current techniques for detecting very small surface connected flaws and ultrasonic techniques for detecting subsurface flaws. Specialized and automated systems have been developed, evaluated and applied to the inspection of critical components in maintenance depots as well as during manufacture. An extremely important part of that development has been the establishment of flaw-containing standards and statistical evaluation methods to provide a clear definition of the reliability of the inspection system.

The system that has served as the catalyst for much of the development effort to define the statistical reliability of the inspection process for engine components is the Retirement or Cause (RFC) system, which was developed on a USAF contract by Systems Research Laboratories (SRL) and which will be described in detail in a subsequent paper in this symposium. It was considered mandatory at the outset of that program that methodology be developed along with the system to clearly and unequivocally demonstrate its reliability to find very small flaws. Consequently, a significant effort was mounted to do just that. A committee of representatives of the major engine manufacturers in the US, along with technical representatives of the USAF, SRL and the other subcontractors on the program, was formed to define not only the flawed specimens that would be required, but reach agreement on the statistical analyses that would be used to determine the performance capability of the system. The basic agreement at the outset of the program was to establish the flaw size which could be found at the 90% probability of detection/95% confidence level. This level of reliability of inspection was established early in the development of the structural integrity programs and is called out in both of the Military Standards. The statistical methods finally agreed upon are those described by Berens (Ref 4). The target surface-connected flaw size for which the system was designed was a 0.005 inch deep by 0.010 inch long or greater fatigue crack. For internal flaws, the target size was a 0.015 inch diameter inclusion.

The RFC system was installed at the San Antonio Air Logistics Centre at Kelly Air Force Base, San Antonio, Texas, and has been in operation since October 1986, inspecting critical rotating components for the F-100 engine. Prior to its acceptance, it was extensively evaluated to validate its performance capabilities. The results of the evaluation have been very encouraging. The system was designed to take full advantage of the latest developments in computer and automation technology to allow it to be essentially independent of operator impact, since that has been traditionally recognized as one of the major sources of error and inaccuracy in most inspection operations. To insure that the system was reliable, an extensive set of fatigue-cracked specimens, where the size, location and orientation of the cracks were very carefully controlled, was prepared and used along with real engine hardware, to test the system. Variables that were evaluated included repeatability, probe changes, load changes, orientation changes and operator changes. In the case of surface connected cracks, the eddy current system has been consistently able to detect flaws in the 0.005 inch deep range. The ultrasonic portion of the system is able to reliably find 0.030 inch diameter maloriented penny-shaped flaws throughout the thickness of the bore region of a disk.

There are a number of other special systems that have been developed for use in both manufacturing and maintenance inspection, including the Eddy Current II system and the Integrated Blade Inspection System (IBIS). These systems have all had to be evaluated to determine their capability and their reliability. Although broad guidelines have been available to generally guide the evaluations, each program has essentially been tailored for the specific system. The same is true for each major new engine program for the USAF that has been required to be designed and manufactured according to the ENSIP Military Standard. Each required demonstration program to quantify the inspection procedures being used on that system has been tailored for the system. It has been recognized that a uniform evaluation procedure is greatly needed to not only make all demonstrations the same, but to reduce the costs entailed in creating a new approach

for each system. With the establishment of the very effective industry/government team that developed and managed the successful full-scale demonstration and qualification of the RFC system at the San Antonio ALC, an excellent opportunity was presented to generate a much-needed Military Standard on System Reliability Assessment. Under the direct support of the Propulsion Systems Program Office of the Aeronautical Systems Division at Wright-Patterson Air Force Base, the same team of experts has been preparing such a Military Standard that should be available by the end of 1989.

This Military Standard for the determination of NDI reliability will address eddy current, ultrasonic, fluorescent penetrant and magnetic particle testing. Although initially intended for those facilities and processes that inspect gas turbine engine components, the methodology incorporated in the standard will be equally applicable to any other class of hardware such as airframe, marine or power generation. The standard will be used to determine the reliability of an existing system, process or facility as well as identify sources of departure from a desired reliability level. Provisions within the standard make it applicable to either manual, semi-automated or fully automated NDI processes. With the standard, it will be possible to make a quantitative comparison of the capabilities of two similar processes or to determine if a facility is able to perform at some target level of reliability.

The standard is based on the statistical analysis obtained from the inspection of a well characterized set of specimens, some of which are not flawed. Requirements are given that describe those features of the production hardware that have to be represented in the specimens for each method. Also specified are the number of flaws and the distribution of flaw sizes as a function of the reliability required and the flaw size for which that reliability is to be demonstrated. Other significant requirements represented in the standard are the statistical analysis methods to be used, data to be collected, and the protocol for the actual conduction of the demonstration. In addition to this, the standard defines the necessary requirements for the handling and cleaning of the specimens as well as how the data results of the demonstration are to be presented.

The need for a uniform evaluation procedure was not simply driven by the fact that the analytical models and conduction of the demonstrations were different among contractors. In fact, a major difference was in the fabrication of the specimen sets themselves. This is extremely important since the response to tight cracks versus open cracks, 3 to 1 versus 15 to 1 aspect ratios, or starter notch versus natural fatigue cracked specimens can give very different results depending on the inspection system. Thus the section on fabrication of specimens is very important to this standard. Since this is the case, when funding becomes available the plan is to have two complete sets of specimens made using all the various geometry and materials which are used in present engines. One set would be kept as a "standards" type set with which the other set would be periodically checked. This "standards" set would never be used for demonstrations. This approach was proposed so that contractor production reliability demonstrations could be quantitatively compared.

ENSIP requires production facility reliability demonstrations to be performed for all new engines. Although the Military Standard has not been approved, its concepts have been used for the new improved performance engines. The specimen sets being used are the RFC sets which are supplemented by the contractors for any new materials and geometry.

To date, the demonstrations have gone well. Automated eddy current inspection flaw sizes that have been demonstrated are .005 - 0.010 inch depth. Automated fluorescent penetrant inspection flaw sizes are .020 - .030 inch depth (approximately 0.060 inch length). Ultrasonic (UT) inspection flaw sizes are .016 - 0.032 inch. Manual penetrant systems and magnetic particle (MPI) systems are scheduled to be evaluated this year.

In the US NDI is used not only because of ENSIP requirements, but also for process control and Retirement For Cause (RFC). Depending on whether the concern is production (contractor dependent) or depot, the philosophy varies. In production, etches are used and billets are inspected with FPI. Sonic shapes are inspected using ultrasonics. At present, the UT requirements are different depending on the contractor. In general, the standard is a No. 1 or No. 2 flat bottom hole. This small size is necessary to meet ENSIP requirements. Initial flaw sizes for embedded flaws are based upon intrinsic materials defect distribution and/or the NDI methods incorporated into the manufacturing process. At present, there are some contractors who have not embraced the concept of inspecting for a No. 1 and/or No. 2 flat bottom hole to satisfy the intent of the ENSIP requirement.

Unique problems at Air Force depots, due to upgrading engine configurations have forced the development of etches for finished parts that will enhance inspection capability without materials property degradation. It also became necessary to UT inspect finished parts and be able to find a mal-oriented defect. The RFC system handles this operation well. In addition to this, a low temperature spinning technique called cryo-spin is now used on some titanium fan disks. If a flaw exists which would cause failure of the disk before the next inspection, the disk will burst during the cryogenic spin test.

In addition to the above problems at the Depot, the Air Force has instituted a Retirement For Cause (RFC) philosophy on some engine models. This concept is based on fracture control philosophy. A component will operate until a crack equal to or greater than the initially assumed flaw is detected. It is clear in applying RFC that the non-destructive inspection becomes a critical factor. The detection of the crack is limited by the

resolution and reliability of the inspection system being used. Thus a uniform, quantitative evaluation procedure is necessary for the determination of NDI reliability.

In the future for production, consideration is being given to using statistical audit of engines with NDI for non-critical areas. If the process changes, then for a specified number of engines, a 100% inspection will be used and then return to the audit plan if no defects are found.

Many of the procedures which have been discussed are only used for military engines. For commercial engines, NDI is more process control oriented and flaw sizes for subsurface defects are larger.

UK Procedures

The significant differences between the USA approach and that used in the UK is where the emphasis for high quality NDI has been concentrated.

It has been shown that the USA approach is to utilize high quality NDI with a demonstratable level of reliability, particularly for surface inspections in both manufacturing facilities and at overhaul depots, and that this (ENSIP) approach has been strongly influenced by the problems encountered by the USAF over the last fifteen to twenty years. Under these circumstances the costs and resources involved in establishing, testing and proving the viability of ENSIP, together with the requirement to enforce the ENSIP rules for future USAF engines, appear to have been justified.

In the UK, however, the historical approach has been to concentrate the NDT activity into proving that the manufacturing process on fracture critical parts is viable and under control and in addition, to conduct expert hazard reviews of the process to recognize and eliminate potential problem sources before the process is standardized and released for production use.

Once the process has been satisfactorily established, the UK philosophy has then been to use high quality NDI to monitor that the process remains within acceptable parameters.

It is also recognized that a much greater emphasis has been placed in the UK on the NDT of critical parts for subsurface defects than that used in the USA, while the USA procedure requires a higher level of NDI reliability for surface defects.

Recent UK/USA engine manufacturer exchanges has shown that major differences exist between the UK and USA practices in the ultrasonic inspection of both compressor and turbine discs, for detecting subsurface defects. These differences (Ref 5) show that the UK approach generally requires a higher standard of subsurface inspection to detect much smaller defects than that required in the USA. It is also an established practice in the UK to use ultrasonic data for trend analysis of the process utilizing ultrasound characteristics, such as attenuation, Grass (structural noise) and defect trends, all of which assist the metallurgist to monitor the process.

The methods used in the UK for establishing that components are free from harmful surface defects, particularly cracks, again rely on a combination of process hazard review and intense surface inspections at the earliest possible stage of the manufacturing process. These surface inspections include the use of acid etchants, both in the initial forging and as a preparation for the inspection of the finally machined surface, which is a practice that has not normally been used in the past in the USA. For some years, these inspections were supplemented by a combination of eddy current and disc spinning to enhance the detection of cracks which may be subjected to compressive stress, but since no surface cracks have been detected in manufacturing, and since the process hazard reviews have proved a total absence of cracking, for many years, the disc spinning has been discontinued.

To date, the service experience on UK engines has not shown the need to develop special depot NDI technologies nor to take a significantly different approach in the manufacturing inspection philosophies.

However, with the advent of the European Fighter Aircraft (EFA), and the involvement of a number of European engine manufacturers in the development and production of the engine, consideration is currently being given to the use of a part ENSIP or Damage Tolerance approach on some of the critical turbine components. At this stage, it is envisaged that a lifing philosophy of a combined fracture mechanics and process approach may be used where the highly stressed areas of a disc would be lifed by fracture mechanics, supported by proven reliability NDI and the low stressed areas traditionally inspected and assessed on a process control basis.

Work as now commenced on a NDI Reliability Program coupled to the EFA Development Program, to establish a data base to support this approach.

No final decision has been taken yet on whether this approach is desirable, but even if a part ENSIP strategy is adopted, it is unlikely that a formal in-service inspection philosophy will be required.

In the UK, the emphasis on high profile process control, coupled with high quality NDI in the early stages of the process, will take on more significance as the desire to use increased stresses and the requirement to detect smaller defects progresses. We are

rapidly approaching (or may possibly have reached) the limits of NDI capabilities, and we are therefore being driven into the need to develop scientific and quantifiable process control parameters. In the UK, a considerable effort is being made to achieve this objective particularly in the area of process modeling, and intense characterization of the process by both destructive and non-destructive examination.

SUMMARY

At present, there are differences between the US and UK philosophies behind the use of NDI. The UK philosophy is mainly one of process control while the US philosophy is based more on damage tolerance criteria. From the previous discussions, it can be seen that even though at present the US has a more rigid and formal approach, it appears that the two approaches are merging to some degree. The UK philosophy is becoming more structured and the US is introducing more process control, particularly for non-fracture critical components. However, it is unlikely that there will be any significant reduction in the current US emphasis on damage tolerance, which carries with it the requirement for full inspection of those areas that are designated as fracture critical. Therefore, there will be continued strong emphasis in the US on the development of automation and the quantitative demonstration of inspection methods. The development of the proposed Military Standard for USAF NDE System Reliability Assessment should greatly assist in the uniform application of this technology for engine programs in the US. The extent to which it may be useful to the UK and the European Community remains to be seen, but the authors strongly recommend a common AGARD approach, particularly for the analytical methodology.

REFERENCES

1. Engine Structural Integrity Program (ENSIP), Military Standard 1783 (USAF), 30 November 1984.
2. Aircraft Structural Integrity Program, Airplane Requirements (ASIP), Military Standard 1530A(1), 26 February 1988.
3. Cowie William D., "Fracture Control Philosophy for Gas Turbine Engines", to be published in Volume 17, 9th Edition, Metals Handbook: Non-Destructive Evaluation & Quality Control, ASM International, Metals Park Ohio, USA, September 1989.
4. Berens, Alan P., "NDE Reliability Data Analysis", Ibid.
5. Taylor, R.G., "Need for Common AGARD Approaches & Actions", AGARD Report No. 768, Luxembourg, 1-6 May 1988.

NDI-CONCEPT FOR COMPOSITES IN FUTURE MILITARY AIRCRAFT

by

Matthias Stoermer
Air Materiel Office, German Air Force
EFA Project Team, Postfach 90 25 00, D-5000 Köln 90
Federal Republic of Germany

Key Words: Advanced Aircraft Structures, Composites, NDI, Artificial Intelligence

Abstract

Helicopters and fixed wing aircraft entering service with the German Air Force, and the use of composites in these aircraft is reviewed. Past experience with composites and with existing NDI techniques are used to identify some of the anticipated NDI requirements for the next generation aircraft.

It is expected that if the level of effort devoted to inspection is to be kept within reasonable bounds, increased effort will be needed to develop improved NDI techniques and to provide training to Air Force craftsmen to make them aware of the characteristics of composite materials and the types of flaws and defects that they are likely to contain. The use of artificial intelligence in NDI is also expected to increase, and a review of some of the German work in the area will be provided.

Introduction

During the next decade, several new aircraft, including both fixed-wing and helicopter systems, will be introduced into all three Services of the Federal Armed Forces. They will all come under German Air Force Single Materiel Management Responsibility.

These aircraft types represent an advanced generation of military aircraft and are characterized by the fact that their airframes are manufactured from composite materials to a considerable extent. In particular, carbon fiber, aramide fiber and glass fiber composites are used.

These advanced technologies will replace conventional metal materials both in secondary (doors, covers, radomes) and primary structure.

Table 1 provides a general survey of advanced European aircraft and the amount of composite materials used.

The first three of them are the above mentioned new German military aircraft.

<u>Aircraft</u>	<u>Composite Proportion of Weight</u>
Attack Helicopter 2	30 %
NATO Helicopter 90	30 %
JF 90/European Fighter Aircraft	40 %
Airbus A 320	17 %
ATR (French Transport A/C)	20 %
JAS Gripen	30 %
Rafale	25 %

Table 1: Advanced European Aircraft and their Proportion of Composites

Preparation of a Inspection Concept

When the European Fighter Aircraft (EFA) is introduced into service, the technical readiness required by the GAF has to be established. Therefore as early as in the development phase GAF will prepare a maintenance concept ensuring technical readiness.

A specific testing and inspection concept for the airframe will be part of this maintenance concept. This testing and inspection concept will inevitably result in a compromise involving several different and sometimes contradictory requirements as shown in table 2:

- Tactical/operational requirements (e.g. availability)
- Flight safety requirements (e.g. inspection intervals)
- Cost-effectiveness (e.g. NDI-Technique)

Table 2: Requirements for an Inspection Concept

Likewise, a distinction has to be made between the test requirements at the different maintenance levels:

- German Air Force Maintenance Levels 1 and 2: Operational/intermediate level
- German Air Force Maintenance Levels 3 and 4: Depot level

Clear distinctions have to be established between cost and effectiveness. In this connection, it has also to be taken into account that depot level maintenance clearly provides a greater technical capability. During the EFA development phase, the Air Force Materiel Office in particular has to provide support to the development of the inspection concept and consequently of the airframe portion of the maintenance concept based on LSA application i.a.w. MilStd 1388.

In the case of EFA, the individual maintenance tasks are identified by a Reliability Centered Maintenance (RCM) analysis process (tailored MilStd 1843).

Moreover, feedback to the design is envisaged within the scope of continuous program progress monitoring: If the appropriate findings are obtained, the EFA design should be influenced within the "maintainability" activities. Where unacceptable logistic consequences are identified, the GAF will try to exert their influence together with the other partner nations.

In this area, the Air Force Materiel Office provides the necessary engineering assessments (Ref. 1).

New Materials Require New Methods

As far as the aforementioned new aircraft generation is concerned, the German Air Force is faced with large-scale application of carbon fiber composites in the airframe structure.

In all weapon system, these materials are used both fully laminated and in sandwich designs.

Previous experience and initial findings obtained from the EFA program already revealed, that the fiber components have their own specific properties. Consequently, they will show their own specific types of damage and faults when put under stress.

Inspection of such damage will also require an inspection technique that is specifically tailored to the component, type of damage, occurrence, and propagation of the fault.

While carbon fibre composites are superior to metal materials as far as fatigue properties are concerned, the crack propagation rates on which are normally the basis for defining inspection intervals, have not been completely described mathematically up to now, a fact which is true even for laboratory models. The model consideration of differing laminate structures, fiber contents, fiber strengths, fiber orientation and types of resin is still in the far future (Ref. 2).

Potential Types of Damage to Composites

At the present time, the German Air Force anticipates the following potential damages shown in table 3 (Ref. 3):

<u>Damage</u>	<u>Reason</u>
Delamination	- impact - local overstressing
Corrosion	- failure of protective coatings due to dynamic load
Moisture absorption	- air humidity - moisture condensation
Ageing	- ultraviolet radiation
Integral tank leakage	- failure of protective coatings due to dynamic load

Table 3: Anticipated Damages to Composite Structures

Potential Test Methods for Composites

At the present time, the following methods shown in table 4 appear to offer themselves for nondestructive testing of composite materials (Ref. 3 and 4):

- Visual inspection
- Tap Test
- Ultrasonic inspection
- Eddy-current test
- X-ray radiography
- Neutron radiography
- Holography
- Laser Interferometry
- Thermography
- Acoustic-Emission

Table 4: NDI-Methods for Composites

Up to now, no individual method has proved to be outstanding and universally applicable. Each method has its advantages and disadvantages in approximately equal shares and, basically, offers itself for only specific applications.

This means that the selection of a test method must first of all be oriented on the faults to be detected and, secondly, has to take into account the specific features of the component (primary or secondary structure). Besides, the inspection interval has to be specified and, finally, accessibility of the area to be inspected shall be considered (e.g. couplant required? Insertion of X-ray film possible? etc.).

For composite materials, there are no material laws available yet from which inspection measures and intervals can be derived similar to those applicable to metal materials. Because of the inhomogeneity of the material (stacking sequence and orientation) they cannot be specified in general terms. Of course, the definition of an inspection concept is more complicated this way.

Due to such considerations, an airframe design philosophy for composite structures differs from previous philosophies for metal structures. Under the fatigue aspect, the safe-life philosophy is used which greatly reduces inspections in this respect.

Yet there is still the hazard of damage by environmental impacts or accidents.

In this context, the vulnerable areas have to be designed to provide tolerance of barely visible impact damage (BVID) throughout the service life (Ref. 5).

However, the GAF must have inspection capabilities to at least assess the technical readiness of the aircraft on the Air Force base.

This applies in particular to the vulnerability of the airframe to environmental impact (runway stones, bird strike, etc.) and accidents on the ground (such as damage occurred during taxiing) (Ref. 6).

Engineering personnel must be provided with appropriate clearly defined procedures and criteria which will enable them to make technically well-founded statements.

Likewise, more extensive, possibly stationary test facilities have to be provided for at the repair depots to permit determination of damage degrees and, consequently, the remaining usable life. In this process, it is easily possible that computer-based evaluations will be done to do that and, in addition to compute the degree of damage, then to define servicing intervals and, in some cases, flight performance restrictions based on strength calculations for the individual airframe.

In this context, a combination of several of the aforementioned NDI-methods may be useful.

An initial and correct step in this direction was taken by the US Air Logistics Center, Sacramento. In particular the full automation of inspection, filing and evaluation processes may result in considerable cost benefits in the long run (Ref. 7).

Requirements for Advanced NDI-Methods

In addition to the aforementioned problems in selecting inspection methods there are other requirements resulting from the tactical-operational demands made on inspection methods for application at levels 1 and 2 as listed in table 5:

- Inspection of large areas of the aircraft in "one look"
- Identification of hidden/unvisible damages
- Identification of delamination and honeycomb separation
- In situ testing of aircraft components wherever possible
- Test results independent of
 - . Fuel condition of integral tanks
 - . Surface protection
 - . Lightning protection
- No special preparations of the item/aircraft before testing.

Table 5: Technical Requirements due to Tactical-Operational Demands

Futhermore, the are additional operational requirements as listed in table 6:

- Airmen being able to handle the test equipment after 2 day training.
- Usage of the system must not require any particular safety precautions.
- Handling of the system by 2 airmen max.
- Test duration less than 1 hour for a selective diagnosis (approx 2 mxm) and no more than 8 hours in the case of larger surfaces.
- Airmen wearing NBC-Clothing during testing.
- Unsusceptibility of the system to environmental conditions as
 - . Noise
 - . Temperatur
 - . Humidity
 - . Fog
 - . Dust
 - . Wet surfaces under test
 - . Different surface temperatures under test.
 - . Poor brightness

Table 6: Operational Requirements

The test results shall be

- reproducible
- recordable
- interpretable without any doubt!

Fault criticality must be readily identifiable.

Of course, it will not be possible to equally meet all the criteria mentioned above when the final procedure is laid down.

However, an optimum compromise should be aimed at.

Research projects in this direction are being supported and pursued by the German Air Force.

Conclusion

The optimum inspection system selected on the basis of the aforementioned constraints and requirements would then represent only one half of the overall concept.

The Air Force engineeres and craftsmen at all maintenance level represent the second half of the concept.

Even most advanced aircraft design cannot enter service without experienced technicians and engineers who have full command of their materials and techniques. This is also true for composite materials. The Air Force metal workers currently employed at levels 1, 2 and 3 will be trained by the GAF to be composite specialists, with special skills in handling composite materials as well as inspection and repair techniques.

Experienced technical Air Force personnel who know their aircraft and materials inside and outside will also - and particularly - be required in the future; otherwise, there will be no confidential relationship between pilots and Air Force craftsmen. Experience gathered during employment of previous weapon systems has shown that the human element can't be neglected in a man-machine-system (Ref. 7).

Consequently, the composite specialist will represent the second aim, which the German Air Force efforts are related to.

His comprehensive training and experience cannot be replaced by automatic computer-based test system. The effort invested in the training of composite materials specialists will pay off when it comes to damage assessment and repair in daily flying operations. The specialist's observations, his experience and ideas will also serve to refine and extend the inspection concept as well.

Besides, it will also be the specialist who initiates and controls an appropriate feedback in continuous coordination between Air Force Material Office and aircraft industry as shown in figure 1. Thus the knowledge gathered in his special field of activity (i.e. maintenance of composite materials) will be incorporated in present aircraft programmes and finally influence design of future aircraft (Ref. 8).

Outlook to Artificial Intelligence

The range of demands made on advanced inspection and test methods described above and the man-machine-system outlined subsequently give rise to considerations how these two aspects could be brought close together and how they could support each other.

The key word in this context is "expert system-artificial intelligence". The idea suggests itself to link an automated test system with the knowledge and experience of technical personnel and thus gradually refine it and make it available for large-scale utilization.

From the authors point of view, the Air Force should take the chance to integrate many other mission relevant and engineering tasks into this expert system which is shown in figure 2.

Thus this system could be designed for a personal computer, and it could be provided with a learning capability; this way it would also be used for assisting the maintenance and repair of composites.

This system could incorporate all component-specific features as well as NDI-Technique, inspection intervals, critical crack lengths and many more. In addition, it could include previous experience gathered in the repair field.

Moreover, the system should be part of the computerbased equipment history records of the entire aircraft. Likewise, an interface with the EFA on-board structure monitoring system should be available to ensure that these data can also be resorted to if necessary.

Thus a computerized maintenance manual would be available, for example in PC or even laptop format. In addition, different levels within the expert system will be possible to adapt it to the requirements of the different maintenance levels or to have a simplified form available for Aircraft Battle Damage Repair (ABDR) Requirements.

Some of these tasks will also be integrated in the Ground Support System (GSS), which is under consideration for EFA.

Research in this direction will be initiated by MOD-GE.

Apparently, we have to get used to the fact that our engineering personnel will no longer carry their hardcopy Technical Orders but will be equipped with laptop personal computers in the future.

However, this will certainly have no adverse effect on the attractiveness of the Air Force engineering units.

When keeping up with advanced technologies and subsequently training our Air Force personnel in such technologies, we will certainly attract sufficient qualified personnel to the Air Force Engineering Organisations.

References

1. Bundesminister der Verteidigung, "Inspektions-, Prüf- und Reparaturverfahren für zukünftige CFK-Flugzeugbauteile", DFVLR Köln-Porz, Oktober 1988.
2. Arbeitskreis Luftfahrttechnisches Handbuch (LTH), Band "Faserverbund-Leichtbau", Ottobrunn 1985.
3. Deutsche Gesellschaft für Metallkunde, Seminar "Theorie, Praxis und Qualitätssicherung in der Anwendung der Faserverbundwerkstoffe GFK-CFK-AFK", Bad Nauheim, April 1989.

4. B.W. Henderson, "USAF Expects Robotic Inspection Facility to Cut Maintenance Costs", Aviation Week/ March 13, 1989.
5. Eurofighter GmbH, "CFC Damage Tolerance Criteria", München, May 1989.
6. Bundesminister der Verteidigung, "Damage Tolerance und Impact Damage Tolerance von GFK im militärischen Flugzeugbau", DFVLR Köln-Porz, März 1989.
7. Rhein-Flugzeugbau GmbH, "Reparaturanweisung für Faserverbundstrukturen am Schulflugzeug FANTRAINER FT400/FT600", Mönchengladbach 1985.
8. Messerschmidt Bölkow Blohm GmbH, "Materialerhaltbarkeit und Zuverlässigkeit von Faserverbundwerkstoffen unter Einsatzbedingungen", Ottobrunn 1989.

BIOGRAPHY

Matthias Stoermer, B.Sc. (Eng.)
 Air Force Materiel Office
 - III B 1 - JF 90/EFA -
 Postfach 902500/503/13
 5000 Köln 90

Matthias Stoermer is Bachelor of Engineering and a regular officer of the German Air Force.

He is assigned to the Air Force Materiel Office, Cologne, where he is employed in EFA program management. He directs and coordinates the Air Force Materiel Office activities as far as technical/technological EFA matters are concerned, including airframe, functional equipment and engine.

1st Lieutenant Stoermer studied aeronautical and space engineering at the Federal Armed Forces University, Munich, where he underwent intensive training in system dynamics. For his diploma thesis in 1985 he chose artificial intelligence. Following his university education, he was in charge of maintenance activities at a German Air Force fighter wing for two years, both at 1st and 2nd line maintenance levels.

Subsequently he was transferred to the Air Force Materiel Office to make use of his practical experience and his engineering knowledge within the EFA Program.

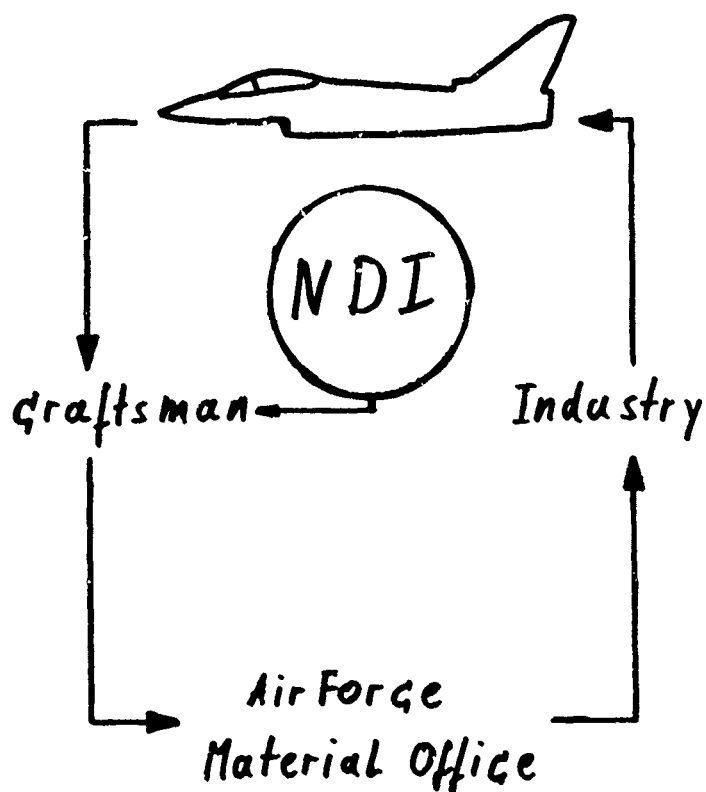


Figure 1: Man - Machine -
Feedback - System

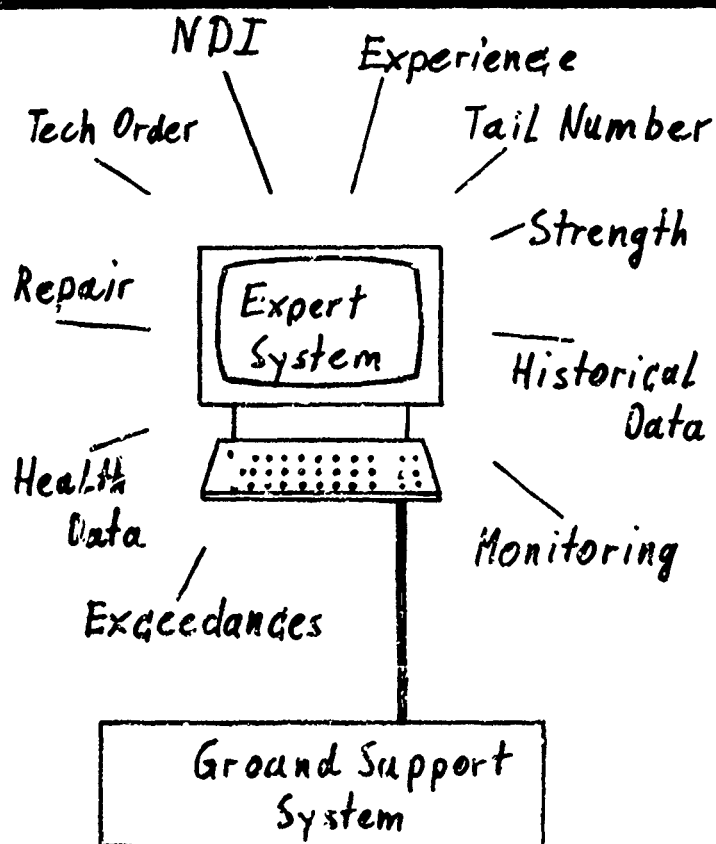


Figure 2: Expert System

ASSESSMENT AND DEMONSTRATION OF THE CAPABILITIES OF NDI PROCESSES, EQUIPMENT AND PERSONNEL*

by

Ward D. Rummel

Manager, Advanced Launch Systems Technology
Martin Marietta Astronautics Group
Martin Marietta Corporation
Denver, Colorado
United States

SUMMARY

The application of modern materials and structural analysis methods and the use of fatigue and fracture analysis in life prediction and life cycle modeling has focused attention on the need for quantitative nondestructive inspection (NDI) methods to quantify materials integrity and life limited component integrity. Advances in both life prediction methods and in quantitative NDI technology have enabled implementation of "retirement for cause"/life cycle management methods. The combined application of life prediction methods and the application of advanced NDI methods have resulted in improvements in engineering system reliability predictions and in quantification of both systems operating levels and systems life cycle operating margins.

This paper discusses the principles of quantitative NDI process characterization, the development of analytical tools for NDI process characterization, and some typical results achieved by quantitative NDI process analysis and characterization.

INTRODUCTION

The need to quantify and validate nondestructive evaluation (NDE)/nondestructive inspection (NDI) performance capabilities has become increasingly necessary with the application of fatigue and fracture mechanics as a basis for design of modern engineering systems. The demand for quantitative characterization of NDI performance has led to the development and application of several analytical tools. NDI process characterization has, in turn, resulted in many NDI process improvements and a great increase in understanding of NDI processes and NDI process capabilities. Early requirements for quantification of NDI process performance arose in the United States on the B-1 bomber program, the NASA Space Shuttle, and in the nuclear power industries. Quantitative NDI capabilities and reliability have become integral factors in the design, production and life cycle management of most modern engineering materials, structures, components and systems.

The result of application of an NDI process is usually a binary, go or no-go decision, thus the methods and tools used in the analysis of NDI processes may be applied to many measurement processes and to automated digital systems decisions based on analysis of analog data. Use of the methods in automated process analysis has, in turn, aided the automation of NDI processes with a resultant overall improvement in both end item system and NDI process reliabilities.

QUANTITATIVE NDI FOR THE B-1 BOMBER PROGRAM

Fracture control technology was applied in the B-1 aircraft program and requirements for quantification of NDI processes were rigorously applied to those structural components whose failure could cause the loss of the aircraft. A flaw length of 0.250 inches and a flaw depth of 0.125 inches, for surface flaws, corner cracks of 0.050 inch radius, and imbedded cracks of 0.250 inch diameter were imposed as initial design constraints. These flaw sizes were selected because it was felt that they could be readily detected by state of the art production inspection processes. If a crack size smaller than that imposed by the design requirements was proposed, a secondary requirement to demonstrate reliable detection at the smaller crack size was imposed.

In conformance to these requirements, a set of test specimens was produced that contained fatigue cracks at each flaw size and material combination. The specimens were passed through the production system inspection lines to assess the capabilities for screening the required flaw sizes. Statistical sampling methods were applied and demonstration to a 95% confidence level was required by repetitive inspections. In the event that the production line methods could not screen at the lower flaw size, redesign of the component and/or improvement of the NDI process/personnel were required. Final design, production requirements were thus satisfied by iterative processes of design, inspection and process improvement.

The difficulty with using a discrete flaw size of range in qualifying a process is that no information is provided on true process capabilities and therefore no information is provided to aid in process improvement when the process fails to meet the

* This paper has been cleared for public release (ASD CASE #89-1595, 22 June 1989). Public domain information has been previously cleared by the authors as referenced. Public release of this paper complies with ITAR regulations for technology transfer.

requirements and no information is provided to aid in assessing process margin when the process meets the requirements. The discrete flaw size method is costly to implement in both the required number of inspection cycles and the need to iterate and improve those processes that do not screen to the required levels (Ref.1).

NASA SPACE SHUTTLE PROGRAM

Fracture control design processes were imposed on all NASA Space Shuttle hardware. It was recognized that all NDI processes have a threshold detection limit and that detection is not a step function at a given flaw size, but varies in the same manner as other measurement processes. A program was initiated to generate a large test sample set containing fatigue cracks of varying sizes and to use those specimens to characterize the capabilities of various production NDI processes. 328 fatigue cracks ranging in length from 0.007 to 0.500 inches were produced in 105 test panels. Thirteen flaw free panels were included in the test set for a total of 118 panels in the test set. The test set was assessed by production X-radiography, ultrasonics, eddy current, liquid penetrant and holographic interferometry procedures in the "as-machined", "after etching", and "after proof test" conditions. A large database was generated by this process and a condensed form of data presentation was required. The characteristic of primary engineering interest was that of crack detection as a function of flaw size. Statistical analysis and sampling methods were used to present data as a continuous function in the form of a Probability of Detection (POD) as a function of flaw size as is shown schematically in Figure 1.

The method of data analysis selected for this presentation was that of a moving average sampling method. In this analysis, the cracks were ordered from the largest crack to the smallest crack. Since observations and cracks were independent, a moving average sampling method can be used to generate the POD function. Crack observations were grouped by counting down twenty nine cracks (from the largest crack size); the point estimate of detection for that sample group was calculated (number of successful detections divided by the number of opportunities); calculating the lower confidence limit for the group sampled, plotting the point estimate of detection and lower confidence limit boundary at the largest flaw size in the sample group; deleting the largest crack from the group and adding the next largest crack in the total data set to the group; calculating and plotting the point estimate of detection and lower confidence limit for that sample group; and continuing the process until data were exhausted (Ref.2). An example of a POD curve, produced by this method, is shown in Figure 2. This plotting method produces the desired, statistically significant relationship between the process detection capabilities and the flaw size. It also produces information that may be useful for process improvement and information on the operating margin for the NDI process. These data were then used to establish the design constraints for the NASA Space Shuttle program and design data were plotted as a function of flaw size and aspect ratio as shown in Figure 3.

The Probability of Detection (POD) method of presenting NDI process information was adopted by both NASA and Air Force programs and has become the industry standard method for NDI process data presentation. The disadvantage of the moving average method of data analysis and plotting is the requirement for a large database in order to provide a continuous function with respect to flaw size. Much work on NDI process assessment and data presentation has been devoted to improved plotting methods and to analysis of smaller data sets. The POD data presentation method is a very useful design engineering tool, but is incomplete in fully characterizing an NDI process. Identifying parametric data, that must be included with all POD data, include the identification of the NDI process operating parameters, such as processing times, calibration methods, and the threshold signal acceptance level (criteria) used as the basis for the flaw/no-flaw decisions. In like manner, the false alarm rate derived from application of the process operating parameters must be identified to fully characterize NDI process discrimination capabilities. Much work has been devoted to the use of all available data to fully characterize NDI process capabilities and to reduce the amount of data required to provide confidence in a derived POD function: action model.

NDI DISCRIMINATION AS A PROBLEM IN CONDITIONAL PROBABILITY

NDI processes involve the control and measurement of complex parameters to produce a final output. The output of the process is, in turn, indirect and a decision must be made on the results of that output. Although many parameters may be varied to produce variations in the output, for example crack presence or absence, the decision process is not binary (go, no-go) as it is frequently envisioned. It is actually the product of conditional acceptance (either by the human operator or by an automated system) due to the interdependence of the output and decision responses. Four possible outcome result from application of an NDI procedure for crack (flaw) detection as shown in the following diagram:

		INSPECTION STIMULI	
		POS a	NEG n
INSPECTOR (SYSTEM) RESPONSE	POS A	TRUE POSITIVE (Crack Detected) $M(A,a)$ $P(A,a)$ (No error)	FALSE POSITIVE (False Alarm) $M(A,n)$ $P(A,n)$ (TYPE II Error)
	NEG N	FALSE NEGATIVE (Undetected crack) $M(N,a)$ $P(N,a)$ (Type I Error)	TRUE NEGATIVE (No crack) $M(N,n)$ $P(N,n)$ (No Error)

To summarize, the outcome of an inspection process are:

- 1) True Positive (TP) — A crack exists and is detected, where
 $M(A,a)$ = the total number of true positive results and
 $P(A,a)$ = the probability of true positive results.
- 2) False Positive (FP) — No crack exists, but one is identified, where
 $M(A,n)$ = the total number of false positive results (false alarms) and
 $P(A,n)$ = the probability of false positive results.
- 3) False Negative (FN) — A crack exists, but is not detected, where
 $M(N,a)$ = the total number of false negative results and
 $P(N,a)$ = the probability of false negative results.
- 4) True Negative (TN) — No crack exists and none is detected, where
 $M(N,n)$ = the total number of true negative results and
 $P(N,n)$ = the probability of true negative results.

The interdependence of these matrix quantities can be expressed as:

$$\begin{array}{ccc} M(A,a) & + & M(N,a) \\ \text{(TP)} & & \text{(FN)} \end{array} = \begin{array}{c} \text{Total opportunities for positive calls} \\ \text{(Total number of defects)} \end{array}$$

and

$$\begin{array}{ccc} M(A,n) & + & M(N,n) \\ \text{(FP)} & & \text{(TN)} \end{array} = \begin{array}{c} \text{Total opportunities for false alarms} \\ \text{(Total number observations of unflawed sites)} \end{array}$$

Due to the interdependence of these two relationships, only two independent probabilities need be considered to quantify the output of an NDI process.

The probability of detection (POD) or probability of true positive results ($P(A,a)$), can be expressed as:

$$P(A,a) = \frac{M(A,a)}{M(A,a) + M(N,a)} \quad \text{or} \quad \frac{\text{total true positive calls}}{\text{total number of defects}}$$

Likewise, the probability of false alarms (POFA) or the probability of false positive results ($P(A,n)$) can be expressed as:

$$P(A,n) = \frac{M(A,n)}{M(A,n) + M(N,n)} \quad \text{or} \quad \frac{\text{total false alarms}}{\text{opportunities for false alarms}}$$

SIGNAL/NOISE RELATIONSHIPS TO NDI PROCEDURE OUTPUT

The desired results of application of an NDI procedure are (crack) detection (signal present) or (crack) nondetection (signal absent). The basis for detection is that of sensing a signal response and determination that the signal response is above a predetermined threshold. Both sensing and interpretation are dependent of the signal (plus noise) and the noise. Since NDI processes produce an indirect signal output response as a function of the characteristic to be measured, other, nonrelevant parameters, such as surface roughness or grain structure, may produce a signal response. Such nonrelevant output is the application noise response for the process and may interact (and interfere) with the discrimination, decision process. This output is normally well above, and should not be confused with, the electronic noise that is inherent to NDI measurements with electronic instruments.

If an NDI procedure is repetitively applied to a single flaw of a given size (in a part with a fixed geometry, surface condition etc.), the output responses may be used to plot probability density distributions of both flaw signal and application noise responses. Under ideal conditions, such as the response from a large flaw, the signal and noise distributions will be well separated, as shown in Figure 4. Discrimination of flaw responses from application noise responses is a simple process and the probability of detection (POD) will be high and the probability of false alarms (POFA) will be low. In practical engineering applications, the flaw size is not fixed (and is rarely large) and the discrimination process is more complex. The discrimination process is indeed applied to a continuous range of flaw sizes and the capability for discrimination is dependent on the separation of the signal (plus noise) and noise responses of the process and is an inherent performance characteristic of the NDI procedure. If the NDI procedure is applied to a single flaw of intermediate size (in a part with the same fixed surface finish, geometry, etc.) the output responses may be used to generate probability density distributions for signal and noise as shown in Figure 5. For this flaw size, the distributions overlap (in part) and the capability for discrimination is dependent on response from a single set of output signals within these distributions. If the single set of output signals are well separated (ie. signals at the outer extremes of the distributions) the output response will be interpreted as acceptable (no flaw condition) for those cases where the threshold response acceptance level is located between the signal and noise signals. If the single set of outputs lies at the inner extremes of the distributions, the output response may be interpreted as acceptable (no flaw or undetected flaw condition) or may be interpreted as unacceptable (false alarm condition) for the same threshold response acceptance level. For this condition, the POD will be lower and the POFA will be higher than for the case of discrimination with positive signal/noise separation margins. If the process is repeated for a small flaw (under the same operating conditions) the signal and noise response distribution will approach coincidence as shown in Figure 6, the POD will be low and the POFA will be high.

INFLUENCE OF SIGNAL/NOISE ON POD

The interaction of signal/noise response on POD is illustrated in Figure 7. For wide separation of probability density distributions for signal (Plus noise) and noise responses, the probability of detection (POD) will be high. A threshold transition in the POD function is obtained when the signal (plus noise) and noise responses overlap. A low probability of detection is obtained when the signal and noise distributions are coincident.

INFLUENCE OF ACCEPTANCE CRITERIA ON POD

It is clear that the performance capability of a given NDI procedure is dependent on the nature and distribution of the signal outputs that are generated under the conditions of application. It is also clear that the threshold acceptance criteria applied in the discrimination process is an important factor in the successful application of a procedure. Consider the application of an NDI procedure to a large flaw under conditions that produce a significant separation of probability density distributions of signal and noise as shown in Figure 8. If the threshold acceptance criteria (represented by the vertical arrow) is placed at too high a level, some of the flaw will be missed (reduce POD). If the acceptance criterion is placed at a proper level, clear discrimination will be realized (high POD). If the acceptance criterion is placed too low, all of the flaws will be rejected, but some false alarms will be realized and good parts will be rejected (high POFA). The respective influence of acceptance criteria on POD for a case of broad signal/noise separation is shown graphically in Figure 9.

The NDI procedure performance characteristics of primary importance are (1) the signal to noise ratio (separation margin) and (2) the threshold acceptance criteria applied in the discrimination process. Optimum NDI procedure performance may be obtained by characterizing an NDI procedure and by matching the threshold acceptance criteria to the performance capabilities of the NDI procedure. Such characterization also enables assessment and quantification of risks that result from changes in acceptance criteria.

VARIATIONS IN DATA ANALYSIS TO PRODUCE POD CURVES

Variations in data analysis and data presentation have been introduced to reduce the amount of data required to generate a POD curve and to smooth the form of the output. Data from controlled NDI processes produced a POD curve having the classic form shown in Figure 1. Berens, et al (Ref.3) proposed that this form could best be described by a log odds or log logistics function as shown in Equation A-1

$$POD(a) = \frac{\exp[\alpha + \beta \ln(a)]}{1 + \exp[\alpha + \beta \ln(a)]} \quad (A-1)$$

This function produces a smooth POD curve from the parameters that are derived from a dataset. Varying methods of reducing the size of the dataset required have been introduced. A useful procedure has been adopted from Berkson (Ref.4) to obtain the α and β estimates by a maximum likelihood method. This method enables the use of binary data to generate the smooth POD curve form. Figure 10 is an example of a POD curve produced by the maximum likelihood/log logistics model method.

Much greater efficiencies in data use can be effected when the NDI procedure output produces discrete quantitative data as a function of flaw size. For example, the output from an eddy current procedure may be obtained in the form of a millivolt response as a function of flaw size. Berens and Hovey introduced an a versus \hat{a} analysis method of estimating POD. This method is based on the probability that \hat{a} (signal amplitude) will exceed the detection threshold (\hat{a}_{th}). To apply the a versus \hat{a} method of analysis, the inspection data must be modeled so that:

$$\hat{a} = f(a) + c + e$$

where $f(a)$ represents the mean trend in \hat{a} as a function of a crack (length or depth) parameter; c is the variance component due to a flaw to flaw variation; and e is the variance component due to inspection variation. A typical plot of signal amplitude as a function of crack length for an automated eddy current inspection is shown in Figure 11. The resulting POD curve for this data is shown in Figure 12.

LESSONS LEARNED FROM ANALYSIS OF NDI CAPABILITIES BY THE POD METHOD

The success of a reliable NDE application to an engineering system is dependent on excellence in:

- | | | |
|----------------------------|---|---|
| * BASIC ENGINEERING DESIGN | } | EARLY DESIGN ANALYSES |
| * NDE ENGINEERING | | — LOW COST CHANGE |
| * NDE MATERIALS | } | NDE PROCESS CONTROL
— HIGH COST CHANGE |
| * NDE EQUIPMENT | | |
| * NDE PROCESSES/PROCEDURE | | |
| * HUMAN FACTORS | | |

When a process fails to meet expectations, the human operator is often approached as the primary problem. Although the human operator may be a cause,

IF INSPECTION MATERIALS, INSPECTION PROCESSES, AND
INSPECTION EQUIPMENT ARE ALLOWED TO VARY, THE
HUMAN OPERATOR DOES NOT HAVE A CHANCE IN CORRECT
DISCRIMINATION AND INTERPRETATION AT THE FINAL
STAGE IN THE PROCESS.

All process factors must indeed be considered and addressed in order to significantly improve process capabilities and reliability.

THE INFLUENCE OF ETCHING ON PENETRANT INSPECTION CAPABILITIES

The need to etch materials before penetrant inspection is often questioned. The influence of performance capabilities on consistent penetrant inspection of etched and unetched parts is readily determined by the POD method. Figure 13 shows penetrant performance on unetched ("as machined") aluminium panels. Figure 14 shows penetrant performance on the same panels after etching.

THE INFLUENCE OF DEVELOPER ON PENETRANT INSPECTION CAPABILITIES

The advantage of using a penetrant developer is readily observed by the POD method as shown in Figures 15 and 16. In this case, the use of developer also reduced the false alarm level while improving penetrant performance.

THE EFFECT OF DEVELOPER FOG TIME ON PENETRANT INSPECTION CAPABILITIES

Process variations in the form of developer fog time in an automated dry powder developer operation are readily observed by the POD method as shown in Figures 17 and 18.

USE OF THE POD METHOD IN OPTIMIZING AUTOMATED PENETRANT INSPECTION PROCESS PARAMETERS

Figure 19 shows the POD capability for an automated penetrant processing station using nominal penetrant processing parameters and an automated read-out. A series of POD assessments were made the progressively optimized penetrant processing parameters. Figure 20 shows the performance capability after process optimization was completed.

USE OF THE POD METHOD FOR SETTING PROCESS ACCEPTANCE CRITERIA

The POD method may be used to optimize process parameters including the acceptance criteria (threshold) used in crack discrimination. Figure 21 is a POD curve for an eddy current inspection using the established acceptance threshold. Figure 22 is the same signal data that has been reprocessed at a more stringent acceptance threshold.

USE OF THE POD METHOD FOR ESTABLISHING FACTORIAL EXPERIMENTS

The POD method is sensitive to slight variations in overall process performance and may be used to assess variations in operator performance. Figure 23 is the POD performance output by an operator that performed at a fixed inspection station on a full time basis. Figure 24 is the POD performance by an operator that performs at that station on a part time (relief) basis. A most frequent use of the POD method is that of establishing operator performance proficiency for an establishing NDI procedure. The POD method may be and is used very successfully to qualify the performance capability of individual operators.

After a process is established and well characterized by use of a test panel set, a subset of the test panels may be used to assess or provide continuing confidence in the performance capabilities of an experienced operator or to qualify a new operator. This is accomplished by means of a Relative Operating Characteristic (ROC) curve. This method balances performance capabilities in terms of detection and false alarms on a set of panels that have been well characterized and related to a specific inspection process (see Figure 25). After a POD performance capability by an experienced and skilled operator has been established for a given set of test specimens, a subset of panels that contain cracks that lie near the threshold detection limit may be removed from the test set for use in qualification by similar performance. Performance by the experienced and skilled operator will result in a level of detection and false alarm rate that are characteristic of the controlled NDI process. When these data are plotted on the ROC curve, the results are a clustering of data points at the high POD and low POFA area of the curve (Ref.5). Additional operators or the same operator are expected to perform to the same level when the subset panels are reprocessed. If data fall outside the required zone of performance, more training and experience are provided or a new level of performance is established by processing the full test set (see Figure 26).

CONCLUSIONS AND RECOMMENDATIONS

The POD method of NDI process assessment and characterization is a powerful and useful tool in establishing and quantifying an operating point for controlled process application. The POD method is useful for any multiple step, multiple variable process that is not readily assessable by more conventional methods and for those methods that produce an indirect measure of a desired output characteristic. The ability of the method to provide information over a range of signal (plus noise) to noise values is useful for those processes where the output response is continually changing. The usefulness of the POD method has been demonstrated in measurement of and optimizing process variables, in optimizing the outputs of automated process acceptance and in measuring and assessing human factor variables within a process application. POD assessments have demonstrated value in both engineering and productivity measurements in quantifying performance capabilities and providing quantitative data for use in life cycle system management.

Challenges in application of the method are those of providing the necessary understanding of the process (prior art) and its performance under controlled conditions, prior to making an assessment. If process controls are rigorous, reduced data sets may be used to characterize process variations. Several methods of operating with reduced data sets have been presented herein and this area provides the greatest challenge for future work. The POD method is recommended as a basic tool for characterizing and communicating the capabilities of an NDI process for purposes of design and acceptance, for purposes of commerce (contractual performance), and for purposes of maintenance and life cycle maintenance of modern engineering systems. It is also recommended as a basic tool in assessing, characterizing and quantifying the results of process improvements and in trade studies to select the NDI procedure that provides the optimum performance capability, reliability and economic value for implementation on an engineering system. The POD method is being incorporated into design specifications, procedures and standards of commerce in U.S. systems. We recommend that this method be given serious consideration for use in internal commerce.

REFERENCES

1. Brent K.Christner
Donald L.Long
Ward D.Rummel *NDE Detectability of Fatigue-Type Cracks in High-Strength Alloys: NDI Reliability Assessments*, Final Report NASA MCR-88-1044, September 1988.
2. Ward D.Rummel
Paul H.Todd Jr.
Sandor A.Frecska
Richard A.Rathke *The Detection of Fatigue Cracks by Nondestructive Testing Methods*, NASA CR-2369, February 1974.
3. A.P.Berens
P.W.Hovey *Flaw Detection Reliability Criteria, Volume I — Methods and Results*, AFWAL-TR-84-4022, April 1984.
4. Joseph Berkson MD "Tables for the Maximum Likelihood Estimate of the Logistic Function", *Biometrics*, V. 13, 1957.
5. Mark K.Davis
Pedro Aguilar *Proficiency Evaluation of USAF SA-ALC Structural Assessment Testing (SAT) Facility Personnel for the Ultrasonic Method*, SA-ALC/MAQCN, June 1987.

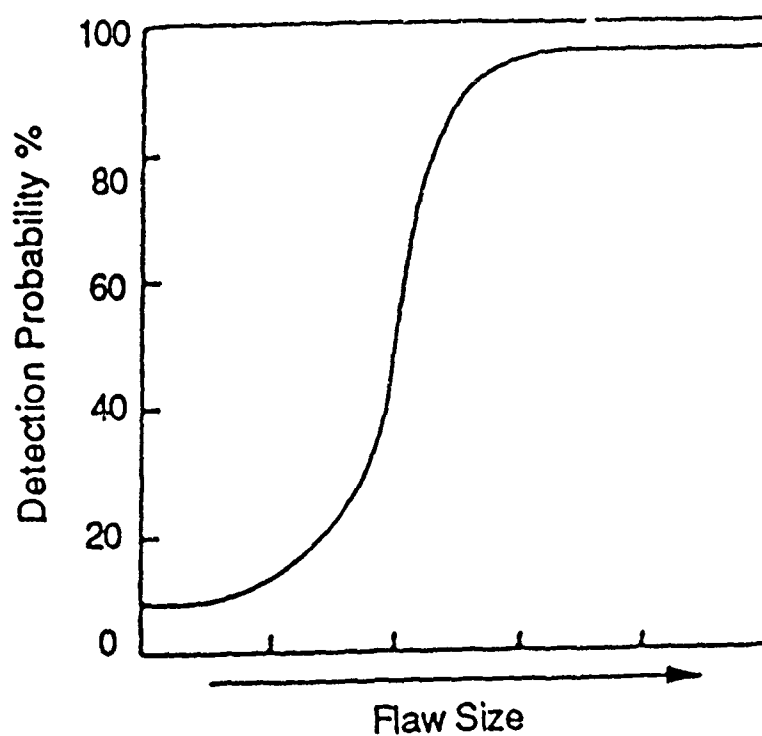


Fig.1 Typical probability of detection (POD) curve

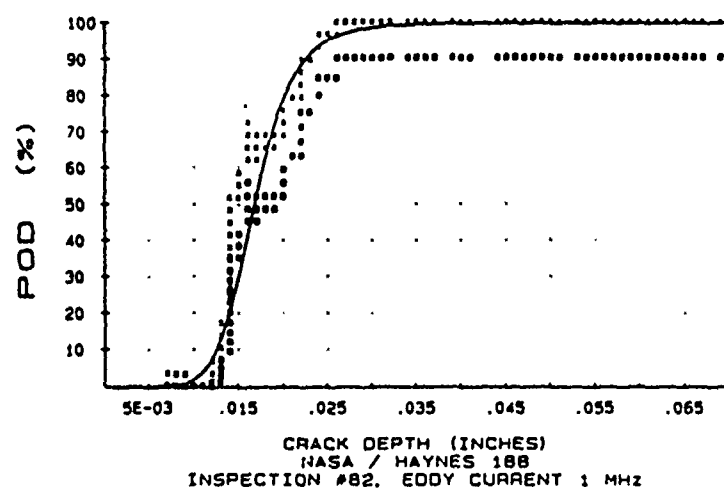


Fig.2 Typical example of a POD curve plotted by the moving average method

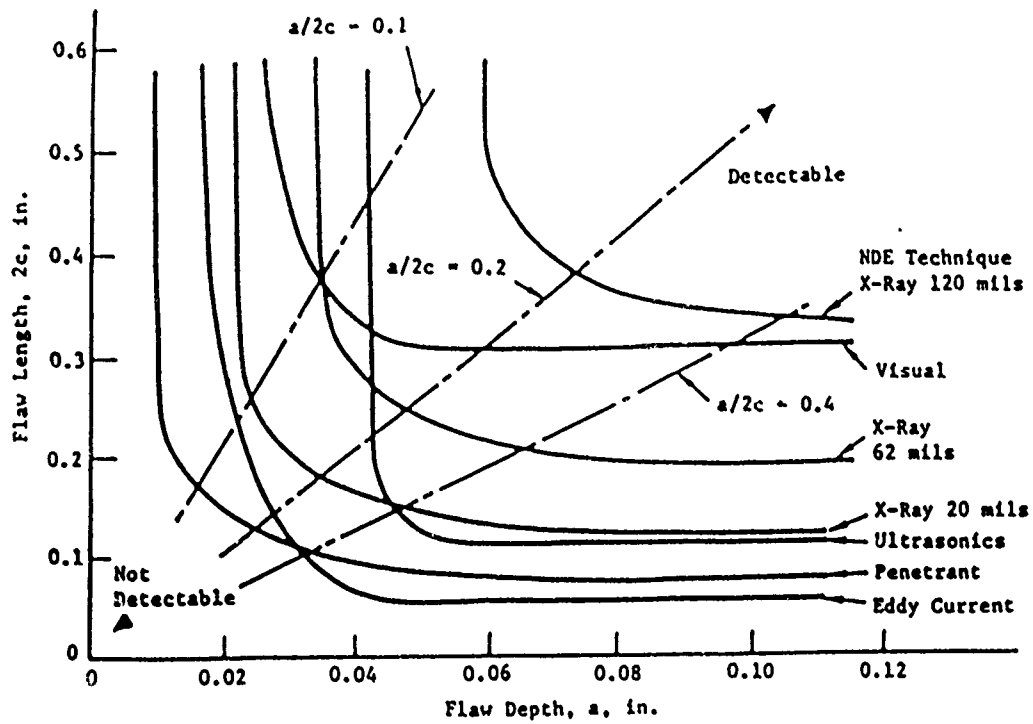


Fig.3a Estimated NDI capabilities for crack detection

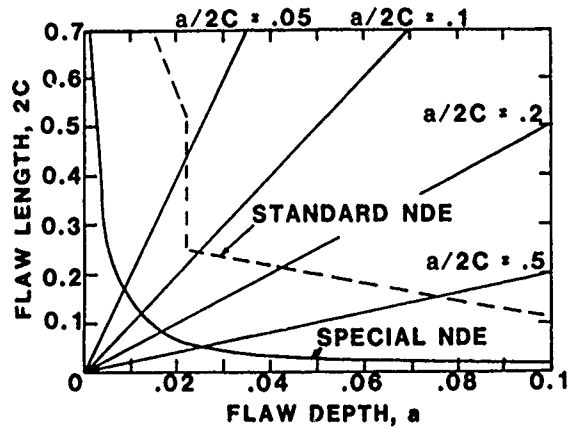


Fig.3b Design/acceptance criteria for general NDE/NDI capabilities

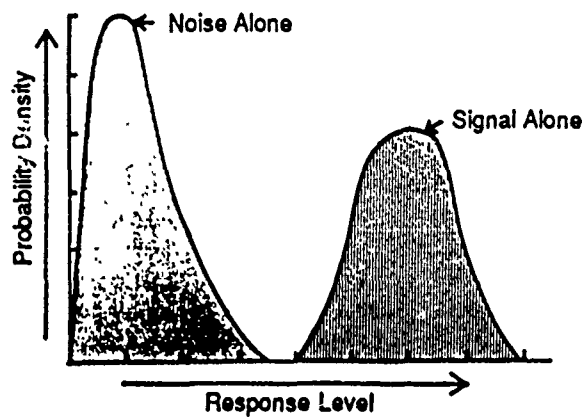


Fig.4 Signal/noise probability density distributions (large flow case)

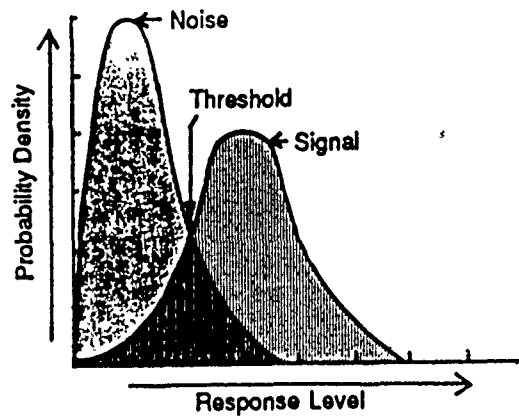


Fig.5 Signal/noise probability density distributions (medium flow case)

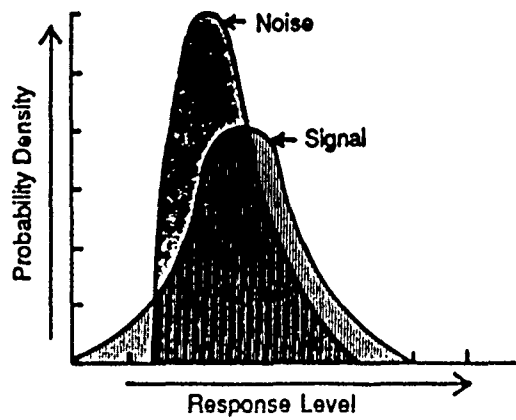


Fig.6 Signal/noise probability density distributions (small flow case)

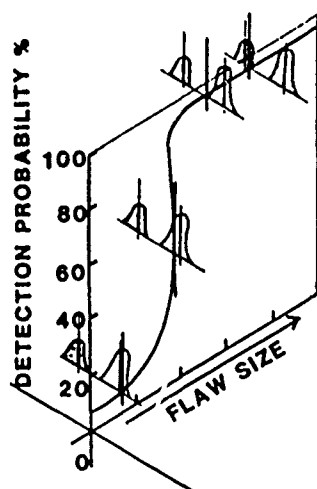


Fig.7 Interaction of acceptance criteria with the probability of detection (POD)

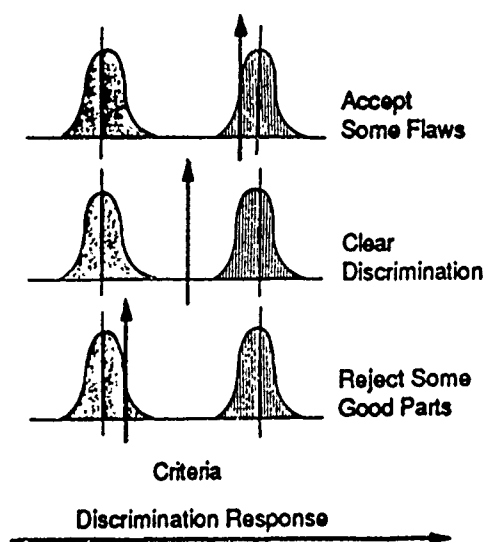


Fig.8 Influence of acceptance criterion (vertical arrow) on process discrimination

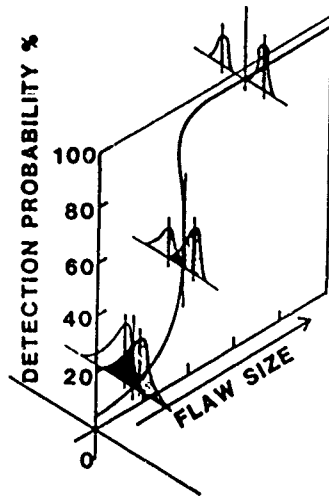
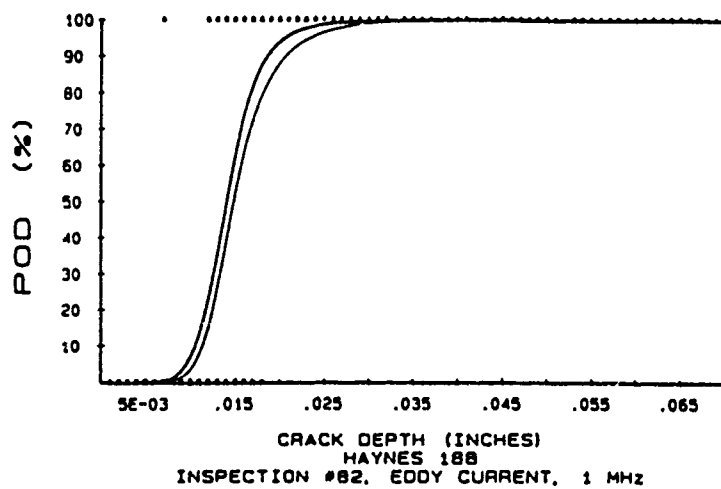


Fig.9 Interaction of signal/noise discrimination with the probability of detection (POD)



*Inspection #82
Haynes 188
102 Specimens
284 Cracks
62.7% Detected
7 False Calls*

Fig.10 POD curve produced by the maximum likelihood method

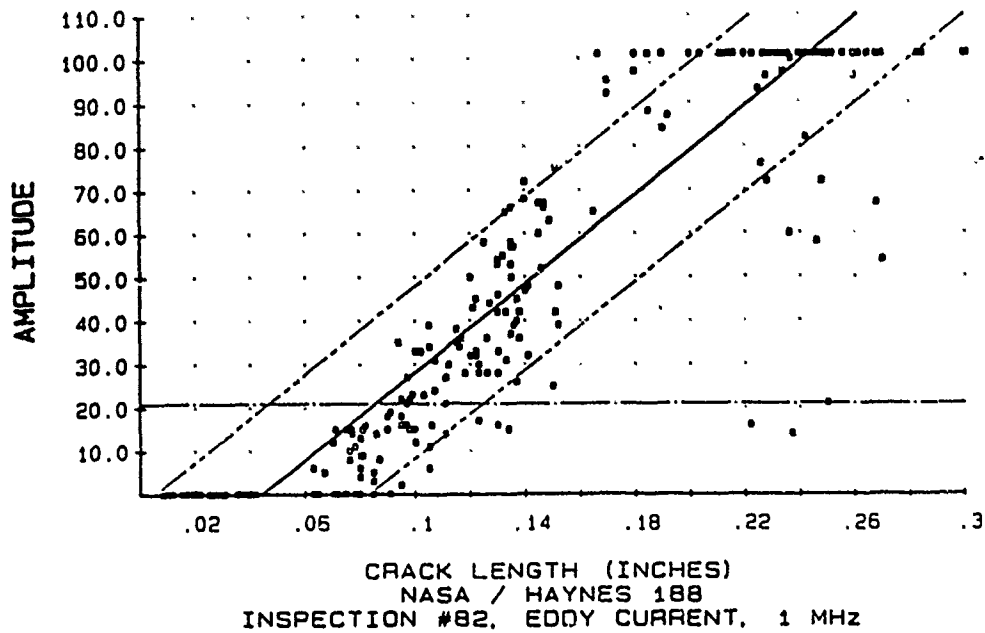
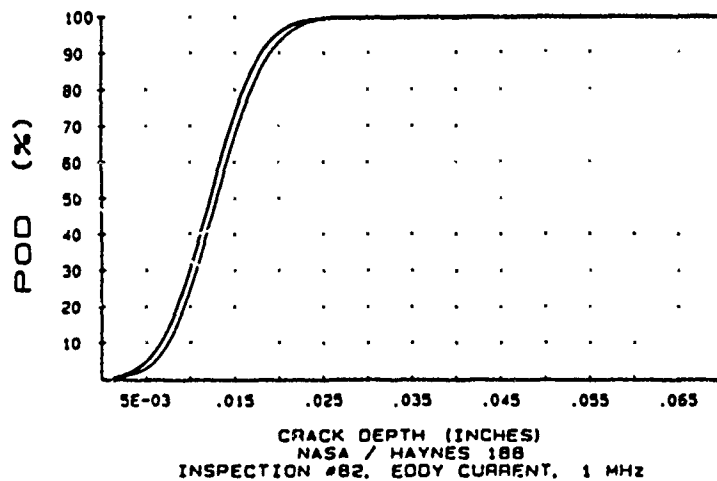


Fig.11 Plot of signal amplitude as a function of crack length for automated eddy current inspection using a 0.125 inch diameter absolute probe



\hat{a} versus a Analysis.

Fig.12 POD curves plotted by crack depth for an automated eddy current inspection using a 0.0125 inch diameter absolute probe

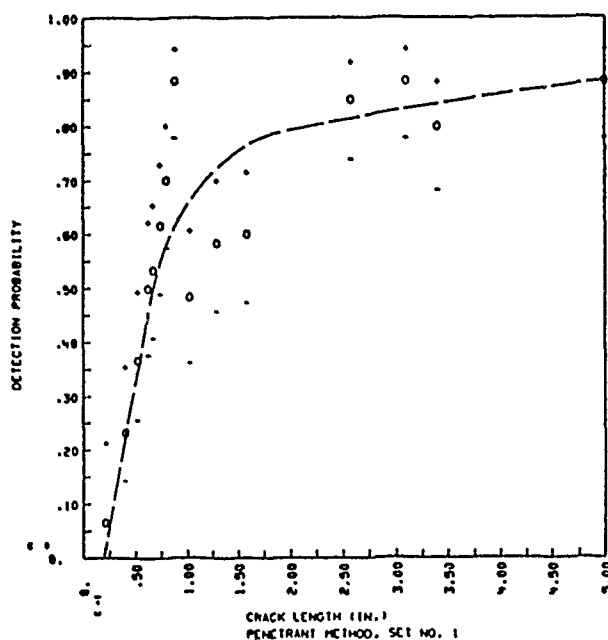


Fig.13 Crack detection probability of the penetrant inspection method plotted by actual crack length at 95% confidence level (all length values $\times 10$) as machined

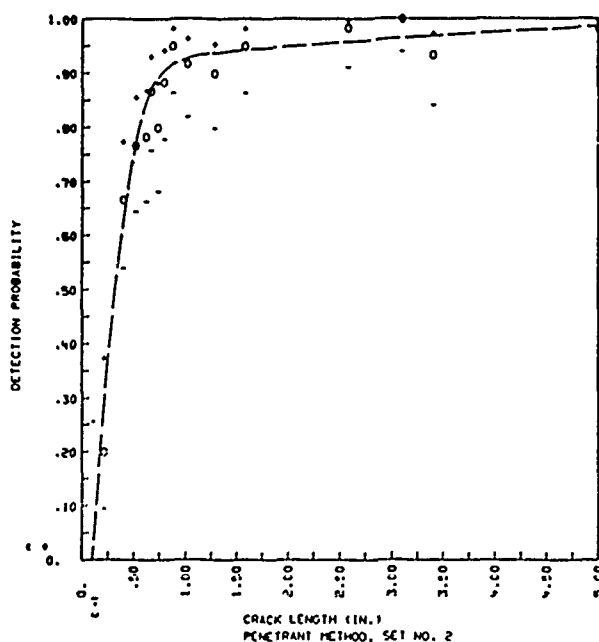


Fig.14 Crack detection probability of the penetrant inspection method plotted by actual crack length at 95% confidence level (all length values $\times 10$) after etch

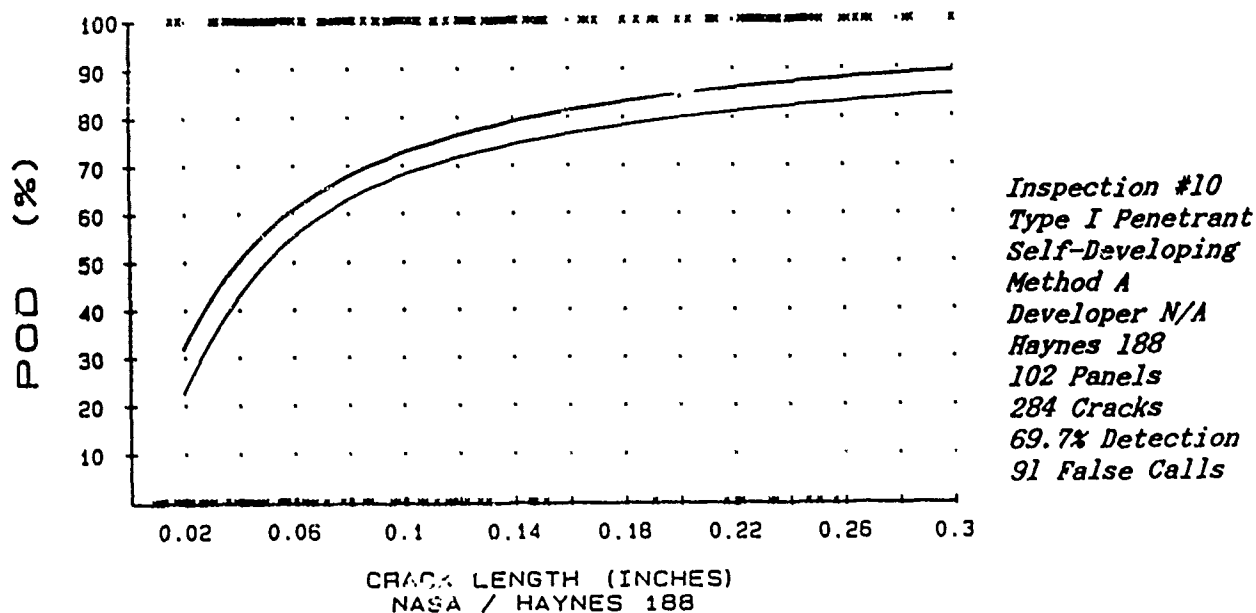


Fig.15 Probability of detection for a self-developing penetrant with no developer

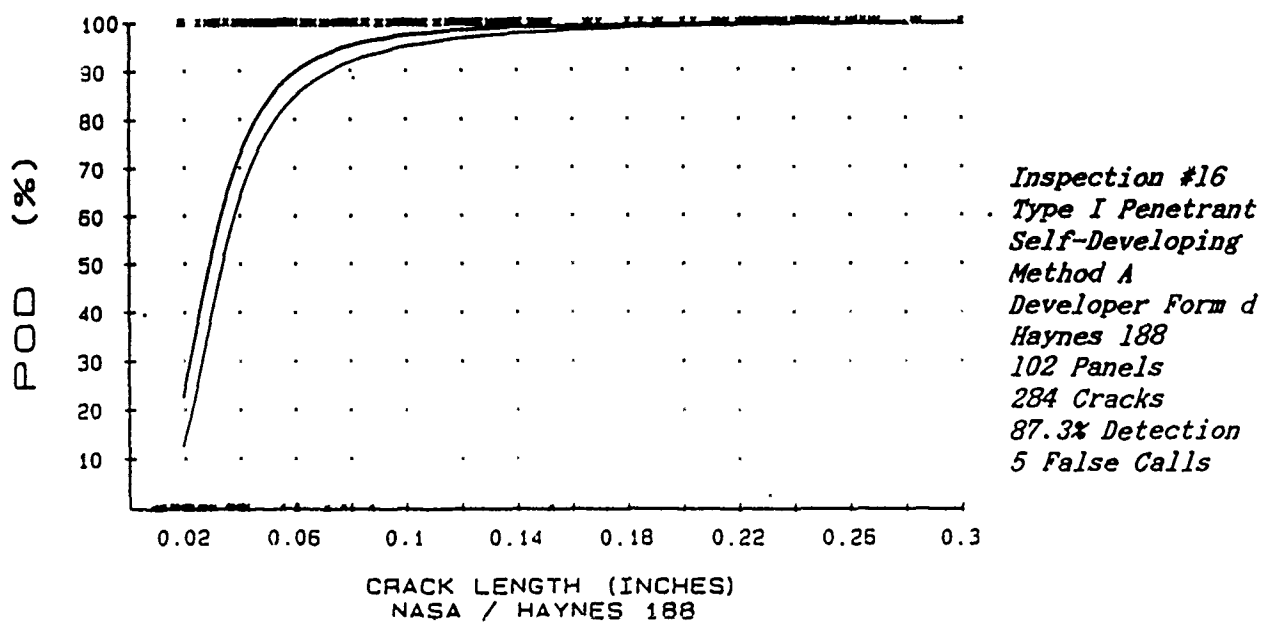


Fig.16 Probability of detection for a self-developing penetrant with developer

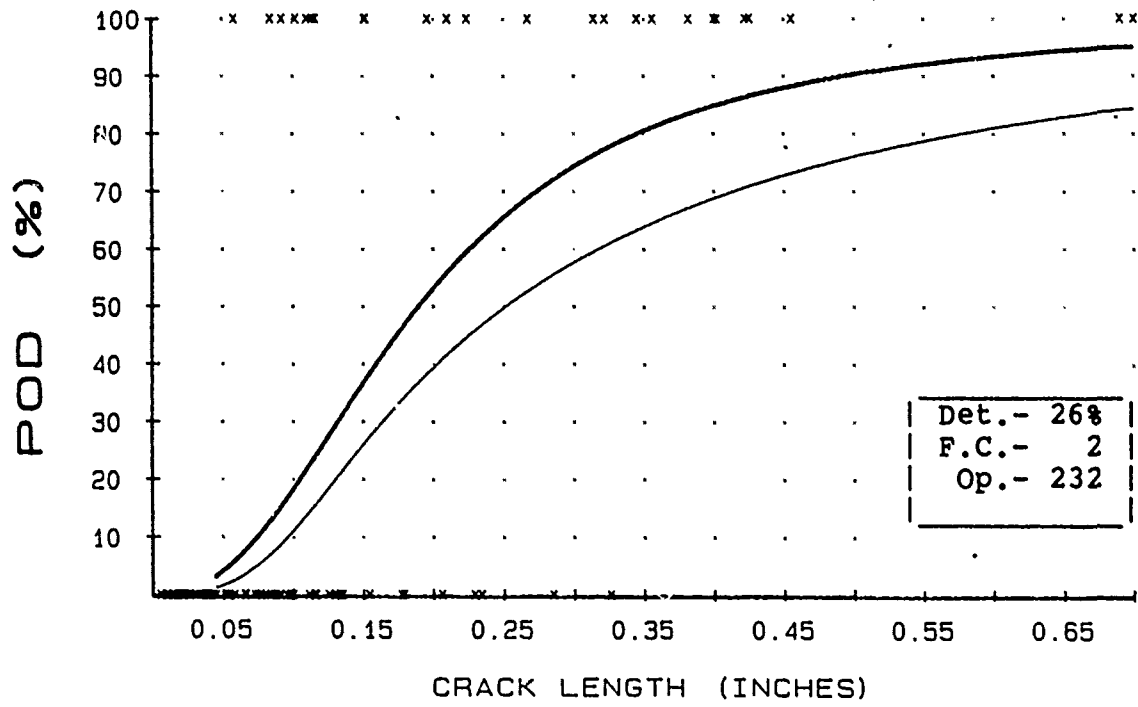


Fig.17 POD curve for penetrant inspection of titanium anti-rotation slot specimens (test set #3) with a one (1) minute dry developer exposure (FOG) time

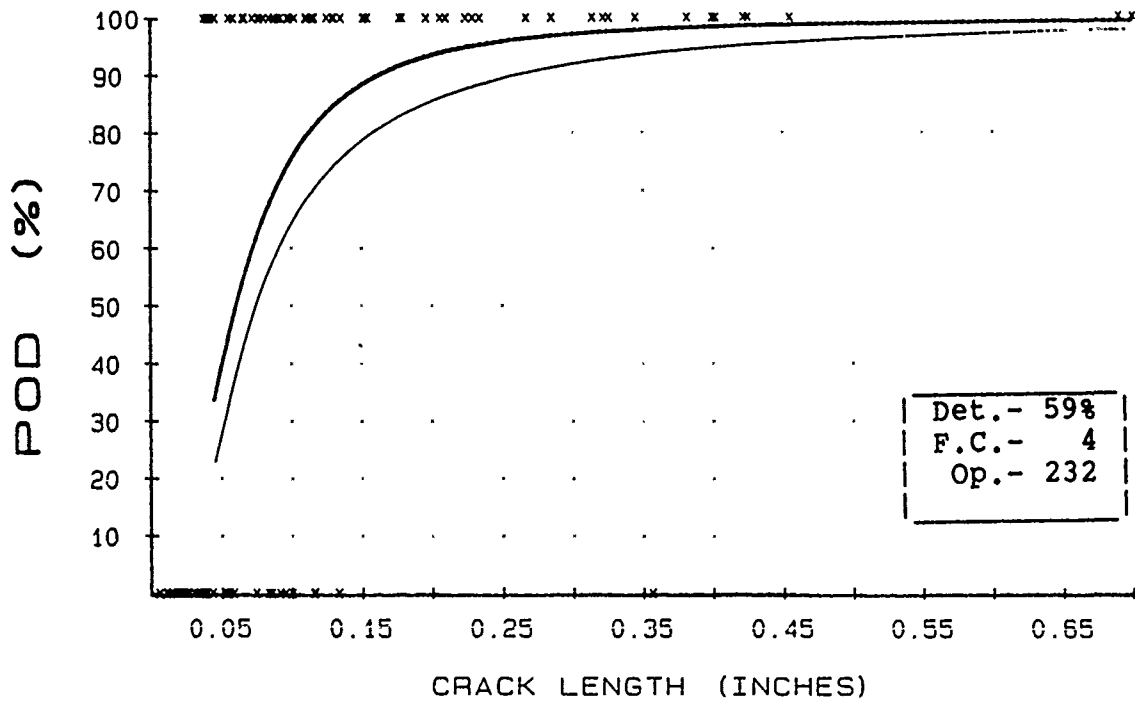


Fig.18 POD curve for penetrant inspection of titanium anti-rotation slot specimens (test set #3) with a three (3) minute dry developer exposure (FOG) time

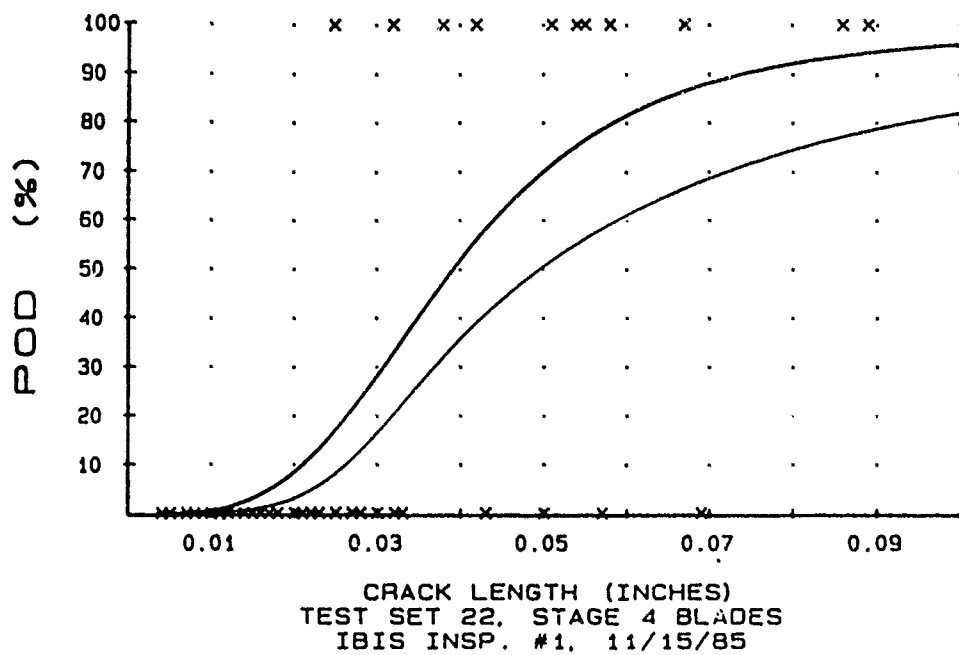


Fig.19 POD curve using the maximum likelihood method of analysis for a penetrant inspection process

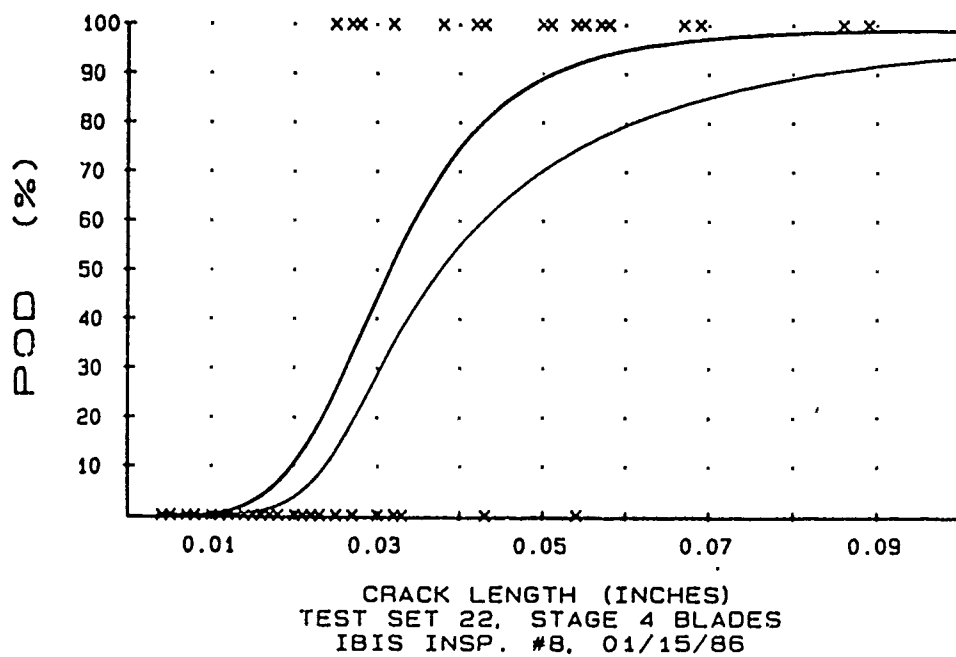


Fig.20 POD curve using the maximum likelihood method of analysis after optimization of the penetrant process shown in Figure 19

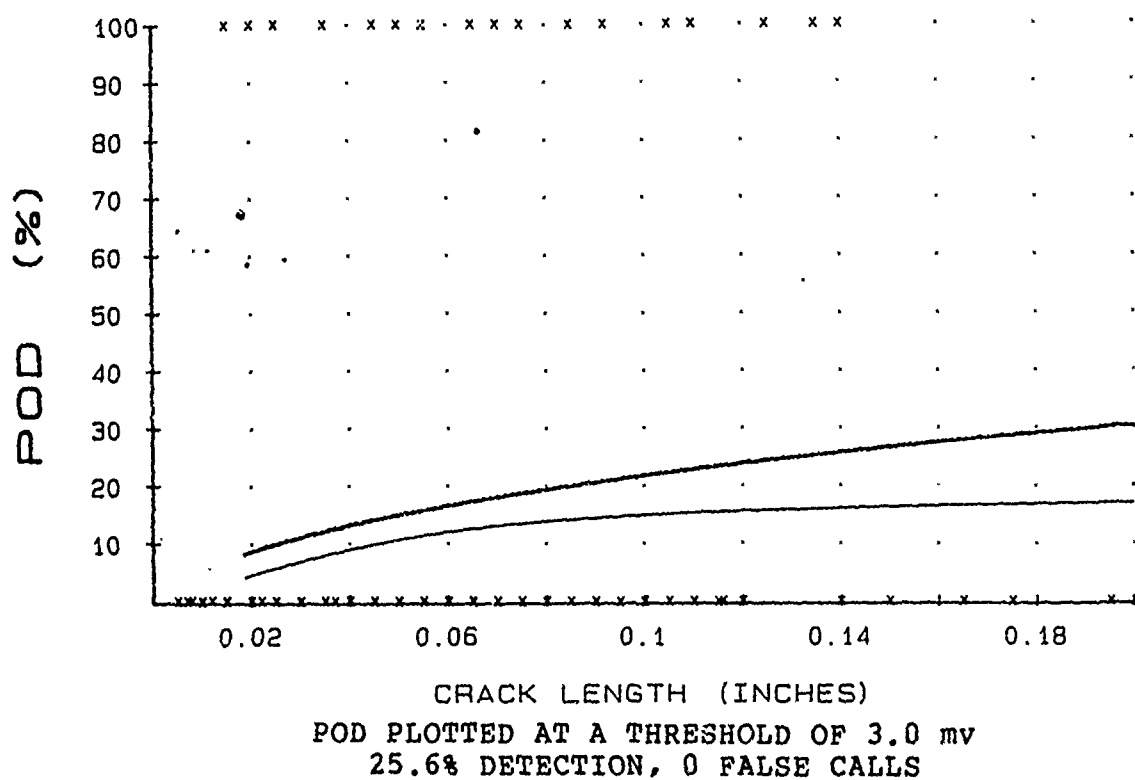


Fig.21 Eddy current inspection data plotted at the production designated acceptance criteria level

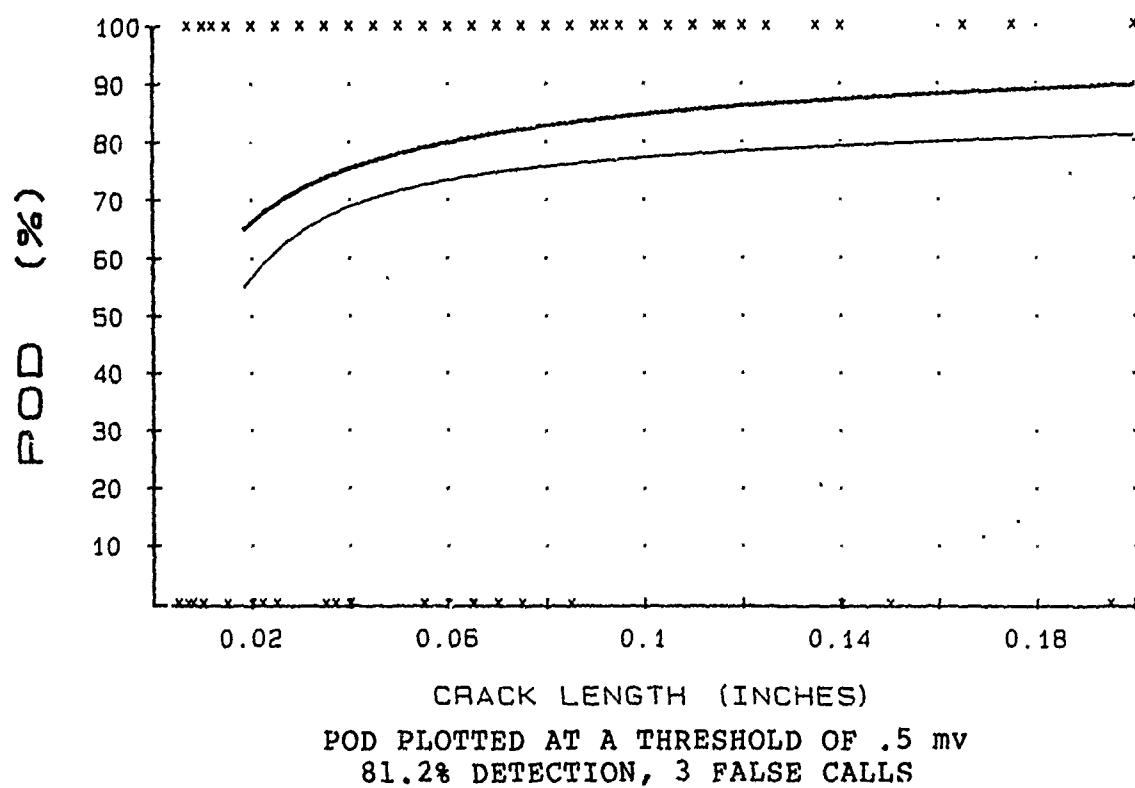


Fig.22 The same eddy current inspection data from Figure 21 plotted at the optimized acceptance criteria level

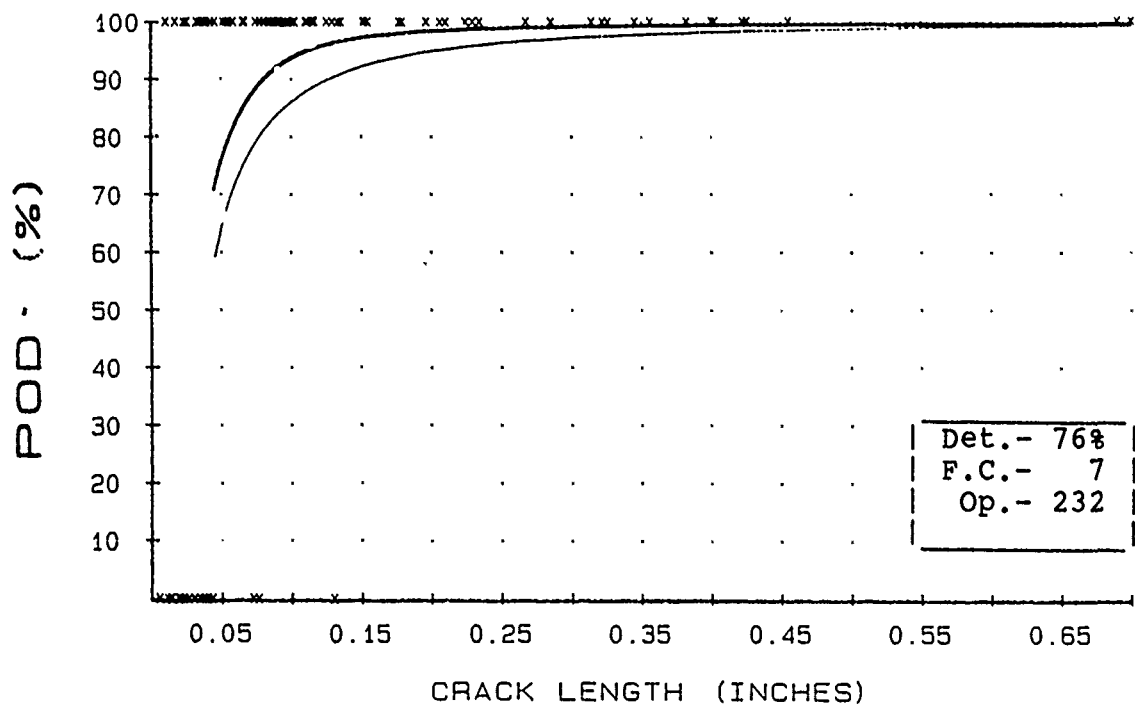


Fig.23 POD curve for a group IV penetrant inspection sequence that was performed by an inspector who had spent seventy-five percent of his time on the penetrant line

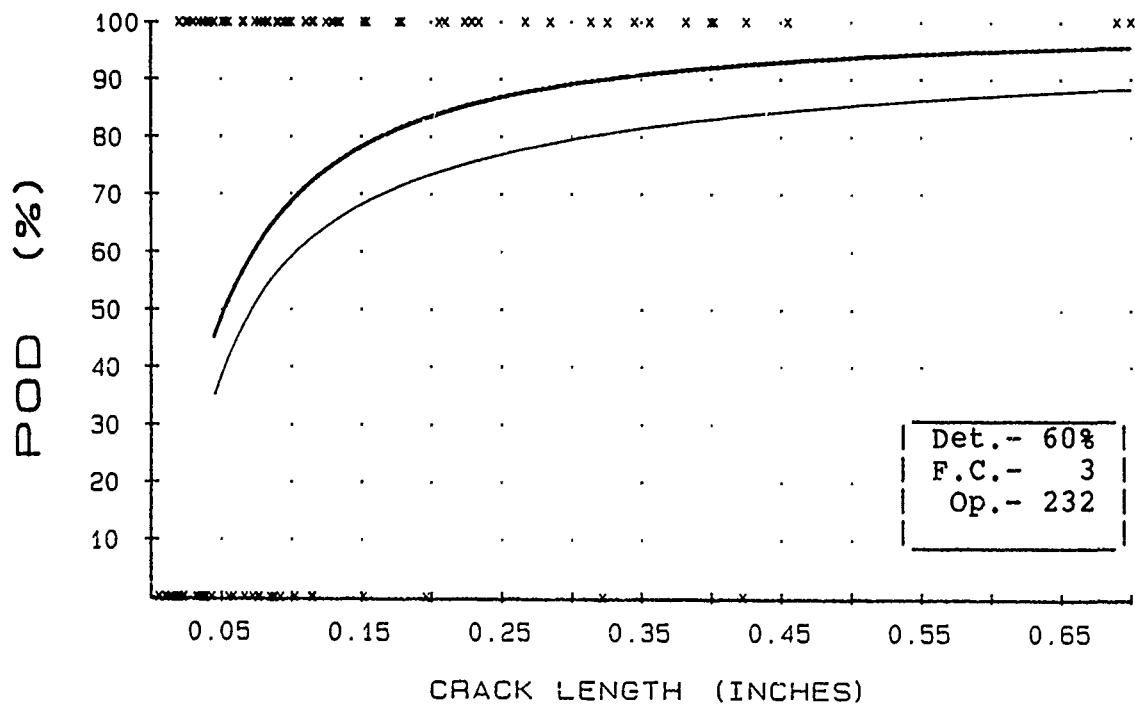


Fig.24 POD curve for a group IV penetrant inspection sequence that was performed by an inspector who had been assigned to the penetrant line for twenty days during the year

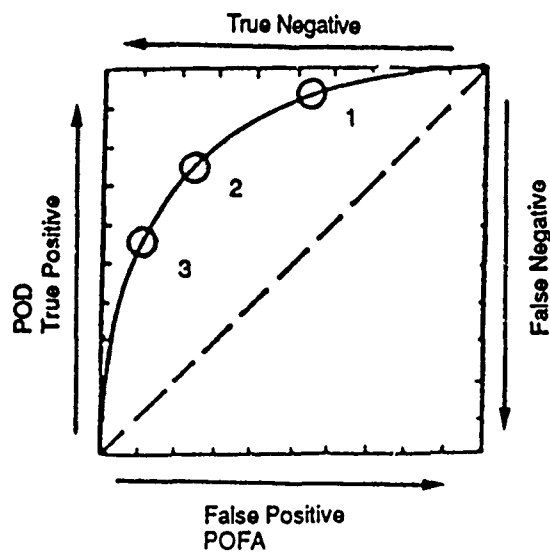


Fig.25 Relative operating characteristic (ROC) curve showing performance at three different acceptance levels

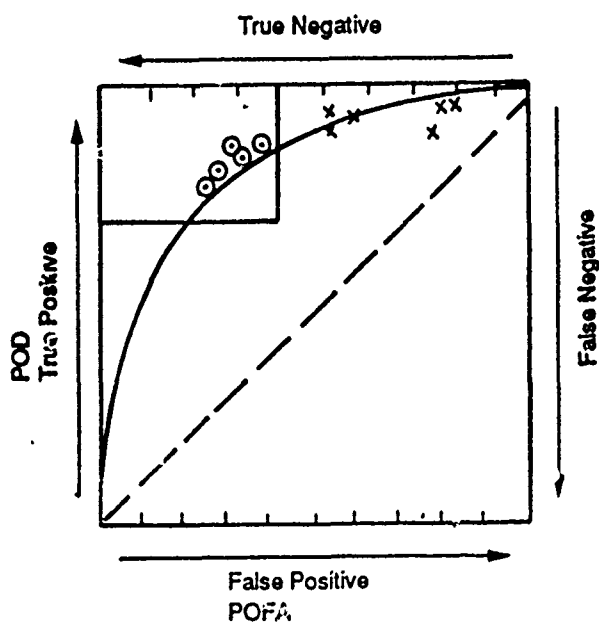


Fig.26 Modified ROC analysis showing relative operator proficiency for two different operators

INSPECTION RELIABILITY

by

David A. Bruce
 Materials and Structures Department
 Royal Aerospace Establishment
 Farnborough, Hampshire, GU14 6TD
 United Kingdom

1 INTRODUCTION

Requirements for NDE of aircraft in service have been determined largely by the prevailing design philosophy. Traditionally aircraft have been designed and operated on a safe life basis, in which the expected life of an airframe component is established by a fatigue test using a predetermined safety factor. Any unknowns, whether in the material properties, the operating load spectra or the allowed flight envelope are allowed for by compensating increases in the safety factor, in an attempt to maintain the desired safety level. In the safe life philosophy, NDE is required only when it has been discovered that the airframe is liable to fail within its safe life, when the operating envelope is modified to include situations which were not adequately represented by the major fatigue test, or when it is desired to extend the operating life of the airframe beyond the established safe life for economic reasons.

As the safe life philosophy accepts that most airframes or components will be scrapped long before their useful life is used up, it is inherently inefficient as a means of life management. An alternative approach, frequently referred to as damage tolerance, was adopted some years ago by the USAF, in which NDE played a central role. In this approach, safety is assured by repeated inspections, on the assumption that NDE can reliably detect potentially serious defects before they reach a critical size. A further development of this approach, now labelled Unified Life Cycle Engineering, has been proposed as the ultimate technique for efficient life management (1).

Whether the requirement for NDE has arisen from the desire to efficiently design and fly damage tolerant aircraft, or from a desire to extend the safe life of traditionally designed aircraft, NDE has in either case become an intrinsic factor in determining the safety level. If it is desired to maintain a pre-determined safety level by inspecting critical components, the safety level attained, and its corresponding inspection interval, can only be estimated if the reliability of the NDE technique can be described quantitatively.

In this paper, the current methods for estimating the reliability of NDE procedures are briefly reviewed. As an example, their application to the results of a recent UK-led "baseline" study of the reliability of rotating probe eddy current inspection, will be described. After introducing definitions of the terminology in section 2, the proposed parametric and non-parametric statistical methodologies will be described in section 3. Section 4 shows the result of applying these methodologies to the actual results of the baseline programme, while the concluding sections examine the implications of the findings in terms of their impact on airworthiness calculations, and the improvements which may be necessary if more reliance is to be placed on estimates of NDE reliability.

2 DEFINITIONS

The usual way of describing NDE reliability is by presenting a "reliability curve", or possibly a single figure for the "probability of detection" of a defect. The implication is that when the inspection task is carried out, the outcome can be described as a random process governed by a well-defined probability (or strictly a true probability), which is usually assumed to depend only on defect size. The figure which is usually quoted is not, however, the best estimate of the true probability of finding a defect, but rather a statistical lower bound on this value at a given level of confidence.

In order to avoid any confusion over definitions, in the following sections two probabilities will be referred to consistently, these will be the mean probability and the probability of detection at the 95% confidence level.

The mean probability will be denoted p , it is the actual fraction of successes obtained in an experiment and is therefore the best unbiased estimate of the true probability. Although p is a property of the test data for the inspection process, since it is an unbiased estimate of the true probability its expectation value is a population parameter.

The probability of detection at the 95% confidence level will, in keeping with notation elsewhere in the literature, be denoted as the POD. Since this quantity is a lower bound on the true probability, it depends systematically not only on the inspection procedure which determines the true probability, but also on the number of trials in the experiment which was used to determine p and POD.

To illustrate the difference between these two probabilities, figure 1 shows the systematic increase in expected POD which may be obtained by increasing the number of trials for a simple experiment with $p = 0.9$.

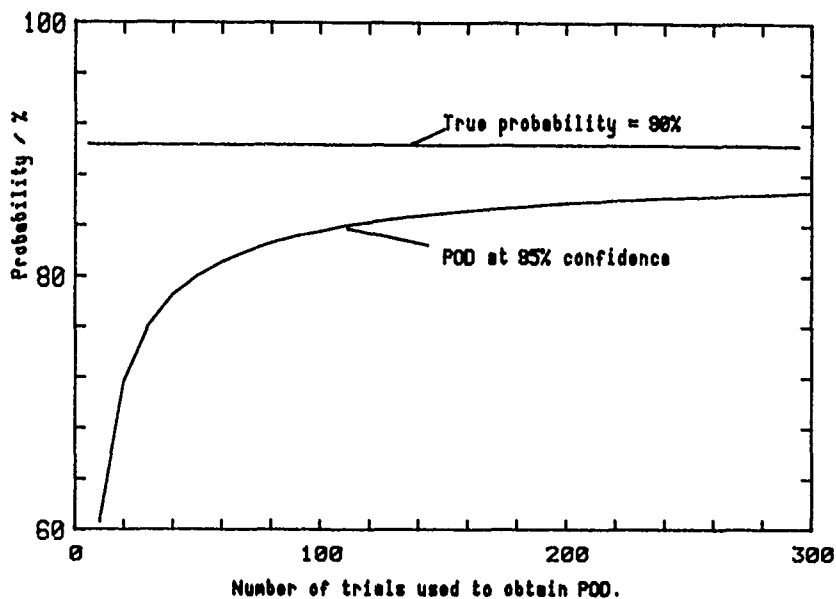


Figure 1

Variation of demonstrated reliability with number of trials

3 METHODOLOGIES

When only a single defect type is to be considered, determination of p and POD results in each case in a single number. If an experiment is carried out in which h successes (hits) were obtained in n trials, then the mean probability is just $p = h/n$. The POD is calculated by an iterative technique using the binomial distribution for n trials to find the probability which gives just a 5% chance of obtaining h or more successes.

In an NDE context, it is more usual to estimate p and POD values over a range of defect sizes where it is anticipated that the values of p and POD will both be dependent on the defect size. Several approaches have been recommended for estimation of these size-dependent probabilities, or reliability curves (2,3). The two main approaches considered here are a non-parametric approach and a parametric approach.

The non-parametric approach, which has also been called the interval method, was recommended some years ago by the ASNT for aerospace practice (4). In this method the desired range of defect sizes is divided into a number of smaller intervals, and the results from each interval are analysed separately to give a p and POD value characteristic of the defect size. The resulting set of values for all of the intervals defines the p and POD reliability curves. The advantage of this method is that, apart from the underlying assumption that the inspection process is inherently probabilistic with essentially a single probability within each interval, no extra assumptions are necessary in deriving the reliability curves. The disadvantage is that since the intervals need to be chosen to be small enough that the probability is approximately constant within the interval, and since an equal number of specimens need to be used in each interval (to ensure that the POD values lie on the same curve), the number of specimens in each interval may be a severe constraint on the POD curve.

The main alternative to the interval method is the parametric approach. This method uses an empirical functional form for the mean probability reliability curve (5). The function chosen will typically depend on two (or possibly three) parameters. These parameters are then estimated from the data by linearising the functional dependence and performing a least squares fit. The 95% confidence limits on the curve are then calculated from the standard deviations of the parameters (assuming a t -distribution for the errors) and this is interpreted as the POD curve. This method has the advantage that the entire set of trials are included in the determination of the POD at any given size, rather than just the fractions of the trials in the relevant size interval, so that the resulting POD curve is much closer to the mean curve. The disadvantage, however, is that an extra assumption has had to be made to estimate the curves, namely the assumption that the variation of the true probability with crack size is accurately given by the chosen empirical function. Provided the probabilities are sufficiently slowly varying functions of defect size this may not cause problems, but if the reliability curve has fairly sharp features the POD curve resulting from this method may be over optimistic in their vicinity.

4 BASELINE STUDY RESULTS

The UK baseline study, and its analysis using the interval method to determine reliability curves, has already been reported elsewhere (6,7). The study involved inspection of a total of 550 fastener hole specimens by 91 inspectors using a rotating probe eddy-current technique. Of the 550 specimens prepared, 250 contained fatigue cracks ranging in length from 0.2 mm to 5.8 mm. The 91 inspectors included UK military and civilian testers and also, through the auspices of TTCP, testers from the USAF and the CAF.

The numbers of specimens and inspectors involved in the baseline study were chosen to be as large as possible to allow a full statistical analysis. If a trial to establish the reliability of NDE techniques is to become a regular feature in the qualification of inspection procedures, the scale of such trials will almost certainly have to be considerably more modest for reasons of time and cost. For the baseline study, the large numbers of specimens and inspectors allowed considerable flexibility in the analysis.

The rotating probe eddy current technique was chosen for the study because, although by no means a fully automated instrument, the rotating probe instrument was the most automated technique currently in use. It was hoped that this would reduce the effect of variations in individual performance which might be expected in a technique requiring greater manual dexterity.

An implicit assumption in producing a reliability curve as a function of crack size is that the various inspectors have a similar performance so that they can all be represented by the same curve. An initial analysis was therefore carried out by grouping the specimens into intervals of 5 specimens and summing the numbers of hits and misses attained by all of the inspectors. The resulting POD and \bar{p} curves are shown in figure 2. Since this approach gave a very large number of trials in each interval, the POD and \bar{p} curves are very close together.

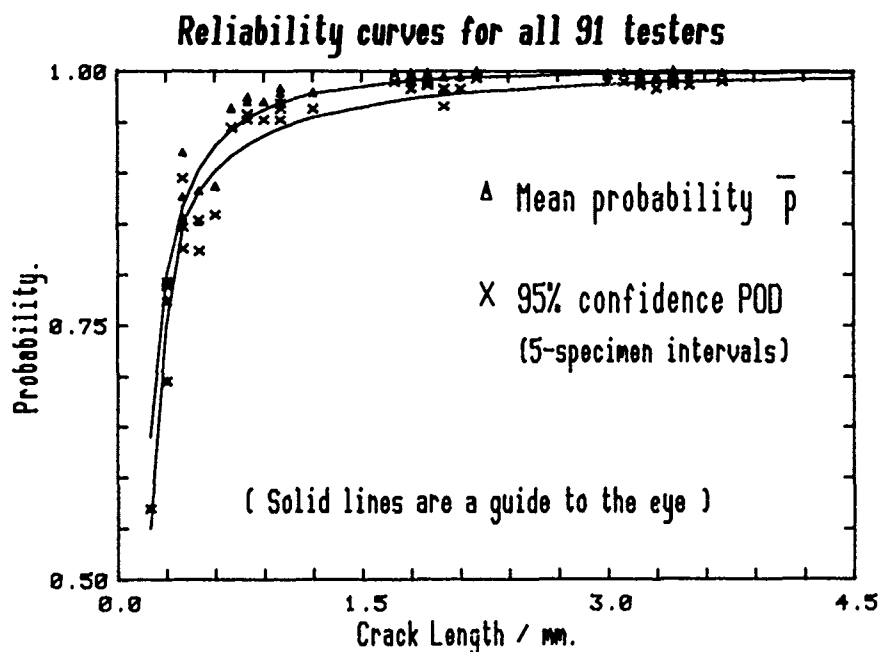


Figure 2

Mean probability and 95% POD curves for all testers

his procedure of summing the results of all of the inspectors to obtain a large aggregate number of trials from which the POD is calculated, is consistent with the underlying assumption that the performance of all of the inspectors is governed by the same true probability. Unfortunately, however, it is apparent from the data that there are several outliers, ie inspectors who have missed more (or in some cases fewer) defects than would be expected. The distribution of the number of misses made by individual testers was therefore checked at each crack size. Even for the large cracks of above 2 mm in length, where the POD does not change measurably with crack size, some of the inspectors missed significantly more defects than their colleagues. When the more obvious outliers were eliminated from the sample, the results for the remaining 77 inspectors were analysed, leading to the reliability curves shown in figure 3.

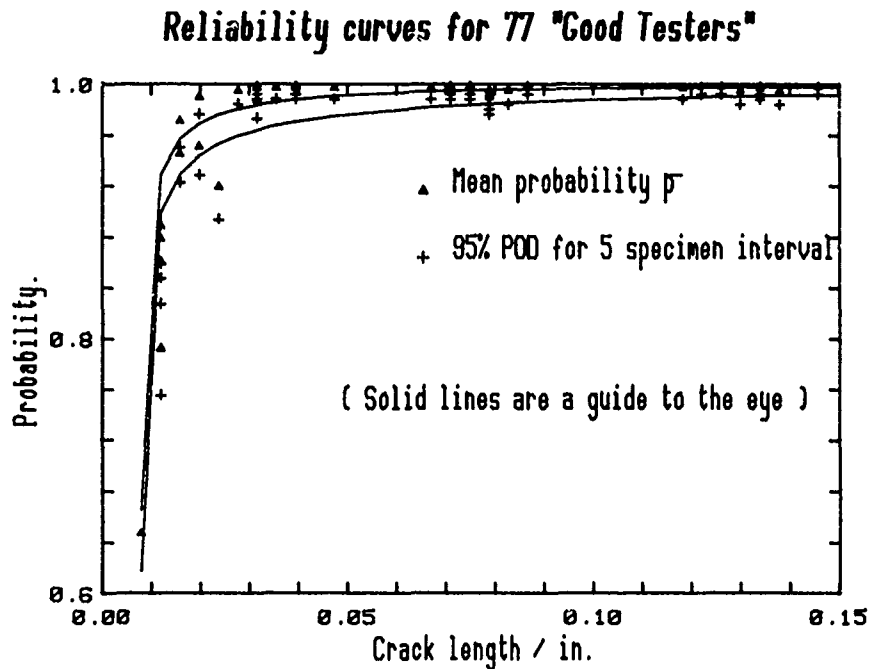


Figure 3

Mean probability and 95% POD curves for testers of approximately uniform ability,
after deleting "outliers"

Where the distribution of misses made by the inspectors corresponded to the expected binomial distribution, it may be assumed that the inspectors were performing with the same probability. The data for inspection of small cracks, those of less than 0.9 mm in length, was clearly not binomially distributed. As an example, the results for the cracks of 0.5 mm in length are shown in figure 4, compared with the binomial distribution which would give the correct mean performance. It is clear from the diagram that there are too many inspectors achieving perfect scores, while most of the misses are made by a fairly small fraction of the population of inspectors. Similar effects were observed at all of the small crack sizes. This shows that for these crack lengths the inspectors were not performing uniformly. Many inspectors were able to correctly locate 100% of the defects while others missed significantly too many to be a part of a homogeneous population. Thus for the entire region where the POD was found to be size-dependent, the POD and p reliability curves are found to be of limited validity as differences between inspectors dominated the results.

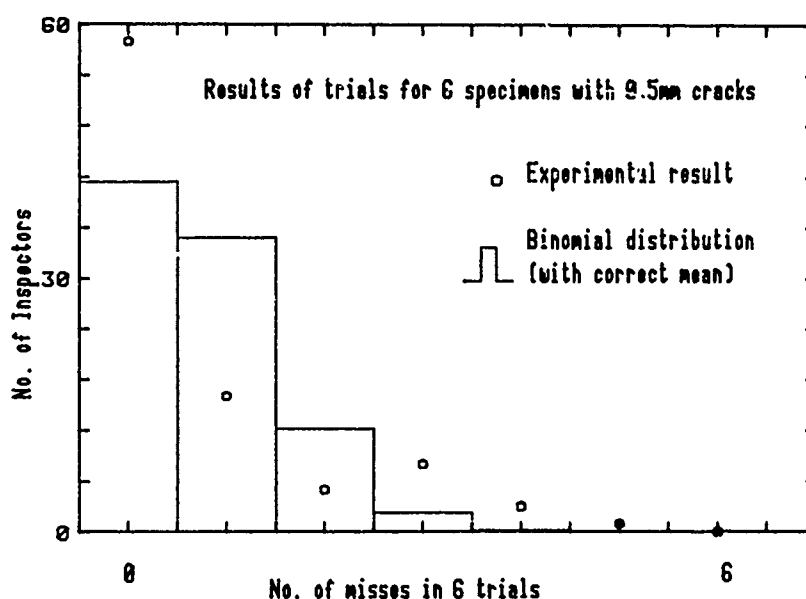


Figure 4

Comparison of the actual and expected distribution of performances for small (0.5 mm) cracks

Since differences between inspectors were shown to be important, the interval method was also applied to the results of individual testers. It was necessary to choose an interval size for the POD calculations which included a sufficiently large number of specimens to allow reasonably high PODs, without making the range of sizes in the interval too large. An interval size of 25 specimens was chosen as this provides 10 points on the curves while allowing a maximum POD of just under 90% (25 hits out of 25 trials gives a POD of 88.7%). The p and POD curves obtained for the best, worst and average testers are shown in figure 5.

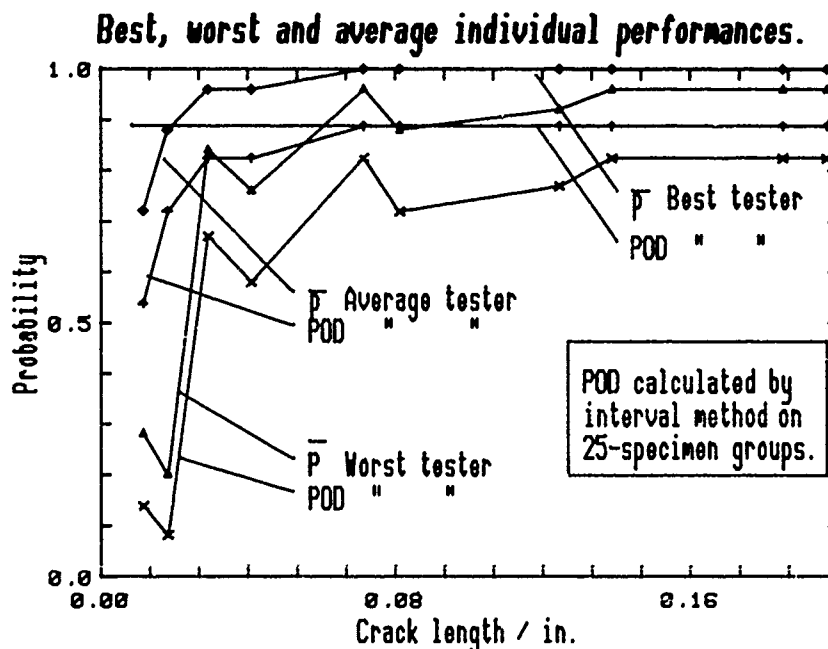


Figure 5

Mean probability and 95% POD curves for individual testers

In the case of the best testers, the reliability curves are simply two straight lines, reflecting the fact that the best testers correctly located all of the defects. These two lines therefore represent the best p and POD that can be obtained by the interval method, when there are 25 specimens in each interval. Increasing the number of specimens in the intervals would increase the limiting POD value, for example intervals of 29 specimens would give a maximum POD of 90%. The performance of the best and the average testers is significantly different only for crack lengths of below 0.7 mm (0.028 in). The worst tester, however, can be seen to be significantly worse than the average, even for cracks as long as 2.0 mm (0.06 in).

In the initial analysis, where the results from all of the inspectors were aggregated to give a very large number of trials for the POD determination, the p and POD curves obtained by the interval method are close together. Because of this, the parametric method of determining a lower bound to the probability of detection does not lead to appreciably higher PODs. When the POD curve is calculated for an individual, however, the interval method suffers from the necessarily much smaller number of specimens in each interval. When the number of trials is small, the parametric method of estimating a 95% confidence curve offers a way of reducing the difference between the p and POD curves, effectively increasing the number of trials. The parametric method was therefore used to reanalyse the individual tester data.

To use the parametric method, it is necessary to specify an empirical function to represent the mean probability of detection as a function of crack length. Several different functions have been proposed (2,5) and for the purpose of this investigation a three-parameter Weibull curve was used. The actual functional form of this is

$$p(a) = 1 - \exp \left(-A (a - a_0)^B \right)$$

where a is the crack length, a_0 is a threshold representing the smallest detectable crack, and A and B are adjustable constants which are fitted by least squares minimisation.

The results for the worst tester are shown in figure 6. The triangles show the actual data points in the 25-specimen intervals. The crosses show the interval-method POD for each interval. The solid line shows the 95% confidence limits on the fitted curve, which in the parametric approach is identified as the POD. It can be seen that the parametric method gives a higher POD than the interval method for the longer cracks. For the shorter cracks, those below about 2 mm (0.08 in), the two methods give similar curves.

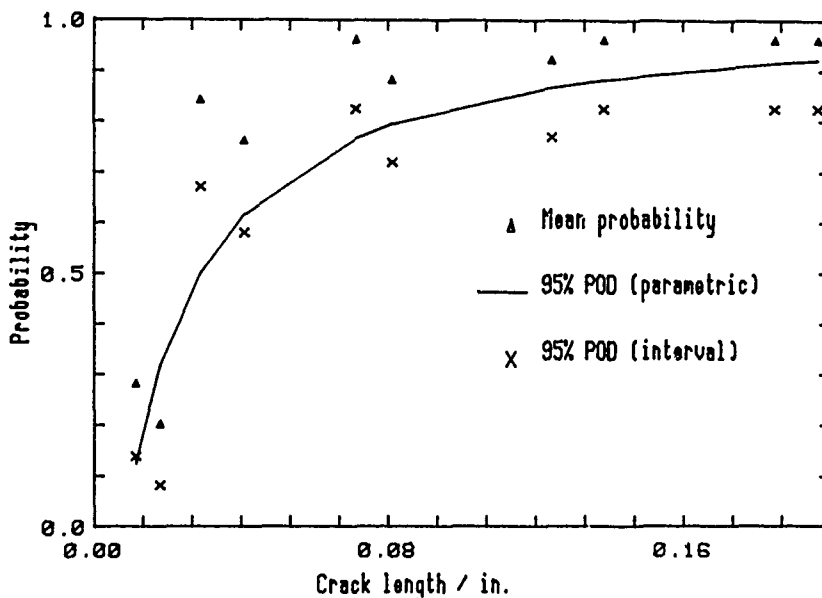


Figure 6

Mean probability, 95% POD calculated by the internal method, and 95% POD calculated by the parametric method for the worst tester

Results for the "average tester" are shown in figure 7. The "average tester" was represented by the average number of misses in each interval, rounded to the nearest integral value. Because of the averaging, the curves are much smoother. The parametric method leads to a POD which is substantially higher than that obtained from the interval method over almost the entire range of lengths. The fitted empirical curve does not seem to reproduce the sharp shoulder of the actual curve very well, and in fact obviously overestimates the probability of detection around .2 mm (.08 in).

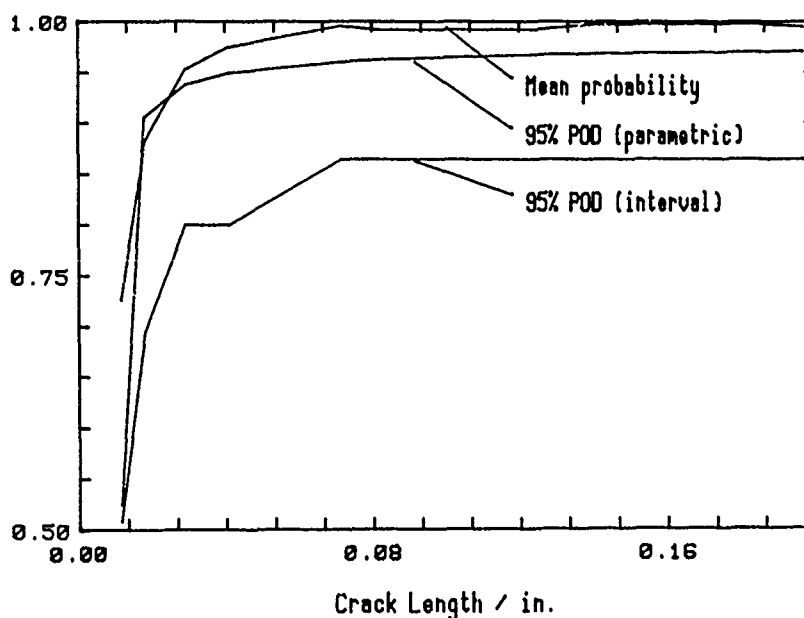


Figure 7

Mean probability, 95% POD (interval method) and 95% POD (parametric method)
for the average tester

5 IMPLICATIONS FOR AIRWORTHINESS

The use of NDE to ensure safety levels requires that NDE reliability is included in the airworthiness calculations. In the simplest treatment it is merely assumed that any defect larger than a threshold size will be detected. All that has to be done in this approach is to estimate the detection threshold. This oversimplification of the problem has two major failings. Even as good a technique as the rotating probe eddy current inspection considered above is not perfectly reliable even for the largest defects, so it is unreasonable to expect 100% detection above a threshold size. The other problem is that it is difficult to measure the threshold size accurately, whether this is done by measuring the mean probability or a 95% confidence POD, unless the threshold size is measured for a fairly low probability of detection (5). The difficulty is primarily caused by the shape of the reliability curve. If this is relatively flat for large defects, the crack length at which the reliability curve attains a specified value is very sensitive to slight changes in the experimental data. It is only in the range of crack sizes below the "shoulder", where the probability is changing rapidly with crack length, that a threshold size can be measured accurately. Clearly this limits the level of probability which may be required at the threshold.

In order to incorporate quantitative measurements of NDE reliability, a Monte Carlo method known as Probabilistic Fracture Mechanics (PFM) has been used (8). In this method, the reliability and crack growth curves are specified, the crack growth between inspections is represented by a random process and the chance of missing a crack in repeated inspections is calculated. These calculations can be used to determine safe inspection intervals or safety levels.

Reliability curves from the base-line study have been used for a set of preliminary inspection interval calculations using the PFM method. The main aim of these calculations was to study the effect of reducing the sample size on the POD curve and, through this, on the safe inspection interval. It was clear from these calculations that reasonable inspection intervals were predicted when using the mean p reliability curve or the aggregate POD curves shown in figures 2 and 3. In contrast, when the POD curves obtained from the performances of individual testers (fig 5) were used, the low POD prevented the desired safety level (1 in 1000) from being attained with a reasonable inspection interval. It was also found that the inspection intervals calculated were quite sensitive to the shape of the reliability curve around the "shoulder" below 1 mm. This is presumably due to the fraction of cracks which grow rapidly from this size to critical size within one inspection period.

The sensitivity of the PFM calculations to the details of the curve implies that the choice of empirical function will influence the results. This reduces the apparent advantage of the parametric method, since the 95% confidence limits on the curve take only the scatter of values around the Weibull curve into account, it is not possible to estimate the effects of systematic differences between the best fitting curve and the true probability.

6 COPING WITH INDIVIDUAL VARIABILITY

The base-line study was exceptional in that a large enough data set was gathered to allow a statistical test of the validity of applying binomial theory. The conclusion that in the small crack region the inspection could not be described adequately by a single probability but depended on the individual tester was not new, similar results having been noted in the "Have Cracks Will Travel" programme (2). The main problem which this variation causes in the application of NDE reliability measurements, is that the probabilities measured by aggregating the results of all inspectors will apply only if a random choice of inspector is made before each inspection. Otherwise either the reliability of each individual must be established, or the theory should be modified to take into account the expected range of probabilities.

In smaller reliability trials, it is unlikely that enough data would be gathered to enable the binomial theory to be tested. Either it must be assumed that all testers will perform with the same probability of detection, or else it might be assumed that the testers would have a given distribution of abilities, reflected in a distribution of probabilities. One approach which appears to eliminate this problem is to use the Bayesian method. In this the aggregate data from the trial is used to estimate the distribution of individual probabilities. This avoids the assumption that all testers have the same reliability without requiring any additional data. In the case of a large number of trials the Bayesian and binomial methods give very similar results. The differences become apparent for smaller numbers of trials when the Bayesian approach gives a considerably longer "tail" to the distribution. This may be seen in figure 8 where the distribution of misses made by the 91 inspectors on the 6 specimens with 0.5 mm cracks is shown, together with a Bayesian (beta-binomial) distribution calculated for the appropriate mean number of misses (9). The agreement with the experimental results is significantly better than that for the binomial distribution of figure 4.

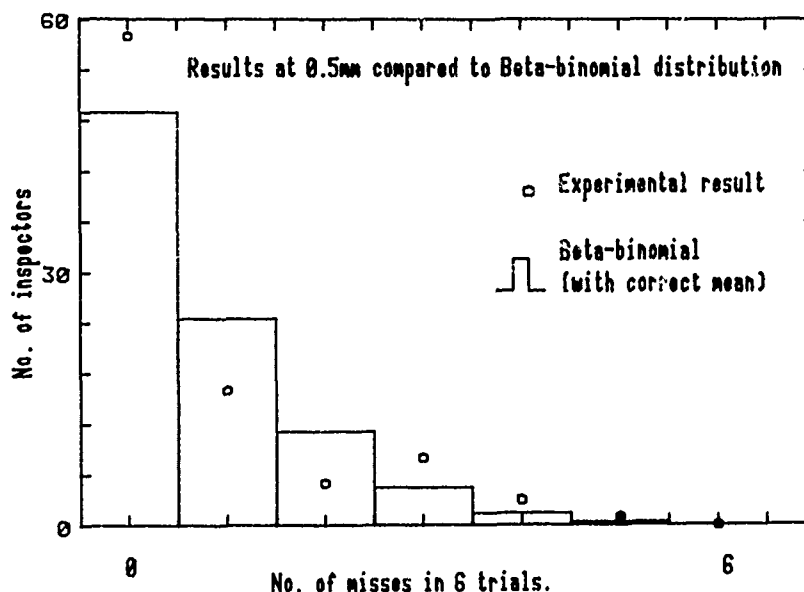


Figure 8

Comparison of the actual distribution of performances with Beta-binomial distribution which arises in the Bayesian approach

An alternative method of incorporating a range of abilities is to assume a particular distribution for the abilities of the inspector population and then to choose values of the mean and variance of this population to fit the experimental data. This approach, which for an appropriate choice of the distribution of abilities leads to the Negative Binomial (or Compound Poisson) distribution for the numbers of misses, has been used in the study of industrial accidents (10). Again in the limit of a small population variance this reproduces the binomial distribution of misses, while if the variance is large, this produces "tails" on the expected results. The negative binomial with the correct mean and variance is compared to the 0.5 mm crack data in figure 9 where it can be seen that it gives better agreement than either the binomial or beta binomial distributions. It was in fact noticeable that the negative binomial with appropriate mean and variance gave a satisfactory fit to all of the data collected in the base-line study at all crack sizes.

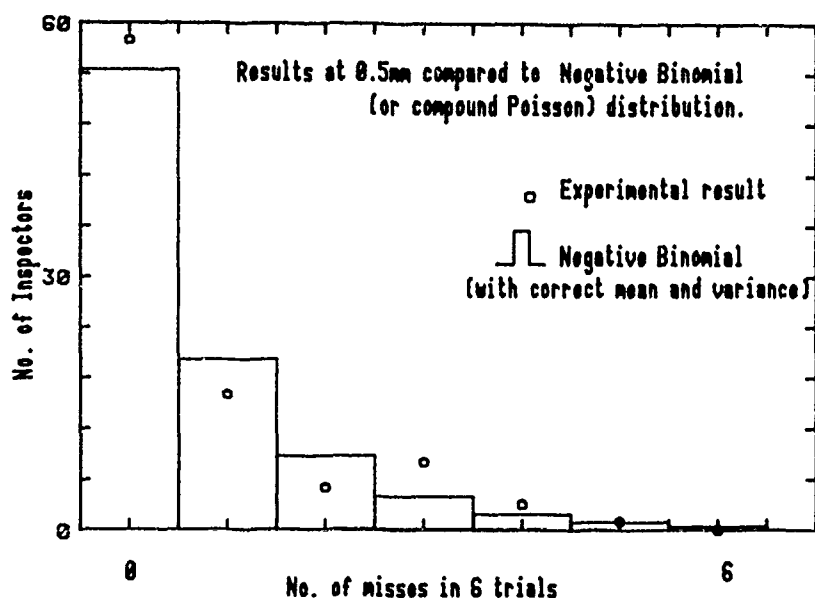


Figure 9

Comparison of the actual distribution of performances with the Compound Poisson distribution with correct mean and variance

Rather than admit the possibility of individual variation which necessitates an extension of the binomial theory, it might be advantageous to ensure that performance is as homogeneous as possible, even at the expense of the ultimate sensitivity. One of the improvements to NDE which is often claimed to lead to higher reliability is an increase in automation. This may have the effect of increasing the mean probability of detection, p . Even if automation is unable to improve the mean probability, it offers two potential advantages from the point of view of measuring reliability. By reducing the possibility of human error and the degree of human judgement present in manual inspections, it may be possible to reduce the variability in inspections to the point where the simple probabilistic model is sufficient. It is, however, important to note that the differences between "individual testers" noted in the base-line study implicitly includes the effects of differences in the calibration and possibly in the performance of their equipment which would not necessarily be removed by automation. A second major advantage of automation may be that it will be possible to generate more data for POD measurements. For example, since an automated test will not be biased by the outcome of a previous test on the same specimen, it may be possible to make repeated measurements on a small specimen set rather than having to manufacture a very large (and costly) specimen set. This increase in the number of trials will reduce the difference between p and POD by increasing the latter even though p may not be increased.

7 CONCLUSIONS

Quantitative measurements of NDE reliability are necessary to enable NDE to be properly incorporated into life management and airworthiness philosophies. Although a framework for this exists through a combination of reliability curve estimation and PFM simulation, the current methodologies rely on the assumption that the inspections can be described by a single reliability curve. This is difficult to substantiate in general and was demonstrably not attained in the base-line study.

In the base-line study, the probability of detection curve was dominated by variations in individual performance throughout the range of crack sizes for which p and POD changed with crack size.

POD curves obtained by these methods do not give a complete description of the expected outcome of a subsequent series of inspections. In view of the necessity of obtaining the best estimate of the expected performance of an inspection technique from the smallest possible set of trials, a better method of parametrising the data would be valuable.

If the reliability of inspections continues to be described by POD curves obtained by the conventional methods, but restricted to smaller sets of inspectors and specimens, then the small sample effects will often prevent the necessary level of safety from being demonstrated, even for the most reliable techniques.

An increase in the level of automation which simplifies the role of the inspector may lead to improvements in repeatability which may prove to be more important than an improvement in average reliability. Although the improvement in repeatability would have to be demonstrated, it may be that highly automated systems would not suffer from the non-binomial variability of results demonstrated above.

8 ACKNOWLEDGEMENTS

The author would like to acknowledge the valuable contributions made to this work by G. Jackson, A. Curtis, D.E.W. Stone and A. Major as well as to the inspection teams from the RAF, RN, USAF and CAF who participated in the base-line reliability programme.

REFERENCES

- 1 Burte H.N. and Chimenti D.E. in Rev Prog QNDE Vol 6B ed. Thompson and Chimenti (Plenum, New York) p1797 (1987)
- 2 Lockheed-Georgia Company, "Reliability of Non-destructive Inspections" - Final Report £ SA-ALC/MME 76-6-38-1, (1978)
- 3 Packman et al. ASM Metals Handbook, 11, p414 (1978)
- 4 Rummel W. Materials Evaluation 40 922 (1982)
- 5 Berens A.P. and Hovey P.W. "Evaluation of NDE Reliability Characterization" Final Report AFWAL-TR-81-4160 (1981)
- 6 Bruce D.A. and Stone D.E.W. in "Reliability in Non-Destructive Testing" ed Brook and Hanstead (Pergamon, Oxford) p45 (1988)
- 7 Bruce D.A. RAE Technical Report to be published (1990)
- 8 Koul F. et al in proceedings of the 66th AGARD specialists meeting on "Damage Tolerance for Engine Structures - NDE" (1988)
- 9 Aitchison and Dunsmore "Statistical Prediction Analysis"
- 10 Greenwood and Yule J. Roy Stat Soc. 83 255 (1920)

CRITICAL INSPECTION OF HIGH PERFORMANCE TURBINE ENGINE COMPONENTS - THE RFC CONCEPT

Bruce A. Rasmussen, WRDC/MTP and Eric L. Pohlenz, WRDC/MTPM
Wright-Patterson Air Force Base, Ohio 45433 USA; and
James D. Hoeffel and Dena G. Williams, SRL/NDE

Systems Research Laboratories, Inc. 2800 Indian Ripple Rd. Dayton, Ohio 45440

SUMMARY

The U.S. Air Force has implemented a new maintenance philosophy, known as Retirement for Cause (RFC), to extend the usefulness of gas turbine engine disks and spacers beyond their original design life. Essential to the successful implementation of this philosophy was the development of a generic, totally-automated engine part inspection system that could reliably detect 5 mil flaws and determine a part's accept/reject status using critical flaw size criteria. Initial implementation of the RFC Inspection System on the Pratt & Whitney F100 engine has significantly reduced the U.S. Air Force engine spare parts inventory requirement and has resulted in a large savings in reprocurement costs.

BACKGROUND

In the early 1970's, jet engines were developed to achieve the higher thrust designs typical of the jet engines used in the U.S. Air Force today. To achieve this level of performance, engine component designs, by necessity, became increasingly complex, required the use of more sophisticated and expensive materials, and had to operate at considerably higher temperatures. As a result, the components became significantly more expensive and their design lives were often less than the design life of the overall engine.

The usefulness of components such as hubs, seals, and disks was based on predicted low cycle fatigue (LCF) crack growth behavior. This predicted LCF life anticipated or modeled multiple engine duty cycles (from idle to full power) to establish the component stresses. This statistical model had inherent risks and made assumptions on the predicted life resulting in a significant degree of uncertainty.

To overcome this uncertainty prior to implementing the "retirement for cause" philosophy, the Air Force used a very conservative approach of retiring components after they reached a given number of operating cycles. In other words, parts were "retired for time"; when 1-part-in-1000 could potentially develop a critical fatigue crack, all 1000 parts were retired to eliminate the possibility of catastrophic failure in flight. The tremendous costs associated with spare parts reprocurement under this maintenance philosophy however, generated a motivation to pursue the development of a safe, more economical means of determining the actual remaining life of high-performance jet engine components.

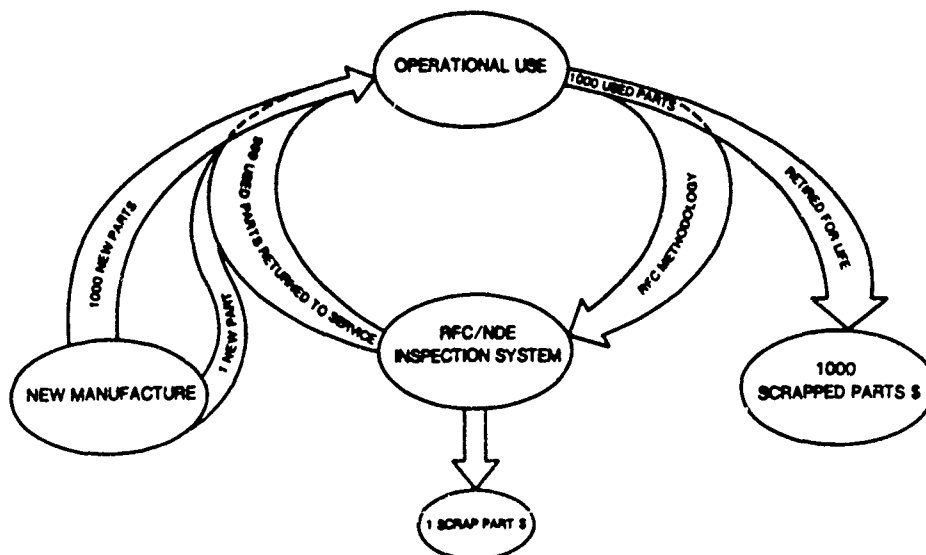


Figure 1. RFC System Concept

The Air Force Wright Aeronautical Laboratories (AFWAL) recognized the potential for significant cost savings in the engine spares business and by the early 1970's, the AFWAL Materials and Propulsion Laboratories conducted a joint in-house research program to evaluate the remaining life of TF33 turbine components beyond their predicted LCF life. Their results showed that 80% of the TF33 components had remaining life equal to five LCF lives and proved that indeed good usable components were being unnecessarily discarded.

Following the TF33 work, the Materials Laboratory initiated a joint program with the Defense Advanced Research Projects Agency (DARPA) to evaluate the technical and economic feasibility of extending the useful life of other U.S. Air Force engine components. The study identified two technology advancements that were essential to a positive "return on investment".

1. Advanced analytical techniques were needed for predicting crack growth behavior in component materials; and
2. Advanced NDE equipment was required that had the inspection sensitivity and reliability to ensure detection of extremely small flaws.

The first category, the development of advanced technology, was addressed in a Materials Laboratory program that established analytical methodology for predicting crack growth in various alloys. The knowledge gained from this program was later used in modeling and predicting component life. The second category, development of the necessary NDE system, became the task of the Manufacturing Technology Division (MANTECH).

In October 1981, MANTECH undertook the task of developing a generic, totally-automated inspection system that could reliably detect 5-mil fatigue cracks in jet engine rotary parts, and the Pratt & Whitney F100 engine was chosen for initial implementation. Emphasis was placed on achieving basic inspection capabilities with automated eddy current and ultrasonic inspection techniques, and improving current flaw detection and characterization techniques by using computer algorithms and eliminating the human decision making process.

Based on past experience with other automated NDE systems, it was clear that this project would require a major Air Force investment as well as universal involvement and acceptance across the engine community. To accomplish the latter goal, MANTECH carefully selected a team of technical experts to design a generic inspection system that could be used to inspect jet engine components from all major U.S. Air Force engine suppliers. This team, as illustrated in Figure 2, consisted of a neutral third-party prime contractor, four major engine manufacturers, systems houses, and science institutes, as well as mechanical and instrumentation manufacturers. In essence, MANTECH brought together the foremost experts in the United States to cover all important facets of nondestructive inspection technology establishment and application.

MANTECH organized the program participants into three specialized Working Groups (Advanced NDE, Systems, and Implementation), a Performance Evaluation Committee, and an Executive Advisory Committee. Each of the program participants were active in the Working Groups and Committees most relevant to their area of expertise.

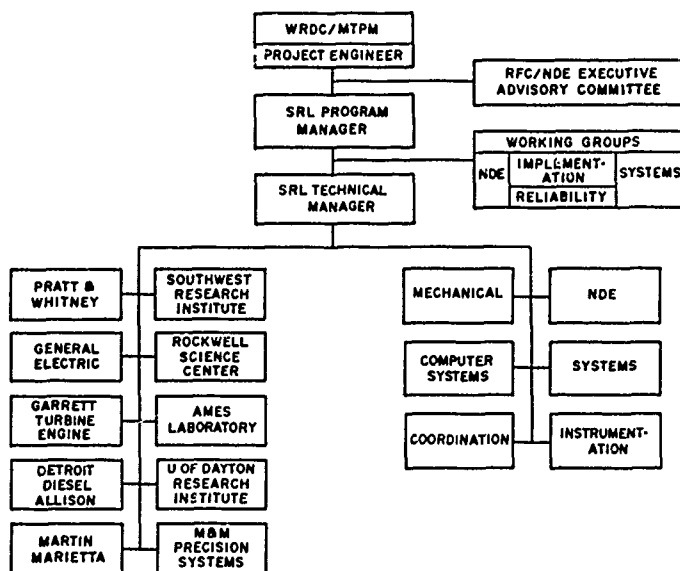


Figure 2. RFC/NDE Program Organization Chart

The Working Groups were primarily responsible for assuring the generic nature of the system design, and applying state-of-the-art technology developed in the laboratory to production practice where possible. The Performance Evaluation Committee, consisting of representatives from each of the major engine manufacturers, developed a comprehensive NDE reliability test plan that included representative specimens from each manufacturer's engine (i.e., Pratt & Whitney, General Electric, Garrett). Air Force representatives from SA/ALC, OC/ALC, ASD, AFWAL, and AFLC were present in all of the working groups and committees and provided information critical to the system's successful transition from laboratory to factory (i.e., facility design, human factors, system operational reliability/maintainability/supportability, data archiving and storage capability, system diagnostics, and security). In addition, representatives from the Navy (NASC) and NASA (NASA Lewis Research Center) were also involved in the working groups and participated in the program technical reviews.

SYSTEM DEVELOPMENT

The RFC Program was broken into three major phases: Prototype design and development, prototype-to-production system upgrade, and production system implementation. The first phase, prototype design and development, began in the fall of 1981 and continued through the spring of 1985. During this phase, the Working Groups and SRL spent considerable time and effort in reviewing existing and current state-of-the-art inspection technology, planning for future technology incorporation, and designing a modular system that could accommodate the future technology as it evolved from the laboratory environments. The modular design concept was carried forward to all aspects of the RFC System - hardware, software, NDE, data acquisition, tooling, etc. Once the top-down modular design was established, the bottom-up system development was initiated. Basic system development was completed and the prototype system was demonstrated at SRL on April 29, 1985. At that time, the feasibility of totally automated part inspection was demonstrated as the stations inspected numerous F100 parts, detected EDM notches, and determined accept/reject status using critical flaw size criteria; the RFC philosophy was determined to be a truly obtainable goal.

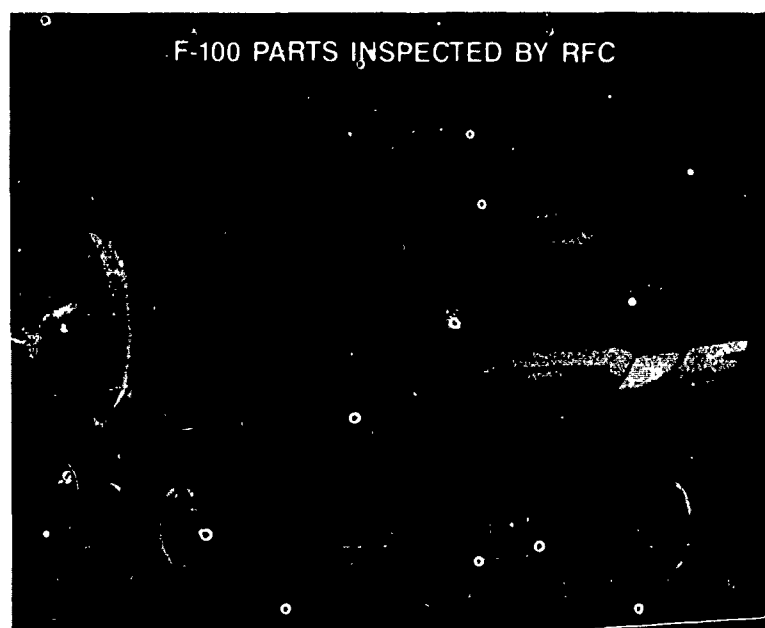


Figure 3. F-100 Parts Inspected by the RFC/NDE System

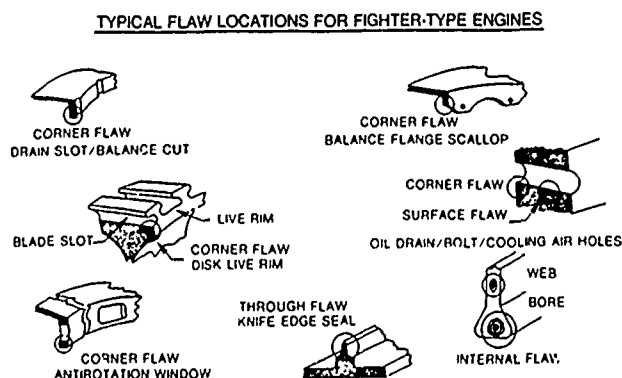


Figure 4. Typical Geometry Inspection Requirements

After the successful prototype demonstration, key features in the system were optimized to withstand production operation. For example, the scanner and probe designs were made more rugged, inspection status display screens and operator control panels were made more user-friendly, communication interfaces were upgraded to provide faster response times and redundancy, and scan plans were optimized to provide greater detection sensitivity and faster part inspection throughput times. This phase of the program lasted roughly 14 months and culminated with preproduction qualification and acceptance testing at SRL.

In August 1985, representatives from the Air Force, Working Groups, and Performance Evaluation Committee met at SRL to perform the Phase I Qualification and Acceptance Tests and the NDE Reliability Tests on the RFC System. The tests examined system reliability and NDE flaw detection capability/reliability under simulated production conditions. NDE tests included automatic scans of engine disks and enough representative fatigue-cracked specimens to yield a statistically significant prediction of detection reliability. The data indicated a 90/95% confidence level for detecting surface flaws in the 5-mil to 10-mil depth range in boltholes and on flat surfaces. An encouraging aspect of the data was a strong correlation between the apparent-vs.-actual flaw depth data. Of particular interest were the variability test results which showed the system to be virtually unaffected by operator changes, probe changes, part loading, flaw orientation and repeated scans. In addition, system uptime test requirements of 80% were exceeded by 11% as the system was operational 91% of the time. The Air Force then authorized SRL to ship the system to the Kelly Air Force Base Jet Engine Overhaul Facility in San Antonio, Texas.

The System was shipped to Kelly the last week of November 1985, and was operational within three days after delivery. Then Phase II Qualification and Acceptance and Reliability Testing were performed. Data resulting from these tests proved the system met or exceeded performance objectives and criteria in each category of testing. Data indicated a 90/95% confidence level for detecting surface flaws in the 4-mil depth range for rivet holes. Bolthole and flat surface data again showed reliable detection in the desired 5-mil to 10-mil depth range. Based on these results, the RFC System was authorized to begin production inspections on F100 engine components in mid-October 1986, and had paid for itself within the first year of operation. Since that time, the system has been running continuously five days a week, at least two shifts a day with no major difficulties or slow-downs in production operation. As of July 31, 1989, production figures at the SA/ALC are 8174 parts inspected, 6916 accepted, and 241 rejected.



Figure 5. Production Facility at Kelly AFB

SYSTEM DESCRIPTION

The basic RFC Inspection System was designed per structured analysis methodology and consists of three primary modules:

- 1) the Operator Console, which is a passive station used to monitor overall system operational status, track the individual part inspections at each NDE station, and generate inspection data reports;
- 2) the System Computer, which performs part tracking, operator console/inspection station interface and communication, NDE data cross-correlation, archival data base storage, system diagnostics, advanced signal processing, RFC proprietary data analysis, and graphics processing; and

- 3) the NDE Inspection Modules, which consist of eddy current and ultrasonic inspection stations. Each NDE Inspection Module consists of three major submodules:



Figure 6. Eddy Current Inspection Module

- a) the mechanical system, which consists of the multi-axis mechanical manipulator with linear X-Y-Z arms and a two-axis robotic wrist; automatic probe changer (EC only); scanners and gimbals; engine part fixture; computer-controlled rotary table; and laser alignment fixture;
- b) the instrumentation cabinet, which houses the NDE instrument; the inspection module's color monitor; station computer; operator push-button control panel; and mechanical manipulator controller; and
- c) the data acquisition module, which consists of all probes, tools, transducers, and squirter; engine part adapters; reference standards and scan plans. (It is this module which is "kitted" to comply with the specific requirements for each unique engine; the other modules and submodules presented above are generic for all engine applications.)

SYSTEM CONFIGURATIONS

The modularity of the RFC Inspection System design has made it a very versatile system which has the inherent capability of cost-efficient technological upgrade. A case in point was the recent upgrade of the inspection station computer from the now obsolete Intel 86/380 to the current Intel Multibus II configuration. With a minimum impact to the station cabinetry, hardware, and operating system software, the Intel Multibus II was integrated into the inspection station providing approximately 5-times greater processing speed.

In addition, the obsolescence of the Digital Equipment Corporation (DEC) VAX 11/780, which is currently being used in the SA/ALC system, prompted the use of the DEC VAX 82/50 in the OC/ALC system. The new VAX 82/50 not only provides greater CPU power in half the physical space, it also costs less than the 11/780. And, as in the case of the Intel system, the transition had virtually no impact on the operating system software.

Other areas of upgrade that are currently being pursued and which will provide significant cost-savings and improved inspection performance are the development of the micro-manipulator for surface inspections, and the development of a variable-diameter probe for RECHII inspections (Rotating Eddy Current Hole Inspections). The micro-manipulator probe will eliminate the need for approximately 50% of the surface probes. Additionally, the variable-diameter probe will eliminate most of the hole inspection probes currently being used. These tooling concepts have the potential for providing significant cost savings to the user in the area of repair, maintenance, and replacement costs. In addition, eliminating the need for the numerous probe configurations has the added benefit of reducing the need for numerous reference standards used for probe check and calibration procedures. Significantly decreasing the number of probes and reference standards will save considerable time during the part inspection, and, most importantly, provide greater inspection integrity by decreasing the variability between reference standards and probes.

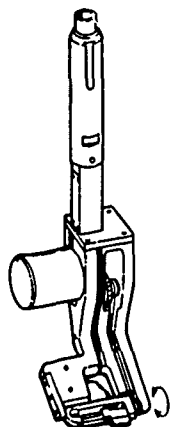


Figure 7. Variable Angle Surface Eddy Current Probe

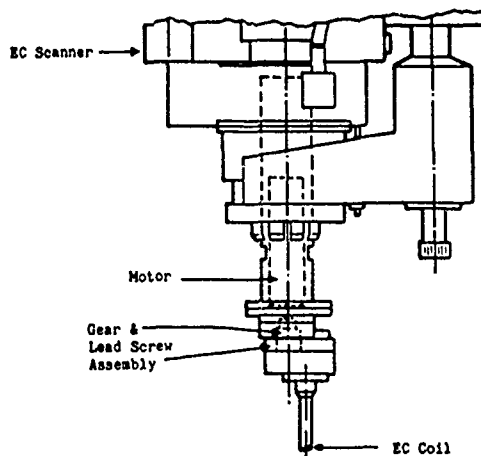


Figure 8. Variable Diameter Rotating Eddy Current Probe

Critical to the future performance of the system is its ability to accommodate future advanced NDE flaw detection and characterization techniques and algorithms. The system's modular software design makes this possible. The system currently uses Fourier analysis and deconvolution, as well as time and spatial averaging techniques during the part inspection process. In addition, research is currently being conducted on the application of various AI and advanced signal processing techniques to the areas of complex geometry inspections and signal-to-noise ratio improvements.

The system's modularity also enables it to easily fulfill the fundamental requirement of providing generic inspection capability for all engine configurations. The basic NDE inspection station (as previously discussed under SYSTEM DESCRIPTION) remains constant for all engine configurations, while the part specific adaptations are made through "kits" consisting of fixtures, adapters, tooling, and scan plans. The generic system design maintains total transportability between stations, ALC installations, engine configurations, etc., while also reducing costs associated with supporting numerous, uniquely-designed inspection systems. To date, the RFC Inspection System can accommodate the Pratt & Whitney F100 and F129 engines, as well as the General Electric F101, F110, and F229 engines through kit modifications to the generic base assembly.

While the SA/ALC and OC/ALC RFC Systems are readily expandable by "plugging in" additional inspection stations, the need for stand-alone station capability has also been recognized. SRL has recently designed such a station which can be effectively used in smaller-scale production operations. The stand-alone station will provide the same critical data processing and level of performance as the full-scale inspection system, but will have less storage capability and will generate hard-copy inspection data directly at the station upon completion of the part inspection, thus eliminating the need for the Operator Console.

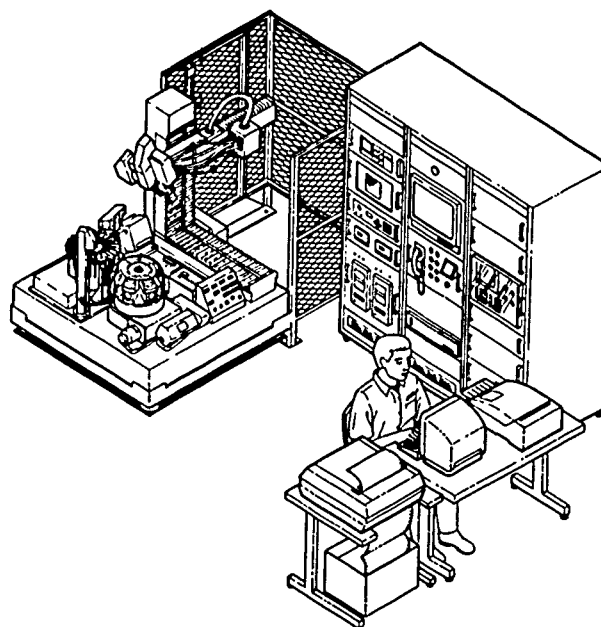


Figure 9. The Stand-Alone Inspection System

CONCLUSION

The RFC Inspection System developed under the direction of the U.S. Air Force has been a very successful project wherein state-of-the-art technology was developed and effectively adapted to practical and productive application. In addition, the manufacturing technology developed under this Government project has beneficial and wide-range application across all facets of the aerospace industry - Government as well as commercial. The technical contributions and cooperative efforts of the RFC program participants are the elements that have made this project a success, whereby individual business interests were often set aside to pursue advancements in technology and industry-wide application. As a result, what was once a concept is now a proven and practiced technology in the critical inspection of high performance turbine engine components.

ACKNOWLEDGEMENT

This work was performed under USAF Contract No. F33615-81-C-5002, "Manufacturing Technology for Nondestructive Evaluation (NDE) System to Implement Retirement For Cause (RFC) Procedures for Gas Turbine Engine Components."

NONDESTRUCTIVE EVALUATION OF ADHESIVELY-BONDED JOINTS

A. FAHR and S. TANARY*
Structures and Materials Laboratory
National Aeronautical Establishment
National Research Council Canada
Montreal Road, Ottawa, Canada, K1A 0R6

Abstract

The structural use of adhesively bonded joints, particularly in aerospace applications, requires nondestructive evaluation techniques for the characterization and qualification of bond integrity. In this paper, the types of defects encountered in bonded joints and the NDE methods available to detect them are reviewed. In particular, techniques which have shown potential for nondestructive characterization of bond strength are described. Finally, experimental results from acousto-ultrasonic (AU) measurements followed by destructive shear tests on single-lap joint specimens made from either metallic or carbon fibre composite adherends and FM 300 film adhesive with different types of bond line defects are presented.

1. INTRODUCTION

Mechanical joining and adhesive bonding are basic methods for attaching components in a structure. In the past, adhesive bonding was used primarily in nonstructural applications. In recent years, however, the use of adhesives has increased significantly both in nonstructural as well as structural applications. Adhesive bonded joints offer advantages in terms of design flexibility, cost effectiveness, stress distribution and strength-to-weight ratio. However, there are some disadvantages in using adhesive joints in structural components. In addition to the tedious surface preparation that is required for adhesive bonding, a major limitation is associated with the difficulty encountered in making an accurate measure of bond quality or potential performance after the joint has been assembled. Furthermore, the performance of bonded joints during service may be affected by environmental conditions or by service induced damage that would result in a requirement for reassurance of bond quality. There is consequently a need for nondestructive evaluation (NDE) techniques that can provide assurance of the structural performance of bonded joints both after fabrication as well as during service life.

In this paper, first the types of defects encountered in bonded joints and the NDE techniques available to detect them are reviewed. Then, the acousto-ultrasonic technique which has shown potential for evaluation of bond integrity is described. Finally, experimental results from acousto-ultrasonic measurements followed by destructive shear tests on single-lap joint specimens with different types of bond line defects are presented.

2. DEFECTS IN ADHESIVE BONDS

Defects in adhesive bonds can be classified into three main categories (1).

- (i) **Physical Discontinuities.** Defects of this type would include voids, porosity, unbonds, inclusions, disbonds and cracks. Voids may be introduced in the bond by lack of adhesive or by air and gases entrapped in the adhesive during fabrication. Porosity may be caused by air bubbles or volatiles in the adhesive layer. Inclusions are foreign materials which inadvertently are introduced into the adhesive during fabrication. Disbond could be created in-service due to impact or fatigue. Cracks are often the result of problems with the cure or by overloading in service.
- (ii) **Poor Cohesive Bond Strength.** The cohesive bond strength is the strength of the adhesive layer itself. Weak adhesive can be due to adhesive aging, incomplete mixing, incorrect formulation or insufficient cure.
- (iii) **Poor Adhesive Bond Strength.** The adhesive bond strength is determined by the extent of molecular attraction of the adhesive to the adherend at the adhesive-adherend interface. Poor adhesion can result from ineffective surface preparation or contamination. This is also referred to as a "zero volume unbond".

3. REVIEW OF NDE TECHNIQUES FOR ADHESIVE BONDS

The majority of NDE techniques currently used for adhesive bond inspection are capable of detecting physical discontinuities. Reference (2) provides a good review of the NDE methods for adhesive bond inspection. This article emphasizes techniques that have shown potential for bond strength evaluation.

Sonic vibration methods utilize frequencies below 500 kHz and are based on the principle that defects cause local changes in the stiffness which in turn affect the vibrational characteristics of the structure. This principle is the basis for several commercial bond testers. Sonic vibration methods use contact probes, dry or wet coupling, and are best suited to in-service inspection of honeycomb structures for gross defects such as disbond.

Ultrasonic methods employ high frequency (>1 MHz) sound waves to interrogate the test material. The use of high frequencies provides better sensitivity but requires a fluid for transducer coupling. The sound waves are transmitted either in a continuous manner (resonance techniques) or in the form of repetitive pulses. The latter is the basis for the widely used ultrasonic pulse-echo and through-transmission techniques.

In resonance methods, the frequency of continuous acoustic waves, which are injected locally to the bonded area, is changed until a resonance condition is produced. At resonance frequency, the wavelength is twice the total thickness of the joint. When there is defect in the bond line, the resonance frequency will change due to the presence of a gap which is seen by the transducer as change of thickness. The principles of ultrasonic resonance are used in some commercial bond testers which are widely employed for in-service inspection of bonded aircraft structures. The resonance method also may be used to indicate changes in the bond strength due to variations of adhesive or adherends thicknesses.

* Department of Mechanical Engineering, University of Ottawa.

In the pulse-echo technique, if the transmitting pulse is sufficiently short, echoes from interfaces may be resolved and their amplitude or position used to detect the presence of physical defects. Using the pulse-echo method, Alers et al. (3) found a correlation between the cohesive shear strength of an aluminum lap joint and the longitudinal velocity of sound waves in the adhesive bond line.

The through-transmission method requires access to both sides of the test component. The contact through-transmission technique has very little practical use because of the difficulty of transducer alignment and the requirement for good contact on both sides. In contrast, using water immersion or squirters for coupling and an automated C-scan for scanning transducers, the immersion through-transmission method has found a major role in production inspection of bonded structures particularly in the aircraft industry (4).

The conventional pulse-echo or through-transmission methods employ an incident beam normal to the plane of the bond and rely on the change in acoustic impedance to indicate defects. These methods could be insensitive to the properties of the bond line which constitute a small fraction of the total beam path length. Other ultrasonic methods which use an oblique incident beam to generate interface or plate waves (Lamb waves) also have been used for bond property evaluation. The interface or plate waves propagate along the bond line and thus are affected to a greater extent by bond line properties. Rokhlin (5,6) employed interface waves to evaluate adhesively-bonded layers using the configuration illustrated in Figure 1. In this way the transmitting probe generates surface acoustic waves (SAW) in the lower substrate which are transformed into interface waves. Since the velocities of the surface and interface waves are close, only a small portion of the energy is transformed into bulk waves. The interface waves leaving the bonded zone are transformed back into surface waves and are sensed by a receiving probe. Rokhlin showed that the velocity of interface waves rises during the course of adhesive polymerization. The measurement of bond strength at different time intervals of the cure cycle also showed trends similar to velocity as illustrated in Figure 2. He concluded that the state of adhesion at the interface affects the interface waves since the weak coupling "shunts" the elasticity of the system as a whole. In another study, Kline and Hashemi (7) monitored fatigue damage development in single-lap aluminium specimens using interface waves, termed guided waves, and noted changes in the transmitted signal amplitude and phase velocity, Figure 3. Bar-Cohen and Mal (8) used immersion techniques to generate "leaky Lamb waves" as illustrated schematically in Figure 4. They found that the destructive interference in the radiated field was sensitive to the properties of the bulk material as well as the interfaces. Figure 5 illustrates the change in phase velocity of the leaky waves with frequency for well bonded and poorly bonded titanium beryllium diffusion bonds. Ultrasonic spectroscopy has also been used to obtain information such as changes in bond line thickness or variations in the strength of the adhesive joints due to fabrication processes and hydrothermal degradation (9, 10).

Acoustic emission techniques rely on the initial response of materials during mechanical loading. An early attempt to use acoustic emission on adhesive bonds was made by Schmitz and Frank (11) who reported a correlation between the density of emissions and the bond strength of aluminium honeycomb specimens. The AE method has also been used to study the effect of temperature, humidity or surface treatment on bond strength (12,13). Figure 6, for example, shows the AE response obtained during tensile loading of two types of specimens, with and without a specified surface treatment. Generally, weak joints show more acoustic emission during loading than do the stronger joints. However, practical application of the AE technique is limited due to difficulties in identifying emission sources and the fact that mechanical loading could result in permanent damage to the bonded joints.

Other NDE techniques such as thermography, optical holography and radiography have also been used for the inspection of bonded components; mainly for the detection of physical discontinuities. Thermography and holography are useful in the detection of surface or near surface defects in honeycomb bonded structures. Radiography is effective in the inspection of complex geometries and honeycomb structures, but X-radiography has found little use in the inspection of metal-to-metal joints because the adhesive layer usually has a much lower density than that of the metallic adherends. In contrast, with neutron radiography, a thin adhesive layer can be detected even through thick layers of metallic adherends (14). However, the practical use of neutron radiography is limited since at present a high neutron flux can only be produced in nuclear reactors or high power accelerators.

4. ACOUSTO-ULTRASONIC TECHNIQUE

Acousto-ultrasonics is a relatively new technique which was first introduced by Vary (15). This method combines the beneficial aspects of conventional ultrasonic and acoustic emission techniques. In this method, which is shown schematically in Figure 7, repetitive ultrasonic pulses are injected into the test material by a broadband ultrasonic transducer. A receiving acoustic emission sensor is placed on the same side of the specimen to intercept the propagating stress waves. In this case, although the transmitting transducer injects compressional waves normal to the surface, the energy transferred into the material will produce stress waves which, like Lamb waves, radiate in the plane of the bond and interact with a significant fraction of the bond line that lies in their path. Recent studies (14-21) have demonstrated that the acousto-ultrasonic technique can be used to provide quantitative information about the mechanical performance of bonded joints by showing a correlation between the AU stress wave propagation characteristics and joint strength.

Williams et al. (16) used the AU technique to evaluate the strength of bonded joints in automotive glass fibre composites, while Kapoor and Prakash (17) applied the technique to evaluate the strength of bonded joints in aluminium. Dos Reis et al (18) showed a correlation between the peel strength for rubber sheets bonded to steel specimens and the stress wave factor (SWF), which is a parameter measurable by the acousto-ultrasonic technique (15). The AU technique has also been used to evaluate the effect of hydrothermal aging on composites (22) and porous metal diffusion bond quality (23).

From the practical point of view, the acousto-ultrasonic technique offers some advantages. The technique requires access to only one side of the structure and thus, it has potential for use on existing structures where two-side accessibility and ability to disassemble the structure may not be possible. In addition, sensitive AE probes are used for receiving stress waves, so that, unlike conventional ultrasonic techniques, precise alignment of probes is not essential. The AE probes are also more effective in overcoming the high attenuation common to most adhesively bonded laminates made of composite materials. Major difficulties associated with the AU technique include obtaining reproducible results and interpreting received signals.

Stress wave propagation can be related to several parameters that are measurable from an acousto-ultrasonic waveform in the time or frequency domain. Important parameters in the time domain, would include signal amplitude, ring-down counts, duration and root-mean-square (RMS) amplitude. Vary (15) defined another parameter known as the Stress Wave Factor (SWF) which is given by.

$$SWF = RTC \quad (1)$$

where R is the repetition rate of the input pulses, T is a pre-determined time interval, and C is the number of oscillations in the received waveform which exceeds a preselected voltage threshold (Ring-Down Count). Williams and Lampert (16) calculated an alternative stress wave factor by summing the amplitudes of oscillations in the received waveform. In our analysis, the Williams and Lampert factor will be referred to as the "acousto-ultrasonic parameter" or AUP to distinguish it from the stress wave factor. The AUP can be calculated using the expression (24):

$$AUP = \sum_{i=0}^P V_i(C_i - C_{i+1}) \quad (2)$$

where V_i and C_i are the threshold and number of counts at the i th level respectively and V_p corresponds to the peak amplitude of the waveform. Since the AUP takes into account both ring-down counts and the amplitude of the signal, it is more representative of AU signals than the SWF.

The AUP provides a means of rating the efficiency of stress wave energy transmission. If the bonded specimen demonstrates a more efficient stress wave energy transmission property (higher AUP value), it is expected that the joint will be able to transfer stress more efficiently (15). Since the AUP provides a relative measurement, it is preferable to normalize the AUP value with that of a calibration specimen or with respect to its maximum value.

Like ultrasonic and acoustic emission methods the results of acousto-ultrasonic measurements are affected by several factors which are related either to the transducer-specimen attachment configuration (e.g. transducer spacing, applied pressure on transducers, coupling fluid) or to the settings and characteristics of the transmitting and receiving instruments (e.g. instrument gain and frequency). Therefore, it is necessary to optimize and calibrate the AU measurement system in order to obtain reproducible and reliable results.

5. EXPERIMENTAL PROCEDURE AND APPARATUS

An experimental study was carried out to assess the feasibility of utilizing the acousto-ultrasonic technique in the characterization of adhesively bonded joints. For this purpose, controlled degradation in bond strength was accomplished by the deliberate introduction of voids in the joints, exposing the bonded specimens to elevated temperatures, aging of adhesives prior to bonding or contamination of adherend surfaces. Single-lap joint specimens (adopted from ASTM Standard D1002-72) were made using either carbon fibre composite or steel adherends and commercial FM300 adhesive film. Also, foam core aluminium panels containing disbands between the aluminium skin and the foam core were tested. Details relating to specimen preparation are provided elsewhere (24,25). Briefly, voids were created in the joint area by removing part of the adhesive film before bonding. After cure, the specimens were inspected using the ultrasonic C-scan technique and the void areas were mapped. Zero volume unbonds were created in the joint by contaminating the surface of the composite adherends with grease before bonding. The bonded test coupons were then inspected by ultrasonic C-scan which showed no clear indication of unbond areas. Specimens with degraded adhesive properties were made by aging the adhesive film at room temperature for periods of 3 to 8 weeks prior to bonding. Also, bonded steel specimens were exposed repeatedly to a temperature of 150°C for about one hour and then cooled down to room temperature in order to degrade the adhesive strength. The bonded specimens were then inspected using the ultrasonic C-scan technique for possible flaws. The C-scan results showed no flaws in the aged samples as well as the heated samples.

The acousto-ultrasonic measurements were carried out using the apparatus shown schematically in Figure 8. An ultrasonic instrument was employed to generate the input signals which, after passing through a repetition controller and reset timer, excited a broadband transmitting transducer with a 500 kHz centre frequency. At a fixed distance away, a receiving acoustic emission transducer was used to intercept the stress waves. Both transducers were coupled to the surface using a coupling fluid. The stress waves received by the receiving transducer were amplified by 40 dB using a preamplifier and filtered by a 125-1000 kHz band pass filter. A representative waveform of the AU signal was digitized using a universal waveform analyzer and stored on floppy disk for further analysis in the time and frequency domains.

After completion of the acousto-ultrasonic measurements, the test specimens were loaded in tension to failure in a universal testing machine and the failure load was measured. The shear strength was calculated by dividing the failure load by the overlap area. After failure, the fracture surfaces were examined using an optical microscope to determine failure modes and the void or unbond areas within each specimen were measured.

6. EXPERIMENTAL RESULTS AND DISCUSSIONS

6.1 Specimens with Physical Defects

The acousto-ultrasonic waveforms in the time domain and corresponding frequency spectra for typical single-lap joint composite specimens without and with voids are illustrated respectively in Figures 9 and 10. In this case, stress waves travel from one adherend across the bond line to the other adherend. Thus, the presence of voids in the bond line reduces the stress wave propagation efficiency due to factors such as acoustic impedance mismatch. In the frequency domain, when there are no voids present in the joint, the frequency spectrum of the waveform consists of a peak occurring at about 350 kHz which is the resonant frequency of the receiving transducer. In the presence of voids, other peaks, occurring at lower and higher frequencies, start to appear in addition to the peak at the resonant frequency of the receiving transducer.

Figure 11 illustrates a three dimensional plot showing the AU inspection results of a foam core panel containing a disbond (26). This was obtained using a commercial AU instrument equipped with a hand-held probe fixture which was dry coupled to the test specimen by two rotating wheels. Inspection was performed by simply rolling the probe manually over the test specimen and taking the RMS amplitude of the AU signals. In this case, since both the transmitting and receiving probes were on the same surface, the presence of fatigue disbond at the interface between the aluminium skin and the foam core caused an increase in the stress wave propagation efficiency as indicated by the increase in RMS amplitude. This increase is attributed to the fact that, when the bond is good, stress wave energy is partially dissipated across the bond line into the foam. However, the presence of disbond prevents the transfer of energy into the foam resulting in an increase in AU signal amplitude.

These results indicate that the acousto-ultrasonic method is capable of detecting physical defects such as voids or disbond in bonded joints. However, the AU response may be different from one material to another. The use of a dry coupling wheeled probe can make the application of the AU method simple and practical.

6.2 Specimens with Zero Volume Unbonds

The AU signals of specimens containing zero volume unbonds created by contaminating the surfaces of adherends with grease did not vary as much as was the case with specimens containing voids. This was expected since the acoustic impedance mismatch, which affects the efficiency of stress wave propagation, is considerably less in specimens with zero volume unbonds. However, the frequency spectra of the acousto-ultrasonic waveforms show variations due to the presence of unbonds in the joint (Figure 12). In the absence of unbonds, the frequency spectrum of the waveform shows a major peak occurring at about the resonant frequency of the receiving transducer (approximately 350 kHz), but as the unbond size increases, there are additional peaks appearing at higher frequencies.

Figure 13 shows the normalized AUP and the joint shear strength for specimens containing unbond areas. The value of normalized AUP in the figure represents an average of 4 measurements on each specimen. Examination of the fracture surfaces revealed that there was generally a mixed mode of failure consisting of cohesive failure in the adhesive, interfacial failure at the free edges between the adhesive and the adherend, fibre pull-off, and interlaminar failure in the first few plies of the composite adherend near the adhesive. It was observed that for joints with larger contaminated areas, interlaminar failure was predominant and the joint strength was generally lower.

6.3 Specimens with Degraded Adhesive

The AU signals in the time and frequency domains for composite specimens made using aged adhesives were not noticeably different from the control specimens. However, the change in normalized AUP with increasing adhesive aging time was more noticeable as illustrated in Figure 14 which shows a reduction of the acousto-ultrasonic parameter with adhesive aging time.

Figure 15 shows the change in the normalized joint strength as a function of aging time of the adhesive film. As the aging time of the adhesive increases, the joint strength tends to decrease. However, the decrease is only about 15% for the aging time of 8 weeks at room temperature. This relatively small reduction in strength with aging time could be due to the fact that the adhesive used in this study was a high temperature curing adhesive. At room temperature, which is below the glass transition temperature of the adhesive, slow cure of the adhesive would normally take place (27).

Comparison between Figures 14 and 15 would indicate that both the acousto-ultrasonic evaluation and the destructive testing results of the specimens with aged adhesive exhibit a similar trend with aging time. The relationship between the normalized AUP and the normalized joint strength is illustrated in Figure 16. Fractographic examination of the fractured specimens showed that the failure modes were predominantly cohesive failure in the adhesive with some interlaminar failure in the composite adherend and interfacial failure at the boundary between the adhesive and composite adherends. It was observed that specimens with longer aged adhesive tended to have relatively more interfacial failure. Similarly, the bonded steel specimens subjected to cyclic thermal exposure generally had lower AUP and average shear strength values than the as-fabricated specimens. The AUP and the shear strength for these specimens is shown in Figure 17.

These experimental results indicate that in many cases the bonded specimens which demonstrated a more efficient stress wave transmission (i.e. higher AUP) resulted in a higher strength values. However, it must be pointed out that these results are obtained on simple single-lap specimens of constant geometry and adhesive thickness and cannot be generalized to other materials, geometries or adhesive systems.

7. CONCLUSIONS

In summary, physical defects in bonded joints can be easily detected with the available NDE techniques although no single method is universally applicable to different types of defects. The problem of detecting poor adhesives has been partially solved and methods such as ultrasonic spectroscopy and pulse-echo using the velocity or attenuation of ultrasonic waves appear to be sensitive to adhesive properties. The problem of detecting poor adhesion due to contamination or improper substrate surface preparation still remains unresolved. Techniques using ultrasonic interface or Lamb waves appear to have some potential for the evaluation of adhesive and interfacial bond properties.

The acousto-ultrasonic method, which is based on the analysis of simulated stress waves, also holds promise for bond integrity evaluation. This technique has some advantages in terms of practical application. A feasibility assessment of the acousto-ultrasonic technique on single-lap joint specimens which contained voids, zero volume unbonds and degraded adhesives indicates that the technique has potential in the detection of all three types of defects in adhesive bonds. It appears that the stress wave propagation efficiency can be related to the bond strength although such relationship may be affected by adhesive and adherend material and geometry. The relationship suggests that the same microstructural and morphological factors of the bond line (both adhesive as well as interface) that affect the joint integrity also influence the acousto-ultrasonic stress wave propagation. Thus, it may be possible to obtain a relative measure of the joint integrity from the acousto-ultrasonic wave propagation characteristics provided that the AU measurement is calibrated with respect to a known sample of the same material and geometry. Further investigation is required to establish the applicability of the AU method on large and complex bonded structures.

REFERENCES

1. Guyott, C.C.H., Cawley, P. and Adams, R.D., The Nondestructive Testing of Adhesively Bonded Structures: A Review, *J. Adhesion*, 1986, Vol. 20, pp. 129-159.
2. Adams, R.D., Cawley, P. and Guyoff, C.C.H., Nondestructive Inspection of Adhesively Bonded Joints, *J. Adhesion*, 1987, Vol. 21, pp. 279-290.
3. Alers, G.A., Flynn, P.L. and Buckley, H.J., Ultrasonic Technique for Measuring the Strength of Adhesive Bonds, *Materials Evaluation*, Vol. 35, No. 4, April 1977, pp. 77-84.
4. Djordjevic, B.B. and Venables, J.D., Nondestructive Evaluation of bonded Metal and Composite Structures, *Proceedings of 13th Symposium on Nondestructive Evaluation*, Leonard, B.E., Ed., San Antonio, Texas, April 1981, pp. 68-76.
5. Rokhlin, S.I., Adhesive Joint Characterization by Ultrasonic Surface and Interface Waves, *Adhesive Joint. Their Formation, Characteristics and Testing*, Mittal, K.L., Ed., Plenum Press, New York, 1984, pp. 307-345.
6. Rokhlin, S.I., Evaluation of the Curing of Structural Adhesives by Ultrasonic Interface Waves. Correlation with Strength, *Journal of Composite Materials*, Vol. 17, No. 1, January 1983, pp. 15-25.
7. Kline, R.A. and Hashemi, D., Ultrasonic Guided-Wave Monitoring of Fatigue Damage Development in Bonded Joints, *Materials Evaluation*, Vol. 45, No. 9, September 1987, pp. 1076-1082.
8. Bar-Cohen, Y., Mal, A.K., Ultrasonic NDE of Bonded Structures, *Transcripts of the Workshop on NDE of Adhesive Bond Strength*, April 13-14, 1988, Orlando, FL, Organized by the Nondestructive Testing Information Analysis Centre, pp. 201-227.
9. Llyod, E.A. and Brown, A.F., Recent Developments in Nondestructive Testing of Adhesive-Bonded Joints, *Adhesion* 2, Allen, K.W., Ed., Applied Science Publishers Ltd., London, 1978, pp. 133-144.

10. Llyod, E.A. and Wadhawani, D.S., Ultrasonic Spectroscopy and the Detection of Hydrothermal Degradation in Adhesive Bonds, Adhesion 4, Allen, K.W., Ed., Applied Science Publishers Ltd., London, 1980, pp. 159-174.
11. Schmitz, G. and Frank, L. NDT Evaluation of the Strength of Bonded Materials, NASA Contractor Report CR-67983, September 1966.
12. Hill, R., The Use of Acoustic Emission for Characterizing Adhesive Joint Failure, NDT International, Vol. 10, No. 2, April 1977, pp. 63-72.
13. Brockmann, W. and Fischer, T., Acoustic Emission Analysis as a Method of Testing Adhesive Metal Joints, 22nd National SAMPE Symposium and Exhibition, San Diego, California, April 26-28, 1977, Diversity-Technology Explosion, Vol. 22, pp. 277-300.
14. Segal, E. and Rose, J.L., Nondestructive Testing Techniques for Adhesive Bond Joints, Research Techniques in Nondestructive Testing, Vol. 4, Sharpe, R.S., Ed., Academic Press, New York 1980, pp. 275-316.
15. Vary, A., Acousto-Ultrasonic Characterization of Fibre Reinforced Composites, Materials Evaluation, Vol. 40, No. 6, May 1982, pp. 650-662.
16. Williams, J.H. Jr., and Lampert, N.R., Ultrasonic Evaluation of Impact-Damaged Graphite Fibre Composite, Material Evaluation, Vol. 38, No. 12, December 1980, pp. 68-72.
17. Kapoor, A., and Prakash, R., Strength of Adhesive Bonded Joints, International Conference on Advances in Fracture Research, Proceeding of the 6th Conf, New Delhi, India 1984, pp. 2649-2655.
18. Dos Reis, H.L.M. and McFarland, D.M., On the Acousto-Ultrasonic Non destructive Evaluation of Wire Rope Using the Stress Wave Factor Technique, British Journal of Nondestructive Testing, Vol. 28, No. 3, May 1986, pp. 155-166.
19. Duke, J.C. Jr., et al., Ultrasonic Stress Wave Characterization of Composite Materials, NASA Contractor Report 3976, May 1986.
20. Green, J.E. and Rodgers, J., Acousto-Ultrasonic Evaluation of Impact-Damaged Graphite Epoxy Composites, 27th National SAMPE Symposium, May 4-6, 1982, pp. 428-439.
21. Kautz, H.E., Acousto-Ultrasonic Verification of the Strength of Filament Wound Composite Material, NASA Technical Memorandum 88827, July 1986.
22. Phani, K.K. and Bose, N.R., Hydrothermal Aging of CSM-Laminate During Water Immersion- An Acousto- Ultrasonic Study, Journal of Materials Science, Vol.22, No.10, Oct. 1986, pp. 3633-37.
23. Vary, A., Moorhead, P.E. and Hull, D.R., Metal Honeycomb to Porous Wireform Substrat Diffusion Bond Evaluation, ASNT Spring Meeting, Massachusetts, April 1982, pp. 185-91.
24. Fahr, A., Lee, S., Tanary, S., and Haddad, T., Estimation of Strength in Adhesively Bonded Steel Specimens by Acousto-Ultrasonic Technique, Mat. Eva., Vol. 47, No. 2, 1989, pp. 253-260.
25. Tanary, S., Characterization of Adhesively Bonded Joints Using Acousto-Ultrasonics, Masters Thesis, University of Ottawa, Ottawa, Canada 1988.
26. Fahr, A., Chapman, T.E., Tanary, S., Farahbakhsh, B., Assessment of NDE Techniques for Foam Core Aluminium Panels, Workshop on NDE of Adhesive Bond Strength, April 13-14, 1988, Orlando, FL., organized by NDT Information Analysis Centre.
27. Lewis, A., Adhesives and Adhesion-Introductory Theoretical Concepts, Adhesives 1979-1980 - Desk Top Data Bank, Cordura Publications Inc., California, p. iii.

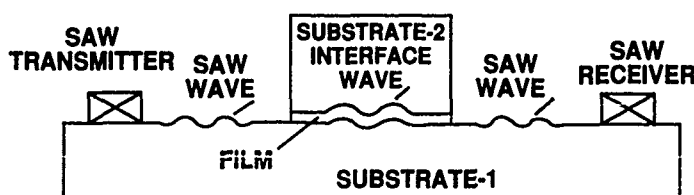


Figure 1. Illustration of the interface wave method (Ref. 5).

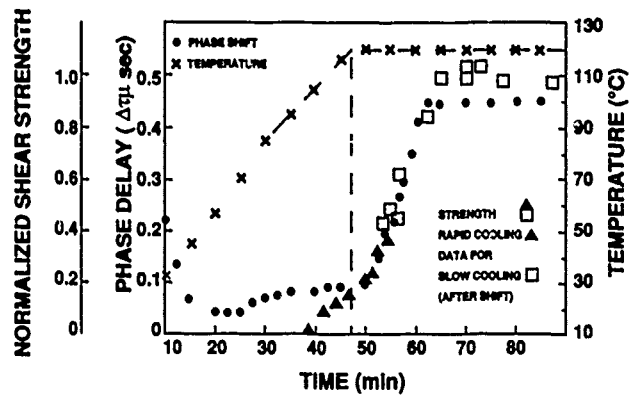


Figure 2. Comparison between the change in the interface wave velocity and the shear strength of the bond in the course of curing FM-73 structural adhesive (Ref. 5).

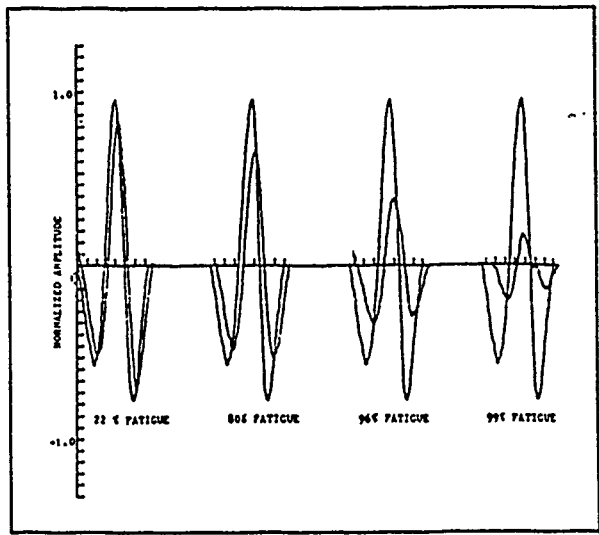


Figure 3. Acoustic waveforms at various stages of cyclic load test as compared to the signal before fatigue cycles which indicate changes in the amplitude and phase velocity (Ref. 7).

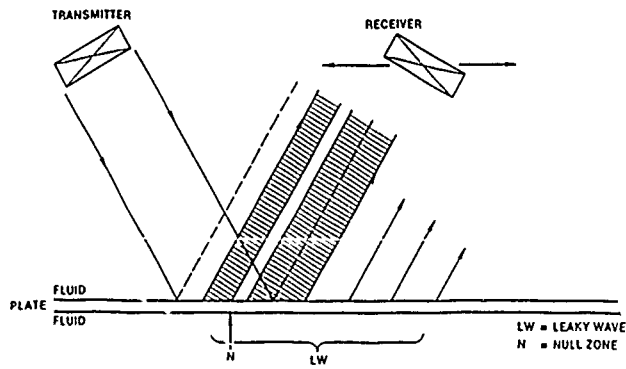


Figure 4. Schematic diagram of the leaky Lamb wave technique (Ref. 8).

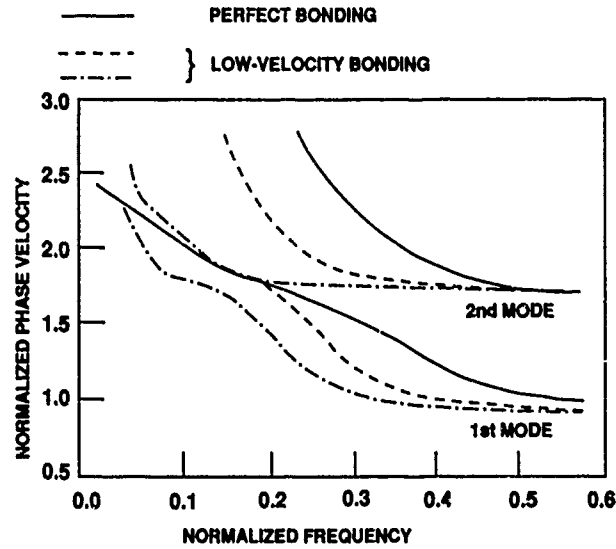


Figure 5. Velocity of the leaky Lamb waves as a function of frequency in a bonded layer with and without interfacial zones (Ref. 8).

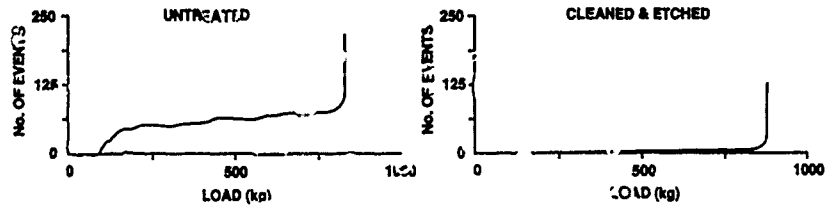


Figure 6. Total AE events vs load for typical specimens made of aluminum adherends and HYSOL 9320 adhesive using different surface treatments.

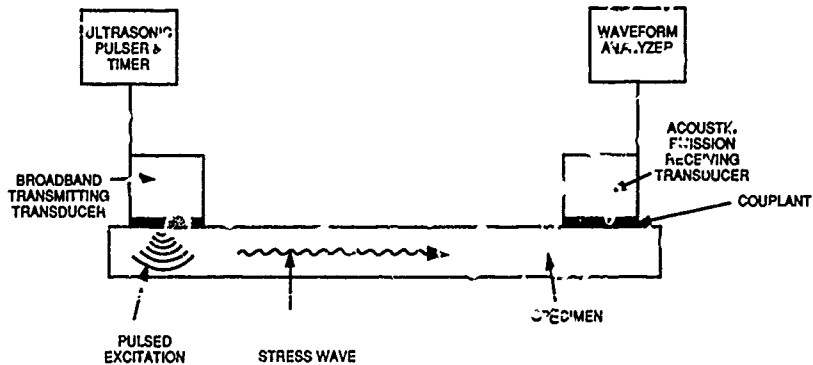


Figure 7. A schematic diagram of the acousto-ultrasonic technique.

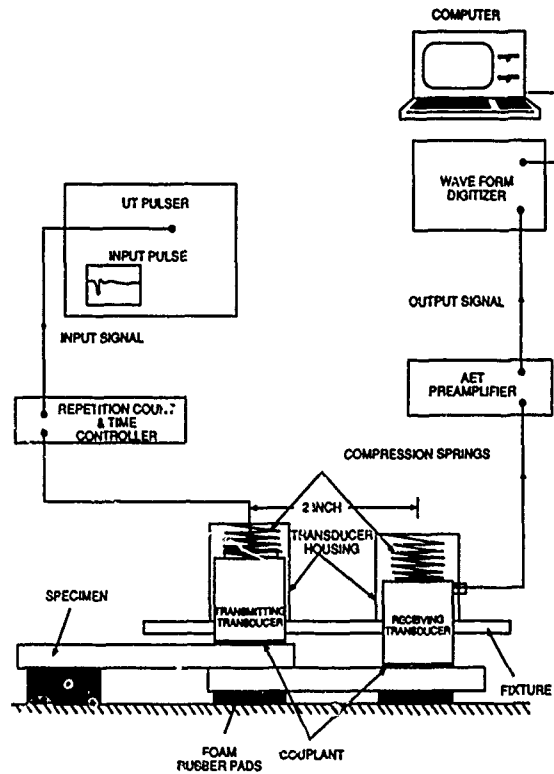


Figure 8. A schematic diagram of the acousto-ultrasonic system as used in the present investigation.

WITHOUT VOIDS

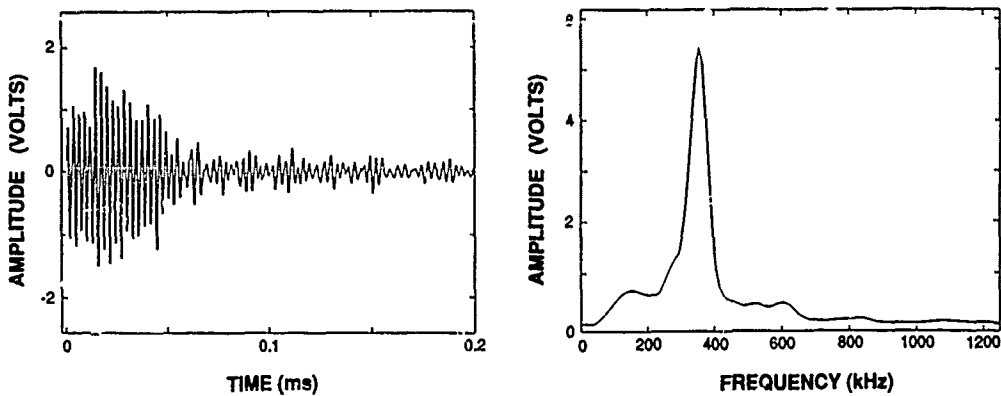


Figure 9. A typical acousto-ultrasonic signal and corresponding frequency spectrum for a well bonded specimen.

WITH VOIDS

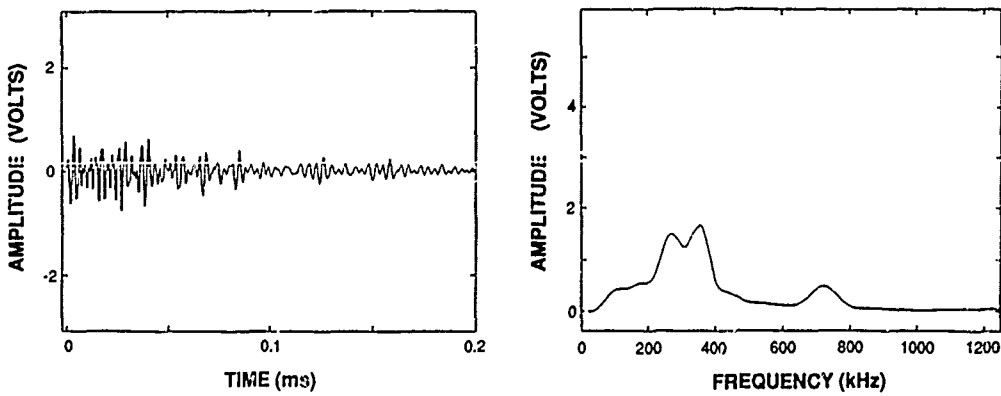


Figure 10. A typical acousto-ultrasonic signal and corresponding frequency spectrum for a specimen containing a void.

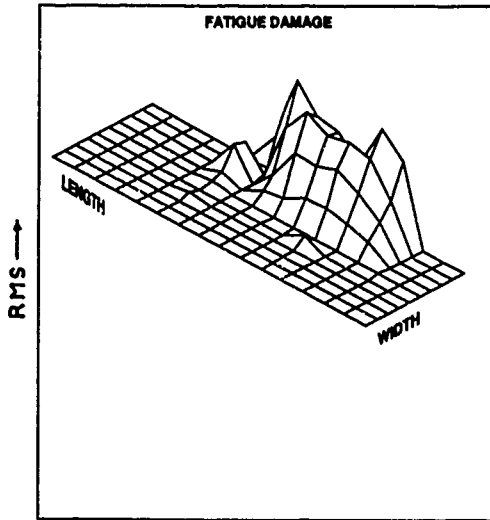


Figure 11. The acousto-ultrasonic inspection results for a foam core panel containing a fatigue disbond.

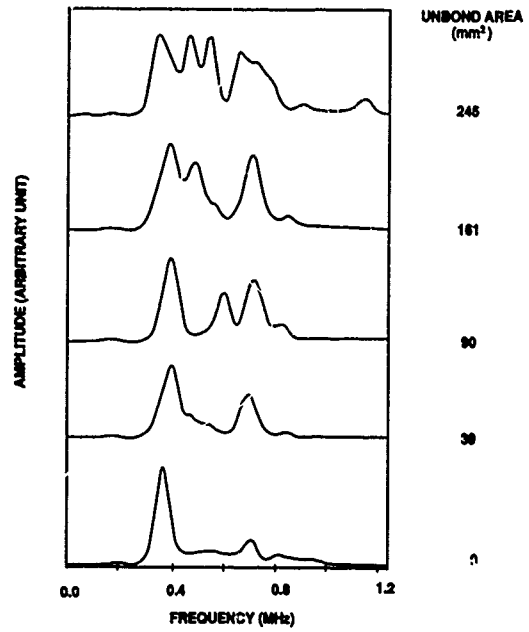


Figure 12. The change in the frequency spectra of the acousto-ultrasonic signals from bonded specimens with contamination unbond areas.

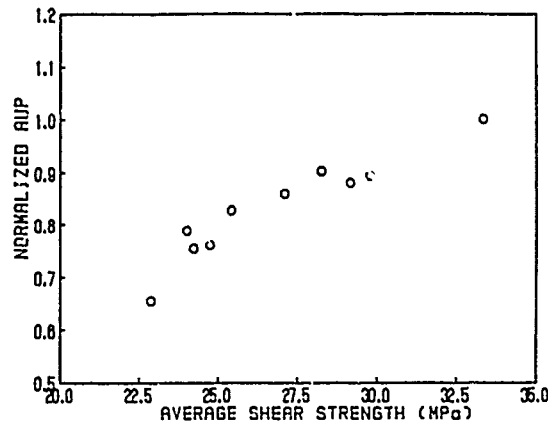


Figure 13. The normalized acousto-ultrasonic parameter (AUP) as a function of the average shear strength for the specimens with contamination unbonds.

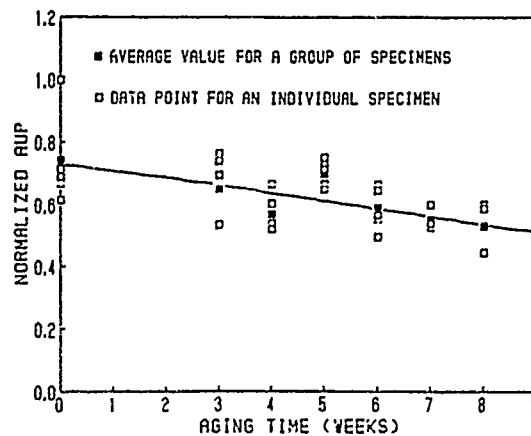


Figure 14. The change in the normalized AUP as a function of aging time.

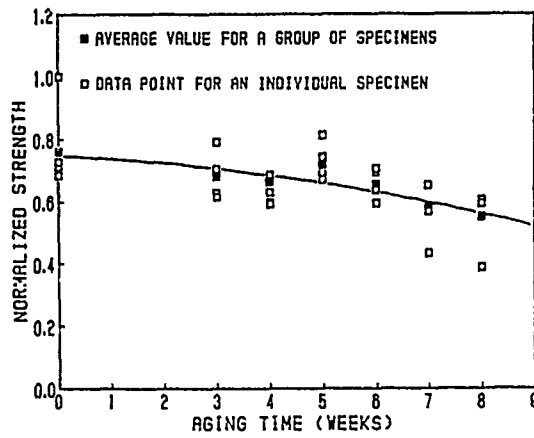


Figure 15. The change in normalized joint strength as a function of aging time.

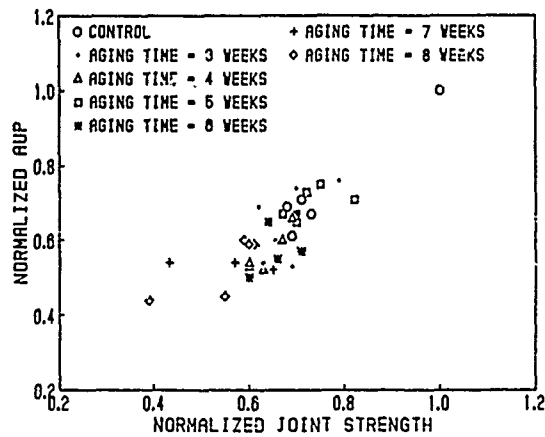


Figure 16. Plot of the normalized AUP vs the normalized joint strength for specimens with aged adhesive.

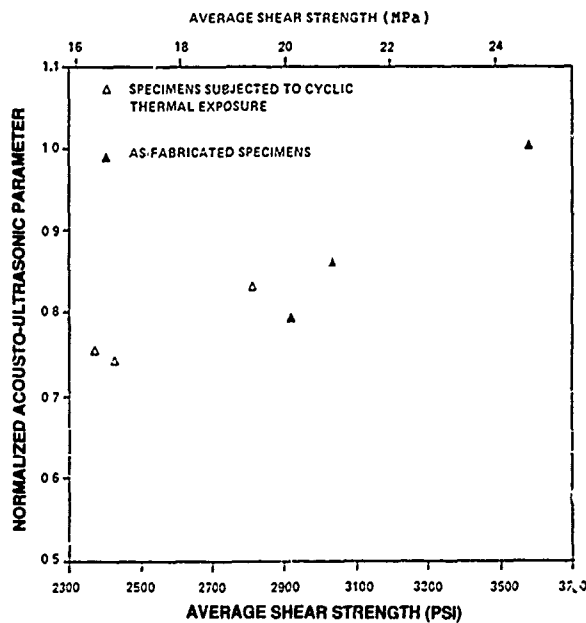


Figure 17. The acousto-ultrasonic parameter as a function of the average shear strength for two groups of specimens; as-fabricated specimens and specimens subjected to cyclic thermal exposure.

ULTRASONIC INSPECTION OF ADVANCED CFRP STRUCTURES BY COMPUTER-CONTROLLED, PULSE-ECHO TECHNIQUE

B. Sainz, J.M. Bernardo, V. Cortés, C. Valdecantos
CONSTRUCCIONES AERONAUTICAS, S.A. (C.A.S.A.)
Project Division I+D.T.M.
Getafe - Madrid - Spain

SUMMARY

A complete system for NDE-NDI of grown defects detection during full-scale fatigue test of a primary CFRP structure has been developed. Both internal and external damages were considered and monitored in order to document its behaviour along the fatigue test for certification purposes.

For external defect, i.e.: those accesible from the outside, a portable, computer controlled ultrasonic system has been designed and proved succesess. Pulse-echo water squirter technique is used and mechanical X-Y frame is able to scan up to 600(X) by 400(Y) mm. Data acquisition is performed for amplitude signal so that C Image can be draw.

Internal damages are controlled by a series of ultrasonic transducers bonded surrounding the damage so that a fixed signal is drawn from each transducer unless defect limit extends and crosses the ultrasonic beam giving a new echo growing from the time base. All the 80 transducers can be checked sequentially by means of a multiplexer. A major-trouble is that the whole structure is aged by 3 months at 70° degrees (centigrade) and 70% humidity. This environment affects both bonding line integrity and piezoelectric parameters of the ceramic, and some design improvements have been introduced to reduce these effects.

INTRODUCTION

One of the main goals of a fatigue test for aircraft structures, besides the certification, is to characterize and to document the behaviour of selected artificial defects, which is very important support for damage tolerance program. To this purpose, several NDT techniques are applied, often more sophisticated than those used in maintenance because technical considerations prevail upon economic ones.

The part to be inspected is a complex CFRP structure (Fig. 1) for the horizontal stabilizer of a commercial airplane. Full scale fatigue test is being carried out for certification purposes. Testing program includes damage tolerance analysis after ageing the structure at controlled moisture/temperature environment. Impact damages are induced in selected critical areas of the structure to simulate accidental damages that may happen during routine maintenance works because tools falls (hammer, screwdrivers, etc.) or other damages simulating production defects.

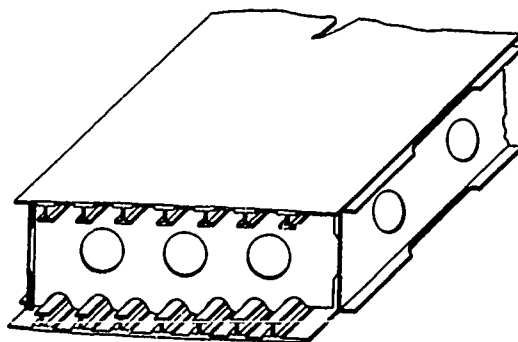


Fig. 1. Structure of the horizontal stabilizer

Fig. 2 shows typical areas to be controlled. Access to some of them is only possible before assembling structure. Spherical impactor coupled to a suitable weight is dropped from up to 2 m to produce low velocity impact that breaks matrix and graphite fibres in an amount depending on the material characteristics lay-up, area geometry and, of course, on the impact energy. Very small or even undetectable damage in the stroke side often come together with big breakage in the opposite surface. Ultrasonic test of pulse-echo or through transmission, easily detects impact damages rather before barely visible surface damage is detected.

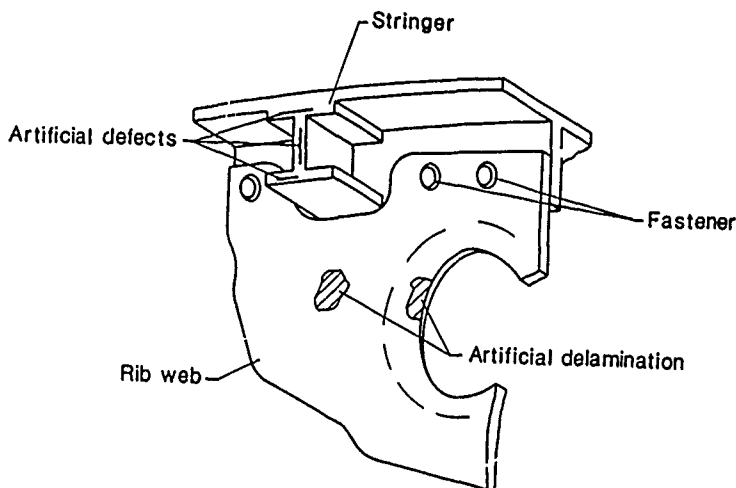


Fig. 2. Stabilizer structure section. Critical area to be controlled

Fig. 3 shows how pulse echo tests behaves in a typical damaged area. But such a test is obviously impracticable in maintenance programmes due to economic reasons and that is because there is a great effort in order to demonstrate how the defects accepted by routine quality control tests in production line behave in service. If, i.e., it is clearly shown that a defect of the maximum acceptable size in a critical area does not grow or its evolution is not significant or even it grows at early stages but stops later, then inspection effort in this particular area can be reduced, making maintenance easier and costly effective.

Access to inspection area heavily affects to the test technique. If damage is in the outside surface, a manual or automatic ultrasonic technique can be used. However some areas become hidden when part is assembled (see Fig. 2) and accesibility is very limited. In these areas an ultrasonic test with fixed transducers around the defect was selected to monitor the defect behaviour (see Fig. 4).

A pulse-echo, water squirter ultrasonic automatic scanning technique was selected to monitor external defects.

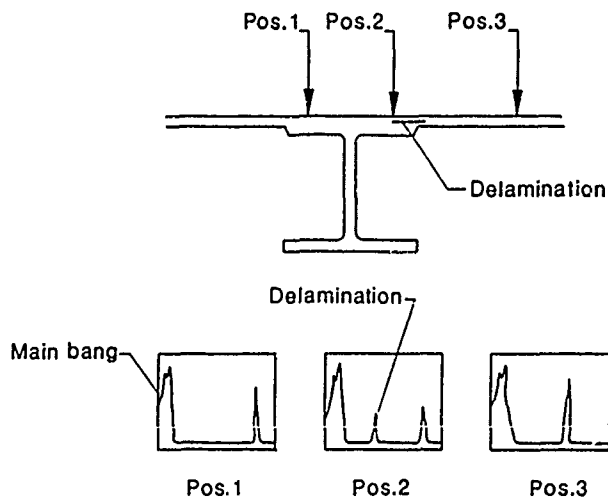


Fig. 3. Typical impact damage (delamination) and CRT display.

EQUIPMENT CONCEPT

Fig. 4 shows the diagram of the system as well as a sketch of the two different problems.

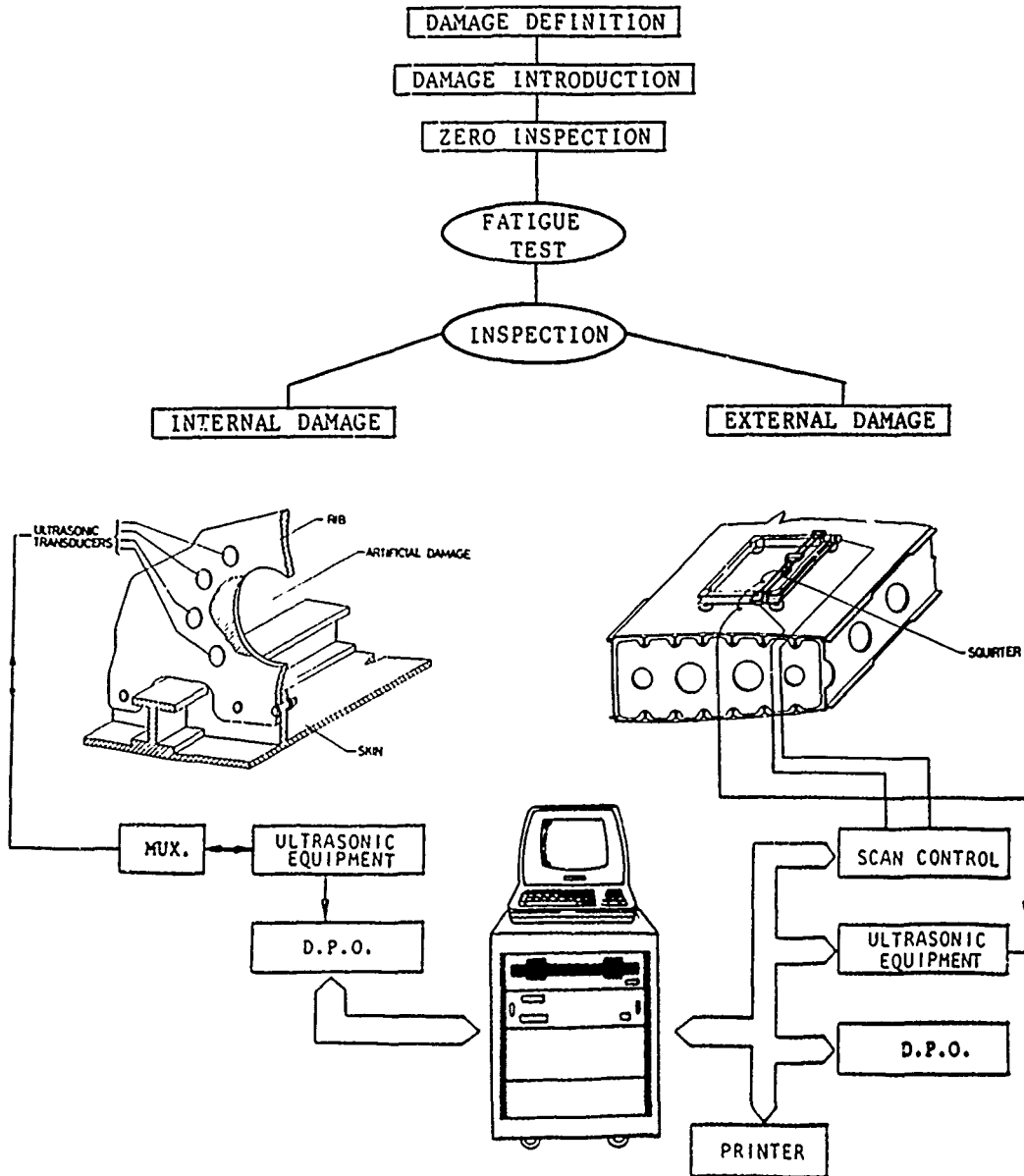
HORIZONTAL STABILIZER FULL SCALE FATIGUE TEST

Fig. 4. Diagram of the inspection techniques for the Horizontal Stabilizer Fullscale Fatigue Test.

Basic ultrasonic equipment is a Krautkrämer USIP-12 with a DTM-12 module able to give digital information from time of flight or thickness through a parallel interface. Transducer for pulse echo test is an H5M, 5MHz frequency, 6 mm diameter. Bonded transducers have been manufactured in our laboratories according with a technique enabling low cost and good repeatability. About 80 transducers have been installed, 5MHz, 5 mm diameter coupled to a 10 mm perspex delay. To improve ageing resistance all the transducers are encapsulated in a suitable aluminium case.

A multiplexer allows to drive any transducer and observe its signal in the screen of the USIP-12. Video output from the rear USIP-12 is feed into a Digital Processing Oscilloscope (Tektronics 2430) able to acquire signal in real time. The operator is allowed via computer to acquire the signal and store it in disk to compare with these from the following test. Comparison is achieved by extracting main features from the raw signals, that is: amplitude and time for each echo higher than 5% of the screen.

Signal coming from external defects is acquired and the following parameters are stored:

- . Amplitude of the maximum echo in the gate
- . Time of flight (or thickness)
- . X and Y coordinate

Scanning of the area is carried out by a computer controlled X-Y scanner able to scan up to 600 x 400 mm at a maximum X axis speed of about 500 mm/sec. Mechanical design enables to achieve 0.2 mm repeatability in X direction and 0.1 in Y direction.

An IBM AT, 20 Mbytes hard disk, 1 Mbytes floppy is used as a computer. Colour monitor driven by graphics adapter card as well as a colour inkjet 3855 IBM printer are used as peripherals.

Besides the printer list of the array, results can be recorded as a C image where Z axis is colour modulated to simulate different signal amplitudes. It is also possible to deflect the pen in the Y direction by a factor proportional to the echo amplitude. If information provided by DTM12 is used, B scan can presented from any part of the scanned area not only in X but also in Y direction. Software enabling this presentation is now being implemented.

Software is designed in a friendly style, and any normally skilled operator can easily be trained as system user. Fully menu structure enables to perform desired operations. A help function is also implemented to support questions at any time. Main menu gives access to the following options:

1. Define Test Parameter
2. Execute Test
3. Print results
4. Files
5. Transducer calibration
6. System Status
7. User's manual
8. End of job

To provide a suitable way to standardize results an automatic cycle to calibrate probe was implemented (option 5). Calibration echo is obtained from a fixed flat piece of glass bonded to the frame close to the coordinate origin. When transducer calibration option is selected by the operator search unit moves to the standard reflector and operator sets it in its maximum echo position. Then a sample is acquired and stored in an adhoc file to be compared with forthcoming ones. Calibration can be programmed to be performed at selected intervals during the test. Windowing and noise suppression algorithms as well as an FFT facility are being implemented to perform signal analysis.

RESULTS

Prior to the start of fatigue testing of the CFRP primary structure, NDI using the neway developed equipment and techniques was performed in the artificially induced defect areas.

Automatic pulse echo scan was performed on the accesible outer skin impact damage.

Pulse echo signals from the bonded probes around each interior defect were transformed through the multiplexor to computer memory.

Figure 5 shows a typical record of an automatic inspection of the external defects during the inspection. Figure 6 shows a group of probes bonded around an artificial defect.



Fig. 5. Impact damage. Typical record

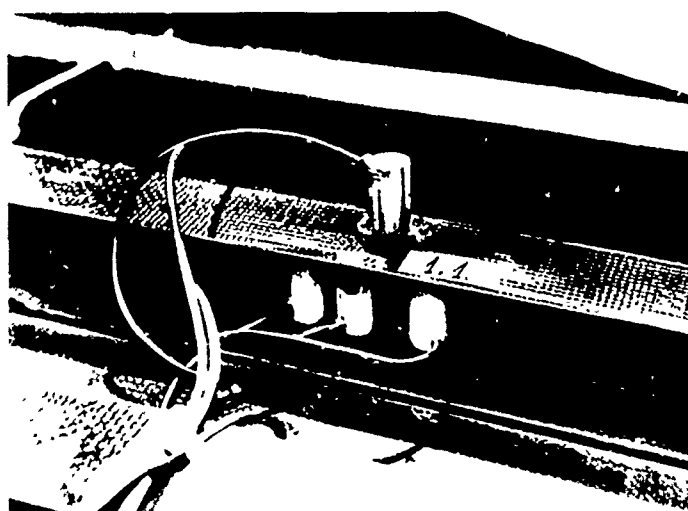


Fig. 6. Probes bonded

During the fatigue test consisting of two fatigue lives, two aging periods of 3 months at 70°C and 70% humidity and a third fatigue life, 15 periodic inspections were performed with the developed systems and equipment.

In summary,

- Outer defects:

A slight growth was observed in 4 of 9 damage areas this growth proceeded until a more or less regular shape with rounded edges was developed and then stopped.

- Inner defects:

No growth was observed in any of the 22 monitored areas.

Another important point, in addition to the inspection results, was the behaviour of the 84 probes that were bonded in different areas of the tested structure. Full 100% (84) finished the first fatigue life and subsequent aging still functioning, and 85% (71) functioned throughout the full test.

REFERENCES

Montero, F. (1986). CSIC. Madrid. Private communication.

Bryan, H. (1982). AGARD-LS-124. Oct.1982. Oporto (Portugal). 22 p.

Segal, E. et al. (1980). Proceedings DARPA/AFML Review of Progress in Quantitative NDE. 209-217.

Willert, V. (1985). MBB Hamburg Report Nr. TN-TE541-2797/85

AN ULTRASONIC SYSTEM FOR IN SERVICE NON DESTRUCTIVE INSPECTION OF COMPOSITE STRUCTURES

by

F.Boschetti, F.Cipri, L.Pugliese and M.Scolaris
Aeritalia — Defence Aircrafts Group — Laboratory Dpt.
C.so Marche 41, Torino 10146
Italy

ABSTRACT

In order to perform, directly on the airfield, the Non Destructive Inspection (NDI) of aerospace composite structures by mean of equipments similar to those already in use in the manufactory workshops, a new ultrasonic system has been developed by Aeritalia.

The system includes an ultrasonic telemetry device for the geometrical location of the U.S. transducer position on the structure to be scanned and an instrumentation for the acquisition and processing of the ultrasonic data by B or C scan representation.

The system operates in pulse-echo mode and provides in real-time a bidimensional representation of the intensity of the U.S. signals as well as the depth of the reflecting surface.

Some typical examples of inspection performed on composite primary structures during fatigue tests simulating service life are presented.

INTRODUCTION

The efficiency of Carbon Fiber Composite (CFC) structures can be optimized by designing and manufacturing monolithic components or assemblies.

Weight and cost savings may be achieved adopting suitable cure or cobonding techniques, and several integral structures have been developed for many new projects of military and commercial aircrafts.

At Aeritalia's Defense Aircrafts Group in Turin, the vertical fin and the horizontal stabilizer torsion boxes of the AMX tactical fighter are produced in fully cured CFC.

If compared with an equivalent design based on conventional light alloys, these primary components have a structural mass about 20% lighter and are 15% less expensive in manufacturing cost. Another example of CFC primary structure having very large integral (cobonded) components is the multispar delta wing box developed for the European Fighter Aircraft (EFA) by Aeritalia, British Aerospace and CASA.

The quality requirements for these primary structures are very severe and evidence must be provided that even very small possible manufacturing defects or in service damages can be detected.

Moreover, in service damages, like impacts, lightning strikes or fatigue delaminations around holes, not always require the immediate substitution or repair of the part in which they occur; periodical monitoring and reporting can be allowed, saving cost and improving the operational efficiency.

Following the above mentioned concepts, in order to enhance the Quality Control standards with improved NDT methods and provide an effective in-service NDI, a new instrumentation has been developed in accordance with these advanced design and manufacturing processes.

This system, identified by Aeritalia as F2, has been studied and integrated under a research program, including laboratory investigations for defect detection and characterization in complex geometry structural components or assemblies.

A special attention has been paid in providing the system of good operational adaptability to different types of composite structures and easy transportability for the handling on the airfields during the aircraft maintenance.

THE F2 SYSTEM

The F2 is a computer-based, flexible and fully transportable U.S. NDI system, able to test CFC structures by means of a man-handled transducer and a telemetry device or by means of a C-scan producing automatic device.

General performances

The F2 can be used to inspect CFC structures in pulse echo mode and provides in real time a bidimensional map of the ultrasonic data relevant to the scanned surface. Therefore, looking at a colour RGB monitor, the operator can immediately detect the presence of defected or damaged areas while inspecting the structural part.

The video image, stored by the computer, is a representation of two ultrasonic values: the intensity of the U.S. signal and the depth of the reflecting surface. The depth variation is represented by a suitable colour scale, while the received U.S. amplitude is represented by a scale of colour intensity (fading to black).

While controlling the scanning, acquisition and storage functions, the system software provides some image processing and statistics capabilities, like low-pass and high-pass filtering on the images, either on amplitude and/or depth data, edge enhancement and area calculation referring to a pre-defined depth. This makes possible to obtain precise data on single defects, like delaminations or inclusions, and raw data on areas in which porosity has occurred.

Finally the video images can be hard-copied on a colour printer. The system block diagram is shown in Fig.1.

F2 SYSTEM BLOCK DIAGRAM

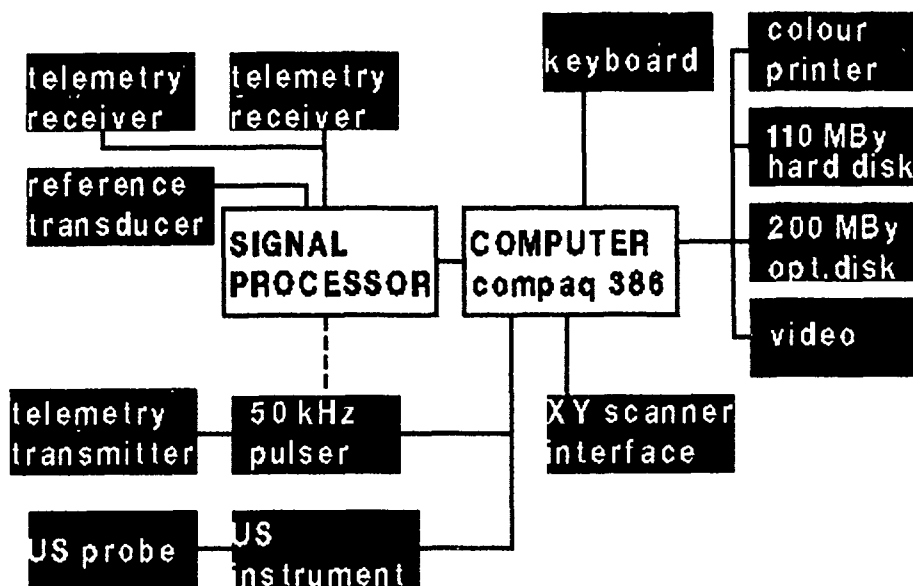


Fig. 1: F2 system block diagram

Scanning systems

In order to generate a map reproducing the geometry of the inspected structural part and to correlate the U.S. measures to the probe location, the F2 system has two operational options:

- a) manual scanning with an ultrasonic location telemetry
- b) automatic X,Y scanning with stepping motors

a) Location telemetry.

A dedicated ultrasonic device, with its own processor, locates the U.S. probe position on the structure surface with an accuracy of 1 mm. In particular the location telemetry is working with three U.S. transducers, one emitter and two receivers. The emitter is fitted to the NDT movable probe and the receivers are installed at the edges of the surface to be scanned.

The location of the probe, handled by the operator, is obtained through the analysis of the delay times of the emitted U.S. waves when detected by the fixed receivers. The scanned area and the probe location are presented in real time on the colour monitor.

b) Automatic X,Y scanning.

The inspection of low curvature surfaces can be performed automatically, moving the U.S. probe by means of a very light mechanical device (1.5 Kg), operated by computer controlled stepping motors. This facility scans the structure surface along two predetermined X,Y axis and allows a limited vertical displacement of the U.S. probe, in order to hold it in contact with the surface.

Ultrasonic instrumentation

A fully computerized U.S. instrument has been integrated in the F2 system. This makes possible to store and recall when needed the calibration data of the typical structural parts to be controlled. The U.S. frequency can be varied between 1 and 25 MHz whilst the sampling frequency variation ranges from 0.5 to 9 KHz. The U.S. intensity measures, expressed in decibels, have a dynamic range of 80 dB, with 1 dB resolution. These measures can be also referred to suitable standard samples.

Data storage and processing

In the F2 current configuration the data processor is a Compaq 386 personal computer, in charge to drive the scanning device, represent and process the acquisition data and print them. The U.S. data are stored on a 110 Mbytes hard disk, with the option of storage, for statistical purposes, on 200 Mbytes optical disks. To successfully drive the instrumentation, though, any AT-type personal computer with a 20 Mbyte hard disk is suitable. The U.S. data achieved by the pulse echo scan are:

- reflected signal intensity
 - depth (time delay between the transmitted and the reflected signals)
- The raw initial data are automatically corrected taking into account the absorption behaviour of the material and are averaged within an area of 1 sq.mm, to obtain the two U.S. values contained in a pixel of the final image.

After these operations then, each U.S. value represents the average response obtained from a number of each of the two kinds of data, depth and U.S. amplitude, coming from 1 sq.mm, which is the size of a pixel. Being 430x430 mm the useful field of the scanning device employed by the system in the current configuration, the usual size of the images is 430x430 pixel. However, there is no reason to be limited by this when working in the telemetry mode.

Alarm thresholds may be setted, in order to automatically detect certain kinds of structural damages; the areas exceeding these thresholds are recorded and computed.

The system can show the collected U.S. data using the following representations, both on the colour video and on the thermal printer:

- colour or B/W map of U.S. amplitudes

- colour or B/W map of reflected signal depths
- enhanced contrast colour map of U.S. amplitudes and depths: sixteen colours are available to define thickness bands selected by the operator, while 16 amplitude bands represented by fading-to-black colour are available for each depth interval.
- false colour map of U.S. amplitudes and depths. The thickness of the piece under inspection is represented by 32 iris colours, each of them can have 8 intensities.

Moreover:

- A zoom function is available on screen, with a range from 1 to 8 times the dimensions of the original image.
- A B-scan representation, either for amplitudes and thicknesses, representing any "horizontal" line of the image, can be shown on screen together with the related C-scan.
- There exists the possibility to study small and unidentified defects detected by the 1-mm-step mechanical device by means of another mechanical device with 1/10 mm steps. This provides a substantial magnification of the area under control; however, due to the time required to scan even a small area with this method, only in very special cases it is convenient to do so.

ALREADY PERFORMED EXPERIMENTAL WORK

Since the F2 system was operational, in order to initially set up it, a test program has been performed on CFC flat specimens simulating manufacturing defects and impact damages, through which the sensitivity in defect detection and laminate thickness measuring has been determined; in parallel the calibration parameters and the U.S. signal processing software have also been optimized.

At the end of this first test phase, the F2 system demonstrated the capability to detect defects smaller than 9 sq.mm (3x3 mm), just below the first ply (0.25 mm) and just over the last one. After that initial activity, a considerable amount of data has been collected on production cobonded structures, in order to characterize the different kinds of defects likely to be found in such cases and to determine the response of the system to them.

The typical geometry of the structures that are to be tested by the F2 system in pulse-echo mode from the external side are double curvature skin panels, stiffened by integral stringers and boxes with cocured/cobonded spars. An example of this kind of structures is shown in Fig. 2.

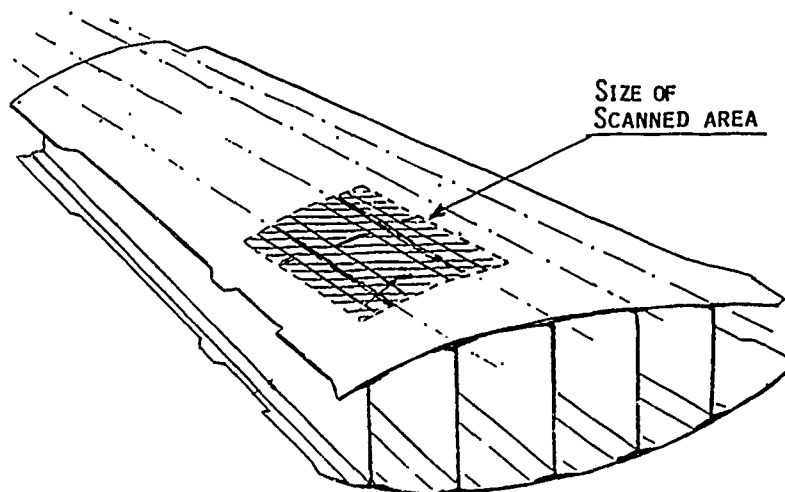


Fig. 2: a typical cobonded / cocured structure to be scanned by F2

Finally, to test the performance of the system on in-service conditions two cocured CLC torsion boxes were controlled during fatigue tests simulating service life. The two structures were affected by some manufacturing defects (mainly porosity), the growth of which was monitored versus simulated flight time, as is shown on Fig. 3.

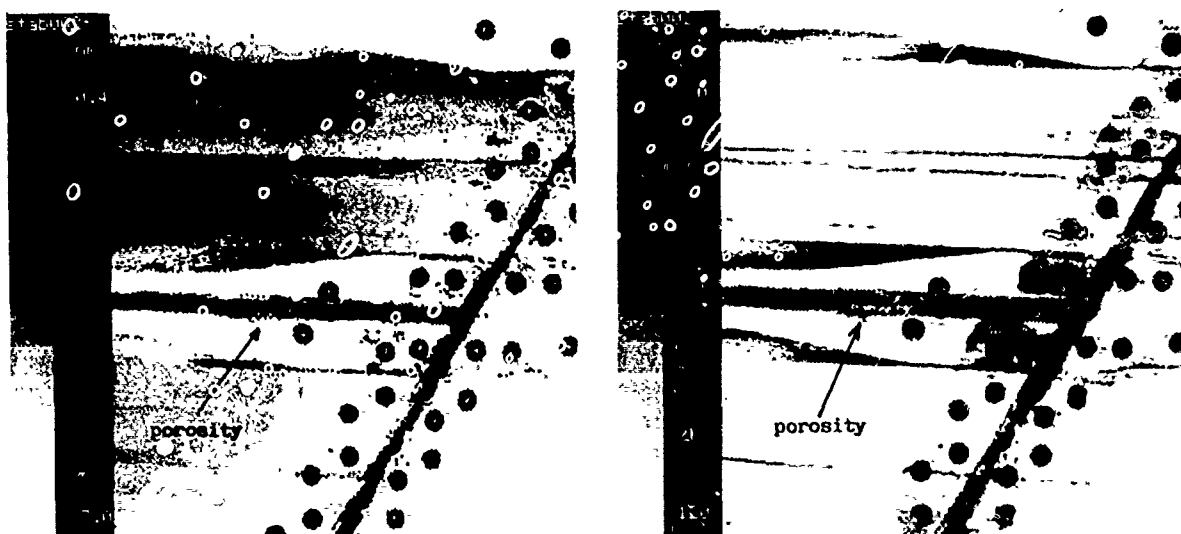


Fig. 3: porosity on fatigue-tested stabilizer scanned in depth (left) and in US amplitude (right).

As some of the defects already present in the structure before it was fatigue tested were repaired, the efficiency of the repair itself was checked (Fig. 4).

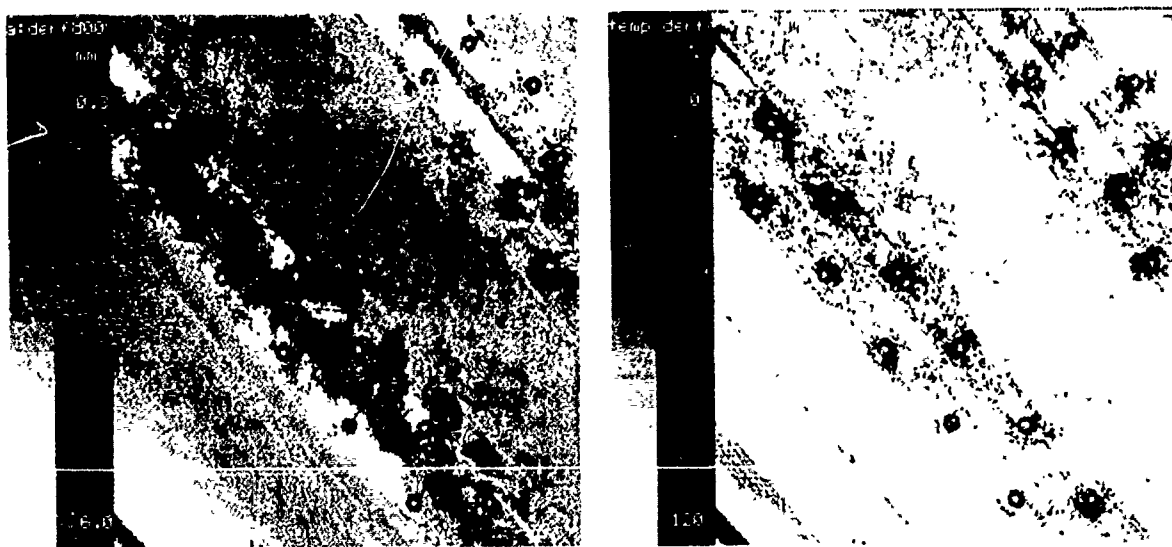


Fig. 4: repair on skin-spar disbonding, scanned in depth (left) and in US amplitude (right).

As was expected, during the fatigue test some more delaminations occurred and developed in stress concentration regions, where the main fittings were located. These delaminations were monitored versus time, too. Figure 5 shows the growth of one of these defects, starting from an aluminum fitting bolted to the CF skin panel.

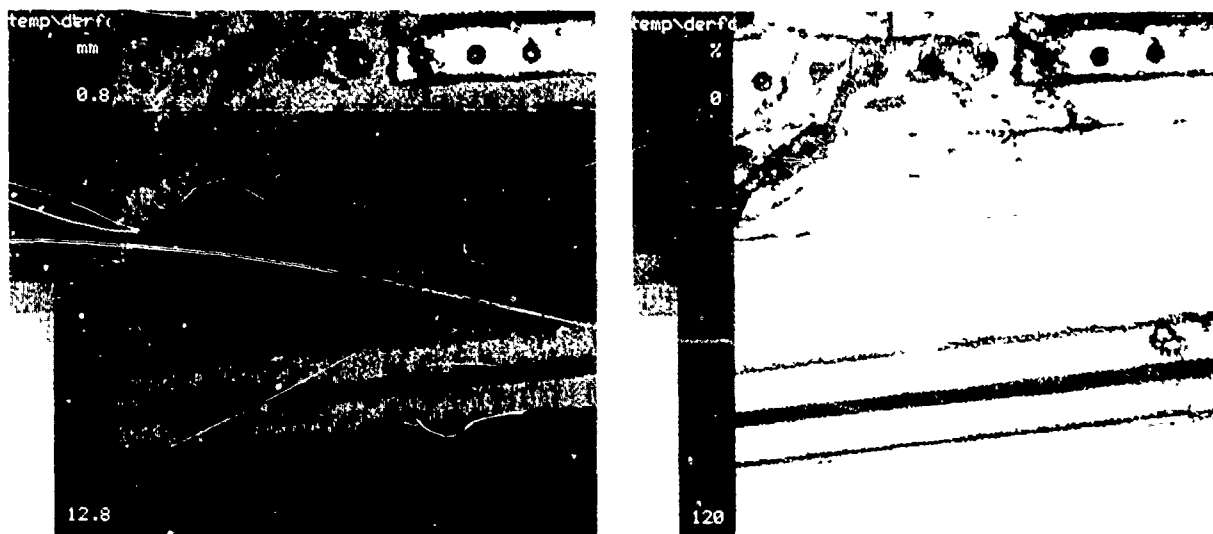


Fig. 5: delamination in stress concentration region, scanned in depth (left) and in US amplitude (right).

After successful completion of this tests program, evidence was provided upon the reliability of the F2 system in in-service conditions. Moreover, the data collected improved the already existing knowledge on the behaviour of composite primary structures during service life.

ONGOING TEST ACTIVITY AND FUTURE DEVELOPMENTS

Additional work is at present in progress to support the preparation of the F2 in-service NDT inspection manual for the CFC parts. This activity requires tests on several structural configurations, taking also into account the various surface treatments of the composite components, which give rise to different responses to the U.S. signals.

As the repair procedures of in-service damages are also to be specified, a significant amount of NDT work on damaged and repaired structures is scheduled in the nearest future. Researches are also in progress in order to provide the F2 system of the capability to automatically recognise the structural areas being inspected. This performance will allow to compare the results achieved on the same structure at progressive flight times, and to compare the U.S. scans of the same area on different structures.

Finally, to give the operator a better support when inspecting CFC structures, the F2 will be implemented by means of a dedicated expert system, able to recognize the presence of the main kinds of defects and to classify them, producing a report to be confirmed by the operator. A first step toward this objective has already been done. Producing a theoretical image of the part being inspected, in which geometrical data are included, allows to obtain an image showing defects only. In this case these are defined as areas with U.S. depth different from design. This kind of image can be generated subtracting the acquisition image from the reference one.

The final purpose is to produce a movable system provided of automatic diagnostic capability, so that the in-service NDT of aerospace composite structures may become more and more objective and cheap.

A Technique for Rapid Inspection of Composite Aircraft Structure for Impact Damage

Jerzy P. Komorowski, Ronald W. Gould

Structures and Materials Laboratory
National Aeronautical Establishment
National Research Council Canada
Ottawa, Ontario, Canada K1A 0R6

and

Walter J. Pastorius
Diffracto Ltd.
2835 Kew Dr.
Windsor, Ontario, Canada N8T 3B7

ABSTRACT

A technique using the Diffracto D-Sight method to locate indentations associated with low energy impact damage is described. In graphite/epoxy specimens good correlation was observed between internal impact damage as shown on ultrasonic C-scan images and indentations detected with the D-Sight method. Test specimens are currently mounted on an aircraft to observe the influence of in-service surface degradation on technique resolution. The method has the potential for inexpensive, rapid and objective detection of low energy impact damage over large areas of composite aircraft structure. Application of this method, because of its inherent reliability, could result in the increasing of the design allowable strain levels for some composite components. Included are two examples of possible application of D-Sight to metal aircraft for inspection of cold worked holes and detection of cracks.

Key words: composite materials, impact damage, D-Sight, barely visible, delamination, aircraft structure, damage tolerance.

Introduction

Advanced composite materials and especially graphite reinforced epoxies have captured an increased share of airframe business over the last 20 years. These materials offer high specific strength and stiffness properties and very good fatigue resistance. Unfortunately, the materials are sensitive to low energy impact damage from such common occurrences as hailstones, stones thrown off the runway or tools dropped by maintenance personnel. These impacts commonly referred to as Barely Visible Impact Damage or BVID can result in barely visible surface damage but significant internal damage.

The sensitivity to impact damage had to be taken into account by designers and certification authorities. Composite aircraft structures are expected to carry ultimate load when damaged. The level of this damage is related to current inspection capabilities and dictated design allowable strain levels for structures fabricated from composite materials. Regular in-service inspections of aircraft with ultrasonic scanning devices are not practical if only due to cost and time required for such inspections. Current inspection practices rely on visual detection of impact damage.

Komorowski [1] suggested the application of a Diffracto-Sight technique to the inspection of composite structures for BVID. Diffracto-Sight or D-Sight (developed by Diffracto Limited of Windsor, Ontario) is a patented [2] method of visualizing surface distortions, depressions or protrusions, as small as 10 micrometers. It is a real-time technique with particular application for the rapid inspection of large surfaces. Computer based image processing has been applied to D-Sight images. An image from previous inspection can be directly compared to current results for quick and operator independent identification of areas where changes in surface features have occurred. This allows an inspection-for-cause approach to be adopted which will reduce the requirement for more costly and sophisticated techniques such as ultrasonic methods.

In a previous paper [3] the significance of D-Sight to composite aircraft structure inspections was explored. Because of D-Sight's inherent reliability, it could be possible to increase the design allowable strain levels for some composite components.

The original experiments in the application of D-Sight to the detection of impact damage [1][3], involved a toughened graphite/epoxy system (IM6/F584). For this paper the existing data were expanded with experiments involving a more popular graphite/epoxy system (AS4/3501-6).

D-Sight

The optical set-up for D-Sight, described in Reference[4] and [5], consists of a light source, a retro-reflective screen and the object being inspected (Fig. 1). The surface being inspected must be reflective, however rough surfaces can be made reflective by wetting with a fluid. The D-Sight effect can be explained using geometric optical principles. If a flat surface with an indent is inspected then the light striking the indent is deflected. It then strikes the retro-reflective screen at a point removed from the light rays reflected from the area surrounding the indent. The retro-reflective screen attempts to return all these rays to the points on the inspected surface they left when first reflected. However, the screen consisting of numerous glass beads, returns a cone of light to the surface, not a single ray. This imperfection of the retro reflective screen creates the D-Sight effect. By backlighting the defect, the technique increases the light intensity on one side of the indent and reduces it on the opposite side. The process

can be viewed as a slope detecting technique with positive surface slope looking dark and negative slope looking light relative to the background. Both flat and moderately curved (in any orientation) surfaces can be inspected using this method.

The D-Sight technique is currently used to inspect car body panels and metal working dies and Diffracto has several commercial versions of D-Sight in production. The most complex systems include video cameras and computer based image processors. D-Sight images can be stored for future reference as video images on tape, digitally on computer storage media, or as video printer output.

Experiment

A total of 27 composite specimens (305x178mm (12x7in)) were manufactured at the Structures and Materials Laboratory of the National Aeronautical Establishment. Eighteen specimens were made using the Hexel IM6/F584 system and later nine specimens were made using the Hercules AS4/3501-6 system. Both systems are graphite/epoxy composites. The AS4/3501-6 is an older system and typical of the first graphite/epoxies used in large production runs (F-18, AV-8B fighters). The IM6/F584 is a system with tougher resin. Panels of three thicknesses (8, 24 and 48 plies) were manufactured using a [0/45/90/-45]_s lay-up. Each panel was numbered and cut into three specimens (A, B and C). The IM6/F584 specimens then received the CF-18 paint finish at the Defense Research Establishment Pacific. All specimens were inspected using ultrasonic C-scan. No manufacturing defects were found.

Before impacting, the specimens were inspected with D-Sight at Diffracto for surface characterization. The results were recorded using a video camera and image processor. A commercial solution of oil and kerosene was used to enhance the reflectivity of the specimen surface. This may not be an acceptable solution for aircraft application so recently Diffracto demonstrated the suitability of a combination of water and detergent for reflectivity enhancement.

The specimens were subjected to various levels of impact energy, ranging from 0.7 to 21.7 J (0.5 to 16 ft*lb), using a Dynatup Drop Weight Impact Test System[6] with a 25.4mm (1in) diameter spherical impactor. The resulting indentations ranged from non-visible to barely visible. Table 1 contains information on the energy level used, indent depth as measured by a micro profiler as well as the maximum dimension of any sub-surface delamination damage as measured using ultrasonic C-scan inspections. The micro profiler used was a Heideheim probe with stylus and optical read out scale mounted on a X-Y table from Anorad. The accuracy of the probe and X-Y table positioning was 1 micrometer. The readout was directly fed to an IBM PC.

A typical C-scan result for an impact damaged specimen is shown in Fig. 2. The damage size as measured on C-scans was plotted against impact energy for all AS4/3501-6 panels in Figure 3 and for 8 ply specimens for both material systems in Figure 4. As expected greater energy is needed to generate damage of a given size in thicker specimens. The brittle resin AS4/3501-6 specimens demonstrated more extensive damage than the tougher IM6/F584 specimens. The straight lines drawn in these plots were hand drawn for clarity of presentation and should not be treated as a rigorous attempt at conducting linear regression of data. Data available to date are preliminary and not numerous enough to conduct statistical analysis especially given the large scatter usually associated with impact studies.

The results of the D-Sight inspections of the impacted specimens along with pre-impact D-Sight images are shown in Figure 5 (for panel 297). To quantify D-Sight indent indication, the diameters of the dark and light spots on the D-Sight specimen image were measured. Since the specimens were compressed in the images to approximately 67% of their full width the measurements were non-dimensionalized. This was done by dividing all measurements by the width of the specimen in the image and multiplying by 100. This eliminated the scaling effect and measures thus produced were called relative D-Sight units. All D-Sight results in this crudely quantified form are included in Table 1.

The zoom lens of the video camera was adjusted such that the (305x178mm (12x7in)) specimens occupied the whole field of view. This made quantification of D-Sight images more precise. Figure 6 shows a D-Sight image of two specimens with impact indents 70 and 55 micrometers deep in the center of an area approximately 0.9 m wide and 2.1 m long (3x7 ft). As can be seen both indents are easy to locate. Without D-Sight these impact sites would be invisible to the unaided eye.

Figures 7, 8 and 9 show plots of D-Sight impact damage indication versus C-scan measured damage for both material systems for 8, 24 and 48 ply specimens respectively. These plots show that there is a correlation between internal damage detected by C-scan and external damage detectable by D-Sight. The more brittle AS4/3501-6 system experiences more internal damage relative to D-Sight detectable external surface deformation. For both systems only at very small internal damage levels was there no D-Sight indication.

The D-Sight based technique of impact damage detection relies on the impacting object leaving a permanent indent on the impacted surface. From the plot in Figure 10 it can be seen that at the low impact energy levels resulting in barely visible impact damage there is a fair correlation between indent depth and impact energy level. This observation is not significantly influenced by specimen material system or thickness.

Discussion

In order to assess the implications of using D-Sight for in-service detection of impact damage in aircraft composite structures a proposed design assumption will be used as a reference. Damage assumptions in the draft USAF damage tolerance design requirements are as follows[7]:

Scratches:

- Assume the presence of a surface scratch 100mm (4.0in) long and 0.4mm (0.02in) deep

Delamination:

- Assume the presence of an interply delamination that has an area equivalent to a 50.8mm (2.0in) diameter circle with dimensions most critical to its location

Impact Damage:

- Assume the presence of damage caused by the impact of a 25.4mm (1.0in) diameter hemispherical impactor with 136 J (100 ft*lb) of kinetic energy or that kinetic energy required to cause a dent 2.54mm (0.10in) deep, whichever is least.

The D-Sight images are very encouraging in that most indentations caused by the impacts were readily apparent. The exceptions are the impacts on specimens 296-A, 296-B and 356-A. The internal delamination damage for these specimens was 8, 8 and 16mm (0.3, 0.3 and 0.6in) respectively as measured from C-scans. The larger damage size was in the AS4/3501-6 specimen. Reference to the damage tolerance assumptions indicate that these delaminations are well below critical size. Hence the damage undetected by D-Sight is noncritical.

The impact indent assumption is well above the D-Sight threshold of 10 micrometers (0.0004in). The D-Sight detected damages are plotted as indent depth versus C-scan measured delamination in Figure 11 and versus impact energy in Figure 12. The damage assumptions from draft USAF damage tolerance design requirements are also shown in both figures for reference.

As part of a preliminary investigation, some of the impacted specimens are being flown mounted behind the nose landing gear of a T-33 aircraft operated by the NAE Flight Research Laboratory. After 56 hours of operation which involved 150 takeoff and landing cycles over a 10 month period, there is no indication that the aircraft service environment will affect the ability of D-Sight to detect impact damage.

Other applications of D-Sight in aircraft structures.

While the main subject of this paper is the application of D-Sight for composite material structures other applications of D-Sight to metal aircraft structures have been proposed recently.

Simpson [8] had suggested the use of D-Sight to detect cold worked holes. The process of cold working of holes introduces compressive residual stresses around the hole which extends the fatigue life of components by delaying crack initiation. The process is being used on aging aircraft as well as on new aircraft in production. Often large numbers of holes have to be cold worked and it is possible that some holes will be missed. Figure 13 is a D-Sight image of a Al 7075-T6 panel with holes. All holes except the middle row were cold worked and this is made clearly visible by D-Sight.

A panel of Al 7075-T6 alloy with a 3.2mm (1/8in) hole was subjected to cyclic loading and then inspected with D-Sight. The cracks extending from the hole can be easily seen. It is speculated that the plastic deformation at the tip of the growing crack leaves permanent deformation of the surface which in turn can be detected by D-Sight.

Conclusions and Recommendations

Based on this preliminary investigations, the following conclusions have been reached:

- D-Sight appears to have sufficient resolution to detect post-impact surface perturbations indicative of significant sub-surface damage;
- The D-Sight method has the potential for the rapid, inexpensive and reliable inspection of large aircraft external composite surfaces and may also be used for metal surfaces;
- Widespread application of D-Sight could lead to higher design strain allowables for some composite structures and it may significantly influence future certification requirements for composites.
- Full correlation studies between the D-Sight detection capabilities and the resultant damage must be undertaken to quantify any application limits. These studies must address the issues of material systems, lay-up, component surface coating, and normal surface degradation. Probability of detection data must be determined before the full potential of the method can be realized.

References

- [1] Komorowski, J.P., Gould, R.W., "A Technique for Rapid Inspection of Composite Aircraft Structures for Impact Damage", NAE LTR-ST-1664, March 1988.
- [2] U.S. Patent #4,629,319, Dec. 16, 1986.
- [3] Komorowski, J.P., Simpson, D.L., Gould, R.W., "A Technique for Rapid Impact Damage Detection with Implication for Composite Aircraft Structures", submitted for publication, April 1989.
- [4] Hageniers, O.L., "DiffraSight - a New Form of Surface Analysis", SPIE Vol.814 Photomechanics and Speckle Metrology (1987), pp.193-198.
- [5] Reynolds, R.L., Hageniers, O.L., "Optical Enhancement of Surface Contour Variations for Sheet Metal and Plastic Panel Inspection", SPIE Vol.954 Optical Testing and Metrology II (1988), pp.208-216.
- [6] Dynatup General Research Corporation, Drop Weight Impact Test System Model 8200 with GRC-730-I high speed data acquisition (Manual).
- [7] Whitehead, R.S., "Certification of Primary Composite Aircraft Structures", Proceedings of the 14 Symposium ICAF 1987, Ottawa, pp.585-617.
- [8] Simpson, D.L., Structures and Materials Laboratory, NAE-NRC, private communication.

Acknowledgments

The authors are grateful to Mr. T. Chapman of National Aeronautical Establishment (NAE) for performing C-Scanning tests and to personnel of the Defence Research Establishment Pacific for painting the specimens. Special thanks should go to the NAE Flight Research Laboratory personnel for flying of specimens on their aircraft.

This work was carried out under NAE Project 07336 task 4269, D-Sight Application to Aircraft Inspection.

TABLE 1. IMPACT AND D-SIGHT TEST DATA

NUMBER OF PLIES	SPECI- MEN	IMPACT ENERGY [J]	C-SCAN DAMAGE [mm]	D-SIGHT INDICATION	PROFILER [mm]
48	294-A	10.85	9.2	3.3	0.018
48	294-B	13.56	48.6	8.8	> 0.1
48	294-C	10.85	51.4	8.4	0.111
48	295-A	9.49	7.3	2.5	0.014
48	295-B	*13.56	44.4	-10.0	-0.137
48	295-C	10.85	18.3	7.0	0.094
24	296-A	4.07	8.3	0.0	n.v.
24	296-B	4.07	8.3	0.0	n.v.
24	296-C	5.42	29.3	8.5	0.051
24	297-A	10.85	33.9	9.5	0.104
24	297-B	8.13	30.3	7.6	0.089
24	297-C	4.75	25.7	6.5	0.07
8	298-A	5.42	22.9	6.8	0.063
8	298-B	0.68	7.3	1.8	0.016
8	298-C	6.78	26.6	6.0	0.07
8	299-A	1.36	12.9	3.3	0.028
8	299-B	4.07	18.6	5.1	0.055
8	299-C	4.07	24.3	7.2	0.055
48	357-A	10.85	32.4	5.5	0.104
48	357-B	16.27	40.5	5.5	0.108
48	357-C	21.69	56.6	7.1	0.235
24	356-A	2.71	15.8	0.0	0.0
24	356-B	5.42	23.7	3.2	0.093
24	356-C	8.13	35.6	4.0	0.133
8	355-A	2.71	22.5	3.9	0.05
8	355-B	1.36	14.8	1.6	0.024
8	355-C	4.07	35.6	5.6	0.067

* - Specimen was impacted from the back side.

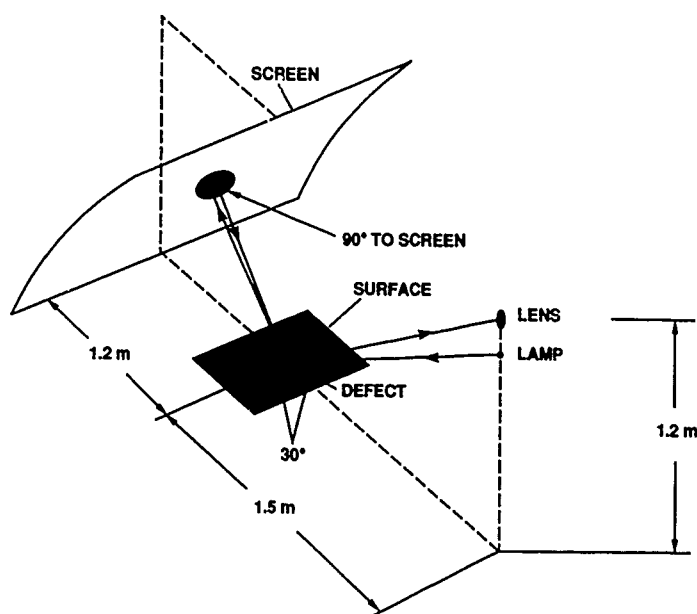


Figure 1. Diffracto-Sight optical set-up

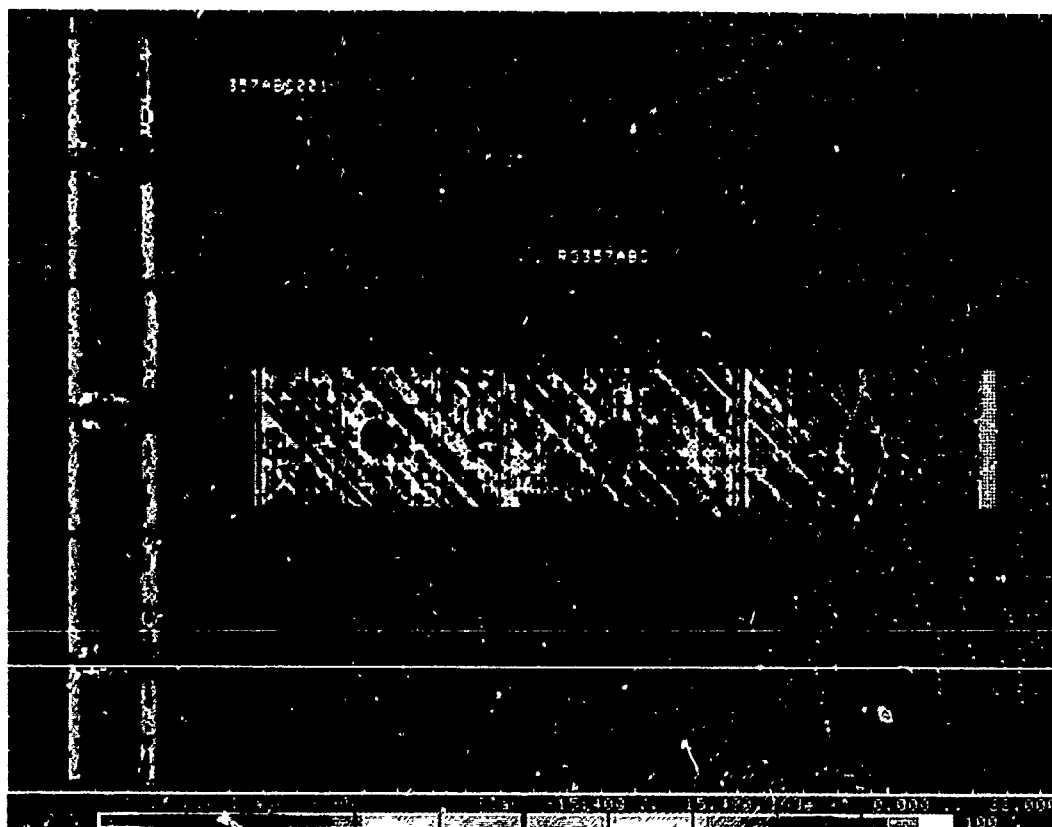


Figure 2. Typical C-scan result for impact damaged specimens
(Panel 357 specimens A, B and C)

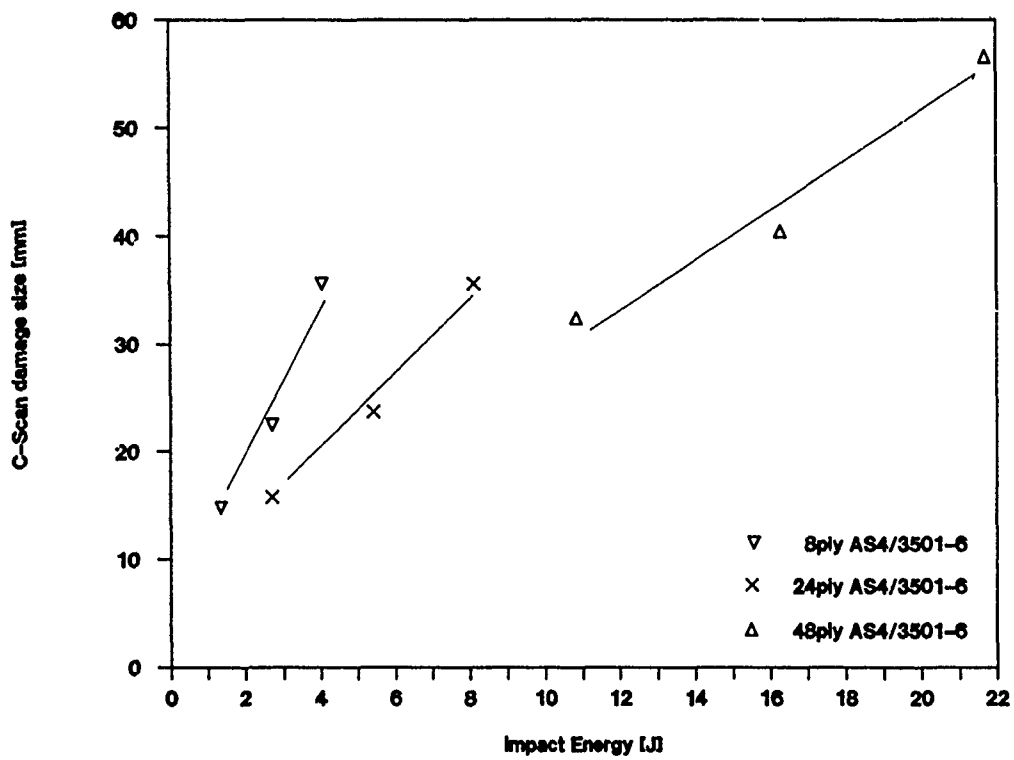


Figure 3. C-scan damage size vs Impact energy

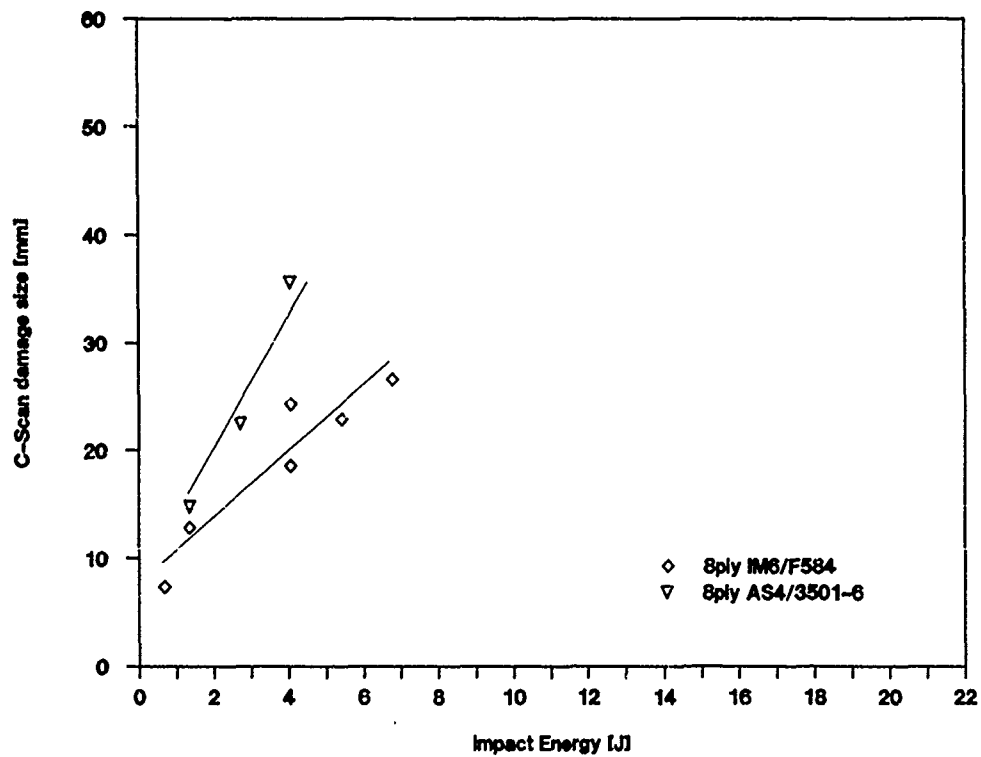


Figure 4. C-scan damage size vs Impact energy

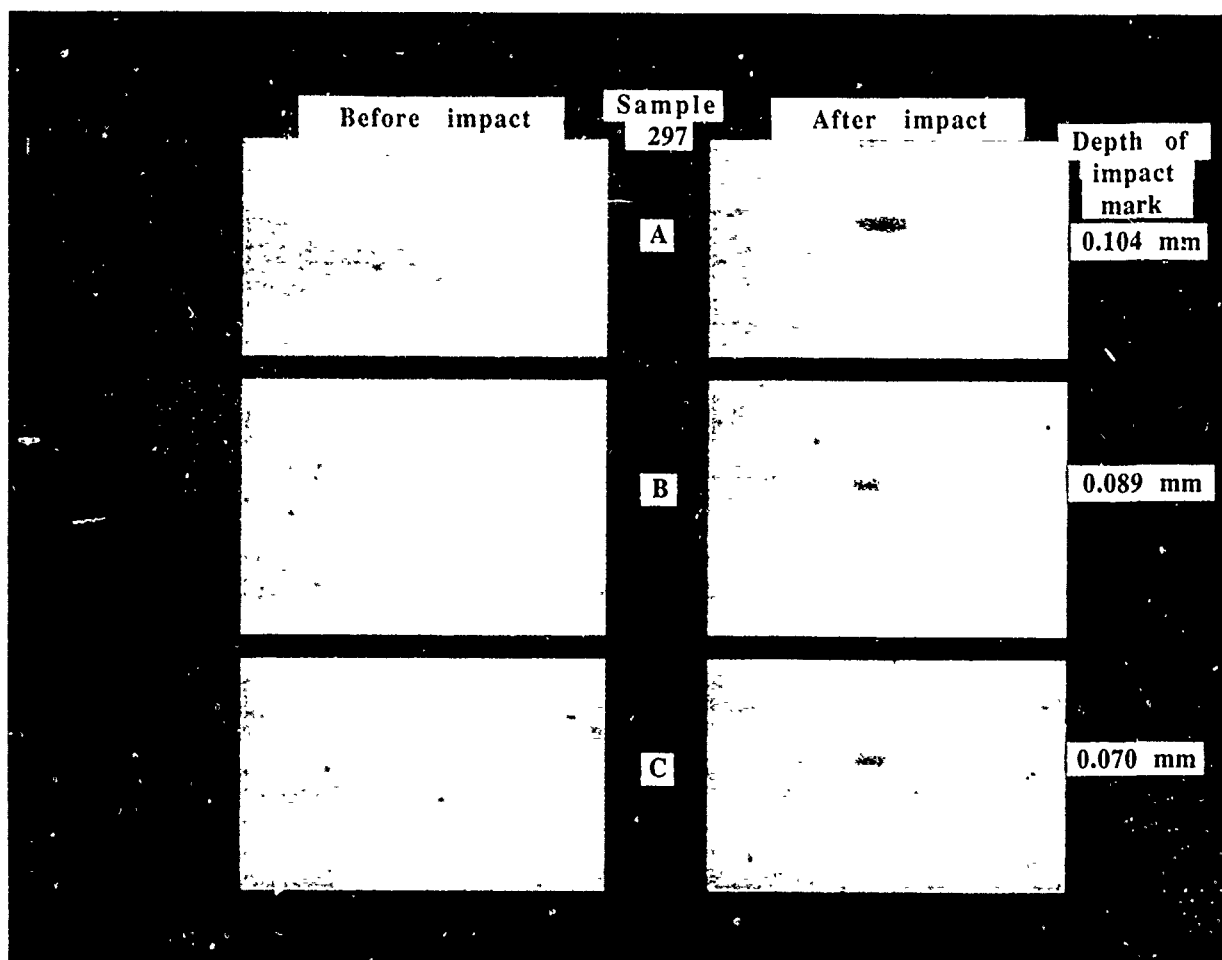


Figure 5. D-Sight images for panel 297

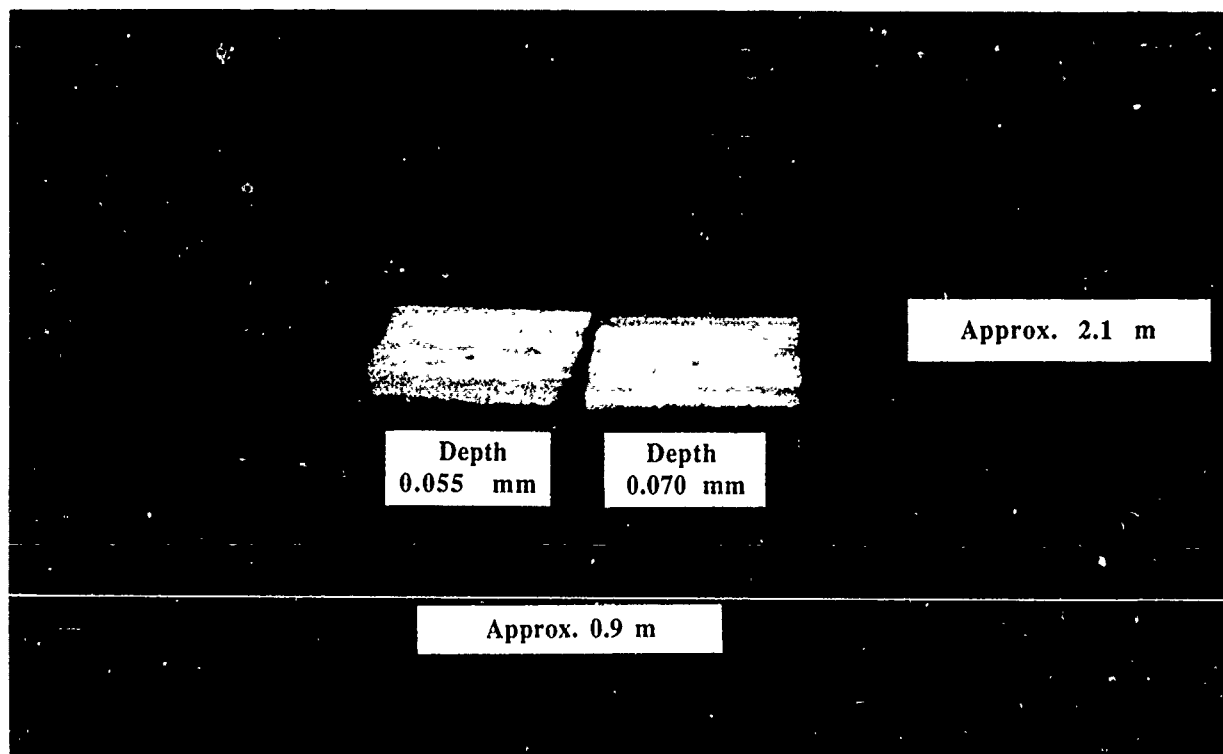


Figure 6 D-Sight image of two impacted specimens.
Field of view 0.9 m wide by 2.1 m deep

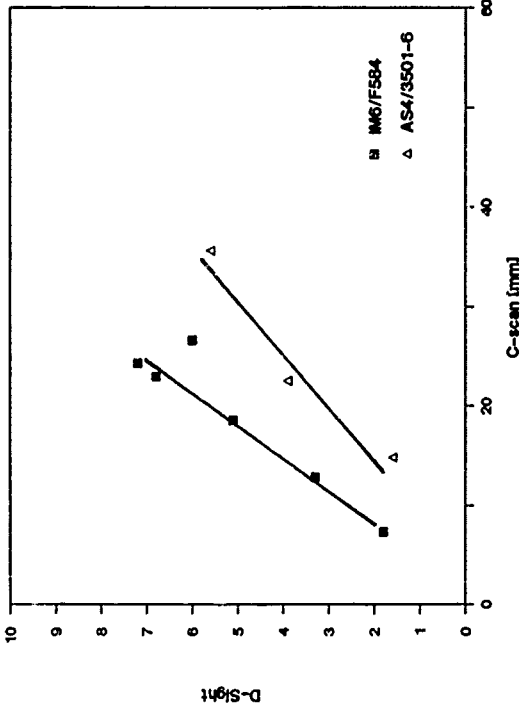


Figure 7. D-Sight vs C-scan for 8 plies thick panels

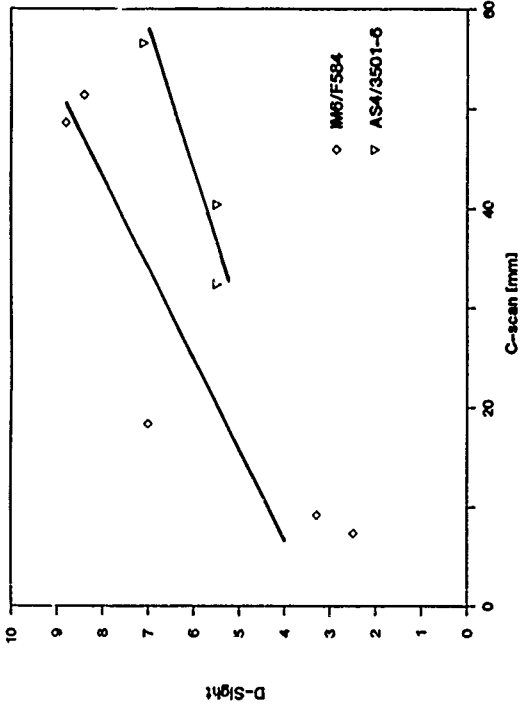


Figure 9. D-Sight vs C-scan for 48 plies thick panels

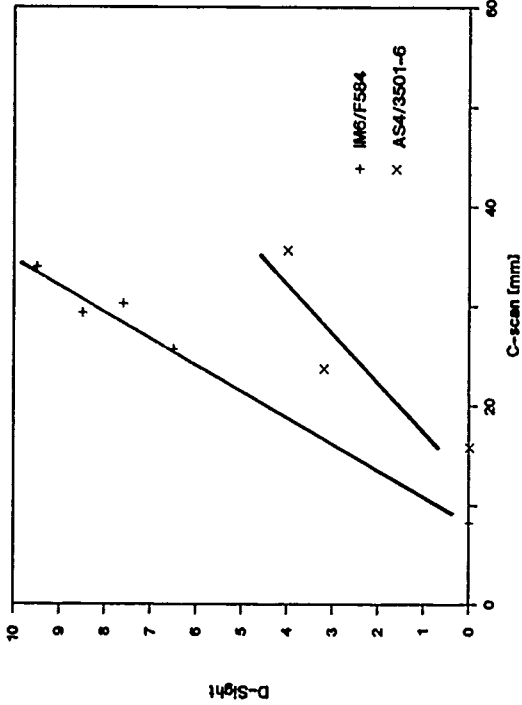


Figure 8. D-Sight vs C-scan for 24 plies thick panels

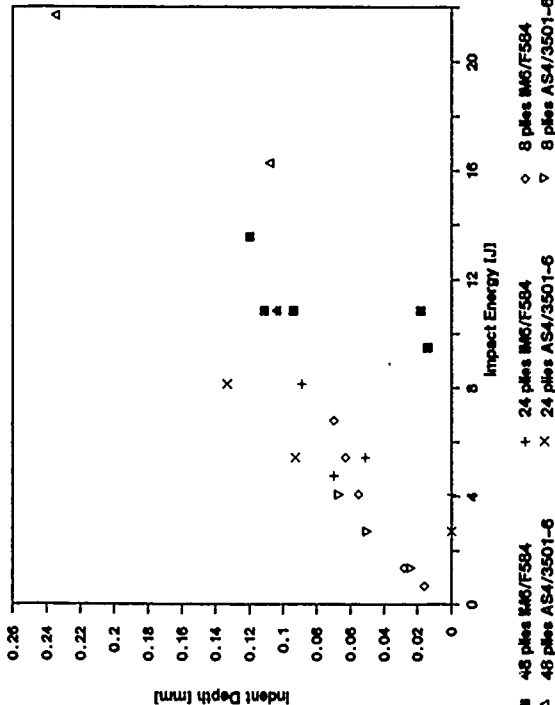


Figure 10. Indent depth vs Impact energy

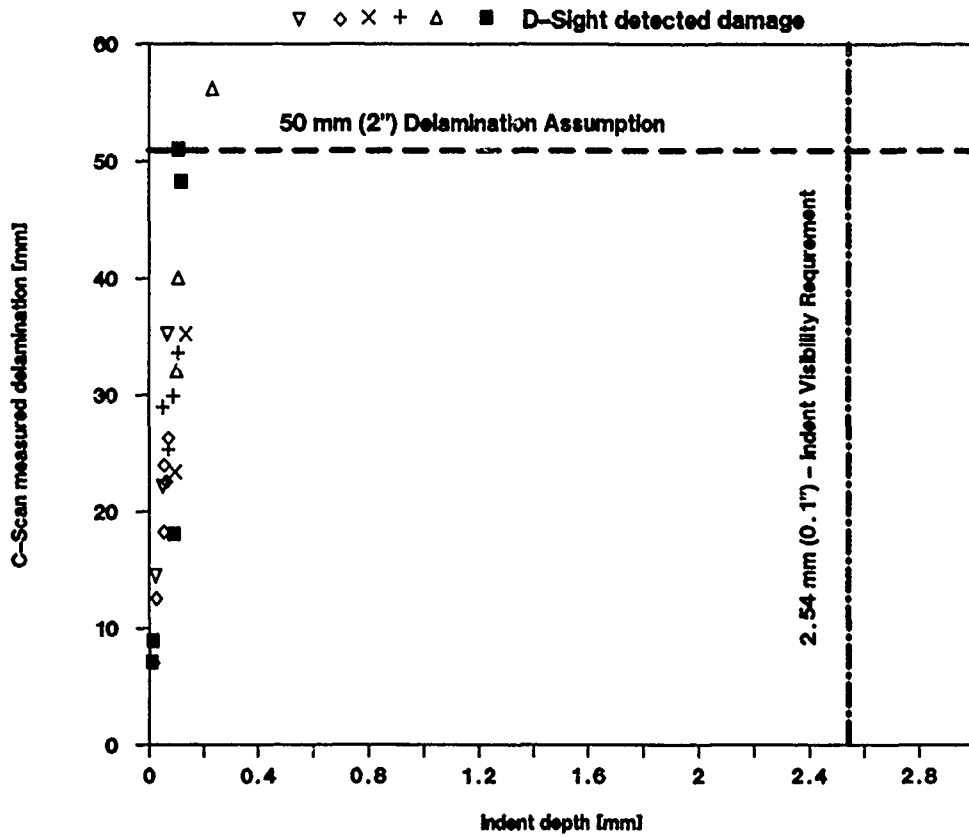


Figure 11. D-Sight and damage assumptions in draft USAF damage tolerance design requirements

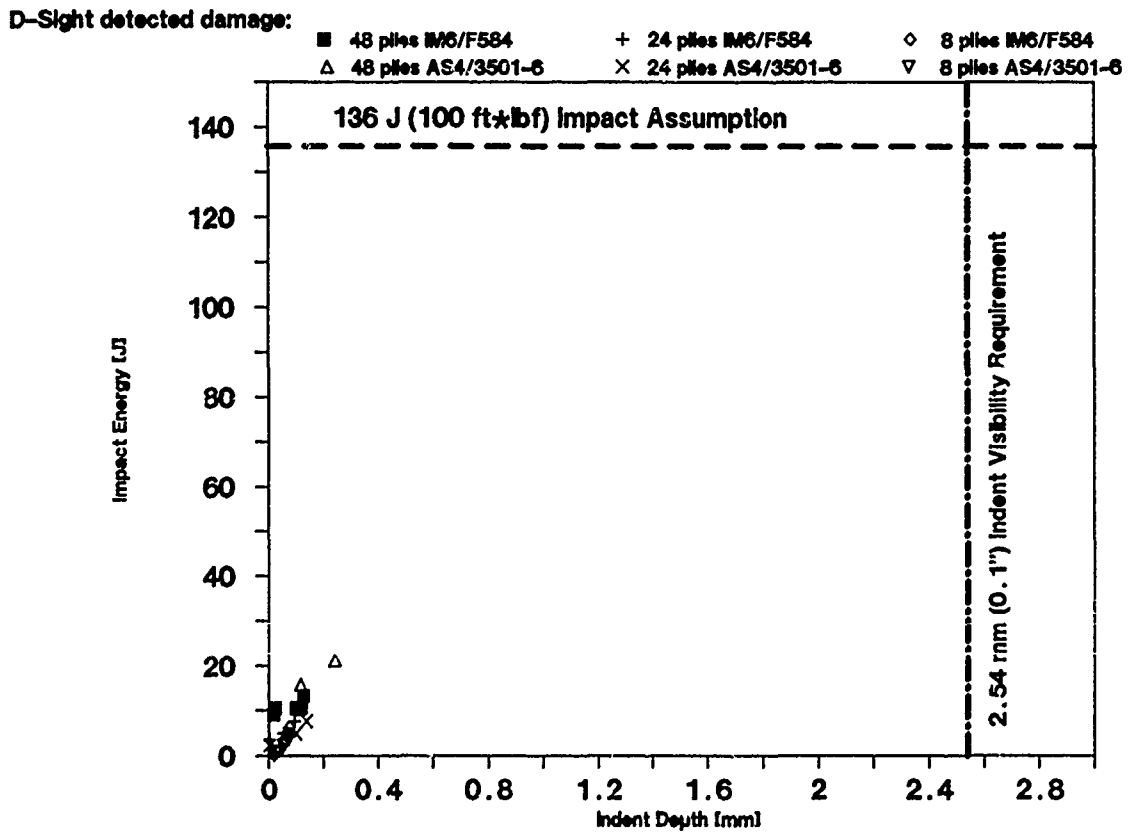


Figure 12. Impact energy vs indent depth and damage assumptions in draft USAF damage tolerance design requirements

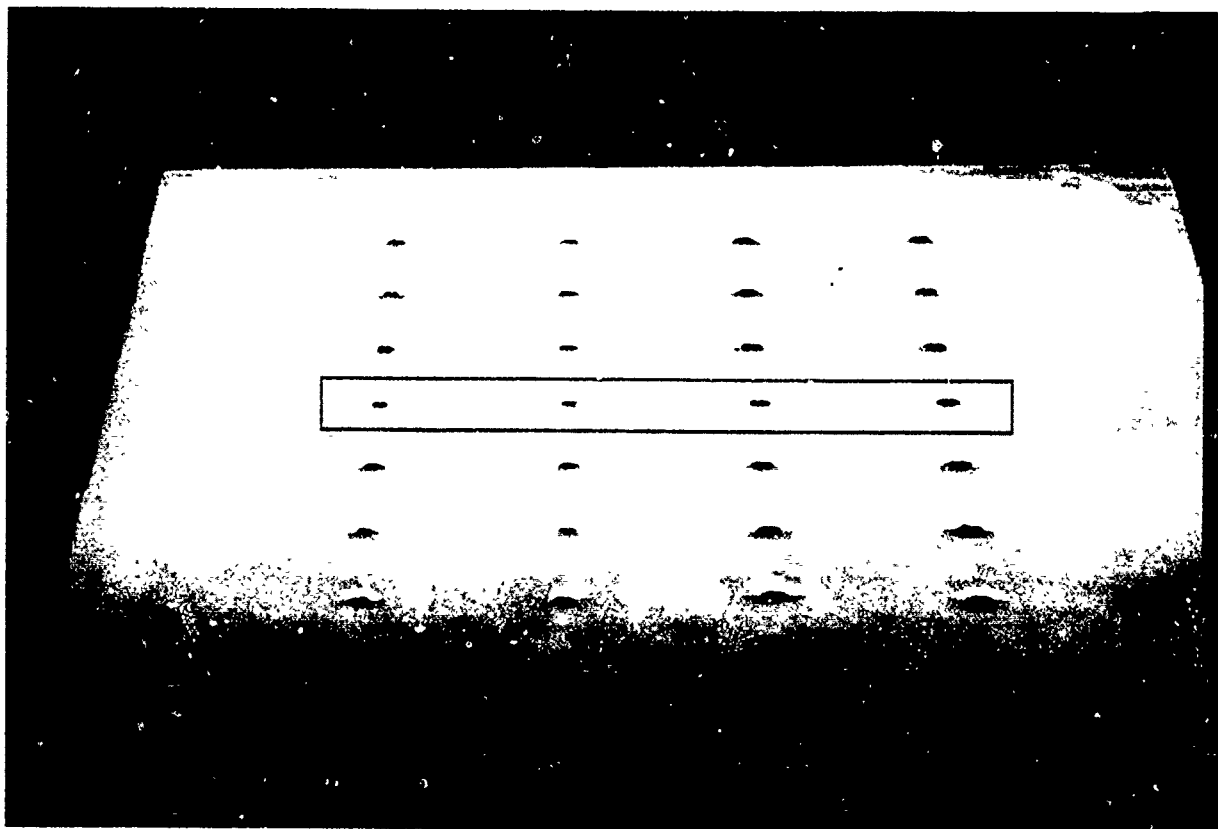


Figure 13. D-Sight image of Al 7075-T6 panel with cold worked holes

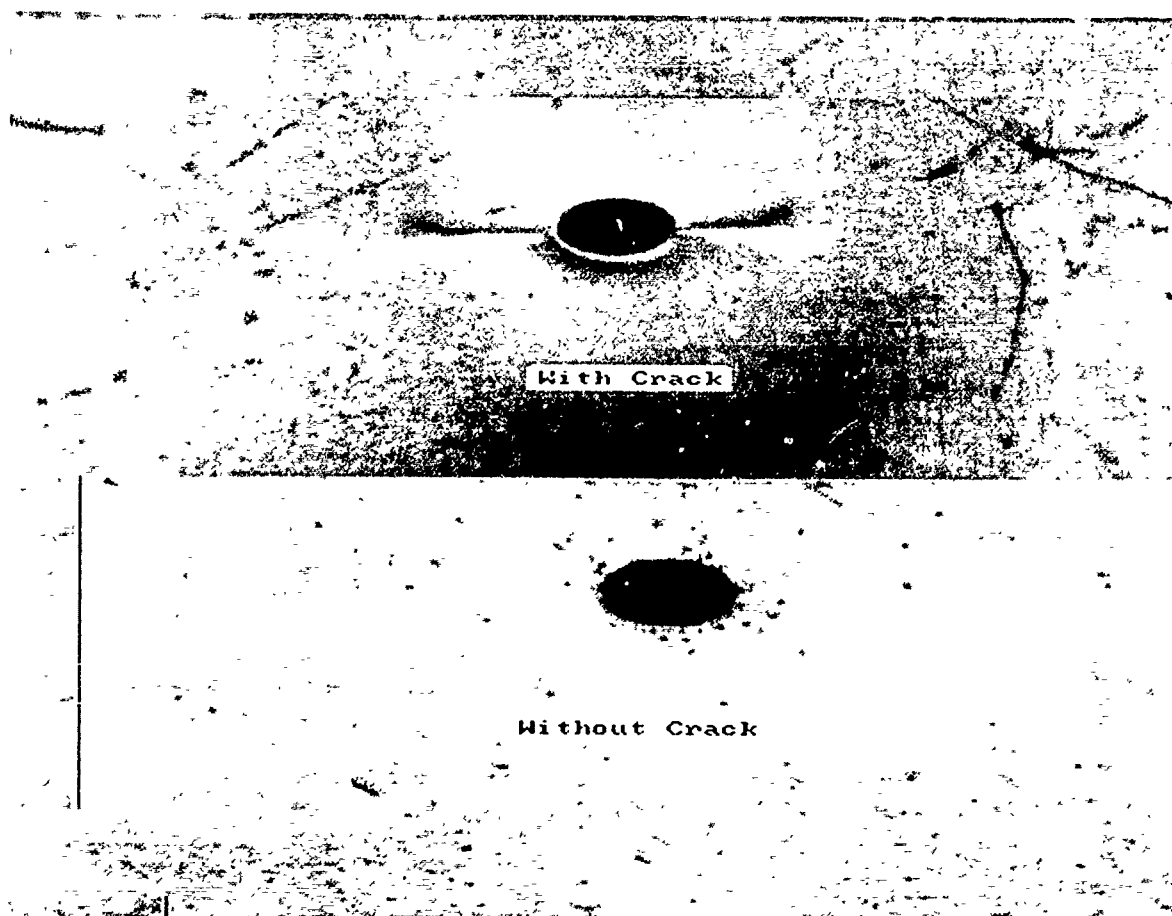


Figure 14. D-Sight image of Al 7075-T6 panel with a hole.
The cracks extending from the hole are clearly visible.

In-service Inspection of Composite Components on Aircraft at Depot and Field Levels

by

Noel A. Tracy
Senior NDE Engineer/NDE Project Manager
Universal Technology Corporation
4031 Colonel Glenn Highway
Dayton, OH 45431-1600
USA

Grover L. Hardy
Project Engineer
Materials Integrity Branch
Systems Support Division
Wright Research and Development Center
Materials Laboratory WRDC/MLSA
Wright-Patterson AFB, OH 45433-6523
USA

Frank J. Fechek
Project Engineer
Materials Engineering Branch
Systems Support Division
Wright Research and Development Center
Materials Laboratory WRDC/MLSE
Wright-Patterson AFB, OH 45433-6523
USA

SUMMARY

ARIS, which is the acronym for Automated Real-Time Imaging System, is a modular, easily transportable, field-ready, ultrasonic system that provides automated, simultaneous recording and real-time display of ultrasonic data and search-unit position during routine manual inspections of laminar and sandwich aircraft structures. The Materials Laboratory of the U.S. Air Force Wright Research and Development Center sponsored the development of ARIS and subsequently evaluated the system in both laboratory and field environments with the aid of an independent contractor. During the evaluation ARIS was used on many aircraft structural components to determine if the system operated according to specifications and to discover ways of improving its applicability and usefulness. Suggested modifications addressed new applications of ARIS, the convenience and comfort of using ARIS, and the appropriateness and logicity of the software. Apart from its use on aircraft parts, ARIS was evaluated for transportability, ease of set-up, operational defects and hardware reliability.

This paper includes pictorial examples of ARIS in use and discussions of all aspects of the field evaluation. The versatility of ARIS is evident through the many features in the original design and the seemingly minor modifications in hardware and software that enhanced the features so that ARIS turned out to be more widely applicable than originally planned. ARIS has a definite place in the portable C-scan arena.

INTRODUCTION

ARIS was developed by Southwest Research Institute on a contract with the Manufacturing Technology Directorate of the Air Force Wright Research and Development Center (WRDC). This development followed a previous contract with General Dynamics, Fort Worth Division that resulted in prototype equipment which established the validity of the concept. ARIS is a modular, portable, field-ready, ultrasonic inspection system which automatically records ultrasonic data and displays it in C-scan format in real time. The system facilitates inspection of laminar structures using existing ultrasonic techniques. An operator can use ARIS programs to analyze data immediately after completing an inspection or can archive the data on 3.5-inch magnetic floppy disks. Archived data can be retrieved at any time for analysis, processing or hardcopy output. ARIS has a unique comparative analysis program which subtracts the original data set from a subsequent data set for the same component and displays only flaw growth.

Universal Technology Corporation (UTC) and WRDC personnel took the first (pre-production) ARIS to Edwards, Hill, Randolph and Charleston Air Force Bases for field evaluations after using the system on laboratory specimens at Wright-Patterson Air Force Base to become familiar with its operation. The evaluation covered both software and hardware capabilities and focussed on features that make the ARIS fail-safe, inspector-proof, versatile and easy to use. Southwest Research Institute implemented some suggested changes between visits to bases and resolved all remaining modification issues prior to assembling four production units which were shipped to Air Logistics, Flight Test and Air Training Centers for extensive field evaluations by Air Force nondestructive inspection (NDI) personnel in their own working environments. The sequence of the discussion and photographs that follow deviates from the chronology of the equipment evaluation and modifications in order to clearly highlight the demonstrated practical aspects and operational features of ARIS.

TRANSPORT AND SET-UP

ARIS was designed to be transportable from one base to another as airline baggage, by one person if necessary. Figure 1 shows an ARIS configured for shipment except for the wheels which are easily removed for travel inside the thin container to which they are attached. Each container meets the airline regulations for baggage and can be easily handled by a fit individual. The equipment inside is padded to prevent damage. The final tally on a production ARIS unit is 13 containers.

Assembling an ARIS into an inspection configuration takes 15 to 20 minutes. It can then be wheeled to the inspection site as shown in Figure 2. Four primary modules remain in their shipping containers which are stacked on the mobile cart made from half the thin container. The other half of the thin container sits on top of the stack and serves as a shelf for the smaller equipment. One group of NDI technicians, that witnessed the assembly process only once, was able to repeat the process a day later on their own, including all electrical connections which are clearly marked and can be made only one way. Straps hold the stack together. Two persons can lift the stack into the back of a

pick-up truck or a van for transportation to sites beyond walking distance. The wheels can be locked when necessary.

HAND-HELD PROBE

The probe (Figure 3) was designed for comfort and convenience. The door-knob handle fits comfortably into an inspector's hand, a prime requirement in the ARIS contract specification. Above the door-knob, out of the way of an inspector's hand, is the sonic emitter which transmits the signals that the computer uses to triangulate the position of the probe. Since the ultrasonic transducer and plastic delay line are held in place with threaded fittings, either can be rapidly exchanged. Instead of a plastic delay-line an inspector can substitute a fluid-filled boot assembly from the through-transmission yoke which is described in a later section.

ARIS ON AIRCRAFT

Figure 4 shows the probe in the hand of an inspector as he scans the composite-laminate wing skin of an X-29. Only the equipment shown needs to be at the inspection surface, which may be up to 50 feet (15.24 meters) away from the rest of the ARIS equipment. The long device in the foreground, the sound bar, contains two microphones which receive the sonic signals from the emitter at the top of the probe. The keyboard allows the inspector to remotely operate ARIS during the entire inspection, even to the point of changing the settings on the ultrasonic instrument. The inspector is watching the generation of the real-time C-scan image of the ultrasonic data on the color monitor as he moves the probe. The packaging of the monitor shown in the figure was temporary pending completion of the evaluation of the color format versus the originally specified shades-of-gray for the data display.

Figure 5 is a typical set-up on a vertical stabilizer on an aircraft. The unevenness of this inspection surface required tape to be used over the suction cups as added insurance against impact damage that would be caused by the sound bar falling onto the horizontal stabilizer. The addition of two more suction cups and other modifications made to the sound bar will be discussed below. The sheathing on the bundle of cables attached to the equipment at the inspection surface was added to prevent the otherwise inevitable tangling experienced early in the evaluation. A further modification resulted in the cables being divided into two bundles over the last eight feet (2.44 meters), one bundle going to the sound bar and the other going to the monitor and keyboard. This logical division reduced the number of cables pulling on the sound bar.

Another thing to note in Figure 5 is the position of the inspector. The position is not uncomfortable, but any crouched or bending position is hard to maintain very long. Through trial and error, an inspection aid (Figure 6) evolved. A lightweight handle assembly allows the inspector to suffer less fatigue while scanning vertical and overhead surfaces. The assembly obviously extends the reach of the inspector also. The handle is detachable so the block holding the probe can be used as another way for an inspector to grasp and scan with the probe (Figure 7). Any variety in handle shape reduces hand fatigue, and the block also provides additional stability to the probe. A slight convex curvature machined on the end of a plastic delay line compensates for any liftoff that is encountered because of the three-point contact that the block/probe assembly makes with uneven aircraft surfaces. Loosening a single thumbscrew quickly releases the probe from the block.

C-SCAN DISPLAY AND ANALYSIS

Figure 8 is a black-and-white photograph of a color C-scan displaying time-of-flight data for a section of the F-16 vertical stabilizer that was being scanned Figure 7. The stabilizer, no longer serviceable for flight, was in a shop prior to some impact tests. The broad bands on the C-scan record indicate the normal pattern of thickness changes in the graphite-epoxy stabilizer skin while interruptions in the normal pattern indicate internal damage not visible on the surface. The color bar to the left of the C-scan quantifies the data. The white cross in the left corner of the C-scan indicates the position of the probe as the inspection of the first region is being completed. The unscanned black area in the middle matches the insignia decal and is a second inspection region, which in this case requires the gain of the ultrasonic instrument to be increased for a proper inspection. When the inspector wants to scan another region, he indicates to ARIS the next region he wants to scan by following prompts that the ARIS software provides. ARIS then automatically loads a new set of predetermined ultrasonic parameters into the ultrasonic instrument and the inspector scans the second region. ARIS provides for up to nine regions and a corresponding number of ultrasonic-parameter sets to accommodate varying structures or inspection conditions within the inspection area covered by one placement of the sound bar assembly.

A region is a polygon of up to 20 sides. Before inspecting a part, the operator outlines the regions on the video monitor by moving the probe to successive vertices of the respective polygonal inspection areas. The complete outlined area (template) for a given placement of the sound bar is referenced to permanent features or known locations (target points) on the inspected part. The template and target points are saved on a floppy disk and retrieved for use at the next periodic inspection, so direct comparison of entire C-scans can be made. The target points are also saved with the data so that after an inspection, during post-processing analysis of the data, an inspector can locate individual data points with respect to the two closest target points. If he selects a data point at the center of a flaw indication, he can locate the flaw on the inspected part with rectilinear coordinate information provided by the ARIS analysis program.

Color presentation of C-scan data was chosen instead of gray-scale because the colors facilitate recognition of abnormal data patterns and visual assignment of quantitative depth or amplitude values (from the color bar) to specific data. The post-processing features of ARIS help to clarify the C-scan data if patterns are not readily apparent. An operator may make selections to have the data presented in seven, five or three colors instead of the maximum fourteen, or he may change the range of data represented by each color. The operator can choose to view a magnified image of any rectangular area of data within the original C-scan (Figure 9) and can also get point-by-point quantitative data values which, for example, can provide a thickness profile with resolution down to 0.001 inch (0.025 mm). The operator can instruct ARIS to produce a hardcopy of any video presentation or any group of digital data. By taking the hardcopy

of the flaw indications to the inspected part, he can outline a flawed area for further nondestructive evaluation or, if necessary, to aid repair.

FLIGHTLINE INSPECTIONS

Inspection of a developmental composite section of the C-141 leading edge was a good test for the remote operation of ARIS. Figure 10 shows the inspector standing on a workstand just inboard of the left inboard engine, still well within the 50-foot (15.24-meter) limit for remote operation. Figure 11 is a closer view of the inspector doing one of the most fatiguing scans (with or without ARIS), the underside of a wing. Since that area of the leading edge was smooth and nearly flat, the suction cups held the sound bar well as long as the cable bundle was secured to prevent unnecessary force on the sound bar. The inspector is watching the C-scan being created on the video monitor resting on the workstand with the keyboard. When the underside of the wing was finished, the inspection continued on top.

The object of the inspection in Figure 12 is the left cargo door at the rear of the C-141 aircraft. Because the sonic emitter at the top of the probe is four inches above the inspection surface, ARIS must correct the probe coordinate information when the inspection surface is curved. ARIS can compensate for a cylindrical surface with a radius of curvature of four feet or more if the sound bar is parallel to the axis at the center of curvature. Even if the radius of curvature is less than four feet, as is the case with the leading edge of the wing, an inspection is still possible. Even though the data will be distorted, data from later scans can be compared as long as the inspector orients the sound bar the same way relative to the curvature each time. He can note the orientation in the comment section of the inspection parameters saved on a floppy disk. He can also comment on the amount of distortion, which he determines by comparing the movement of the probe to the corresponding movement of the cursor on the video monitor.

During flight-line inspections electrical power is provided by mobile generators (Figure 12). These generators are not noted for their stable voltage outputs, but ARIS operated well with them. If the voltage suddenly drops below the minimum requirements (or somebody pulls the plug), the internal batteries in ARIS take over and supply power to the volatile memory. The inspection can continue when the power is restored; the inspector simply resumes scanning as if nothing had happened.

The inspector needs reasonably fair weather to use ARIS on the flight line. However, too much sun is disadvantageous when trying to view video monitors (Figure 13). A glare screen and a light shield on the monitor provide some relief. The light shield in the form of an extension of the monitor enclosure on the front of the ultrasonic instrument are seen in Figure 14. Mounted inside the shield on the ultrasonic instrument is a video camera which transmits the A-scan to the video display at the touch of a key on the keyboard during remote operation. The availability of the A-scan at the remote inspection surface was requested so that ultrasonic responses can be monitored if the inspector has to alter the ultrasonic instrument settings or if he wants to investigate the cause of a certain data point on the C-scan. He can also save A-scans for reference. The C-scan image returns with another touch of the same key.

ADDITIONAL MODIFICATIONS

Figure 14 shows the configuration of the ARIS production units which incorporate modifications suggested as a result of the evaluation of the pre-production unit. A handle, adjustable front legs, and strain relief improvements that were added to the new enclosure for the video monitor. The modified sound bar assembly has more suction cups, and each pair can rotate and slide along slots in the bracket to accommodate various surfaces and conditions. The sound bar itself rotates around its axis so the inspector can adjust the angle for optimum reception of the signals from the sonic emitter in the probe if the sound bar assembly cannot be mounted on the surface as the probe is scanning.

The sound bar can also be removed from its base and mounted on a tripod. In Figure 15 the inspector is scanning a graphite-epoxy frame on a 5-ton truck which was a composite demonstration vehicle built for the Army. Without a tripod this inspection cannot be done because the sound bar cannot be attached to the truck in a manner required for a proper inspection. The idea for a tripod originated when the evaluation team tried to scan doors on the F-18 landing-gear wells. When the sound bar was mounted on the small nose gear door, little of the door surface was available for scanning. If the tripod had been available to hold the sound bar adjacent to the door, the entire door could have been scanned. The main landing-gear doors were larger but still had less than the 16 ft² (1.49 m²) which can be inspected with one placement of the sound bar. Therefore, an entire door could be scanned more efficiently with the sound bar on a tripod next to the door.

THROUGH-TRANSMISSION CAPABILITY

The through-transmission yoke is another unique feature of ARIS that is useful for inspecting honeycomb sandwich structures, such as the F-16 ventral fin in Figure 16. Compressed springs within the lightweight tubular members at the hinged end of the yoke provide the force to keep the transducers in contact with the surface of the part as the inspector moves the yoke back and forth. A closer view of the parts of the yoke are shown in Figure 17. A pair of extension tubes (pictured below the main frame) slide into the respective center tubes at the end of the frame. Quick-release pins hold the extensions in positions appropriate to the width of the part being inspected. At full extension the yoke will extend over a part three feet wide. Longer extensions, allowing a reach of four feet, have been used to successfully scan all empennage components of F-15 and F-16 aircraft.

At the bottom of Figure 17 are two nylon blocks with fluid-filled boot assemblies that hold the probe and a second ultrasonic transducer. To keep the sonic emitter facing the microphones in the sound bar, the inspector rotates the probe within the boot assembly by loosening a thumbscrew. Each block has a gimbal to allow slight pitch and roll movements so the blocks will conform to contours on the part being inspected. The inspector mounts the blocks on the extension tubes by inserting the boss on the gimbal into the hole in the end of the respective extension, adjusting the yaw angle of each block so the boots are facing each other, and inserting the quick-release pins to hold the bosses in

their respective holes. The inspector can change the yaw angle as necessary to allow him to scan the boot assembly up to and along all edges of a part while keeping the blocks on the part or away from adjacent, interfering structures. A set-up showing both probe rotation and block angulation is shown in Figure 18. The versatility and light weight of the through-transmission yoke is illustrated again in Figure 19.

OTHER APPLICATIONS

The boot assembly with the probe can be detached from the block in the through-transmission yoke and used separately. A nylon ring slides onto the bottom of the assembly and provides three-point contact with the inspection surface to maintain a constant delay-line length and to keep the probe from wobbling. The boot facilitates consistent ultrasonic coupling between the probe and the part being inspected, especially on curved surfaces such as the radome in Figure 20. ARIS has been used to inspect the same type of radome mounted on top of a C-18 aircraft.

Figure 21 shows the object of successful periodic inspections with ARIS — the irregularly shaped nose on the SR-71, a section of which is depicted in the lower right corner of the figure. Personnel at an Air Logistics Center developed a pulse-echo ultrasonic technique using the boot assembly for this application. ARIS has been transported thousands of miles to conduct some of these inspections.

CONCLUSIONS

ARIS is a unique system that is well-suited for field inspection of laminar structures, provided that basic pulse-echo or through-transmission ultrasonic techniques can produce the required data. The system has many novel features and can be readily applied to many components. It does not require unique fixturing for each part inspected.

Although ARIS has a definite place among transportable ultrasonic systems that provide permanent records of data, a user of the system must recognize that trade-offs are involved. ARIS provides a permanent record of an inspection that can be used at any time to directly locate areas of a part that produced ultrasonic data of interest. However, the price of the permanent record is the time needed to set up ARIS on the part. Ultrasonic techniques can be stored on magnetic disks for efficient calibration of the ultrasonic instrument at the beginning of an inspection, but establishing a technique the first time an inspection is done requires more time for an ARIS inspection than for a totally manual ultrasonic inspection. ARIS requires that the ultrasonic instrument be set up precisely since the real-time interpretation of ultrasonic A-scans by the coordinated effort of the human eye and brain still cannot be matched by ARIS.

ARIS provides assurance that 100 percent of a selected area is inspected, but scanning literally 100 percent does take longer. It was demonstrated during the evaluation of ARIS that the traditional method for obtaining what was thought to be 100 percent coverage (by monitoring transducer overlap according to tracks of displaced couplant) actually left about 20 percent of an area uninspected. Furthermore, small data elements selected by an ARIS operator to give maximum spatial resolution, increase the time it takes to inspect 100 percent. Fortunately, ARIS provides a choice of data elements to permit reasonable inspection times, 0.4 inch (10.16 mm) elements for minimum inspection time as well as 0.2 inch (5.08 mm) and 0.1 inch (2.54 mm) data elements for more detailed C-scans of smaller areas of interest. With the 0.4 inch element a through-transmission inspection of an F-15 horizontal stabilizer takes approximately three and one-half hours. That includes everything from the time an inspector rolls ARIS up to the plane till he packs up and rolls it away after completing the inspection.

ARIS is not a panacea for inspecting laminar structures in all situations. However, experience with ARIS will enable selective use at successive intervals to record data that can be directly compared to graphically show the effects of service on the part being inspected. The uniqueness of ARIS stems mainly from its versatility. The various features enabling the versatility have been successfully demonstrated, so now they may be incorporated as needed into future ARIS units to meet specific inspection requirements.

ACKNOWLEDGEMENTS

The authors gratefully acknowledge Daniel C. Laufersweiler of Universal Technology Corporation for his extensive contributions to the evaluation; Bruce Jacobs, Dennis Hamlin and Robert Spirks of Southwest Research Institute for their support of the evaluation; and personnel at Edwards, Hill, Randolph and Charleston Air Force Bases who made aircraft available for the evaluation. The participation of Universal Technology Corporation in this program was sponsored by the U.S. Air Force Wright Research and Development Center, WRDC/MLSA.

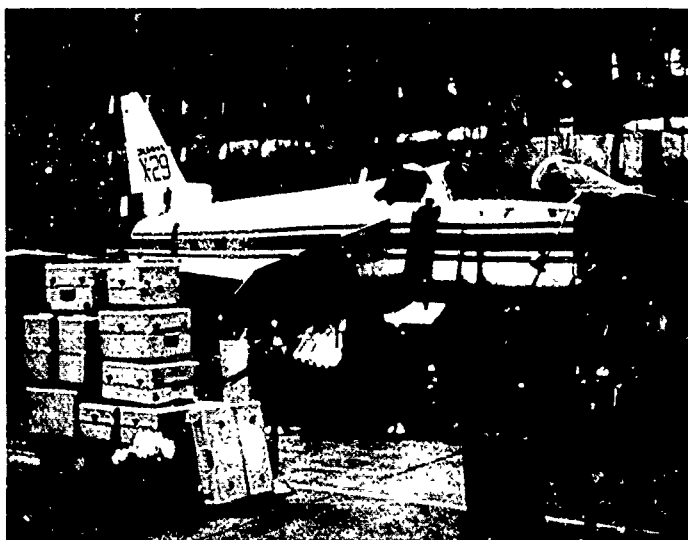


Figure 1. ARIS containerized for shipment or storage.



Figure 2. ARIS being wheeled to an inspection site on the flightline.

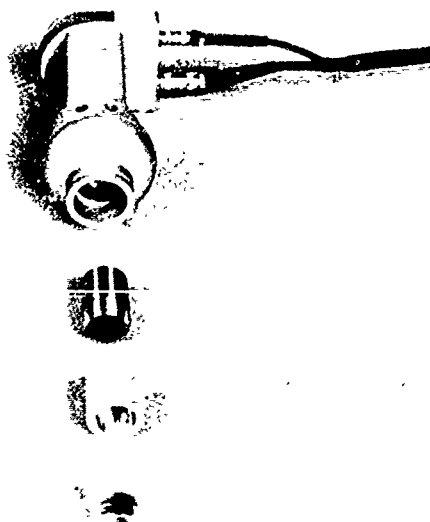


Figure 3. Exploded view of the probe.

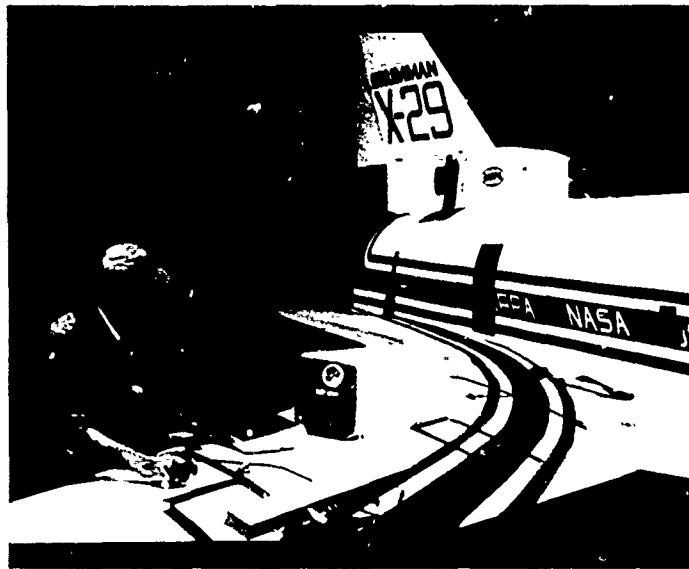


Figure 4. Inspection of an X-29 wing.



Figure 5. Inspection of an F-16 vertical stabilizer.



Figure 6. Lightweight probe handle being used on the vertical stabilizer.



Figure 7. Probe stabilizer block detached from lightweight handle and being used on an F-16 vertical stabilizer torque box in a shop.

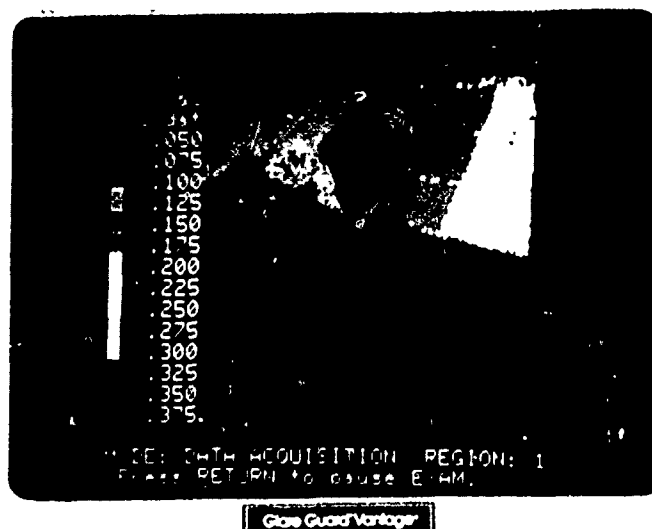


Figure 8. C-scan time-of-flight data from the F-16 stabilizer graphite-epoxy skin.

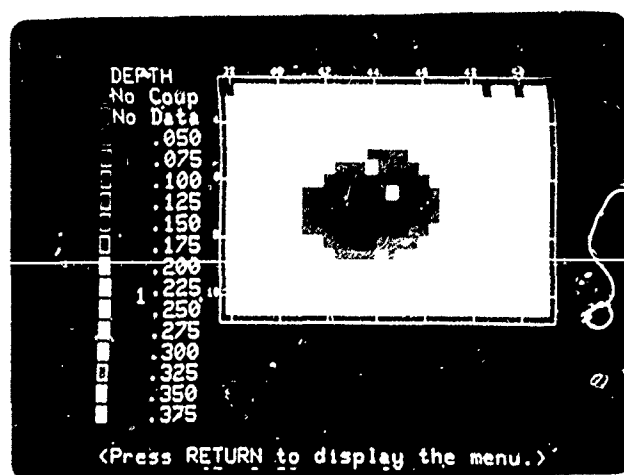


Figure 9. Magnified image of time-of-flight C-scan data indicating impact damage in the F-16 stabilizer skin.

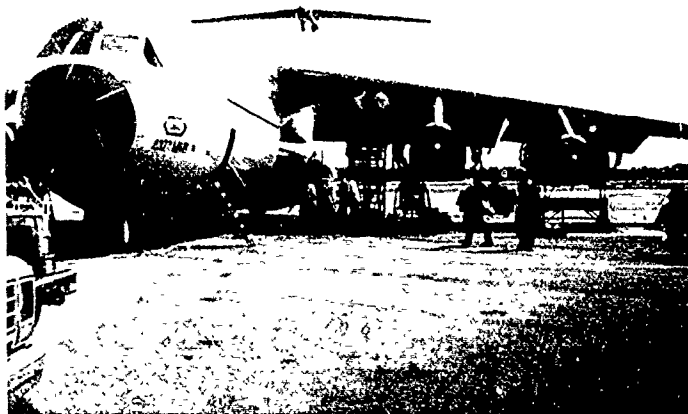


Figure 10. Inspection of a C-141 wing leading edge.



Figure 11. Close-up view of an inspector using ARIS on the under side of the C-141 leading edge.

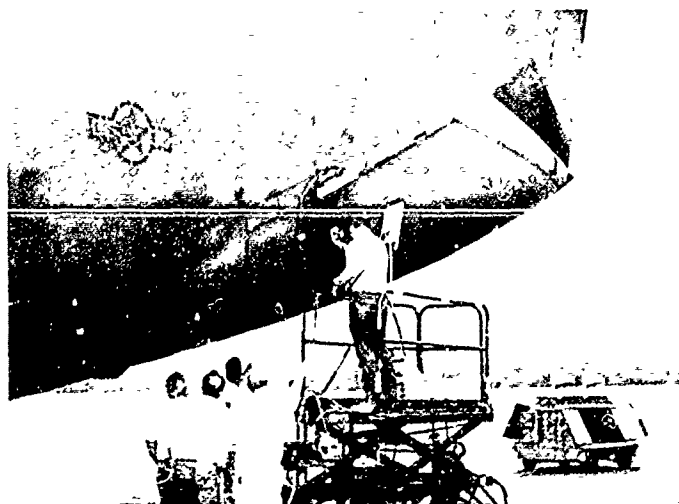


Figure 12. Inspection of a C-141 cargo-bay door.



Figure 13. Photograph showing the difficulty encountered when trying to view the video monitor in bright sunlight on a flightline.

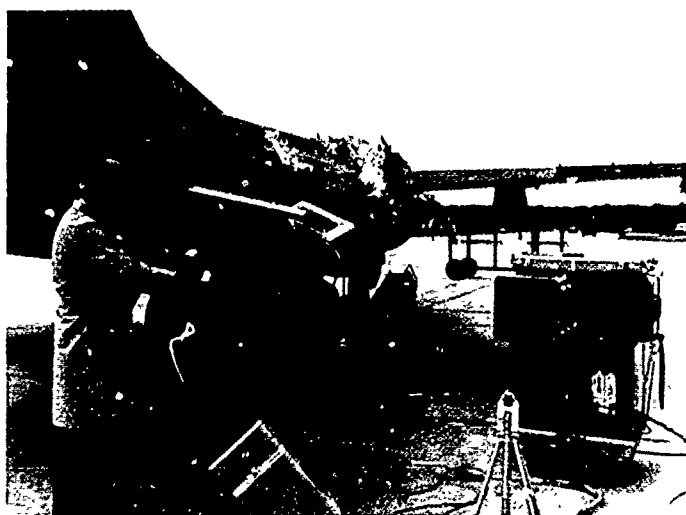


Figure 14. Inspection of an F-16 horizontal stabilizer with an ARIS production unit incorporating the hardware modifications.



Figure 15. Example of an ARIS set-up with the sound bar mounted on the tripod.

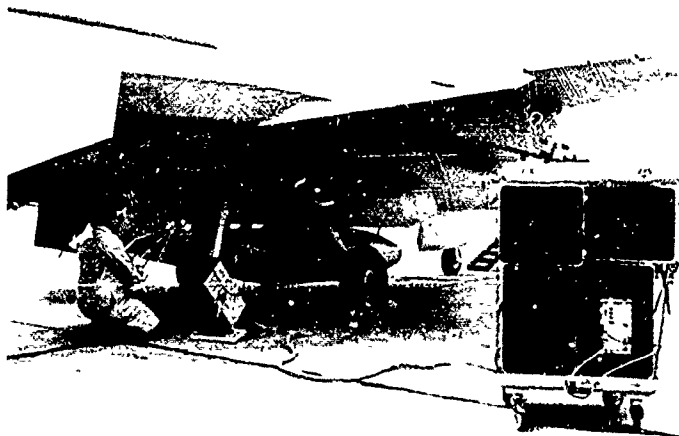


Figure 16. Through-transmission inspection of an F-16 ventral fin.

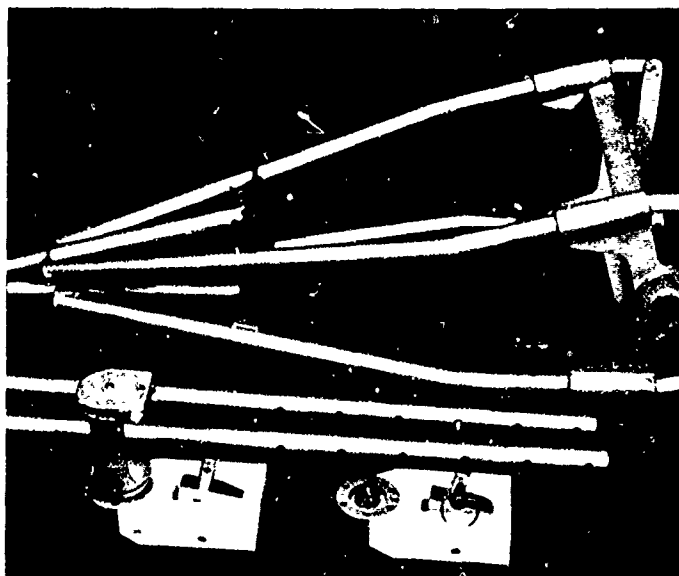


Figure 17. Close-up view of a disassembled through-transmission yoke.

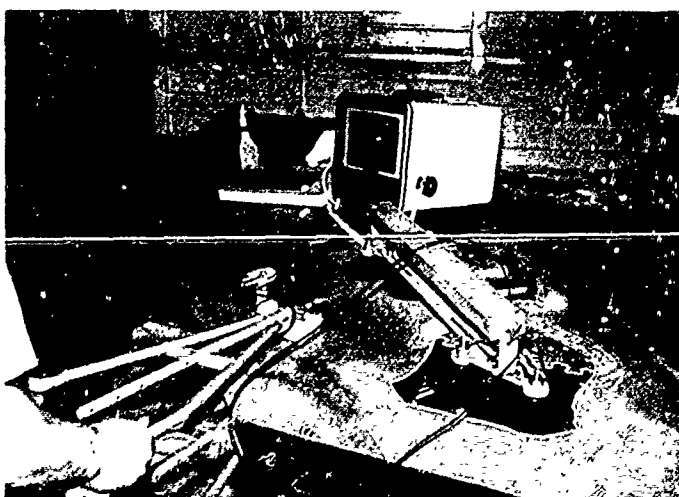


Figure 18. Through-transmission inspection with the probe rotated and the probe-holder block angulated.



Figure 19. Through-transmission inspection of a B-1B weapons-bay door.



Figure 20. Pulse-echo inspection of a radome with the boot assembly on the probe.

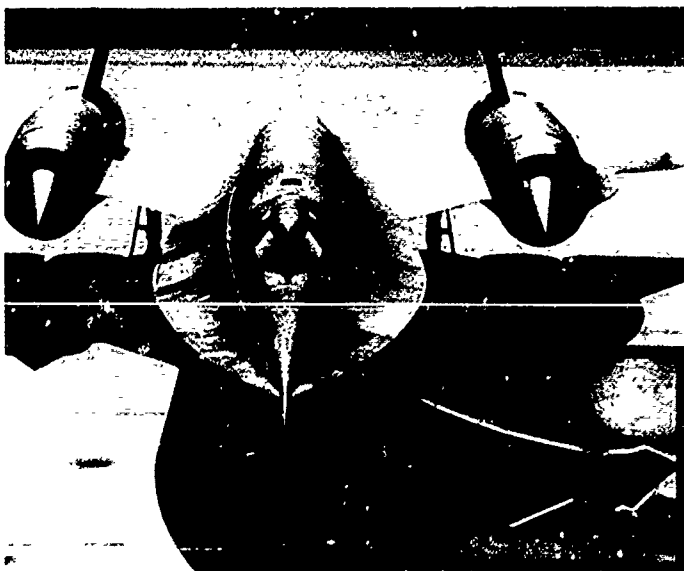


Figure 21. View the streamlined nose of an SR-71, successfully inspected with an ARIS.

Development of an Automated Ultrasonic Inspection System for Composite Structure on In-service Aircraft

W.R.Sturrock*, R.W.Ramsbottom**, and Major W.J.Miller***

*Defence Research Establishment Pacific,
Victoria B.C. Canada.

**Galatea Research, Brentwood Bay, B.C. Canada.

***DND/NDHQ, Ottawa, Ont., Canada.

ABSTRACT

Composite honeycomb (carbon/epoxy facesheets bonded to aluminum honeycomb) control surfaces for the CF-18 are inspected at the time of manufacture using (among other methods) ultrasonic through-transmission, but there is no automated ultrasonic inspection system to verify structural integrity of the honeycomb on in-service aircraft. Manual methods of ultrasonic contact scanning or even local through-transmission can be performed over small areas, but it is impossible to reliably inspect a complete control surface, such as a trailing edge flap on the wing or a horizontal stabilator, with hand-held transducers.

A description is given of the development and characteristics of an automated scanner and ultrasonic system to perform through-transmission inspections of honeycomb structure on the CF-18 without removal of the part from the aircraft. The prototype system, including a mobile lift table/platform, was demonstrated on an aircraft at CFB Cold Lake, Alberta, and examples of C-scan images obtained are shown. Recommendations are made for further improvements.

Introduction

With the introduction of the CF-18 aircraft into the Canadian Forces (CF), it was recognized that a requirement would exist to inspect composite materials, covering large surface areas.

While a number of nondestructive methods are used for the inspection of composites, ultrasonics is preferred for the detection of delaminations in the graphite/epoxy skin, as well as skin-to-aluminum honeycomb disbonds. To address quality control requirements, manufacturers have developed large, automated ultrasonic through-transmission equipment for factory inspections of large areas. Currently, however, only manual techniques are approved for use on in-service aircraft at the Main Operating Bases (MOB's).

Experience has clearly demonstrated that for inspections covering any appreciable surface area, manual ultrasonic methods are labour intensive; this increases aircraft downtime and maintenance costs and reduces inspection reliability. A recent special inspection (SI) on the leading edge (LE) flap of the CF-18 aircraft required approximately forty (40) manhours/flap (i.e. 80 mhrs/aircraft) to

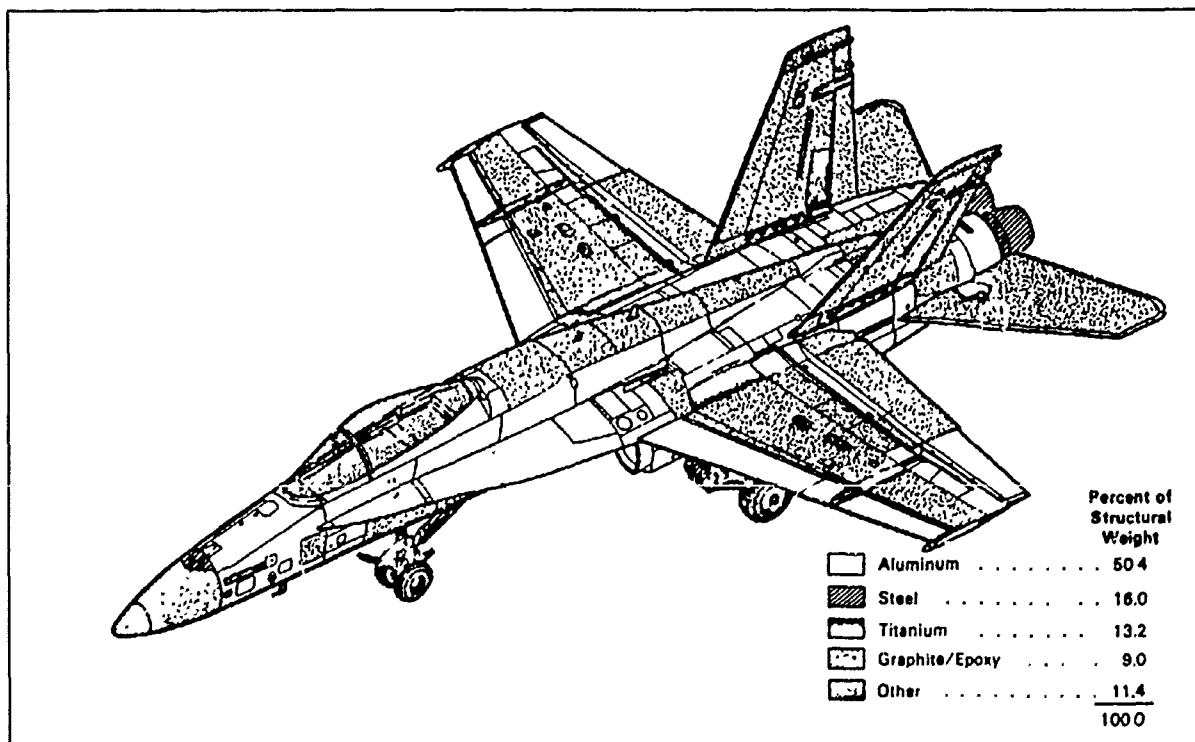


Figure 1. CF-18 Showing Areas of Graphite/Epoxy (courtesy of McDonnell Douglas).

complete and required the removal of the part from the aircraft. Considering the relatively small surface area of the LE flap (1.5 m^2) and the likely requirement to inspect larger components such as the horizontal stabilator (8.2 m^2), the inefficiency of a manual inspection method is evident.

This paper describes the development and characteristics of a prototype automated through-transmission ultrasonic inspection system. Initial field trials indicate the potential for improved inspection reliability and repeatability with significant reduction in aircraft downtime. It is evident that as requirements for additional inspections increase, the need for additional manpower resources can be avoided with systems such as this.

Background

The CF-18 is the first aircraft to be purchased by the Canadian Forces that makes extensive use of graphite/epoxy (GR/EP) composite materials. Approximately 93 m^2 (1000 square feet) of wetted surface area of the aircraft are GR/EP material as shown in

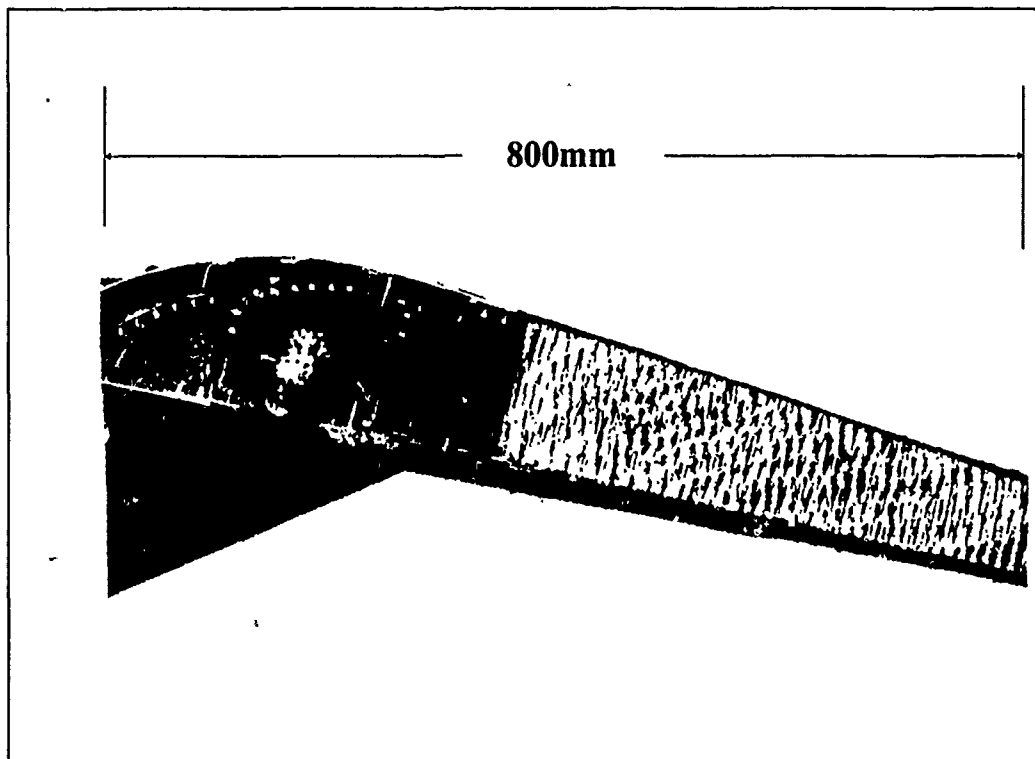


Figure 2. Section of Trailing Edge Flap Showing Honeycomb construction.

Figure 1. In addition to GR/EP laminates bolted to aluminum spars, many control surfaces such as the horizontal stabilator, rudders and trailing edge flaps are constructed of GR/EP bonded to full depth aluminum honeycomb (see Figure 2). Visual, ultrasonic, bondtest and radiographic (X-ray) examinations are the main NDT techniques used to determine the structural serviceability of the aircraft; however, ultrasonic techniques are specified by the manufacturer to detect delaminations in the GR/EP skin as well as skin-to-aluminum honeycomb disbands.

As early as 1982, through-transmission ultrasonic inspection of the horizontal stabilator was identified as being physically impossible for inspectors to perform manually. The potential need to inspect large areas for hidden impact damage made the development of an automated ultrasonic through-transmission scanning system, which could be applied to an aircraft in the hangar, a priority. Fully automated scanning systems were implemented by the aircraft manufacturer to provide fast, repeatable, archivable ultrasonic inspections of parts prior to being assembled on the aircraft. C-scan equipment has been available in factory based systems for many years. Early systems produced an archivable hardcopy image on paper. Later, large computer based ultrasonic data acquisition systems were developed to store the scan data on magnetic media as well as produce hardcopy and display the image on a television monitor (e.g. MCAIR's AUSS shown in Figure 3). Some manufacturers have developed portable semi-automated systems (requiring manual movement of the transducers) primarily for ultrasonic inspections of pipeline welds. Most recently personal computers have permitted the development of small, portable ultrasonic systems using magnetic or optical disk storage of the data (e.g. AMDATA, DREP's SPUD system).

In all of the above systems, a mechanism is used to move or guide the transducers in a raster pattern to fully cover the scan area and provide position data for the C-scan plot. Factory systems (Figure 3) actively move the transducers with motorized gantry axes, using water jets to couple the transducer with the part to perform through-transmission inspections. The majority of portable systems (see Figure 4) are intended for small (30 cm X 30 cm) area pulse-echo scanning using a track secured to the part to guide a single transducer, manually moved by the operator, along the straight lines required by the search pattern and provide position data to the data acquisition system. ARIS (Automated Real-time Inspection System) is another portable system developed for the US Air Force

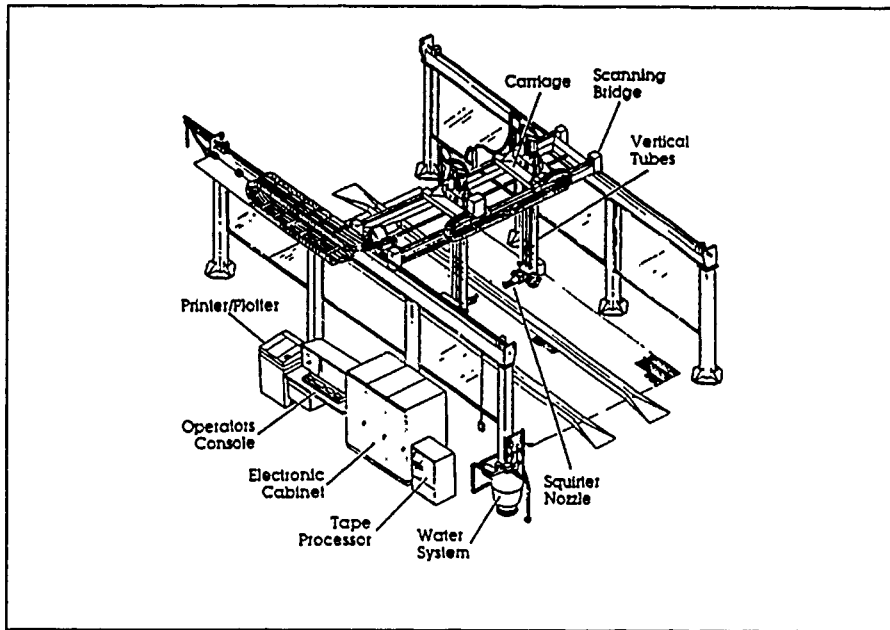


Figure 3. Automated Through-Transmission Ultrasonic Scanning System (Courtesy McDonnell Douglas).

which uses a "freehand" scanning technique. Position data for the C-scan are provided by an acoustic ranging system secured to the inspected part. The transducers use a fluid filled polyurethane boot to acoustically couple with the part.

Faced with the need for repeatable ultrasonic inspections of large honeycomb areas as well as localized repairs, tasking was authorized in 1983 to develop a transportable, easily applied automated scanning system which could:

- provide repeatable archivable results (C-scans);
- relieve technicians of the mechanics of transducer movement;
- perform fast scans of large areas on the aircraft, primarily the horizontal stabilator;
- be transported to the aircraft in the hangar rather than require a dedicated facility.

Such a system would also allow for a significant increase in the output and reliability of ultrasonic inspections without requiring a commensurate increase in staffing.

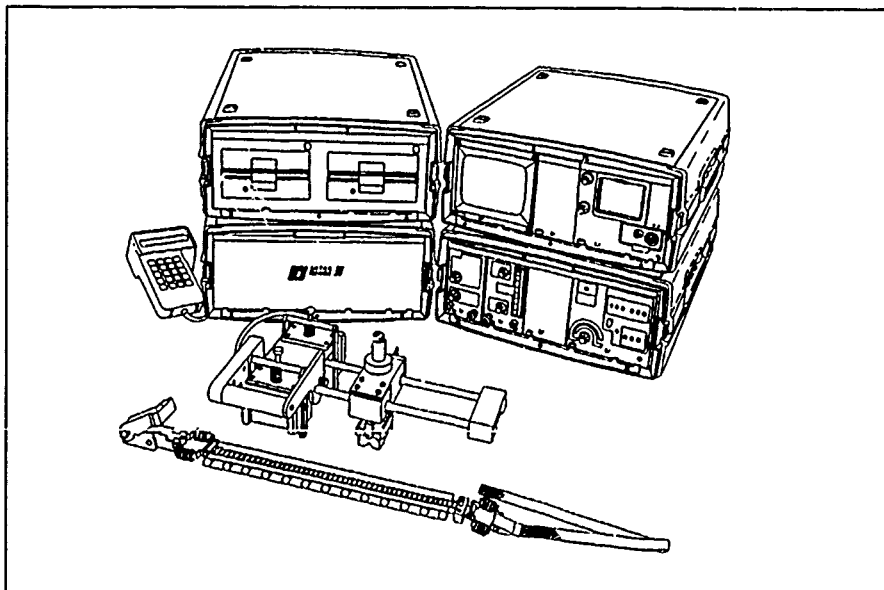


Figure 4. UltraImage III Computerized Portable Ultrasonic Inspection System (Courtesy SAIC).

Prototype Scanner

The prototype scanner initially developed for DREP by Robotic Systems International, Sidney, B.C., consists of two subsystems: the scanning yoke and the electronic controller console. Figure 5 shows a block diagram of the system. The maximum yoke scan area (500 X 1000 mm), is adequate to reach all inspection areas on the stabilator when used in a batch mode.

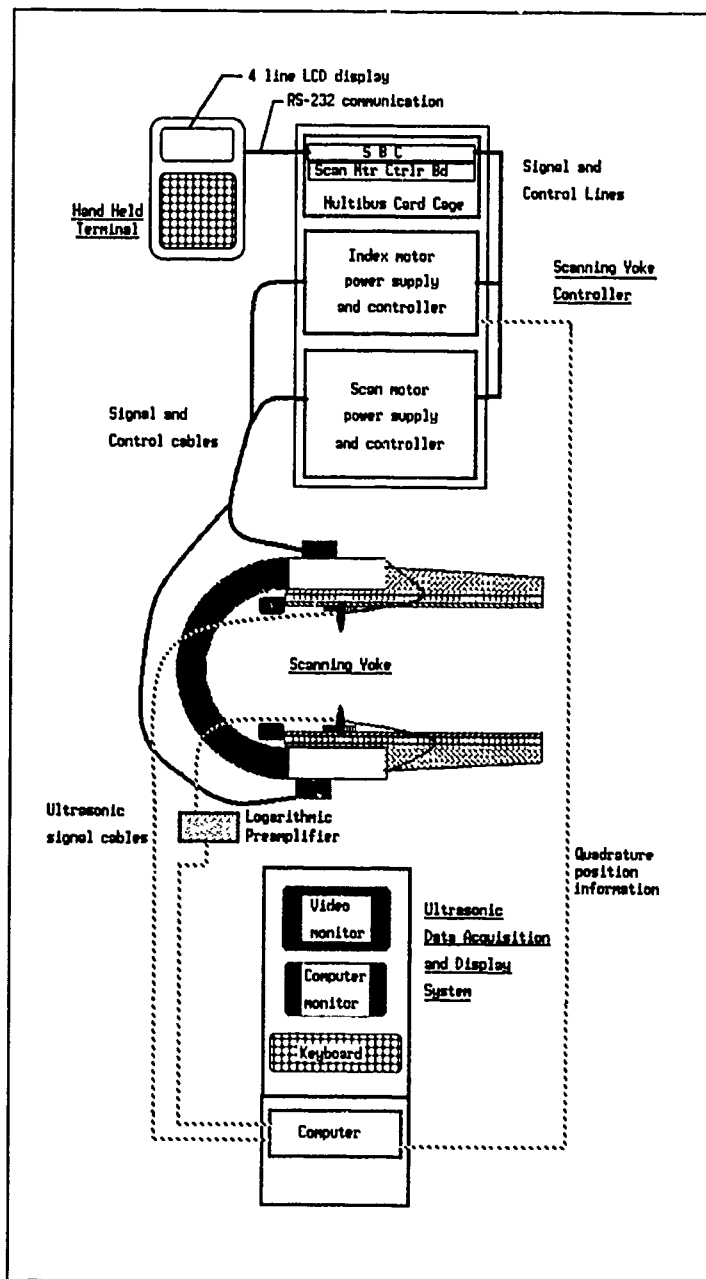


Figure 5. Block Diagram of Scanning System.

The yoke is made up of welded aluminum frames with the two identical scanning frames linked by a C-frame as shown in Figure 6. Scan axis movements are produced with a lead screw with a pitch producing 25 mm of linear motion for each revolution. The lead screw is driven directly from the shaft of an AC brushless motor whose position is sensed using a resolver attached to the rear of the motor shaft. A stepper motor is used to drive a gear reduced ball screw for index axis movement. The position of the scan axis is sensed using a linear position transducer attached to the index frame. Since each of the four actuators is controlled separately the potential exists for transient misalignment of the scan heads.

The scanning yoke user interface is a hand held terminal (HHT) with 4 line LCD display. The operator selects the required function from the displayed menu or submenu. The program constructs the correct command sequence and sends it to a single board computer (SBC) in a Multibus rack via a RS-232 link.

The SBC controls the stepper motors by sending a sequence of pulses to a stepper motor controller clock card. The AC brushless motors are controlled by a Multibus board which receives commands from the single board computer via the bus. The quadrature pulse position information required by the data acquisition equipment is provided by an optical encoder driven by the scan axis lead screw and derived from the index axis stepper motor clock output.

Ultrasonic Data Acquisition Systems

The ultrasonic data acquisition system used for approximately half of the project was the UltraImage III system manufactured by Science Applications International Corp. of Two Shaws Cove, CT. The physical design of the scanning yoke was based on interfacing with this unit. It is capable of acquiring and processing ultrasonic data for 20,000 position points in a 100 X 200 matrix and storing the data on floppy disk.

A second system, Signal Processing and Ultrasonic Display (SPUD) designed and developed by the DREP NDE Group was used for the final two months of the project, for two reasons: first, the system was untried in a practical application and therefore would benefit from a period of debugging, and second, the

UltraImage system was restrictive in its speed, storage, display formats and scan size and was being superseded by the DREP system. Therefore it was reasonable to store as many scans as possible in a format which would probably become the future format for C-scans at DREP and the Aerospace Maintenance Development Unit (AMDU), CFB Trenton.

Couplant System

The water-jet coupled transducer system (Andec Laminar Link, Model WCP-104) has a focal length matched to the laminar flow transducer housing. The frequency of the transducers (1 MHz) was selected as the most suitable for the range of composite/honeycomb thicknesses in the horizontal stabilator. The couplant system, comprised of a containment, reservoir, pump, filter and valves is shown in Figure 7. The containment consists of curtains and support structures that direct the flow of water from the inspection surface to the reservoir. The reservoir is a container for the water supplied to the pump with sufficient capacity to allow for some loss of couplant due to leaks in the containment system. The pump supplies the water to the squirter heads from the reservoir. The filter removes particulate material picked up from the inspection area and traps air bubbles which may be entrained in the water. The valves are used to independently control the volume of water flowing to each of the squirter.

Operation

The scanner is set up for an area scan using the HHT by commanding the scan and index axes to move to the starting point of the inspection area and recording the position as "home". The size of the scan area is then entered as offsets from this home position in the scan and index directions. The distance the index axis moves after each scan motion is calculated by the SBC to be 1/100th of the index offset distance. This in turn determines the resolution of the scan. During an area scan, the transducers move to the limits of the scan axis, then retrace the path prior to indexing over to the next scan position. This results in the scan axis data being acquired twice for each data point.

As the transducers move along the scan axis, a series of pixels is displayed as a horizontal line starting at the upper left hand corner of the video monitor (see Figure 6). The intensity of each pixel on the monitor corresponds to the digitized peak amplitude. Each index motion then steps the trace down one line on the left hand side of the image. For the majority of the C-scans in this project the images were set to 200 data points horizontally (scan axis) and 100 data points vertically (index axis). At the end of an area scan, the entire C-scan image is displayed on the monitor and may be saved to disk.

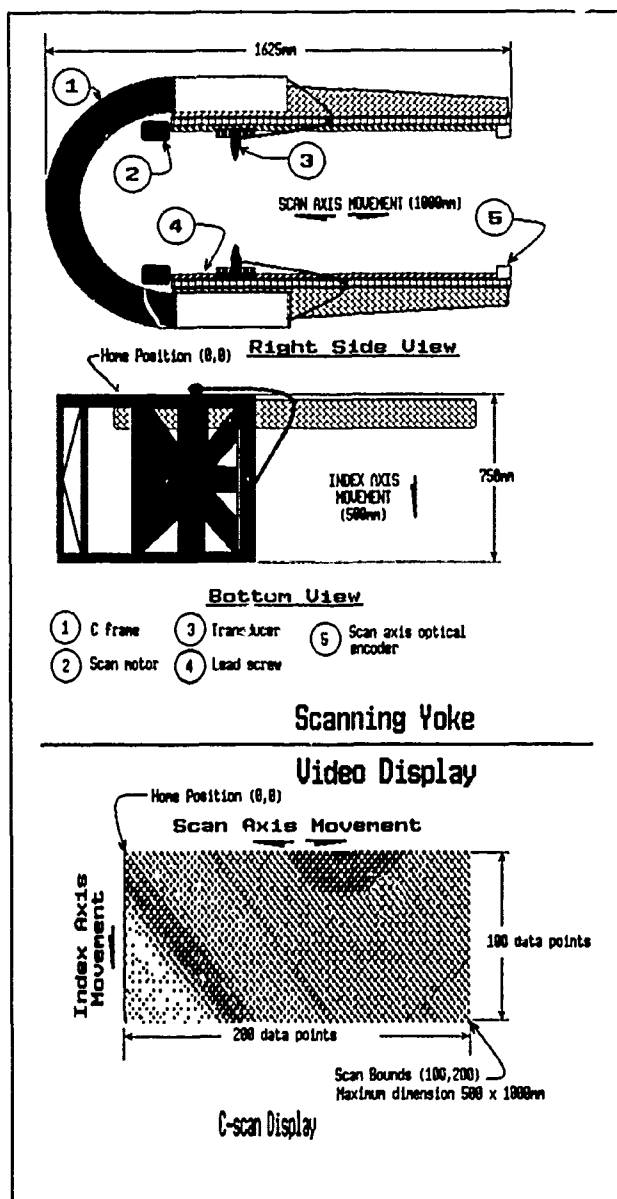


Figure 6. Scanning Yoke Prototype.

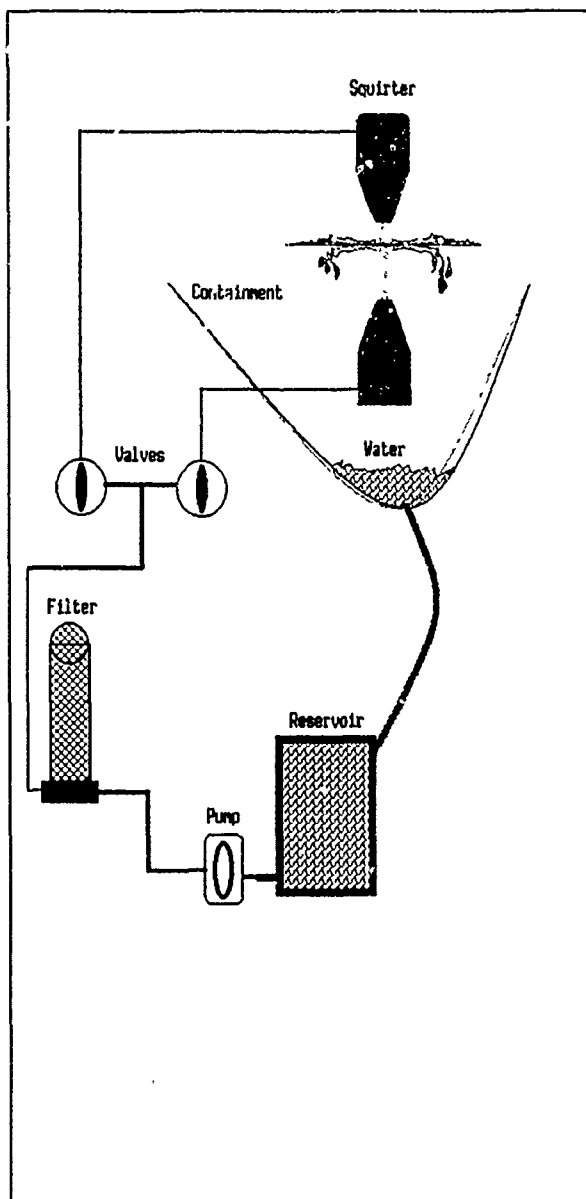


Figure 7. Water couplant System.

The distance between data points in the C-scan image is determined by the scanner index step size and is referred to as the scan resolution. The data acquisition system must also be told how many position pulses to count before capturing data for the next point in the display. For the majority of the stabilator images in this paper the scan resolution was 5 mm. Images of test specimens are displayed at 2.3 mm resolution.

It was obvious from visual observations of the scanner during a scan, that the upper and lower scan frames moved relative to each other. Misalignment transients are of primary concern because of the momentary drops in signal amplitude which can introduce spurious results. Steady-state misalignments and misalignments which occur gradually (e.g. from one corner of the scan area to the opposite corner) are of less concern since the evaluation of the C-scan involves comparing the amplitude of an area relative to the amplitude of its closely adjacent areas.

Scanner Evaluation

Two methods were used to quantify variations in transducer head alignment. The first derived the magnitude of alignment variations from C-scan images. The second method used a machinist's dial gauge to measure the direction and magnitude of both steady-state and oscillatory movements.

Results

The results of a C-scan of an aluminum plate with simulated defects are shown in Figure 8. The most striking feature is the vertical banding which is consistent with, but not a conclusive indicator of, variations in alignment of the transducers. The amplitude difference between bands is about 20%. A quick check of the amplitude variation for various offsets of the transducers showed that a 20% change corresponded to an offset of about 2 mm.

The results of the dial gauge measurements are summarized in Table 1. The measurement of index offset was found to be position dependent, *i.e.* the amount of offset depended on the position of the scan heads in the scan area. The measurement of the offset in the scan direction showed a gradual change in position (delta) as well as rapid oscillatory behavior.

Following this evaluation of the prototype scanner by Galatea Research, it was concluded that with some additional hardware and software improvements and the addition of a positioning system, the prototype was capable of performing ultrasonic inspection on an aircraft.

Table 1
Monotonic and oscillatory behavior (peak-to-peak) of scan head alignment along scan axis during area scans at different scan speeds:

Speed (mm/s)	Delta (mm)	Oscillation (mm)
25	1.0	0.25
75	2.0	0.40
150	2.3	1.00
225	2.3	0.50

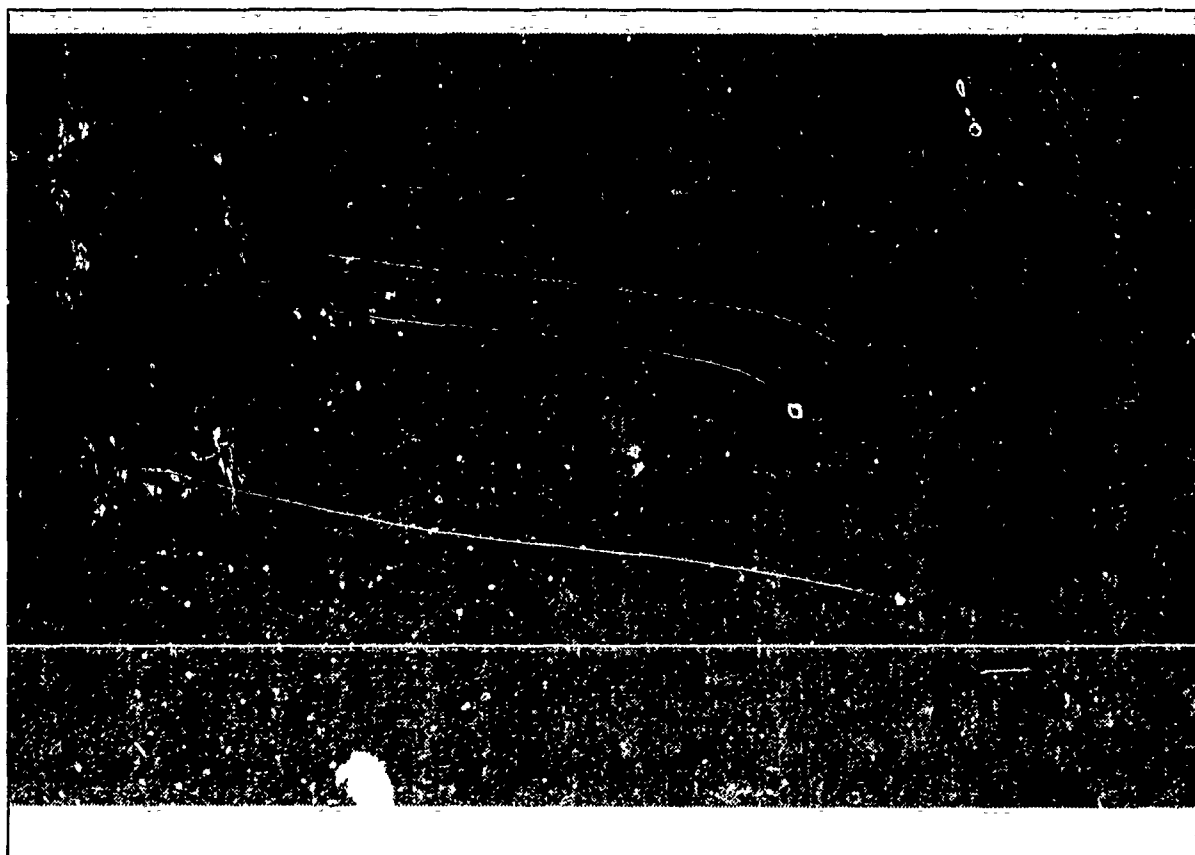


Figure 8. C-scan of Aluminum Plate at a Resolution of 5 mm.

Laboratory Simulations of On-Aircraft Inspections

Before testing the prototype system in an aircraft maintenance environment, additional laboratory tests were performed to provide answers to a number of questions.

These tests were intended to:

- discover the physical problems encountered in deploying the prototype scanning system around a horizontal stabilator, mounted at the same height and orientation as it would be found on an aircraft;
- determine the effects of scan speed and misorientation on the quality of the C-scans and determine if the data were repeatable.

Tests included scans of test specimens (of the same construction and cross-section as the stabilator) with known defects, and of a stabilator mounted on a spindle secured to a test stand fixed to the floor, as shown in Figure 9. A threaded rod was attached to the control arm on the stabilator allowing the pitch to be adjusted from 15 degrees nose up to 15 degrees nose down (see Figure 9).

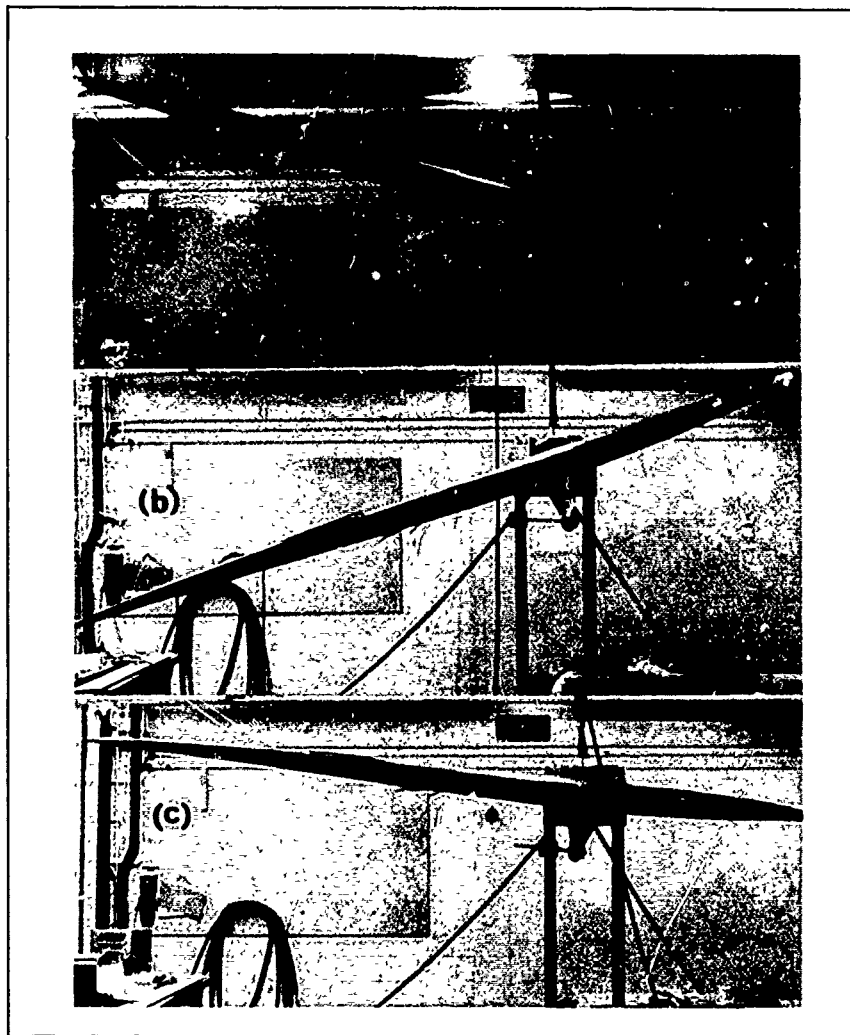


Figure 9. Laboratory Setup: (a) Stabilator 15 degrees nose up; (b) 15 degrees nose down; (c) 5 degrees nose up (ground lock position).

It was decided early in the project that from an operational standpoint, one fixed stabilator pitch would be better than making pitch a function of the chosen inspection area. It was the understanding of DREP staff, that regulations required the installation of a ground lock when the aircraft was in the hangar, to prevent damage to personnel and equipment. For these reasons the ground lock position was assumed for all scans and the tests were performed on this basis. Some water runoff tests were attempted with both positive and negative pitches; however, the results did not justify changing the ground lock restriction.

In order to position and orient the prototype scanner over the stabilator, an experimental positioning system was developed. The materials and design were based on off-the-shelf equipment obtained locally. The only exception was the hydraulic lift table. A commercial hydraulic scissor lift table (weight approximately 580 kg) was procured with a wheeled support base and a lockable rotating axis secured to the platform. The height of the platform was variable from 700 to 1500 mm using push buttons controlling a hydraulic pump for upward motion and a solenoid valve for downward motion. The speed of upward motion was fixed at about 12 mm/s by the 1/2 horsepower hydraulic pump and the rate of downward motion was adjusted by a flow control valve to about 6 mm/s.

The selection of the lift table was based primarily on availability and lift range. The entire assembly was rated for a payload of 450 kg based on the strength of the casters; however the lift table was capable of handling 1500 kg. The use of a table with a payload safety factor of 13:1 ensured a stable platform and a hydraulic system that would not creep downward during a scan. (The lift table was left at a fixed scanning height for over two weeks with no noticeable change in elevation). Caster and floor locks were provided to prevent movement during a scan. A steering mechanism was added to the platform casters as shown in Figure 10. Pitch and roll movements were provided by mounting the base of the scanner on three screw jacks attached to the top of a rotating platform (yaw axis) as shown in Figure 10. This design permitted roll and pitch adjustments in excess of 15 degrees and also provided about 200 mm of vertical Z-axis adjustment. The ideal jacks would be stiff in all directions and provide the scanner with a stable base. The scissor style of jack was chosen for its availability but was not laterally stiff. Automotive ball joints were used as a mechanical interface between the scanner base and the top of the jacks.

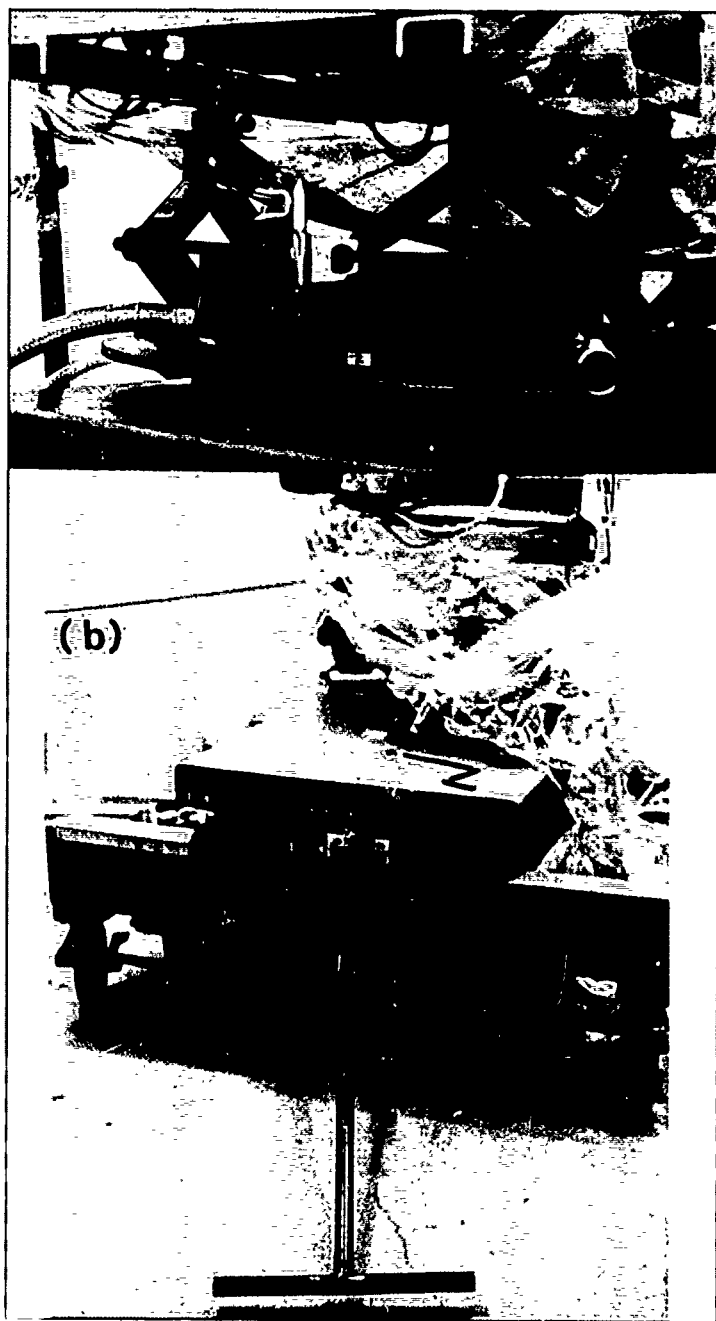


Figure 10. Positioning Platform: (a) right-hand side view of the scissor jacks used to provide roll and pitch orientation mounted on the yaw axis rotating platform, the containment membrane is visible in the right hand side, (b) front view of positioning platform showing the steering mechanism and pull handle. An identical arrangement was installed on the rear of the platform.

to be easy to position, conformed to the shape of the stabilator and could be placed such that 100% of the water from both top and bottom sides of the stabilator was recovered. The flexibility of the membrane permitted the edges to be positioned where water was flowing. When moving the scanner to a new position, the containment was easily folded in on the scanner resulting in the smallest possible volume to be moved around the aircraft. The final version of the containment replaced the polyethylene with 0.2 mm (8 mil) vinyl sheet. This material provided a clearer view of the scanner, had superior puncture and cut resistance, and could be easily repaired.

Preliminary tests showed that water on the upper surface flowed toward the leading edge with some lateral flow towards the tip when scanning the trailing edge. Lateral flow also occurred on the lower surface; however gravity generally caused the water to bead and drip within 0.5 m of the contact point at the flow rates used. From the beginning of the project, the ability to capture and recirculate all of the water from the squitters was considered an important goal for operational and safety reasons. In addition, an upward automation path (automatic movement from one scan area to the next) required that the ideal containment system would not need human intervention. Rigid containment systems, integral with the scanner and wheeled platform, were felt to offer the best chance of achieving future automation goals.

Two different sizes of rigid containment system were assembled and tested. The smaller of the two extended about 1.2 m in front of the base and the largest extended 2.4 m. The width of both containments was the same as the scanner (about 1 m). However, the smaller unit was unable to catch leading edge water when scanning the inboard trailing edge. The large unit was too long and bulky to move easily around the aircraft without colliding with the aircraft. Neither of the two designs was able to collect the water for all scan positions without additional barriers being placed on the upper surface to control lateral flow, i.e. operator intervention was required to place the barriers. In addition, the rigid sides restricted visual and physical access to the lower scan axis when positioned against the lower surface of the stabilator.

A second approach used a channel secured to the edge of the stabilator to capture all the upper surface water without requiring the operator to repeatedly move a lateral flow barrier. The intent was to have the operator install the continuous channel around the stabilator prior to positioning the scanner. The experiments included passive collection as well as applying a vacuum to the channel to actively collect water. Flow rates and water velocity were too great for the initial designs resulting in the water stream flowing over the channel. In addition, lower surface water had a tendency to drip outside the rigid containment and the flexible hose linking the channel to the reservoir limited the movement of the lift table. At this point, the requirement for the operator to position the containment was accepted and the goal of using a rigid containment system to allow future automated movement was discarded. A flexible containment made of 4 m X 2 m polyethylene sheet and secured to the stabilator with plastic covered metal clips was found

Test Procedures

Twelve overlapping 500 X 1000 mm scan areas were marked on the lower side of the stabilator to provide guides for positioning the scanner. The separation of the sensor holders was set at the maximum for all scan areas for a number of reasons. Although the length of the water column was known to affect signal amplitude and turbulence, the range of thickness of the inboard areas required the maximum separation. The design of the sensor holders made it difficult to reduce the separation for thinner, less tapered areas at the stabilator tip without affecting the alignment of the transducers. Finally it was desirable to determine if one separation could be used for the entire stabilator to simplify the setup procedures.

Once positioned and oriented, the flexible containment was secured to the stabilator using spring clips and in some cases, waterproof tape. The data acquisition system and scanner controller were then initialized, and the scan was performed. The through-transmission testing of the 12 areas laid out on the horizontal stabilator required approximately 30 minutes per scan at a scan speed of 225 mm/second.

Some scans were repeated on specific areas of the stabilator under the following conditions:

- position and orientation unchanged, scan speeds set to 25, 75, 225 mm/second;
- position and speed unchanged, scanner visibly misoriented;
- scanner moved away from scan position and orientation altered; scanner then returned to original scan position, oriented and scan repeated at same speed.

The purpose of the first test was to determine the effect of different scan speeds on the quality of the data. The second test was to determine the effect of a visible misorientation of the scanner. The final test was intended to simulate the comparison of archived data to a more recent scan, i.e. could the scanner be returned to the same position as a previous scan and could the resulting C-scan be easily compared to earlier results?

For the orientation tests, the scanner was aligned with reference to the stabilator using a scale to measure upper and lower standoff distances at the left and right edges of the scan frame and the tip of the scan arms. The screw jacks were then adjusted to equalize the upper and lower standoff measurements. Measurement of standoff distances was ultimately abandoned in favour of visually aligning the edge of the stabilator with the horizontal arms of the C-frame.

Ensuring correct alignment with the markings on the stabilator was difficult for a single operator; however, it was made easier by the use of the yaw axis. The throat of the scanner occasionally contacted the stabilator when the casters swiveled in the wrong direction during movement; however, the addition of a steering mechanism on the lift table eliminated this problem. Securing the containment curtains was not difficult and 100% water recovery was achieved in all but the inboard edge areas where some splashing was expected due to interference with the spindle.

Once the pitch and yaw axes were set, it was possible to move the scanner parallel to the leading or trailing edge of the stabilator for successive scans with only Z-axis adjustments, i.e. the orientation remained the same. The scanner could also be removed from the stabilator by pulling it away in a direction normal to the edge without the tip of the scanner touching the stabilator.

Test Specimens

Test specimen 13T4B was constructed of full depth honeycomb and graphite epoxy facesheets with defects ranging in size from 50 mm to 6 mm on the upper and lower sides. The section was supported on a frame at different angles and with the defects closest

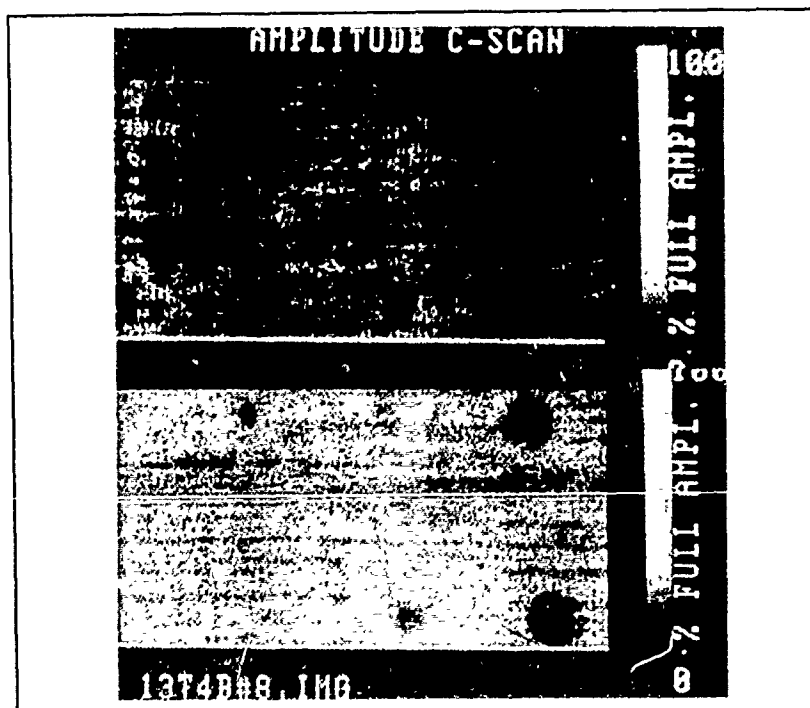


Figure 11. C-scans of Test Specimen 13T4B: top: aligned; bottom: 8 deg pitch misorientation.

to the transmitter or to the receiver. An example of the results is shown in Figure 11. These tests strongly suggest that misorientations as much as 8 degrees to the honeycomb axis have little effect on the ability of the through-transmission C-scan to detect flaws as small as 25 mm with a scanner resolution of 2.3 mm. The most noticeable effect is the shift in position of the flaws on the lower surface due to the angle of the test piece and the "waveguide" effect of the honeycomb.

Repeatability

Two methods were employed to determine the repeatability of C-scans. The first was to repeat a scan with the same parameters, *i.e.* without changes to orientation, position or scan speed. The second method was intended to simulate returning to an inspection area to repeat an inspection and compare the new data with previously archived data. These results showed that repeating a scan with the same position and orientation resulted in virtually identical images; the only major differences occurred at areas of turbulent flow near the edges of the part. Returning to the same location was impossible; however, the images were virtually identical.

Resolution of the Image

Scans were made of the outboard tip of the stabilator (area L7), at resolutions of 2.5 and 1.25 mm at a speed of 75 mm/s, to

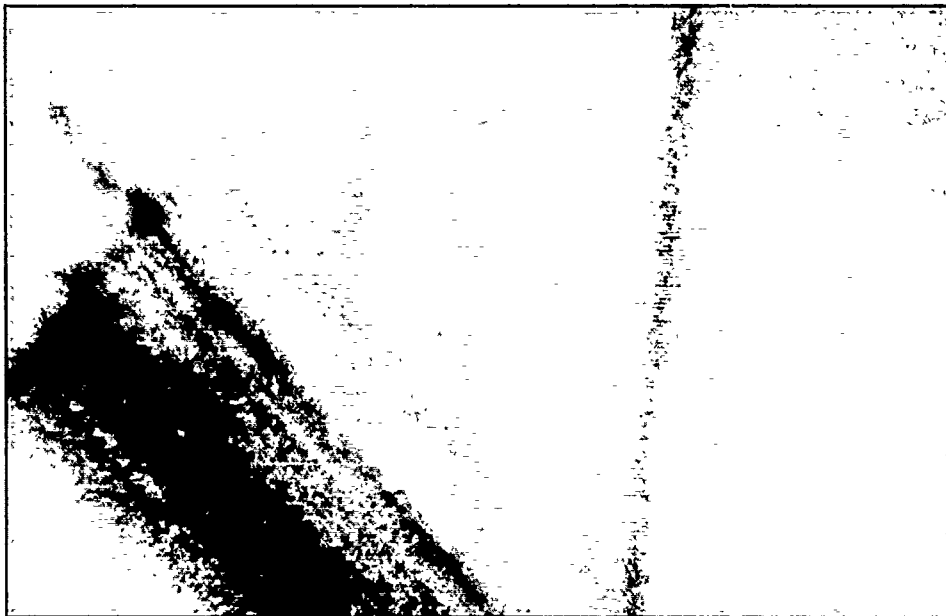


Figure 12. C-scan of Area L7 at Scan Resolution of 1.25 mm.

determine if a smaller scan pattern would reveal additional useful detail in the image. The results of the 1.25 mm scan are shown in Figure 12. Portions of the right hand side of the image appear to show the edges of the honeycomb cells and strips of amplitude changes which may be due to adhesive thickness changes or honeycomb machining marks.

Results

The practical speed limitation for the data acquisition equipment was found to be 225 mm/s. Above this limit, position data were lost, and the resulting scan was skewed and had "drop-outs" (loss of amplitude data). The noise level of an image increased with higher scan speeds, probably as a result of motion induced turbulence in the water column. The results of two successive scans at 75 and 225 mm/s showed that, although there are small differences in the images, all major flaws are visible in both images. To determine the effect of a misorientation, two successive scans of the same area were performed with proper alignment and visible misalignment, and with all other variables held constant. The only apparent effect of misorientations is a distortion of the image of a geometric feature. Scans of test specimens were used to further investigate misorientation effects.

The tests demonstrated that although increased scan speed had some effect on the C-scan image, a speed of 225 mm/s produced an almost identical image to one produced at 75 mm/s. Orientation of the scanner with the structure was not critical and resulted in acceptable images at up to 6 degrees of tilt; however the scanner could be aligned with the stabilator to within 0.5 degrees with visual alignment techniques. Returning the scanner to the same location and detecting the same features is possible; however it is very difficult to eliminate some shift in the position of the features in the two images. A simple wheeled platform and three orientation axes were sufficient for one operator to employ the scanner in a practical application. The ability to recognize a flawed area is dependent on the size and relative amplitude of a flaw. The results of scans of test specimens with known flaws suggests that for a flaw to be recognized in a noisy image it must be a contiguous group of at least 0.5% of the total data points. Using this rule of thumb, a scan resolution of 5 mm would reveal a 50 mm square flaw in a noisy image.

Based on the above results it was concluded that the system was ready for field tests.

Field Tests

The laboratory results indicated that flaw detection using the scanner was robust, requiring only visual confirmation of orientation prior to beginning a scan and the application of standard inspection procedures in the set-up of the ultrasonic equipment. The field tests were intended to confirm these findings and discover if hangar conditions would create unforeseen problems. The system was disassembled and the components mounted on pallets designed to cushion against shock. Both the UltraImage III and DREP ultrasonic systems were loaded with support equipment and driven 1550 km to CFB Cold Lake.

The system was unpacked, assembled, and operational in 2.5 hours and, with the exception of two minor failures, operated flawlessly for the entire four days of testing. The original goal was to scan two horizontal stabilizers on a CF-18; however, since a special inspection was in effect on the leading edge flap, the test plan was changed to scan the starboard leading and trailing edge flaps and one horizontal stabilator.



Figure 13. Prototype Scanner Scanning Horizontal Stabilator of CF-18.

A CF-18 was moved to a location in a hanger to within 50 feet of the three phase power required by the scanner. Although the aircraft was unserviceable (U/S) because the port engine was removed, this caused no observable tilt in the attitude of the aircraft. An external ground lock was installed on the starboard horizontal stabilator. The scan areas were laid out on the lower surface using PVC tape with the same 500 X 1000 mm template used in the laboratory tests. The layout differed slightly from the laboratory pattern on the inboard leading edge, resulting in a reduction from 12 to 11 scan areas.

The set-up is shown in Figure 13. Scans L1 to L7 on the stabilator were performed, then the scanner was moved to the leading edge flap. Once the LE flap was scanned, the transducers were readjusted to the left hand side position in order to scan T1 through T4 of the stabilator trailing edge. Although the trailing edge flap could not be scanned due to a shortage of ground locks to hold the flap near the horizontal (stowed) position, it is believed that the prototype scanner would have been capable of performing the complete inspection without any difficulties.

Results

The first scan revealed a previously unknown anomaly on the inboard leading edge of the horizontal stabilator as seen in Figure 14. Manual pulse echo tests confirmed that the anomaly was on the lower surface. Core splice lines and other internal structures were easily visible as were the PVC tape boundaries.

The scan of the leading edge flap, which was in its fully extended position required the scanner to be oriented at 1 degree roll and 15 degrees pitch. A lead tape simulated flaw (13 mm square) was secured to the upper surface to determine if it could be detected. The results are shown in Figure 15. The scanner performed the leading edge flap inspection in 3 1/2 hours, the recently issued SI order for the manual inspection of this part was estimated to take 30 to 40 hours.

Water recovery was about 80% efficient with the majority of water spillage occurring near the fuselage. A number of drips were caused by problems with the hose layout and the inexperience of the technicians in positioning the containment curtains. However,

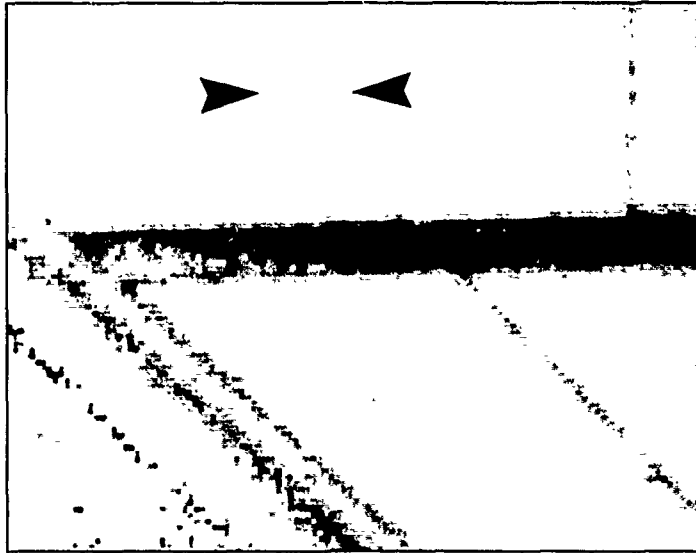


Figure 14. Area L1 of the Horizontal Stabilator Showing Anomaly.

water drips could be captured in the standard floor trays used to catch hydraulic oil leaks in the hangar. Much higher recovery was achieved in the laboratory and it is believed that 100% recovery could be realized with some refinements in the containment design.

Although the scanner had been maneuvered successfully by a single operator in the laboratory with an uneven floor surface, additional personnel were available during field trials. One person viewed the system from about 2 meters away, to give instructions on orientation and position and to control the vertical movement of the lift table, while two others pushed or pulled the table into position, locked the floor locks, operated the screw jacks, and positioned the yaw platform. Although this was the most efficient method given the extra manpower, it gave the misleading impression that three people were required to operate the system. However, being able to view the positioning of the scanner from a position 1 to 3 meters behind the scanner is an advantage. Thus, if the operator were provided with actuated control of all orienting and positioning functions with a control pendant, it would allow positioning by a single operator without sacrificing safety concerns or increasing setup time.

Small lateral (X-Y) movements could only be accomplished by releasing the floor locks and using repetitive back and forth movements. This experience suggests that a lockable sliding platform mounted on the yaw axis and capable of moving 100 mm in X and Y directions would simplify the positioning of the scanner. Alternatively if the base wheels were actuated for 360 degree rotation, it may be possible to provide finer movements than were possible with the manual steering mechanism on the prototype platform.

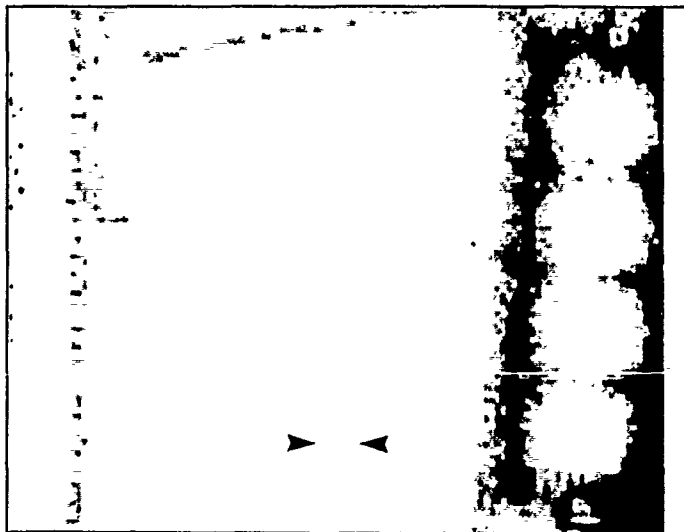


Figure 15. Area of the Starboard Leading Edge Flap Showing a 13 mm Square Lead Tape Flaw on the Upper Surface.

Conclusions and Recommendations

The prototype scanner and positioning system are a viable method of producing through-transmission ultrasonic amplitude C-scans of the CF-18 horizontal stabilators and leading and trailing edge flaps. Although improvements in design and construction are strongly recommended, the system could be successfully deployed in the field in its present configuration.

Scan speed and orientation of the scanner affect the repeatability of the C-scan far less than was originally thought. Although the scanner could be easily oriented to within 0.5 degrees of the stabilator, C-scans produced with scanner misorientations of up to 6 degrees showed good correlation with correctly aligned scans. A scan speed of 225 mm/s and a scan resolution of 5 mm results in a C-scan production rate of about 30 minutes (including the setup time) for a 1000 X 500 mm scan area. Although the prototype scanner produced acceptable C-scans, the alignment of the scan heads varies to an unacceptable degree. A close inspection of some of the images shows the faint banding indicative of scan head oscillation. The scanning yoke and controller should be redesigned both mechanically and electrically to ensure more accurate transducer alignment and to simplify the controller. Recirculation of 100% of the water is possible with a flexible containment system.

The minimum detectable flaw size is dependent on the noise level, flaw impedance relative to the surrounding material and the resolution of the scan. Field tests showed that a 13 mm square lead tape flaw was clearly visible on the middle of the leading edge flap in a C-scan with a resolution of 5 mm. Other tests on GR/EP test sections suggest that a minimum recognizable flaw size in a noisy image would be 50 mm at a 5 mm scan resolution.

Multiple transducers should be implemented to reduce the scan time or to increase the scan resolution of the images. The time required for a scan could be reduced by a factor proportional to the number of transducers per side. If a requirement is established for the detection of 25 mm diameter flaws, increasing the number of transducers will provide the additional resolution without an increase in the time taken to perform a scan. However, the additional water volume may cause some loss of signal and/or water recovery problems.

Transducers capable of maintaining a fixed standoff distance and normality to the surface should be developed to permit pulse echo scans with the scanner. Since through-transmission C-scans do not indicate on which side of the part a flaw may be located, time consuming manual pulse echo techniques to determine the flawed side are needed; this would be unnecessary if an improved contact transducer could be developed for the scanner. Image processing techniques for comparing current C-scans to archived scans of the same area should be developed.

Acknowledgements

Initial prototype development was conducted by Robotic Systems International, Sidney, B.C. under DSS Contract #97708-4-5575, and is documented in DREP CR-86-3. Further development and demonstration at CFB Cold Lake was performed by Galatea Research under DSS Contract #W7708-7-8978, and is documented in DREP CR-88-9. The efforts and contributions of RSI, Galatea, CFB Cold Lake, AMDU Trenton, DSS (Richmond B.C.) and DREP personnel in making these projects a success are gratefully appreciated. In particular, Mr. Terry Miller, of the DREP NDE Group, not only persevered with his calm diligence, but made many valuable technical contributions.

NEUTRON RADIOGRAPHY - APPLICATIONS AND SYSTEMS*

by

H.-U. Mast and R. Schütz
Industrieanlagen-Betriebsgesellschaft mbH (IABG)
Einsteinstraße 20
8012 Ottobrunn
Fed. Rep. of Germany

SUMMARY

In accordance with previous results obtained in the US, a recent research project at IABG showed neutron radiography to be a nondestructive testing (NDT) method of potential value in aerospace maintenance and quality assurance, complementing conventional inspection methods. Applications include the detection of corrosion products, entrapped moisture, adhesive defects as well as some defects in carbon fiber composites. For years the large-scale use of neutron radiography was delayed due to the lack of small and inexpensive but powerful neutron sources. Recent progress in this area led to the present development of a new generation of small neutron sources, such as compact cyclotrons and powerful neutron generators.

1. INTRODUCTION

Neutron radiography is a nondestructive testing method similar and complementary to radiography with X-rays. As seen in figure 1¹, thermal neutrons - i.e. slow neutrons that are in thermal equilibrium with their environment ($E_n = 0.025$ eV) - are predominantly scattered or absorbed by nuclei of some elements with low atomic numbers, such as hydrogen, carbon and boron, whereas most metals, in particular aluminium, are comparatively transparent to neutrons. Hence neutron radiography may be used to detect hydrogenous or other light materials, e.g. plastics, adhesives, corrosion products and explosives, as well as flaws or defects in nonmetallic components, particularly when these are covered or surrounded by metals.

Subsequent to the development of the scientific and technical foundations in the UK and US in the early sixties the first major applications of neutron radiography outside the nuclear industry were the detection of defective spacecraft ordnance^{2,3} and of residual ceramic core in cast turbine airfoils⁴.

Based on a large number of research and development projects (e.g.⁵⁻⁹) in the US, the employment of neutron radiography in aircraft maintenance is now in preparation on the basis of several recently constructed, mobile and stationary neutron radiography systems at the US Air Force's Sacramento Air Logistics Center^{10,11}.

As part of an IABG research project funded by the Federal Ministry of Research and Technology the applications of neutron radiography in aircraft maintenance, materials development as well as industrial quality assurance have been investigated with the aim to supplement previous results, particularly with respect to modern materials and recent inspection problems, and to increase the acceptability of this NDT method in the Federal Republic of Germany.

In the course of this research project^{12,13} aerospace components and materials with defined defects or damages were examined with a mobile neutron generator-based radiography system now in operation at IABG and other accelerator or reactor radiography facilities as well as, for comparison, with conventional NDT methods (X-radiography, ultrasonic and eddy current techniques, etc.).

Furthermore, IABG is cooperating with SODERN (France), SENER (Spain) and LTV Aerospace and Defence Company (USA) in the EUREKA-project "DIANE" with the object to develop and construct the prototype of a more powerful mobile neutron generator-based radiography system than hitherto available^{14,15}.

2. NEUTRON RADIOGRAPHY SYSTEMS AND TECHNIQUES

A neutron radiography system is schematically depicted in figure 2. A source emits neutrons - for practical purposes at a rate of at least 10^9 ns⁻¹ - with energies, depending on the nature of the source, of usually several 10^6 eV. Since high-energy neutrons would penetrate the object to be examined without undergoing the desired interactions with light nuclei, the emitted neutrons need to be slowed down to thermal energies by scattering collisions in a moderator consisting of hydrogenous or carbonaceous materials.

A collimator of length L and base diameter D directs a nearly parallel beam of neutrons to the object. The geometrical resolution of the assembly is proportional to the ratio L/D , whereas the neutron flux at the object (governing the exposure time) is proportional to $(L/D)^{-2}$. Therefore every radiograph taken implies a compromise between geometrical resolution and exposure time. At present only test reactors and large accelerator systems produce neutrons at a rate to render possible the geometrical resolution as obtained in X-radiography.

Since neutrons are not electrically charged, they do not form images on conventional X-ray films. Therefore converter foils frequently consisting of gadolinium, dysprosium or indium with a typical thickness of 25 - 250 μ m are used. By absorbing thermal neutrons these emit charged particle radiation that blackens X-ray films. Light-emitting converter foils, as generally employed in electronic neutron cameras, reduce exposure times by several orders of magnitude, however at the expense of image resolution.

*Work supported by the Federal Ministry of Research and Development (BMFT)

By further reducing neutron energies, as done in neutron filters called "cold sources", higher thicknesses of some metals (several centimetres of steel/iron and several ten centimetres of aluminium) can be penetrated and the contrast for homogeneous or other light materials is enhanced. However, such filters are only installed in test reactors, for they considerably reduce neutron fluxes.

For years the large-scale application of neutron radiography was delayed due to the lack of small and inexpensive yet powerful neutron sources. But recent progress in this area led to novel applications of neutron radiography, which, in turn, accelerated the development of small sources and radiography systems. Neutron sources at present available may be classified in six groups in descending order of neutron yield:

- Test and research reactors

Test and research reactors have been the most prolific source of neutrons, providing radiographs with a resolution comparable to that of X-radiographs. However, shielded experimental areas at reactor radiography facilities are generally small, permitting merely small objects to be radiographed for quality assurance purposes, and, for safety reasons, the usefulness of most reactors with regard to testing aerospace ordnance is limited. Furthermore, because of complex licensing procedures and high cost only a limited number of new reactors is likely to be built in the future.

- Cyclotrons

For a few years small compact cyclotrons¹⁶ and even smaller cyclotrons with superconducting magnets¹⁷ have been available. With these cyclotrons reactor-quality neutron radiographs can be produced within exposure times of several minutes up to one hour. Even superconducting cyclotrons cannot be considered as mobile, e.g. as required for aircraft maintenance, but they are transportable.

Cyclotrons will for some time be the most powerful non-reactor neutron sources available, but their cost of several million US-\$ and their operating complexity restrict their employment to rework centres with a high throughput of test objects.

- Van de Graaff accelerators

Stationary Van de Graaff accelerators were employed very early as in-house neutron sources, in particular for the inspection of ordnance. They may now be considered as less attractive, since small cyclotrons with a higher neutron yield are available. A project to develop a mobile Tandem- Van de Graaff accelerator in the US was terminated in 1987 for apparent lack of success.

- Neutron generators

Neutron generators, consisting of a sealed neutron-emitting tube with a weight of a few kilograms as well as separate, readily transportable high-voltage and cooling supply units represent the most promising source for mobile neutron radiography systems. They are attractive because of the comparatively low cost and simple, essentially maintenance-free operation. The first mobile sealed-tube neutron generator-based radiography system in Europe, recently equipped with a handling system designed for the inspection of combat aircraft, was installed at IABG in 1988 (figure 3).

Major drawbacks of sealed tube generators are as yet the low neutron yield, further enhanced by the high energy of 14 MeV of the emitted neutrons and therefore low fraction of neutrons thermalized in the moderator, as well as a short target lifetime of a few hundred hours with a continuous drop in the neutron yield.

In order to overcome these remaining drawbacks a EUREKA-project with the aim to develop a powerful mobile neutron radiography system, "DIANE" (Dispositif Integre et Automatique de Neutrographie) was initiated by SODERN (France), SENER (Spain) and IABG in 1987, now joined by LTV Aerospace and Defence Company (USA)^{14,15}. The essential part of this system is a new sealed-tube neutron generator, "GENIE 46", to be developed by SODERN, with a considerably higher neutron yield and target lifetime than hitherto achieved with such systems. The first "GENIE 46"-prototype will be installed into the IABG-system for test purposes in early 1990.

- Linear accelerators

Electron Linear accelerators that were used in some research centres for neutron radiography are now known to be unsuitable for this purpose because of the high electromagnetic background radiation produced and the comparatively low neutron yield. Compact ion linear accelerators are currently being developed as (potentially transportable) sources for radiography¹⁸, but no experimental results on their performance have been obtained, yet.

- Radioisotope sources

Radioisotope facilities on the basis of californium (Cf^{252}) have been the most widely used neutron sources for radiography in the US, since they are simple to operate and require little maintenance. Furthermore, californium has been supplied free of charge in the US as part of a government program, although a continuation of this service is presently being reconsidered. Most existing systems, designed for research purposes, produce low neutron fluxes, but a high neutron yield can be obtained by adding up a sufficient amount of the isotope, provided the assembly is cooled and the permanent biological shield appropriately dimensioned.

Major radioisotope systems (e.g. as used at McClellan AFB, Sacramento) with a neutron yield comparable to that of accelerator-based units contain several ten milligrams of californium, surrounded by a moderator and a biological shield with a weight of usually several tons.

Apart from safety aspects, which would make licensing of a radioisotope facility in most countries difficult if not impossible, a disadvantage of californium is the short half-life of 2.65 years. One milligram of californium produces $2.3 \cdot 10^9$ ns⁻¹ at a cost of approximately 10000 US-\$. In order to replace a powerful neutron generator, a radioisotope source of about 60 mg of californium with an equivalent neutron yield may be chosen, which requires an annual replenishment of 16 mg to maintain the initial neutron yield. This exceeds the purchase and annual cost for the neutron generator several times.

The above comparison between neutron sources shows that small cyclotrons and neutron generators are likely to be dominant for neutron radiography purposes in the foreseeable future. The former may be installed as stationary systems for industrial quality assurance, while the latter represent inexpensive, simple to operate neutron sources for mobile use in aircraft maintenance both in rework centres and in the field.

3. APPLICATIONS IN AEROSPACE MAINTENANCE AND QUALITY ASSURANCE

Taking into account previous results obtained in the US, a large number of potential applications of neutron radiography in aerospace maintenance and quality assurance has been investigated during the above mentioned research project at IABG:

- Corrosion

Corrosion can be made visible by neutron radiography because of hydrogen contained in corrosion products. The hygroscopic character and hence the moisture content of corrosion products additionally represent an important factor with respect to their detectability.

Particularly surface corrosion, exfoliation corrosion and generally corrosion accompanied by sufficient corrosion products (e.g. in aluminium honeycomb structures) were found to be detectable with neutron radiography. Intergranular, stress and pitting corrosion in an advanced stage were also revealed.

The minimum thickness of corrosion products visible depends strongly on a number of factors, such as the moisture content of the corrosion products, the neutron radiography system and film/electronic camera employed and on how well the corrosion boundaries are defined. Under optimum conditions the minimum thickness of corrosion products detectable with small accelerator-based radiography systems is of the order of 0.01 inches.

Figure 4 shows the neutron radiograph of a combat aircraft wing with integral fuel tank. An aluminium plate with surface corrosion was placed inside the tank. The corrosion products are clearly visible.

Figure 5 shows the neutron radiograph of a fuselage section of a passenger aircraft consisting of, from the inside out, interior panel, glass fiber insulation and a lap joint section. The lap joint contains corrosion (barely detectable by visual inspection from the inside of the fuselage after removing interior panel and soundproofing) that is seen in the radiograph.

- Entrapped moisture

Neutron radiography was found to be by far the most sensitive NDT method to detect entrapped moisture or liquids. Moisture films, e.g. in honeycombs, with a thickness of less than 0.004 inches can be made visible.

Figure 6 shows the neutron radiograph, recorded with an electronic neutron camera, of an experimental passenger aircraft spoiler, consisting of a carbon fiber composite (CFC) sandwich with honeycomb core. Entrapped moisture and water, causing severe disbonding between honeycombs and CFC-layers, are clearly visible as dark patches.

- Adhesive defects

Neutron radiography can successfully complement conventional inspection methods in case of adhesive defects caused by too much or too little adhesive, voids or cracks in the adhesive and/ or when the affected parts are not accessible.

Figure 7 shows the neutron radiograph of a stringer consisting of several adhesively bonded aluminium layers that was taken from the tail section of an in-service helicopter. The radiograph reveals voids in adhesive layers. For comparison the X-radiograph of the same stringer is added in figure 8.

An example demonstrating by comparison the applicability of neutron and X-radiography with regard to the detection of corrosion, entrapped moisture and adhesives is given in figures 9 and 10, showing the neutron and X-radiograph of a section of a helicopter rotor blade with aluminium honeycomb core. A part of the honeycombs was removed and replaced by corroded honeycombs (1) taken from a naval reconnaissance aircraft, discernible as dark lines in the neutron radiograph. The honeycomb image (2) seen in the neutron radiograph does not, as in the X-radiograph, originate from absorption of radiation in the aluminium (which is transparent to neutrons), but from compressed layers of adhesive between the honeycomb core and the outer aluminium profile. Entrapped water that was injected into the honeycombs (3) produces comparatively high-contrast images in the neutron radiograph. Several wedges of different materials were added for calibration purposes.

- Defects in carbon fiber composites

Conventional NDT methods are in most cases superior to neutron radiography with respect to the detection of defects, e.g. impact damages, in CFC-structures. However, neutron radiography becomes useful, when defective CFC-layers are covered by metals or in case of resin inhomogeneities.

Figures 11 and 12 show the neutron and X-radiograph of a CFC-panel (containing a tube section) with resin inhomogeneities. Neutron radiography provides a higher-contrast image of this defect.

- Defective O-rings

Defects in O-rings between metals, e.g. between different sections of booster rockets, are difficult to detect by conventional NDT methods. In the course of the IABG-research project a section of the projected booster of the ARIANE 5 containing two O-rings with different simulated defects (cuts, notch (upper O-ring) and displacements (lower O-ring)) was examined with neutron radiography (figure 13). The O-rings with a diameter of approx. 0.3 inches were situated between steel layers of a total thickness of approx. 0.9 inches (upper O-ring) and 0.8 inches (lower O-ring). All defects are clearly visible in the radiograph that was produced at a "cold source" reactor facility.

- Further applications

The examination of ceramics components (particularly those on the basis of silicon carbide (SiC) that is increasingly used for some parts of spacecraft) by neutron radiography revealed defects, e.g. porosity and inhomogeneities, that frequently lead to the failure of the affected components, yet could not be found with any other NDT method¹³.

Neutron radiography has been also successfully applied to the detection of cracks, particularly in thick metallic objects and in the potting of electronics components. By using gadolinium-based contrast agents that have considerably higher attenuation coefficients for neutrons than comparable contrast agents for X-rays, hairline cracks or delaminations with a width of a few micrometres in or between metals, composites, plastic materials and adhesive layers could be seen in their full extent¹³.

Figure 14 shows the neutron radiograph of a segment of a SiC -based ceramics ring with porous regions and a hairline crack that was made visible with the contrast agent described above.

CONCLUSIONS

Neutron radiography was found to be a useful, supplementary NDT method with regard to the detection of some types of corrosion, entrapped moisture and liquids, certain defects in adhesive layers and carbon fiber composites, defective O-rings, cracks particularly in thick metallic objects and in the potting of electronics components as well as some flaws in ceramics.

A new generation of accelerator-based neutron radiography systems is likely to provide the technical basis for the economical application of this NDT method in an aircraft maintenance environment and possibly in industrial quality assurance.

The present development^{10,11} points in direction of a future employment of neutron radiography combined with X-radiography, ultrasonic and other techniques, integrated in fully automated inspection systems in aircraft rework centres.

REFERENCES

1. Hawkesworth, M.R., "Basic Principles of Thermal Neutron Radiography", Proc. of the First World Conf. on Neutron Radiography, San Diego, USA, 5.-9. Dez. 1981 (D. Reidel Publishing Company, Dordrecht, Holland, 1982) pp. 5-21.
2. Golliher, K.G., "Neutron Radiography of Apollo Ordnance", Ref.1, pp. 325-332.
3. Bouloumie, J.-P., "Aspects Qualitatifs du Controle Neutrographique Applique aux Chaines Pyrotechniques du Lanceur ARIANE", Proc. of the Second World Conf. on Neutron Radiography, Paris, Frankreich, 16.-20. Juni 1986 (D. Reidel Publishing Company, Dordrecht, Holland, 1987) pp. 263-270.
4. Edenborough, N.B., "Neutron Radiography to Detect Residual Core in Investment Cast Turbine Airfoils", Neutron Radiography and Gaging, (Berger, h., Ed.), ASTM STP 586, Philadelphia, 1976, pp. 152-157.
5. Dance, W.E., "Neutron Radiographic Nondestructive Evaluation of Aerospace Structures", Ref. 4, pp. 137-151.
6. Larsen, J.E., Baltgalvis, J., Patricelli, F., Gallardo, M., and John, J., "Evaluation of a Portable Neutron Radiographic System for the Detection of Hidden Corrosion in the Wing Fuel Tank of the E-2C Aircraft", IRI Corp. Techn. Rep. INTEL-RT 6081-001, 1975.
7. Patricelli, F., Larsen, J.E., Baltgalvis, J., Marks, R., and John, J., "Californium-252 Based Neutron Radiography for the Detection of Disbands in the Spar Closure Area of 540 Series Helicopter Blades", IRI Corp. Techn. Rep. INTEL-RT 6085-001, 1975.
8. John, J., "Californium-Based Neutron Radiography for Corrosion Detection in Aircraft", Ref. 4, pp. 168-180.
9. Fromm, D.A. and Barton, J.P., "Plans for Aircraft Maintenance Neutron Radiography Systems", Ref. 3, pp. 431-438.
10. Henderson, B., "USAF Expects Robotic Inspection Facility to Cut Maintenance Costs", Aviation Week and Space Technology, March 13, 1989, pp. 53-57.

11. Froom, D.A. and Barton, J.P., "Aircraft Neutron Radiography - An Overview", Proc. of the Third World Conf. on Neutron Radiography, Osaka, Japan, May 14-18, 1989 (in print).
12. Mast, H.-U., Knorr, E., Stein, P., and Richter, R., "A Comparative Study of Neutron Radiography and Conventional Nondestructive Testing Methods for the Inspection of Aircraft", Ref. 11.
13. Mast, H.-U., Brandler, T., and Richter, R., "Various Industrial Applications of Neutron Radiography", Ref. 11.
14. Dance, W.E., Huriet, J.R., Cluzeau, S., Mast, H.-U., and Albisu, F., "DIANE: Advanced System for Mobile Neutron Radiology", Nuclear Instruments and Methods in Physics Research B40/41, 1989, pp. 1316-1321.
15. Dance, W.E., and Mast, H.-U., "Performance of Operational Mobile Accelerator Neutron Radiology (NR) System as Scale Factor for DIANE", Ref. 11.
16. Fukushima, J., Nakamura, T., Hiroaka, T., Sekita, J., Yokochi, H., Yamada, T., and Yamaki, S., "Neutron Radiography Using Ultra-Compact Cyclotrons", Ref. 3, pp. 215-221.
17. Wilson, M.N., and Finlan, M.F., "The Superconducting Cyclotron as a Transportable Neutron Source", Ref. 3, pp. 199-206.
18. Hamm, R.W., "Compact Ion Linear Accelerators for Neutron Radiography", Ref. 11.

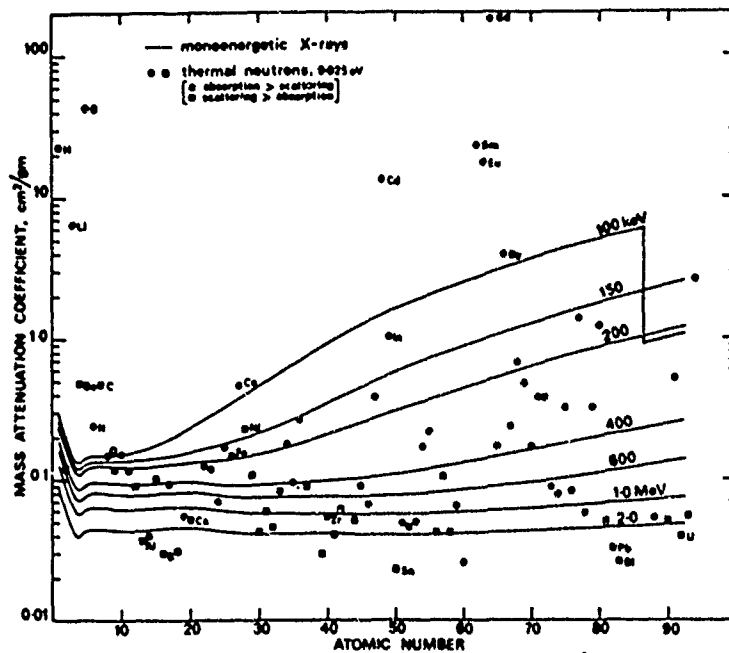


Figure 1 Mass attenuation coefficients of the elements as a function of atomic number for X-rays with energies between 100 keV and 2 MeV (lines) and for thermal neutrons (dots)

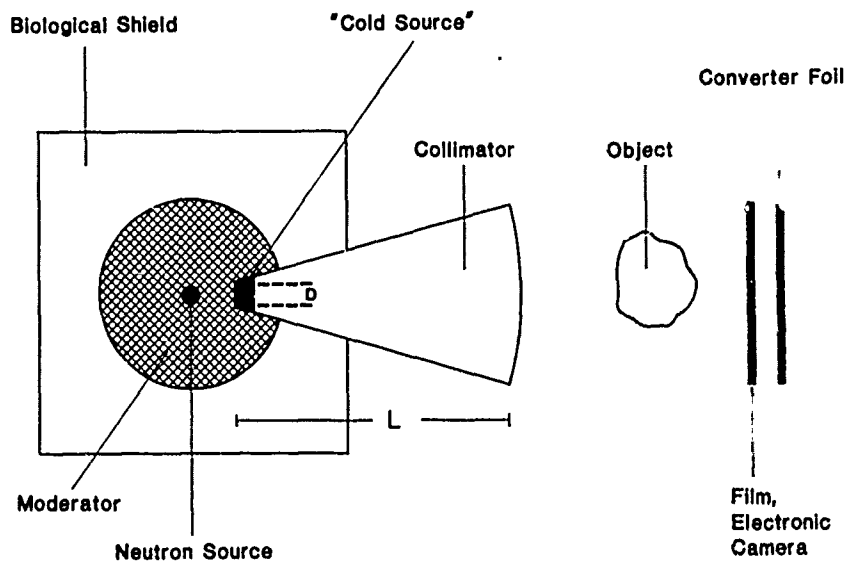


Figure 2 Principle of a neutron radiography system

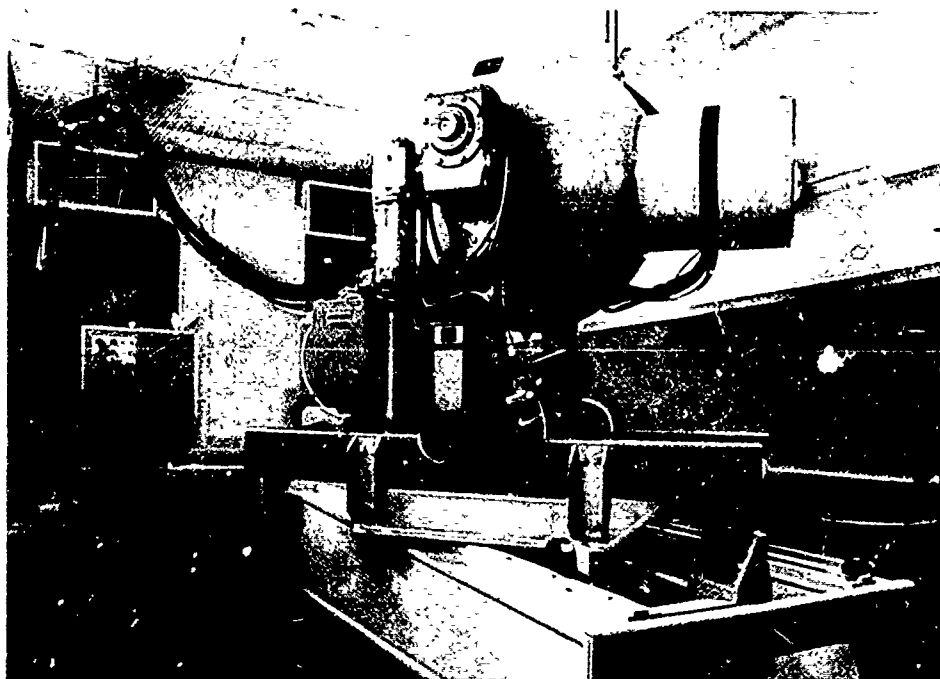


Figure 3 Neutron generator-based mobile radiography system at IABG

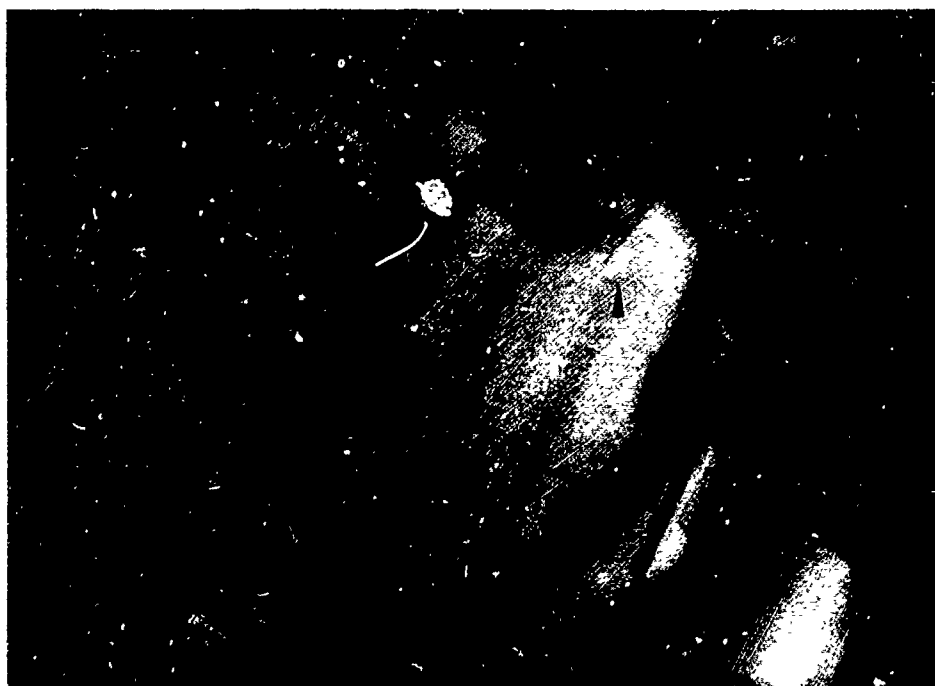


Figure 4 Neutron radiograph of surface corrosion in the integral wing fuel tank of a combat aircraft (IABG-system)



Figure 5 Neutron radiograph of a passenger aircraft fuselage section with lap joint corrosion (IABC-system)



Figure 6 Neutron radiograph of an aircraft spoiler with entrapped moisture and water (IABC-system)



Figure 7

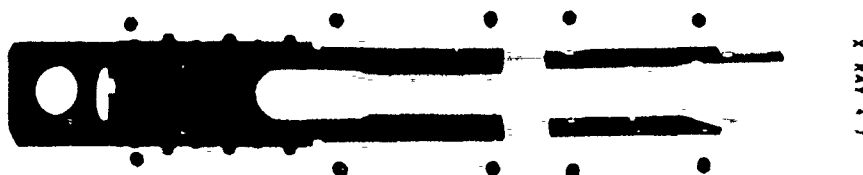


Figure 8

Figure 7 Neutron radiograph of a helicopter stringer revealing adhesive defects (Van de Graaff radiography system)

Figure 8 X-radiograph of the stringer shown in figure 7 (60 kV)

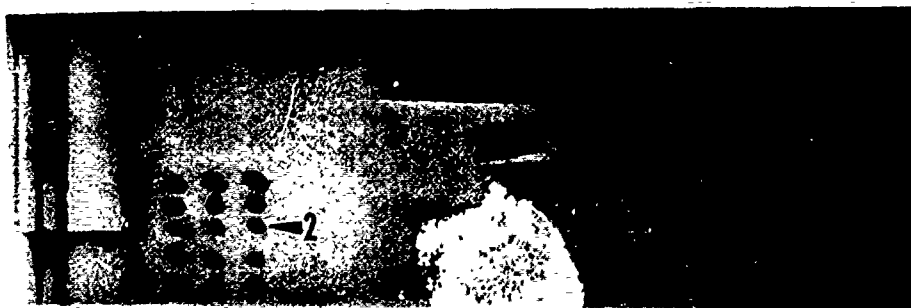


Figure 9



Figure 10

Figure 9 Neutron radiograph of a section of a helicopter rotor blade with various simulated defects (Van de Graaff radiography system)

Figure 10 X-radiograph of the rotor blade section shown in figure 9 (60 kV)



Figure 11 Neutron radiograph of a CFC-panel with resin inhomogeneities
(research reactor facility)

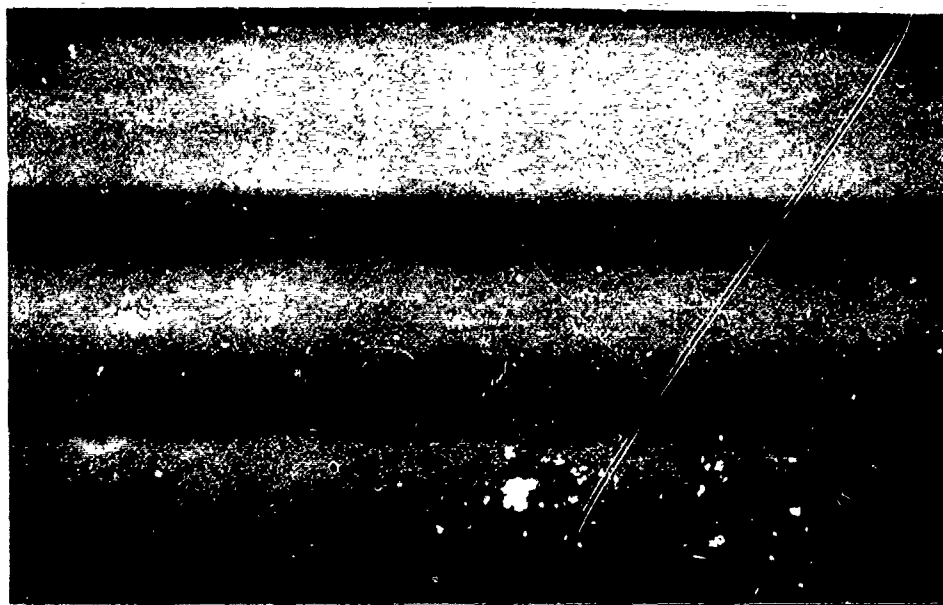


Figure 12 X-radiograph of the CFC-panel shown in figure 11 (30 kV)

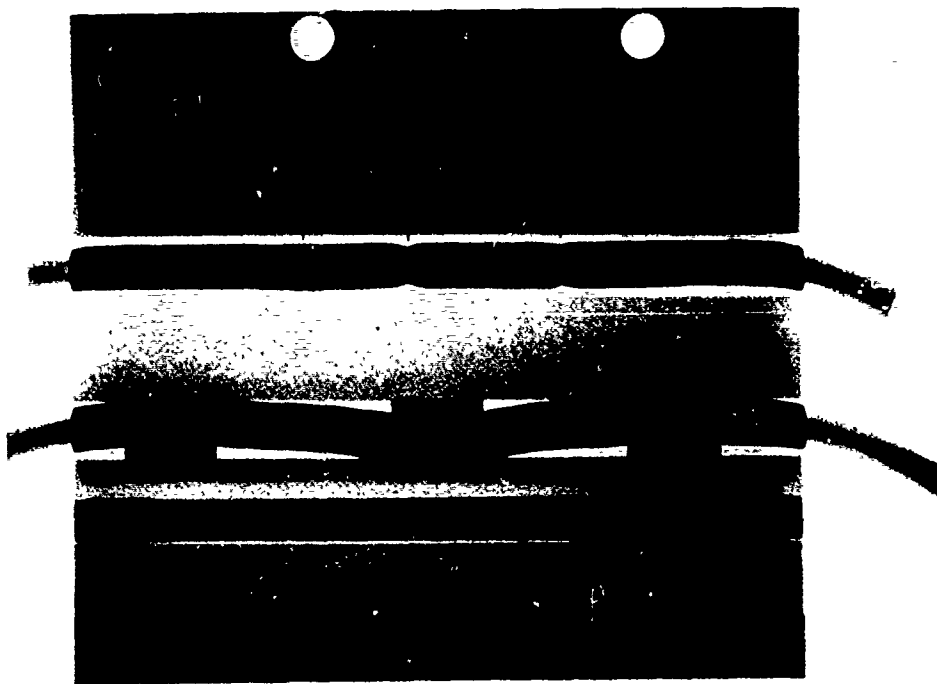


Figure 13 Neutron radiograph of a booster section containing O-rings with various simulated defects (research reactor facility)



Figure 14 Neutron radiograph of a segment of a ceramics ring with porous regions and a crack (research reactor facility)

PROGRESS IN THE DETECTION OF CRACKS UNDER INSTALLED FASTENERS USING EDDY CURRENTS

D J Harrison

MOD(PE)
Materials and Structures Department
Royal Aerospace Establishment, Farnborough
Hampshire, GU14 6TD
United Kingdom

SUMMARY

The detection and characterisation of fatigue cracks growing radially from fastener holes continues to be a major problem in the non-destructive inspection of aircraft. In general, it is highly desirable to be able to detect cracks in the skin and sub-structure without the need to remove fasteners. Eddy-current methods are in principle well-suited to the detection of cracks in metals but, in this case, difficulties of interpretation can arise as a consequence of the relatively complicated geometry. For example, the effect of the fastener itself or a nearby edge can easily mask the effect of a crack. If the effects of irrelevant geometric features can be identified and removed then the ability of eddy-current systems to detect cracks reliably under these circumstances can be considerably enhanced. An intelligent eddy-current instrument has been developed specifically for this problem. The Eddiscan uses a rotating transducer to map precisely any variations in the induced electromagnetic field around the circumference of the fastener. By using pattern recognition and other analysis techniques, the presence and position of cracks can then be inferred. Using this method, cracks in the skin and sub-surface layers can be detected with either ferrous or non-ferrous fasteners installed.

INTRODUCTION

One of the problems associated with the maintenance of the structural integrity of aircraft arises from the growth of small radial cracks beneath the heads of rivets and bolts. In the vast majority of cases these are fatigue cracks generated by the cyclic stresses induced by service loads. Such cracks may occur through deficiencies in the original design or poor quality control during manufacture, but, especially for military aircraft, their occurrence is often due to changes in the usage of the aircraft or the need to extend the life of the structure.

Whatever the cause, the possible presence of these cracks is proving of increasing concern to both civil and military operators and there is a clearly defined need to be able to detect them well before they approach a critical size. There are, of course, considerable economic advantages to be gained if these cracks can be detected while they are still small, because the costs of repair are usually much lower.

The number of fastener holes requiring inspection is often quite high and it is usually impractical to remove the fasteners in order to inspect the holes; indeed the act of withdrawal itself can cause sufficient damage to lead eventually to cracking. Although the exact requirement varies quite widely from component to component, there is in general a need for an instrument that can detect small radial cracks in the skin and subsurface layers under both ferrous and non-ferrous installed fasteners.

Existing in-service methods of inspecting installed fasteners are based primarily on ultrasonic and eddy-current techniques. The disadvantage of ultrasonic methods is that paint must be removed prior to inspection and re-applied afterwards. Furthermore, although automated ultrasonic instruments exist, they are cumbersome and very expensive and so many applications still rely on the use of hand-held transducers. Eddy-current methods also rely on the use of hand-held transducers; this limits the performance and also requires a sustained high level of concentration by the operator. The only semi-automatic approach is based on the sliding probe in which a probe, constrained by a straight-edge, is moved by hand along an entire line of fasteners. This method is fast although not particularly sensitive and relies on the fasteners being exactly colinear.

Eddiscan is an eddy-current inspection method that was originally developed to detect cracks specifically in the outer layer, or skin, of aircraft structures beneath installed non-ferrous fasteners (1), (2). Since then, the requirement has expanded to include cracks in subsurface layers of multi-layered structures and also ferrous, as well as non-ferrous, fasteners. The original instrument has been modified in order to meet the new requirements. Prior to discussing the basic principles and performance of the modified Eddiscan, it is necessary to consider the two developments that have made the modifications possible.

EDDY-CURRENT INSPECTION OF SUBSURFACE CRACKS

The detection of subsurface cracks using eddy currents has several features that make it distinct from the more common problem of detecting surface-breaking cracks. It is appropriate therefore to discuss the underlying theory in general terms in order to see how, in principle, to design a practical inspection technique that is optimised for this application.

The basic elements common to all eddy-current inspection methods are represented schematically in figure 1. An electromagnetic field source, usually a coil, induces eddy currents in a nearby conducting body. Within a conductor, eddy currents propagate in the form of attenuated travelling waves and so their interaction with cracks may be regarded as a scattering problem. Any crack that is "illuminated" by incident eddy-currents develops a charge distribution at its surface that radiates a scattered eddy-current field. Part of this propagates to the surface of the conductor where its associated magnetic field, H , can be measured by a suitable sensor as a function of position and time (or frequency). Depending on the amount of data that is gathered, various options are available ranging from simply detecting the presence of a crack to estimating its size, shape and depth.

It can be seen that the aims of good design include maximising the incident eddy-current field at the site of and normal to the plane of the crack and also measuring the scattered magnetic field at the surface with as much sensitivity and resolution as is reasonable, taking into account the

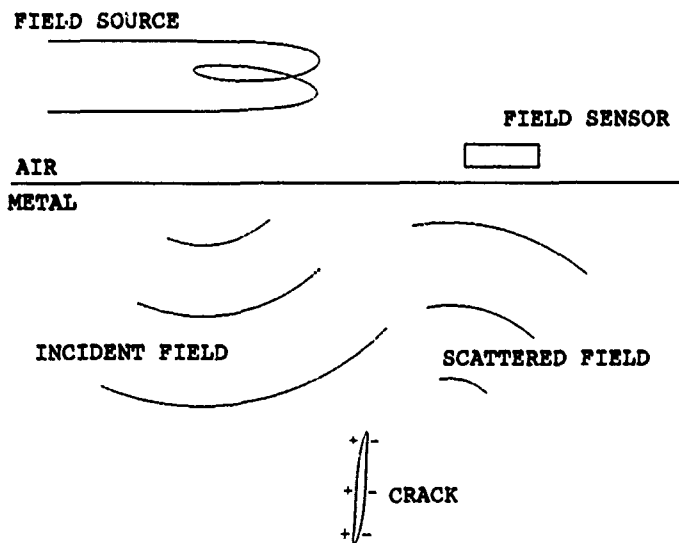


Figure 1. The basic model of eddy-current inspection

prevailing signal-to-noise ratio. In virtually all in-service applications, coils are used both as field source and field sensor and frequently the same coil is used for both. This latter arrangement is quite effective for detecting small surface-breaking cracks but is not appropriate for use with subsurface cracks. First, as eddy currents propagate through a conductor they become considerably attenuated particularly at high spatial and temporal frequencies. Thus in order to maximise the incident eddy-current distribution at the site of subsurface cracks, a large coil should be used as field source and the current through it should contain predominantly low temporal frequencies. Second, if used as a field sensor, a coil measures the time-derivative of flux linkage rather than magnetic field. At the low temporal frequencies that must be used, a coil becomes ineffective as a means of measuring magnetic field. The use of a Hall device as an alternative has the advantages that it is very sensitive to magnetic field at a point over a frequency range from DC up to 100 kHz. The combination of a large coil as field source and a Hall device as field sensor offers a substantial improvement in the detectability of subsurface cracks by virtue of its superior sensitivity and resolution compared with conventional techniques.

TRANSIENT EDDY-CURRENTS

It is frequently desirable or even necessary to be able to determine the depth of cracks or defects, either so that cracks can be better characterised or so as to help resolve genuine cracks from other defects which have no structural significance.

A particular problem that can arise with fasteners is caused by the identification marks that are often stamped on the heads. Since they can interact with the incident eddy current distribution they can cause a magnetic field perturbation that is measured by the field sensor. Although small, they are at the surface, and so the effect that they have is emphasised relative to the effect of a large crack that is some distance below the surface. It is essential in this case to be able to distinguish cracks from miscellaneous surface effects. These requirements have led to the development of a novel transient eddy-current method.

In conventional eddy-current techniques the field source is excited with a sinusoidal current and measurements are made at one or more fixed frequencies. Measurements made at a single frequency contain only a fraction of the information that is available. Measurements at different frequencies can be combined in order to improve the characterisation of cracks but the method of combination tends to be empirical since it lacks an intuitive interpretation. In Eddiscan the field source is driven by a square wave current, as shown in figure 2a. This generates impulses of EM radiation at each transition which propagate comparatively slowly into the conductor where dispersion and interaction with cracks and other electrical discontinuities causes radiation to be scattered back to the surface where it can be measured by the field sensor in the form of a bipolar series of magnetic field transients (see figure 2b).

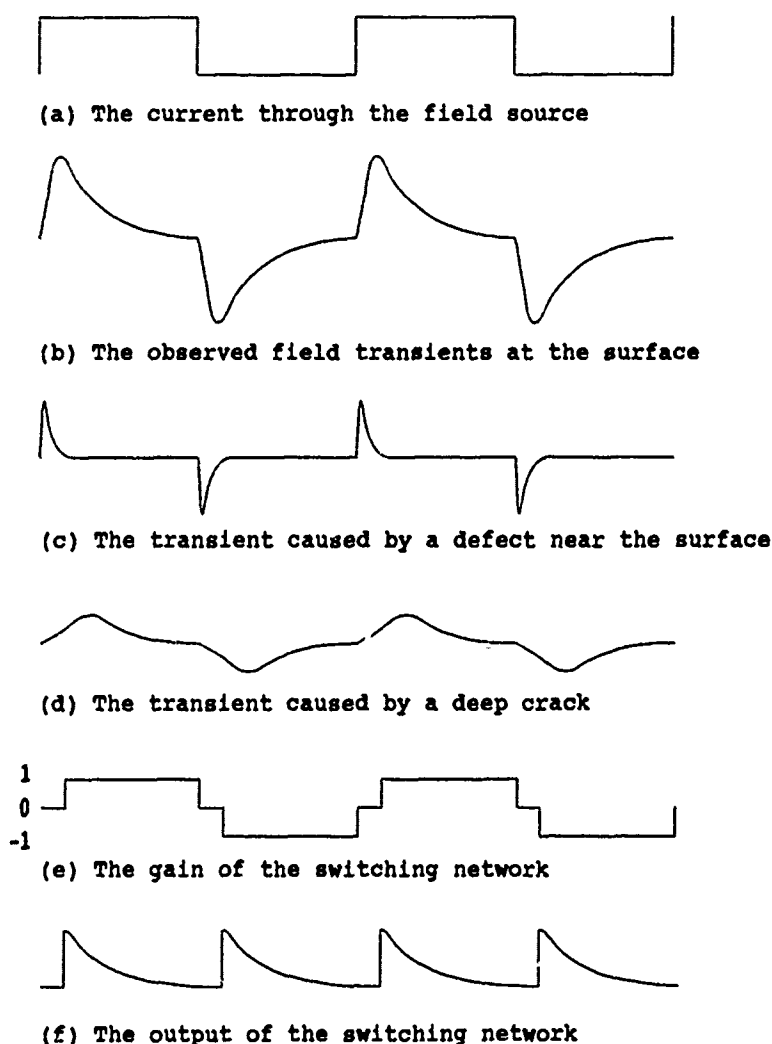


Figure 2. The shapes and timing of the basic waveforms

If interpreted correctly, these transients can be analysed to yield information about the depth of any cracks present. Most of the transient is caused by the high level of dispersion in the material. This remains constant and can be ignored. Superimposed on this are the smaller transients caused by cracks and defects. Because of the finite time taken for EM radiation to propagate down to a crack and back, the deeper the crack the longer the delay in the arrival back at the surface of the associated scattered field pulse. Thus the transient caused by a defect near the surface arrives back first (figure 2c) while the corresponding transient from a deep crack arrives later (figure 2d) and is characteristically broadened as a consequence of its longer path through the highly dispersive conductor. That is, different parts of the transient contain information about different depths; it is similar in principle to radar or ultrasonic pulse-echo techniques. Using synchronous gating methods, different parts of the transient may be selected and integrated to give an output that is an estimate of the total amount of radiation scattered from the corresponding depth band. This output is therefore sensitive only to cracks and defects that are present at that depth.

Using this technique it is easy to eliminate the effects of indentations and other surface artifacts. The initial part of each measured transient is discarded since it contains predominantly information about defects at or close to the surface. Information about subsurface layers is not lost since does not arrive at the sensor until later in the transient.

THE EDDISCAN SYSTEM

Eddiscan is a microprocessor-based instrument which uses a rotating transducer to detect cracks in multi-layered structures under installed fasteners. It is a software-configured instrument in which all operations including transducer control, data acquisition, analysis and display are controlled by means of programmed instructions.

An example of a fastener and its environment is shown in figure 3. This situation is typical of aircraft structures in which an outer skin is fastened to a substructure by means of rivets. Fatigue cracks can grow radially, as shown, in either layer. So far as eddy-current inspection is concerned, problems arise because of the dominant effect that the fastener and fastener hole have on any incident eddy-current field. In particular, the partial or total electrical discontinuity at the boundary of the hole and the different conductivity and permeability of the fastener can combine to generate a very large response in an instrument and hence mask the effect of genuine cracks that might otherwise be readily observable. This is particularly so in the case of ferrous fasteners. Also, as previously indicated, indentations

and other identifying marks in the heads of many fasteners can also cause problems. The purpose of the Eddiscan instrument is to make measurements in such a way that these disruptive signals are either eliminated or drastically reduced.

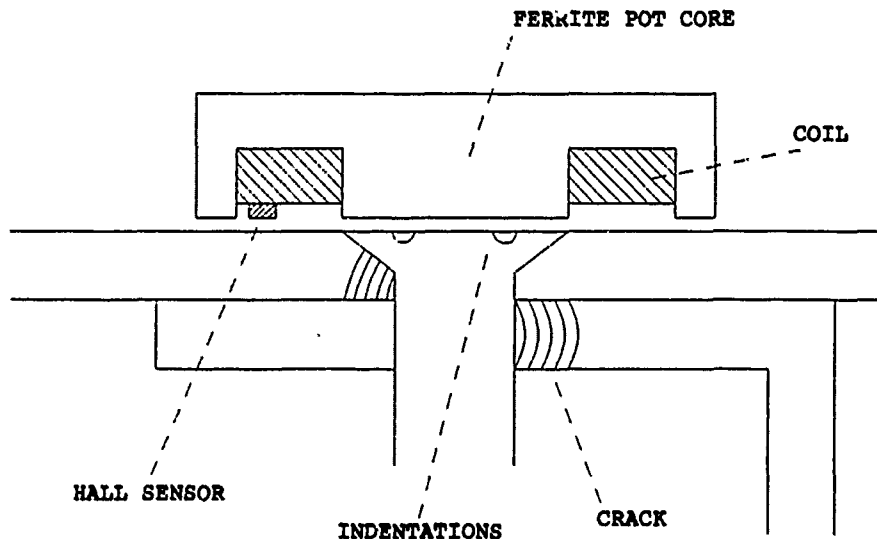


Figure 3. The transducer positioned over a typical fastener

Recalling the foregoing discussion on optimising the detection of subsurface cracks, a cylindrically-symmetric ferrite pot-core and coil are used as field source and a Hall device is used as field sensor. This is illustrated in figure 3 with the pot-core positioned coaxially above the fastener. A square-wave current is passed through the coil and induces pulsed eddy-current loops around the fastener which propagate down into the conductor. If there are no cracks present, then as the pot-core is coaxial with the fastener the current loops are concentric and consequently all magnetic fields have circular symmetry about the axis of the fastener. Measurements are made at the surface using a Hall device which measures the component of magnetic field perpendicular to the surface. The sensor voltage, as a function of time, represents the train of transient magnetic fields that are scattered back to the surface (figure 2b) as a result of the square-wave current excitation. If the sensor is rotated about the axis of the fastener then the shape of the transients will remain constant since all the fields are circularly symmetric. If however a radial crack is present, then the induced currents are distorted in its vicinity and no longer circularly symmetric. Consequently the magnetic field at the surface exhibits a perturbation above the crack. Under these circumstances, when the sensor is rotated about the axis of the fastener the shape of the observed field transients changes as the sensor passes over the crack. This change in shape is due to the small additional transient field scattered by the crack and is the basic data that is used to detect and characterise the crack.

Three distinct axes are involved: the axis of the pot-core, the axis of the fastener and the axis about which the sensor is rotated. If they are all coincident as described above then the fastener and hole are effectively transparent and small cracks can easily be detected. In order to simplify the transducer, the Hall sensor is attached to the underside of the pot-core and they are both rotated together about the axis of the pot-core by means of a stepper motor as illustrated in figure 4. In principle there is no need to rotate the pot-core but this procedure eliminates one of the independent axes. Connections to the coil and Hall sensor are made via slip rings. A magnetic pick-up is incorporated in order to give a pulse once per revolution so that the absolute angular position of the sensor can always be determined.

A simplified block diagram of the electronics is shown in figure 5. A microcomputer is the main component of the system and communicates with several peripheral devices including a graphics processor by means of an address and data bus. The drive current for the field source is derived from a digital-to-analogue converter (DAC1) which generates a square wave under programme control. The timing of this signal, in common with all other signals, is determined by programmed instructions which are synchronised to a free-running counter-timer in the microcomputer.

The output of the Hall sensor is a bipolar series of transients as shown in figure 2b. It is amplified and processed by a switching network which can reverse the polarity of the input signal or set it to zero under programme control. If switching changes are synchronised to the square-wave source current then predetermined parts of each transient can be selected or suppressed. Figure 2e summarises the switching strategy that is used in this case. The trace represents the gain of the switching network. At the beginning of each transient the gain is switched to zero in order to discard the signals arising from surface defects. Note that since the transient series is bipolar, alternate transients must be reversed in polarity in order to obtain a non-zero mean. The output of the switching network is a series of unipolar transients (figure 2f) that represents the energy scattered from below the surface but not from the surface itself. The mean level of this signal is therefore sensitive to subsurface cracks but unaffected by surface artifacts and so when the transducer is rotated about the axis of a fastener the mean level will be perturbed as the sensor passes over a crack.

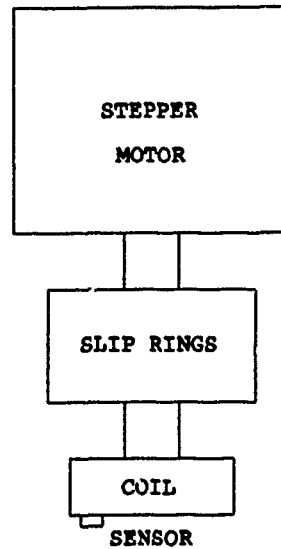


Figure 4. The Eddiscan transducer

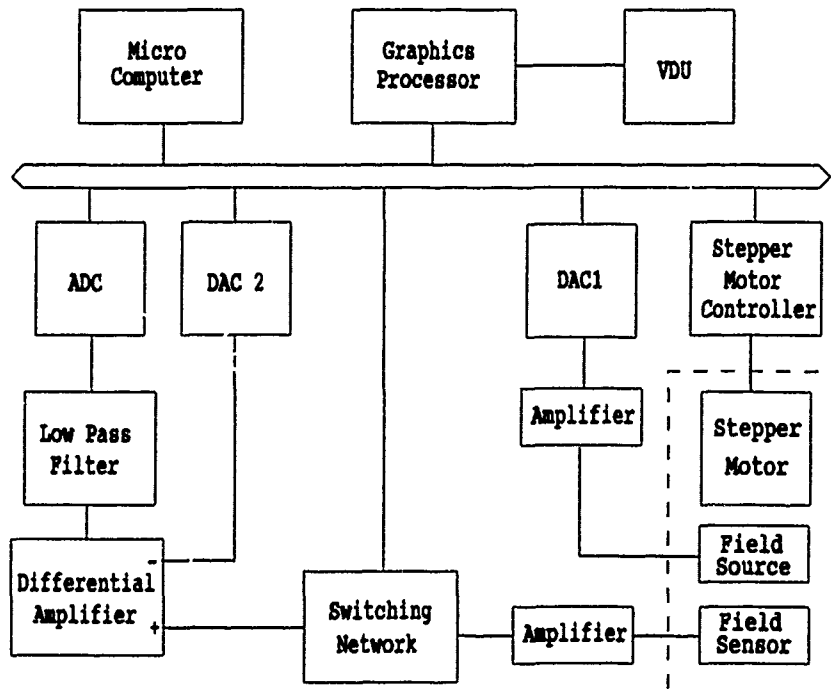


Figure 5. Block diagram of the electronics

The mean level can be extracted by low pass filtering but, since the variations due to cracks are small, the signal must first be amplified. However, the mean level contains a comparatively large DC offset which depends on material properties and which must be removed first. This is done by generating a quasi-DC voltage using DAC2. This is adjusted under programme control in order to balance out the offset. The output of the low pass filter then represents the amplified mean level variations and can be sampled by an analogue-to-digital converter (ADC) and stored in memory.

In terms of the hardware implementation of an eddy-current system, the use of a transient technique enables the analogue electronics to be greatly simplified. It is no longer necessary to generate sinusoidal driving signals or use techniques such as analogue synchronous demodulation. Apart from signal amplification, everything can be accomplished by means of synchronous switching circuits. This type of circuit is ideally suited to microprocessor control.

SYSTEM OPERATION

The system operates in the following way. The transducer is driven at a constant speed of approximately 300 rpm and measurements of the low pass filter output voltage are continually sampled by the ADC as a function of angular position and stored in memory, each measurement overwriting the previous one at that position so that a constantly updated scan is available in memory. This scan is the basic unit of data that is used in all subsequent calculations.

If the transducer is rotated about the axis of a fastener then the resulting scan represents a map or image of the magnetic field variations around the circumference of the fastener. For the case when no cracks are present, since everything is cylindrically symmetric, the scan yields a straight line. If, however, a radial crack is present, the scattered field from it causes a peak in the resulting scan as the sensor passes over the crack as shown schematically in figure 6a. This data can be processed by software techniques to identify the presence and angular position of any cracks.

The transducer can be used as described above to detect small cracks when it is rotated about the axis of a fastener. However, in general it is not possible to position it with sufficient precision; indeed, the fastener may be covered with paint and thus not visible. If the transducer is misaligned and rotates about an axis that is off-centre from the fastener then the induced current interacts with the boundaries of the hole and is severely distorted even in the absence of any cracks. Also, if the Hall sensor rotates about a different axis to that of the fastener then large magnetic field variations are observed even if the induced current is circular and the resulting scan is dominated by an error (figure 6b). This makes the transducer ineffective even though it is very sensitive to small cracks since their effect can be dwarfed by the error signal as shown in figure 6c.

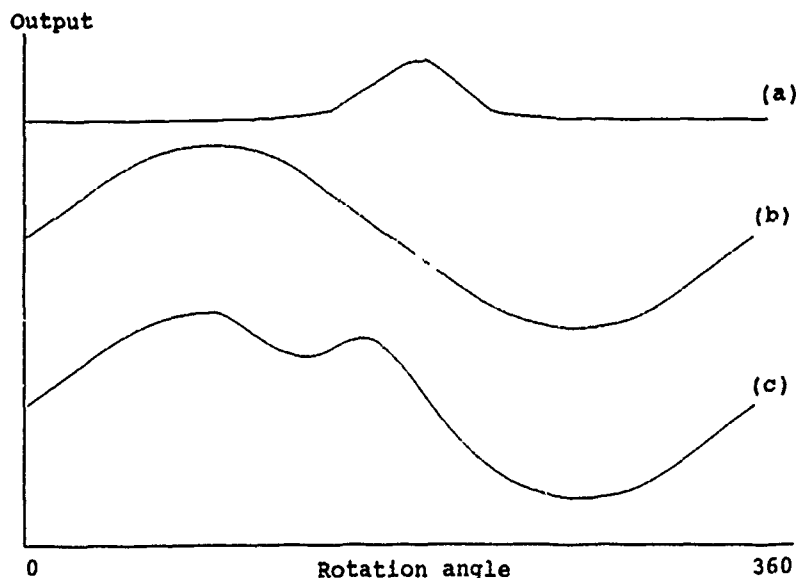


Figure 6. Scans for one complete revolution: (a) for a crack, (b) due to misalignment and (c) for a crack when the transducer is misaligned

The problem of centering can be overcome since the characteristics of the error signal due to misalignment are uniquely determined by the relative position error of the transducer. Thus, software techniques can be used to continually analyse the scan, identify the error signal and generate a real-time centering display as shown in figure 7. The axes represent the position of the fastener and the small cross represents the position of the transducer. As the transducer is moved around over the fastener, the small cross moves in unison with it. This display enables an operator to centralise the transducer and hence eliminate the error function.

This process rapidly enables the removal of gross misalignment signals but, and particularly with ferrous fasteners, the transducer is so sensitive to small movements that it is virtually impossible to centralise it precisely within a reasonable time. Software, in the form of pattern recognition techniques, is used to identify and remove the residual misalignment signal so that approximate centering is sufficient as well as rapid. The ability to centralise and hence make use of this type of rotating transducer depends totally on the use of software techniques.

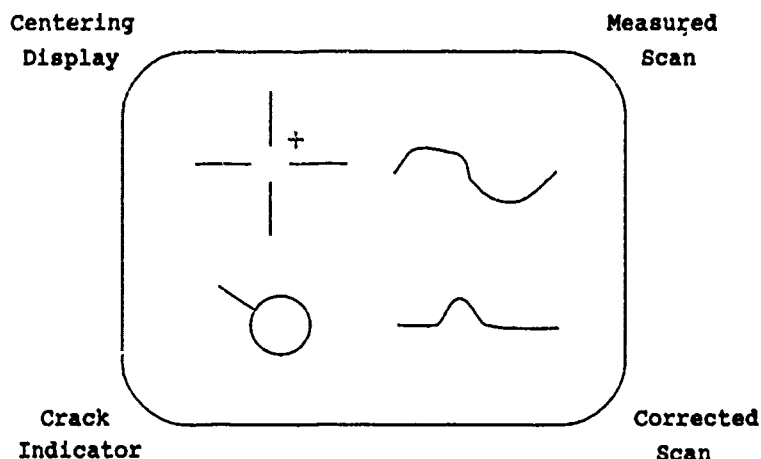


Fig 7. Information displayed on the screen

Thus the original measurements of a series of transients are processed by hardware and software to generate a one-dimensional scan or image of any cracks present from which the effects of transducer misalignment and surface artifacts have been removed. Although this image can be further analysed in order to reconstruct and display a pictorial representation of the crack, the basic version of the instrument described here displays results and information to the operator on a VDU in the form shown by figure 7. The measured scan is a direct display of the raw data for one complete revolution and is continually updated. The corrected scan shows the corresponding results after the residual alignment error has been removed. This shows the isolated peak due to a crack. The crack indicator is a plan view of the fastener head showing the angular position and size of detected cracks.

PERFORMANCE

A prototype instrument has been constructed on the basis of these principles. In order to indicate the performance that can be obtained, some results are shown of measurements made on a multi-layered specimen comprising seven sheets of aluminium alloy, each 2.5 mm thick, fastened together with 5.0 mm diameter ferrous rivets with irregular indentations stamped in the heads. Genuine fatigue cracks of various sizes are simulated by EDM slots.

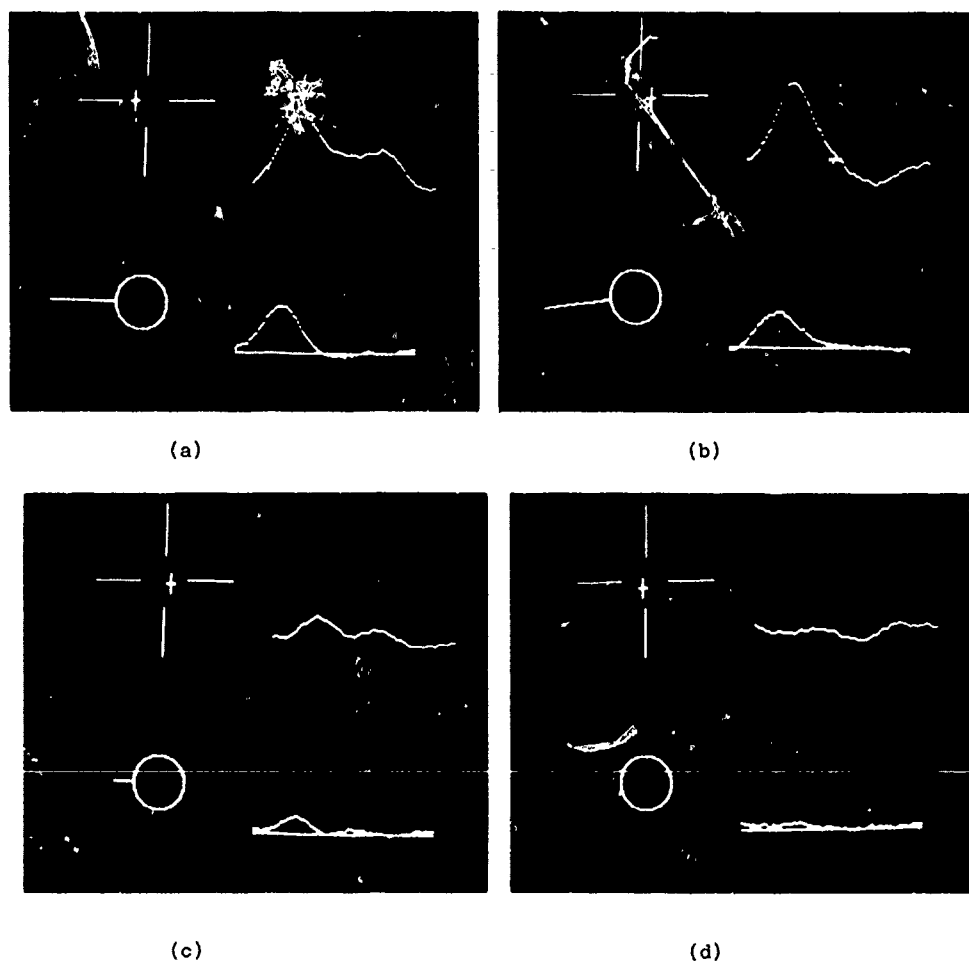


Figure 8. Results for EDM slots in the second layer: (a) 5.0 mm, (b) 3.0 mm, (c) 1.5 mm and (d) no crack

The transducer can be centralised over a fastener and measurement completed within approximately ten seconds. As an example of the performance of the system, results photographed directly from the screen are shown in figure 8 for EDM slots of sizes 5.0 mm, 3.0 mm, 1.5 mm and 0.0 mm radial length in the second layer. They were all at the 9 o'clock position relative to the transducer. The presence of these slots is readily apparent from visual inspection of the corrected scan and the crack indicator shows the correct angular position. However, it is not intended that an operator should rely on this type of display. Ultimately, these results will be further analysed and presented in a more detailed and comprehensive graphical form.

CONCLUDING REMARKS

Consideration of the physical principles underlying eddy-current inspection has led to an improved method of detecting subsurface cracks. This has been applied to the problem of detecting cracks under installed aircraft fasteners and it has been shown that a prototype Eddiscan system (3) has a satisfactory performance.

The use of microprocessors is critical for the type of instrument described here. It is by means of extensive analytical techniques and digital processing that gains in performance can be made over conventional analogue instruments.

REFERENCES

- 1 D J Harrison, "The Detection of Cracks under Installed Aircraft Fasteners by means of a Scanning Eddy-Current Method", in *Review of Progress in Quantitative NDE*, Vol 6A, D O Thompson and D E Chimenti, Eds., Plenum Press, 1987, p. 1013.
- 2 D J Harrison, Royal Aerospace Establishment, "The Detection of Cracks under Installed Aircraft Fasteners", 1987, TR87040.
- 3 The Eddiscan device as described in this paper is the subject of British patent application 8916423 made on 18 July 1989.

ACOUSTIC EMISSION DETECTION OF CRACK PRESENCE AND CRACK ADVANCE DURING FLIGHT

S.L. McBride, M.D. Pollard, J.D. MacPhail, P.S. Bowman, D.T. Peters

Department of Physics
The Royal Military College of Canada
Kingston, Ontario, Canada K7K 5L0

SUMMARY

Results are presented which show that it is possible to detect crack growth and crack presence in airframe components during flight.

To accomplish this, a data acquisition system has been developed specifically for in-flight applications. It is shown that crack advance of less than 1 mm^2 was readily detected during flight and the fracture-related acoustic emission signals unambiguously identified.

INTRODUCTION

Since the mid-1970s, several studies have investigated the feasibility of using acoustic emission (AE) to monitor the integrity of aircraft structural components during flight. These studies are completely catalogued in an annotated bibliography of acoustic emission [1,2]. AE has the advantage of being capable of monitoring large components with a single sensor, is truly a passive technique, and can be conveniently used in hard-to-reach locations. Successful development of this technique will offer tremendous savings by reducing the need for major disassembly in order to inspect critical load-bearing components.

The principal problem of acoustic emission monitoring is the unambiguous identification of signal sources (eg, crack growth, crack face rubbing, structural noises). This problem is addressed here, using a multiparameter criterion to identify signals originating at a crack in the presence of airframe noises. To accomplish this, we have developed a data acquisition system specifically for in-flight AE monitoring. This system is stand-alone, is battery-powered, and allows for dual-channel multiparameter processing of the data during flight. This multiple-criterion system greatly enhances the confidence level for the unambiguous separation of crack-related data from airframe noise.

This study also includes the use of an inertially-loaded specimen, containing a well-documented crack, which is attached to the support frame in the instrumentation bay of a Tornado aircraft. Aircraft manoeuvres produce crack advance in the specimen under known g-loading conditions and with superimposed airframe noise. This test apparatus, along with the prototype data acquisition system, has been flight tested in both the Canadian CF-5 and the British Tornado aircraft.

EXPERIMENTAL

The Data Acquisition System

The dual-channel, digital data acquisition system used here was designed and constructed specifically for the recording and interpreting of acoustic emission data during flight. The design is based on criteria derived from the RMC work of almost a decade in the area of acoustic emission monitoring during flight [3,4,5]. These studies established the importance of the difference in arrival time of an event at different locations, signal risetime, and the magnitude and variation of the applied stress at the time of occurrence of the event. All of these parameters are necessary to isolate crack-related events from other noise sources during flight and are recorded by the data acquisition system used here. To provide maximum flexibility, the data acquisition system can be powered either by the aircraft electrical system or by batteries.

The output of each of the two piezoelectric sensor elements is amplified by an integrated preamplifier (with nominal gain of 40 dB) located inside the sensor casing. The resulting signal is buffered, logarithmically amplified, envelope followed and peak detected. These operations are accomplished using signal conditioning boards custom-made for the purpose (figure 1a). The output of each envelope follower is separately fed into the digital data acquisition system where the times of preselected amplitude threshold crossings 6 dB apart are recorded (figure 1b). The output of the peak detectors and accelerometer are digitized by an A/D converter and stored in memory.

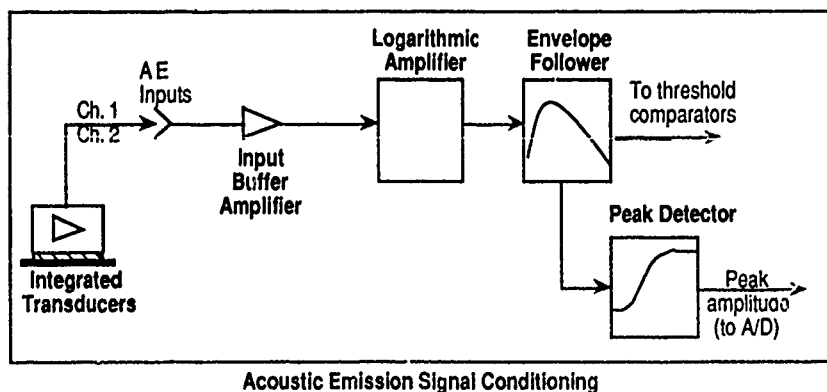


Figure 1a - Schematic diagram of the acoustic emission signal conditioning.

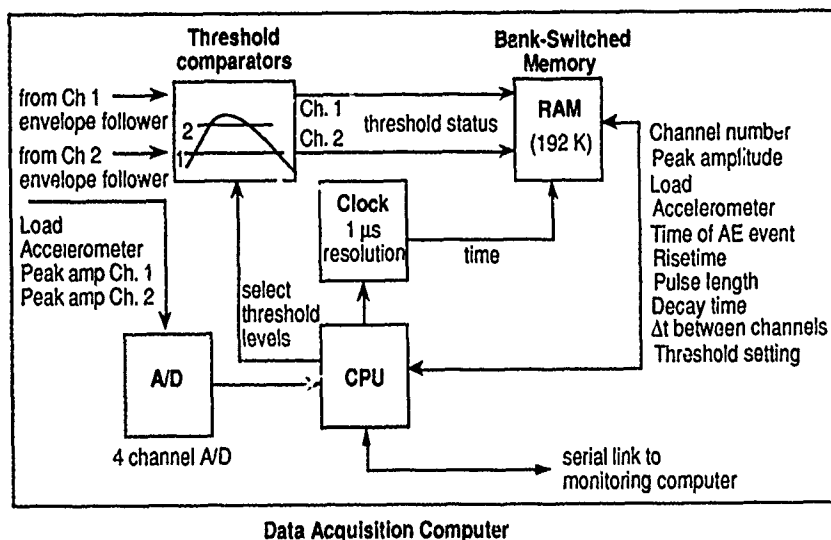


Figure 1b - Schematic diagram of the acoustic emission data acquisition computer.

All of the above data are compressed into an event record which includes the time of occurrence of the event at each sensor, the difference in arrival times at two sensors (Δt), event risetimes for 6 dB change in amplitude, event durations, event decay times and event peak amplitudes. The resulting data set is then extracted from the data acquisition system via an RS-232 interface and stored on disk on a portable personal computer. Extensive screening of data, field analysis and interpretation can be carried out immediately. Final analysis and interpretation are accomplished using spread-sheet software. Table 1 lists the general specifications of the apparatus.

Table 1 - General specifications for the RMC digital data acquisition system for in-flight acoustic emission monitoring applications

2 Channels AE	60 dB dynamic range
2 Analog Channels	0-10 V full-scale deflection
Power	10 Watts maximum
Memory	192 Kbyte RAM with battery back-up
Dimensions	23 cm x 13.5 cm x 25 cm
Weight	2 kg
Mass Data Storage	transfer to portable PC via RS232 interface

The Inertially-Loaded Specimen

Figure 2 shows a schematic diagram of the inertially-loaded 7075-T651 aluminum fatigue specimen clamped in the inertial loading frame support. Silicone fluid provides proper acoustic coupling of the fatigue specimen to the loading frame to ensure that airframe noises are transmitted to the fatigue specimen for detection by the acoustic emission sensors. Prior to mounting in the loading frame, the test specimen was precracked to a crack length which would cause crack propagation when the 0.9 kg inertial load was subjected to an acceleration in excess of 3 g. The aircraft acceleration is sensed by an accelerometer (Entran Devices, Inc., model EGD-240) mounted in the loading frame support block. The inertially-loaded specimen was acoustically coupled to the aircraft support frame in the instrumentation bay.

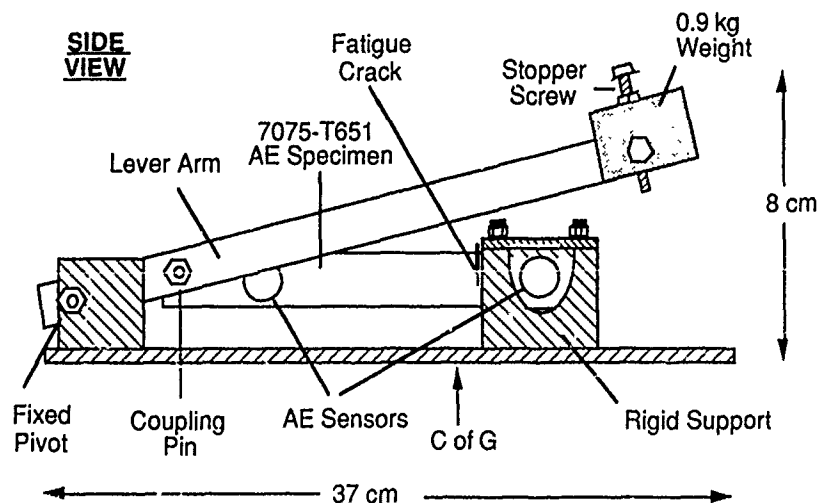


Figure 2 - Schematic diagram of the inertial loading apparatus and precracked 7075-T651 aluminum test specimen.

System Calibration

A detailed calibration of the acoustic emission system (inertial-loading frame, fatigue specimen, sensors and data acquisition apparatus) was carried out for source signals injected at various locations. The source signals used are the helium gas jet, pencil lead fracture, pulsed YAG laser and fracture-related events generated during fatigue crack growth and overload in the laboratory. The measured mean arrival time differences (Δt) and mean risetimes are listed in Table 2 for various locations. These two parameters were extremely efficient at isolating crack-related events from incoming airframe noise, as indicated in table 2 and shown in figure 3. Figure 3 shows the measured results obtained using 0.5 mm diameter pencil fracture as a simulation source.

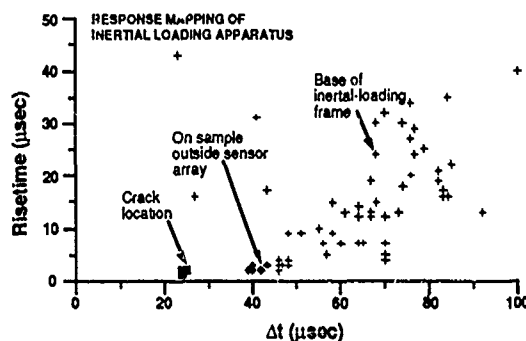


Figure 3 - Measured values of Δt and signal risetime for various locations.

Table 2 - Measured mean values of Δt and signal risetime for various locations.

Position of source	Δt (μsec)	risetime (μsec)
Crack location	24	2
On specimen, outside sensor array	41	2.5
Base of inertial-loading frame	65	16

The Test Flight Results

Figure 4 shows the test flight profile as measured by the data acquisition system. Each recorded data point corresponds to the detection of an event. These events result from crack advance, crack face rubbing and airframe noises. Included in the flight profile are three aircraft manoeuvres at 15 min 12 sec, 67 min 38 sec and 68 min 30 sec, respectively, relative to take-off. These manoeuvres resulted in successively increasing maximum g values of 2.7 g , 4.3 g and 5.2 g , respectively, and applied a sequence of increasingly large stresses to the fatigue crack through inertial loading. Electron microscopic examination of the fracture surface revealed that an increase in crack face area of 0.63 mm² resulted from the 4.3 g_{max} manoeuvre. Fracture of the specimen occurred during the 5.2 g_{max} manoeuvre.

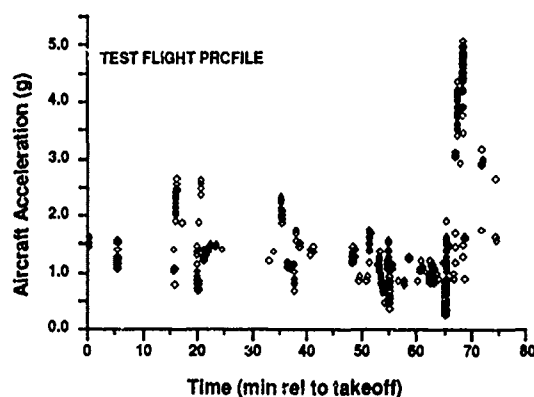


Figure 4 - Aircraft acceleration as a function of time for all of the events detected during flight. These include all sources (crack advance, crack face rubbing and superimposed airframe structural noises).

Figure 5 shows the scatter plot of signal risetime and difference in arrival time of each acoustic emission event and noise signal detected during the test flight (figure 4) for comparison with the calibration data (figure 3). Comparison of figures 3 and 5 show that the majority of detected signals arrive at the sensors via the base of the inertial-loading frame. Based on this comparison, only those events with $\Delta t = 24 \pm 6 \mu\text{sec}$ and risetimes of $3 \pm 2 \mu\text{sec}$ were accepted as crack-related events.

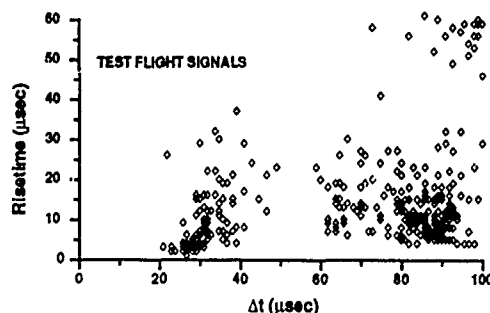


Figure 5 - Signal risetime as a function of difference in arrival time.

Figure 6 shows the effect of applying these conditions to the data of figure 4. Note that all but the final two high-g manoeuvres are removed from the data set by the dual-parameter filter.

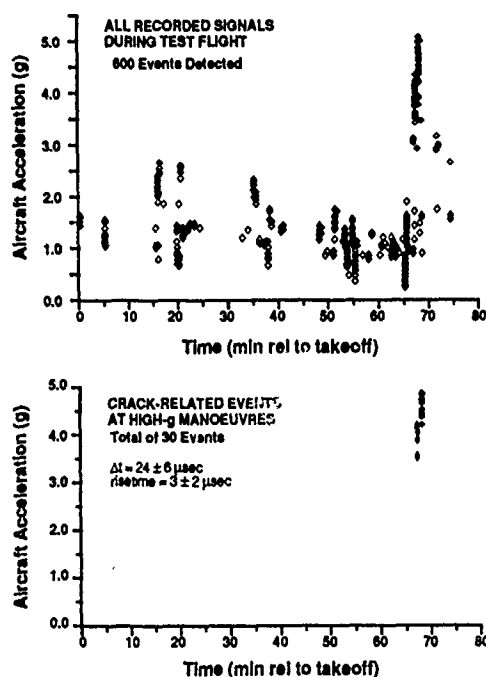


Figure 6 - Comparison of the occurrence of all events detected during the test flight (upper graph) with the occurrence of events unambiguously identified as crack-related ($\Delta t = 24 \pm 6 \mu\text{sec}$ and risetime of $3 \pm 2 \mu\text{sec}$). Note that these latter events occur only during progressively high-g manoeuvres which provide the stresses required for crack advance.

Figure 7 shows an expanded view of the data recorded during the $4.3 g_{\text{max}}$ manoeuvre which resulted in crack advance. In the lower graph, only the crack-related events are shown. By application of the Kaiser Effect, these events are identified separately as crack advance and other crack-related events.

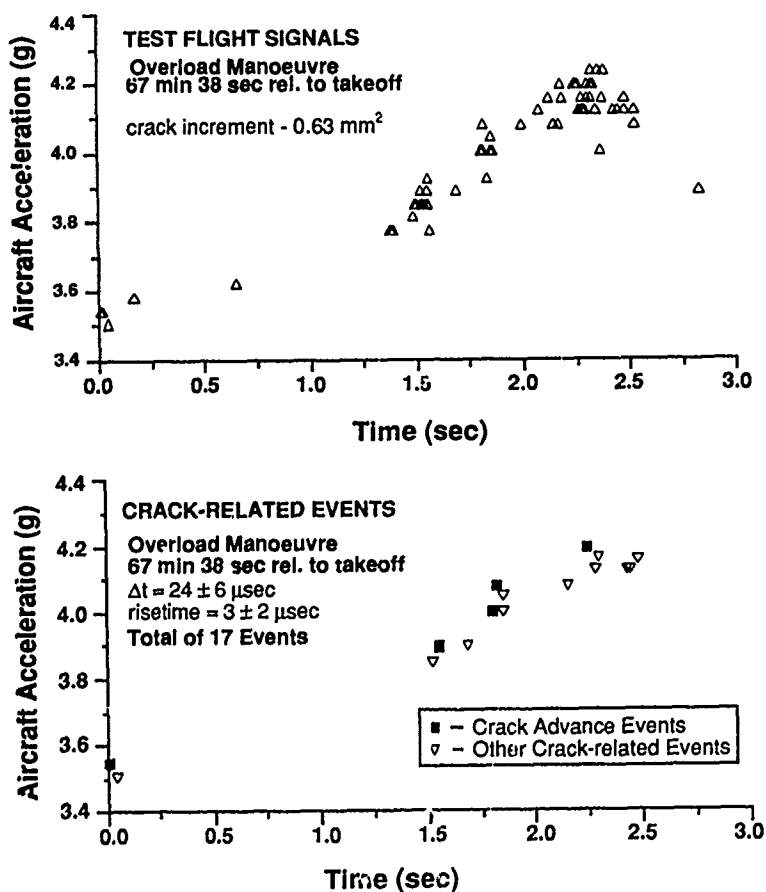


Figure 7 Crack-related signals detected during the $4.3 g_{\text{max}}$ manoeuvres. The upper graph includes all detected events, while the lower graph includes only those events which are crack-related. The distinction of crack advance events from other crack-related events can be accomplished using the Kaiser Effect.

SUMMARY AND CONCLUSIONS

A precracked 7075-T651 aluminum specimen mounted in an inertial loading apparatus was subjected to stresses large enough to propagate the crack during flight. These crack propagating stresses occurred during specific test flight manoeuvres of a British Tornado aircraft. The specimen and loading apparatus were part of a secondary structure bolted directly to the support frame in the instrumentation bay of the aircraft. Acoustic emission data and aircraft acceleration were recorded using a data acquisition system designed at RMC specifically for in flight monitoring applications. The crack-related events were isolated immediately following the test flight. More detailed analysis was later carried out to confirm the results and to separate crack advance events from other crack-related events.

The selection of events which are unambiguously caused by crack-related sources was carried out using a very restrictive dual criterion ($\Delta t = 24 \pm 6 \mu\text{sec}$ and risetime of $3 \pm 2 \mu\text{sec}$) derived from specimen calibration and comparison of the test flight data with laboratory crack growth results obtained for 7075-T651 specimens with geometry and sensor configurations similar to that of the specimen used for the test flight. The 30 crack-related events selected in this manner from 600 events detected during the test flight occurred as the result of high-g manoeuvres during which crack advance would be expected. Eleven of the 30 crack-related events are attributed to crack advance by application of a temporary Kaiser Effect criterion. Thus, we confirm the feasibility of the unambiguous detection of crack growth and presence in 7075-T651 during flight, provided that detailed calibration of the structure is carried out.

Continuing work in this area includes the application of the RMC data acquisition and analysis system to the monitoring of airframe fatigue tests, the monitoring of a slowly growing fatigue crack in a secondary structure during flight, and the in-service monitoring of failure-prone airframe structural components during flight.

REFERENCES

1. T. F. Drouillard, Acoustic Emission, A Bibliography with Abstracts, Plenum Data Company, New York, N. Y., 1979
2. T. F. Drouillard, "Bibliography Update", J. Acoust. Emiss., 1982-87
3. S. L. McBride and J. W. MacLachlan, "In-Flight Acoustic Emission Monitoring of a Wing Attachment Component", J. Acoust. Emiss., 1, 223-228, October, 1982
4. S. L. McBride and J. W. MacLachlan, "Effect of Crack Presence on In-Flight Airframe Noises in a Wing Attachment Component", J. Acoust. Emiss., 1, 229-235, October, 1982
5. S. L. McBride and J. W. MacLachlan, "Acoustic Emission Due to Crack Growth, Crack Face Rubbing and Structural Noise in the CC-130 Hercules Aircraft", J. Acoust. Emiss., 3, 1-10, January, 1984

ACKNOWLEDGEMENTS

Supporting funds were provided by the Department of National Defence, Canada (ARP 3610-208, CRAD 144688RMC01 and DAS Eng 84778ACCA01). The project was monitored by Mr. W.R. Sturrock of the Materials Section, Defence Research Establishment - Pacific, Victoria, British Columbia, and Major W.J. Miller, National Defence Headquarters, Ottawa, Ontario. The Tornado test flight reported here was provided by British Aerospace, Warton, England, under contract to Dr. D.E.W. Stone of the Royal Aerospace Establishment, Farnborough.

DEVELOPMENT AND APPLICATION OF COMPUTED TOMOGRAPHY (CT) FOR INSPECTION OF AEROSPACE COMPONENTS

by

Thomas J. Moran
In-house Research Group Leader
Nondestructive Evaluation Branch
Wright Research and Development Center
Materials Laboratory, WRDC/MLLP
Wright-Patterson AFB, OH 45433-6533
United States

SUMMARY

The requirement for quantitative characterization of flaws and material properties in advanced aerospace system components has led to extensive DOD efforts in the area of X-ray Computed Tomography (CT). This technology, which was originally developed for medical applications, generates quantitative cross-sectional images of the density of the component being inspected. After an in-house Materials Laboratory team provided an initial demonstration of its industrial and aerospace applications potential ten years ago, the Air Force initiated several contract programs to construct military inspection CT systems and demonstrate their potential. From the time the first small (XIM) and large (AFACTS-I) CT systems began operation, the quantitative potential of this methodology has been demonstrated for a wide range of applications. This paper will discuss a representative sampling of these applications in order to provide a balanced picture of which applications are suitable for CT and which are not suitable, either as a result of technical deficiencies or economic limitations.

INTRODUCTION

One of the major thrusts of research in NDE during the past two decades has been the development of quantitative techniques. This is due to the fact that the design philosophy for aerospace systems has been modified to require an acceptance of the fact that flaws always exist in a structure and that the structure must be able to function for its design life containing the largest flaw that was likely to be missed without failure. Thus, the use of a more sensitive NDE technique than had been assumed during design could lead to the scrapping of usable hardware unless that technique produced quantitative information.

X-ray Computed Tomography (CT) was initially applied to applications in medicine where it produced quantitative images of the density of soft tissues and permitted accurate diagnosis of anomalous conditions such as cancerous tumors [1]. The instrumentation developed for this application operates in the 160 keV range and is optimized for low dose, rapid data acquisition. Thus, the vast majority of high density metallic aerospace components were uninspectable at the medical energy levels for variation determination and only metrological applications were investigated. However, the development of composite materials provided a new class of component which could be inspected on medical CT instrumentation.

Approximately 10 years ago a team from the Air Force Materials Laboratory used such a medical system to demonstrate that CT could be used to inspect carbon/carbon materials and provide quantitative measurement of the linear x-ray attenuation coefficient which is related to density information when there is little variation in material type in the component, and also detect almost closed delaminations. The results were so striking that Laboratory management agreed to fund several exploratory development and manufacturing technology programs to provide a quantitative inspection capability for space applications ranging from small engine and missile components to Peacekeeper motors. In order to produce systems for this wide range of applications, the instrument manufacturers had to develop methods to handle the effects of beam hardening (selective attenuation of lower energy photons which effectively increases the average energy in a broad spectrum x-ray beam), develop new detectors to handle x-ray energies up to 16 MeV, and component handling systems which could accurately and rapidly move components up to 10 feet in diameter, weighing many tons. These requirements were met and this paper will describe the resulting systems, their capabilities and performance on selected applications.

X-RAY CT SYSTEMS

A block diagram of a typical industrial CT system is depicted in Figure 1. The major components are the X-ray source, detector array, mechanical specimen holder and motion stage and a computer/display system for system control, data acquisition, image reconstruction and display. The typical X-ray source is of the tube type for energies in the 160 - 420 keV range or a linear accelerator for higher energies up to 16 MeV. The mechanical portion of the system is required to have machine tool accuracy and ruggedness in order to move relatively large objects with position accuracy better than 0.1 to 0.3, depending on data acquisition method, of the pixel size desired in the final image.

The detector array typically is composed of as few as 64 elements up to several thousand depending on the configuration of the system. There are two common modes of operation for industrial systems. The most common is the second generation or

translate-rotate mode of operation which generally utilizes a smaller number of detectors and translates the specimen across the x-ray beam in order to acquire data for each pixel at every angle. The third generation, rotate only configurations are typically utilized with the higher resolution, microfocus systems whose greater position accuracy requirements are more economically met by restricting the number of axes which must be controlled. Third generation systems are more susceptible to errors generated by variations in detector performance and object size is limited due to the requirement that the object must fit within the fan shaped x-ray beam.

Individual detector elements are typically composed of scintillation counters or gas ionization chambers. For energies above 420 keV the scintillation counters are the detector of choice due to the poorer stopping efficiency of the gas ionization chamber at those energies. Special piggy-back detectors have been developed for applications which require energy sensitivity. For such applications, the first detector stops the lower energy photons and the rear detector detects the remaining higher energy photons.

The final major element in a CT system is the computer(s)/display system. In many instances, a separate dedicated scan control computer is utilized to control the mechanical motion and synchronize the source (if necessary), detectors and motion. The primary computer requires a high capacity array processor to transform the raw data into an image, significant quantities of non-volatile data storage (hard disk and/or tape) and a graphics display capable of displaying at least 1024 x 1024 points.

PERFORMANCE PARAMETERS

When one wishes to characterize the operation of a CT system, there are a relatively large number of parameters which have to be considered [3]. In many instances the performance to be obtained for a specific application is determined by system configuration, operator choice and material being inspected. The parameters can be considered in two different categories; (1) Input parameters - radiographic, system, etc. settings, and (2) Output parameters - image quality. Examples of each are as follows:

(1) Radiographic, system, etc. parameters

- a. Source - type, energy, focal spot size
- b. Magnification - Ratio of source-detector distance to source-object distance
- c. Scan or Data Acquisition Time - the lower limit is set by the mechanical motion capabilities of the system, with increased time required for more attenuative materials which require increased detector integration time for an acceptable signal to noise ratio.
- d. Image Reconstruction Time - dependent on image size, array processor, and reconstruction method; can be as short as one minute for a 1024 x 1024 image.
- e. Slice Thickness - source, detector collimator opening.
- f. Fan Beam Width and Height - source collimator dependent.
- g. Detector Quantity and Individual Width - width is a variable in some systems.

(2) Image Quality

- a. Resolution - field of view, image size, point spread function
- b. Contrast Sensitivity - smallest difference in contrast resolvable.
- c. Signal to noise - variation in CT number in an image of a uniform object.
- d. Density standard error - since the CT number is related to the X-ray attenuation coefficient, the relationship between CT number and density should be linear only when the specimen is composed of a single material. However, this quantity is of value to the user after it has been determined for his application.

The majority of today's industrial CT systems were developed for specific applications. Thus, the performance of those systems is optimized for selected parameters with severe degradation possible in some of the others. For example, a system designed for scanning objects 100 inch (250 cm) diameter will typically generate images with 0.10 in. (2.5 mm) pixels, use a 16 MeV source and require more than 10 minutes to acquire the data for one slice. Such a system would produce relatively poor images for objects under 10 in. (25 cm) diameter since it would not be able to resolve defects smaller than 1% of the object diameter. If the X-ray spot size were small enough and the system had magnification and detector aperture variability, it would be possible to reconfigure the hypothetical system described above to achieve better resolution for smaller objects. However, its overall performance would probably not be as good as a system designed specifically for such an application.

Some efforts are currently under way to characterize system performance under optimized conditions so that the best system design for a specific application may be

identified. Phantoms for spatial resolution, contrast sensitivity and system noise have been prepared by Boeing under an Air Force contract from the Materials Laboratory and are being circulated to as many system owners as possible in order to develop a standard data base on system performance. Examples of typical images of these phantoms are shown in Figures 2, 3 and 4.

APPLICATIONS

Initial industrial applications of CT exploited its capability to provide metrology of cooling passages in engine components which were previously inaccessible to other NDE techniques and its ability to provide quantitative density information. Examples of these applications are shown in Figures 5 and 6.

Current application efforts in the aircraft community have demonstrated that CT should be able to provide greatly improved failure analysis and reverse engineering capabilities for components that are inspectable using current CT instruments. An example of the detail achievable is shown in Figure 7 for a hydraulic actuator. Disassembly of a failed part could cause the loss of the desired information due to all of the small components in such a part. Another potential application for CT is to quantitatively characterize the features which are generated using another NDE method. An example is shown in Figure 8 where an unambiguous interpretation of ultrasonic scattering from low density, porous areas in a filament wound composite was possible after the component was inspected using CT.

More recent work has shown that another medical technique, dual energy Radiography/CT, could also be utilized industrially for such applications as chemical separation of the materials in a component. An example is shown in Figure 9. In addition to chemical separation, dual energy also can be utilized to eliminate beam hardening effects and produce a more quantitative density or attenuation coefficient image by eliminating the energy dependence of the attenuation coefficient. An example is shown in Figure 10.

A second variation on CT, Laminography, has also been implemented for use with CT instruments. A series of preview scans or digital radiographs is generated for a relatively large number of angles. The images are then superimposed in software to create images of individual planes or lamina in the object. This methodology is analogous to the classical method of laminographic imaging which required multiple films to be exposed and mechanically aligned and superimposed to bring the layers into focus. Figure 11 shows an example for a composite cylinder.

CONCLUSION

CT has provided the quantitative capability that has long been sought for NDE. Unfortunately, the capability has not yet been fully exploited due to the cost of the systems, their lack of portability, the long data acquisition times for many applications, and finally, the requirement to qualify the CT inspection for specific applications by demonstrating the detection limits on a relatively large number of specimens. As the data base for the technology evolves, it should be possible to predict its performance on a given application and design cost effective special purpose systems for those applications.

REFERENCES

1. H. J. Scudder, "Introduction to Computer Aided Tomography", Proc. of IEEE, vol. 66, pp. 628-637, 1978.
2. R. P. Kruger and T. M. Cannon, "The Application of Computed Tomography, Boundary Detection, and Shaded Graphics Reconstruction to Industrial Inspection," Materials Evaluation, vol. 36, pp. 75-80, 1978.
3. "New Standard Guide for Computed Tomography (CT) Imaging," proposed ASTM Standard (1989).

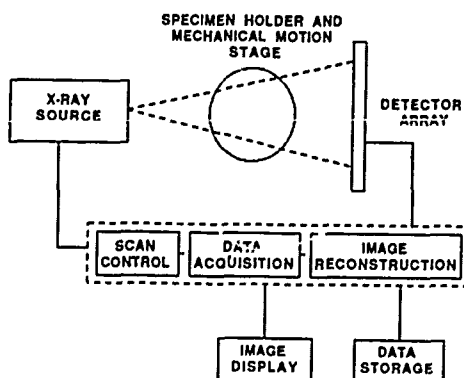


FIGURE 1. CT SYSTEM BLOCK DIAGRAM

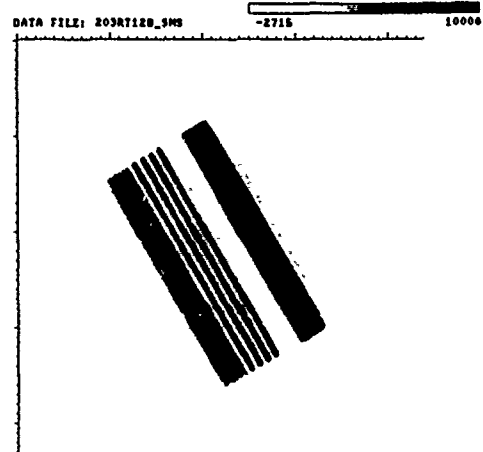
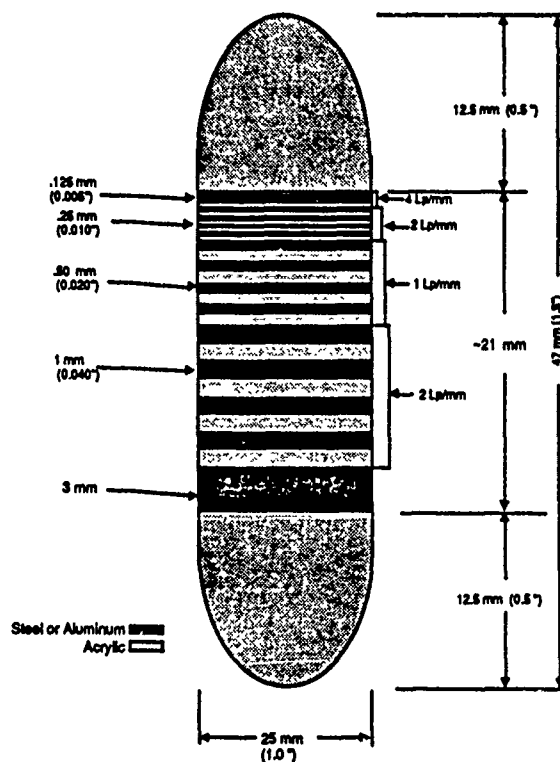
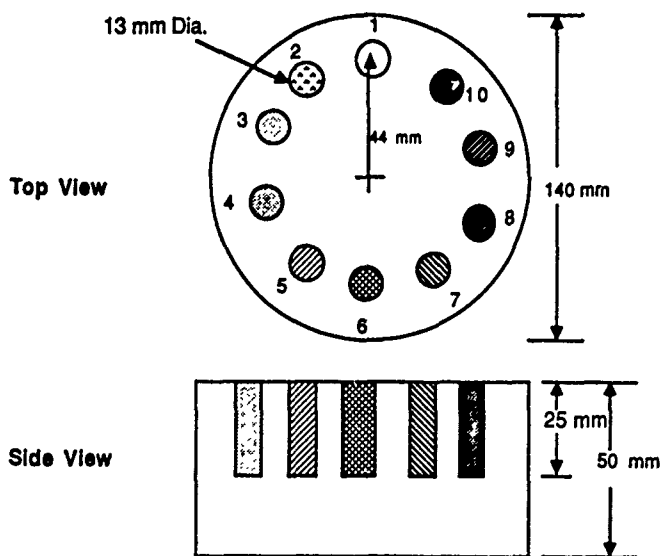


FIGURE 2. CT SPATIAL RESOLUTION STANDARD (LEFT OF FIGURE) AND CT IMAGE OF STANDARD (RIGHT OF FIGURE).



Each density phantom is a cylinder measuring 13 mm dia. x 25 mm (1/2" dia. x 1" $\pm .001$).

The cylinders and their corresponding densities are listed below.

Material	Density (g/cc)
1 Air Gap	
2 High Molecular Weight Polyethylene	0.945
3 Nylon	1.156
4 Nylatron	1.165
5 Acrylic Plexiglas (core material)	1.193
6 Delrin	1.507
7 Magnesium	1.784
8 Teflon	2.179
9 Aluminum	2.704
10 Titanium	4.423

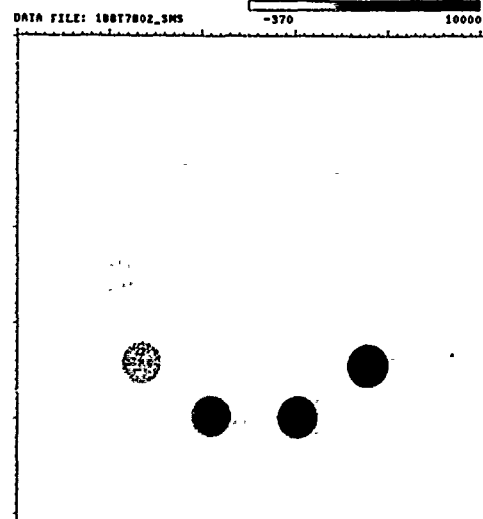


FIGURE 3. CT CONTRAST RESOLUTION STANDARD (LEFT OF FIGURE) AND CT IMAGE OF STANDARD (RIGHT OF FIGURE). NOTE THAT MATERIALS 3 THRU 5 ARE NOT RESOLVED.

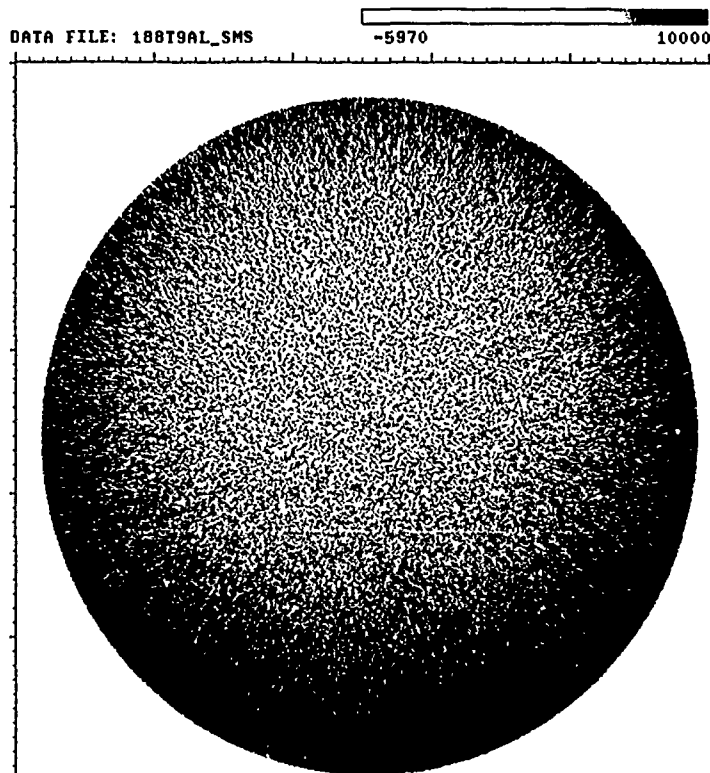


FIGURE 4. CT IMAGE OF ALUMINUM (16cm DIAMETER) NOISE STANDARD. NOTE COMPRESSED GRAY SCALE AND RELATIVELY UNIFORM IMAGE OF STANDARD. SLIGHTLY LIGHTER AREA IN CENTER OF IMAGE DUE TO UNCORRECTED BEAM HARDENING EFFECTS.

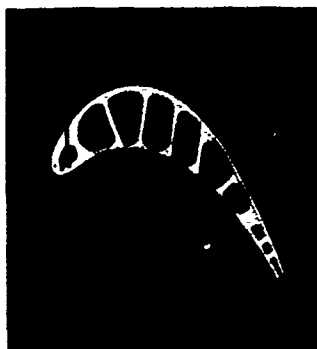


FIGURE 5. SINGLE CT SLICE OF ENGINE TURBINE BLADE. FINE RESOLUTION OF COOLING PASSAGES ALLOWS DETECTION OF THINNING EFFECTS.

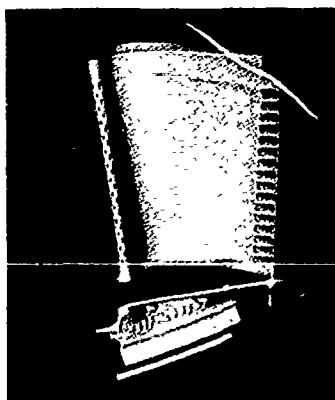


FIGURE 6. 3D RECONSTRUCTION OF ENGINE TURBINE BLADE FROM MULTIPLE SLICES OF THE TYPE SHOWN IN FIGURE 5.

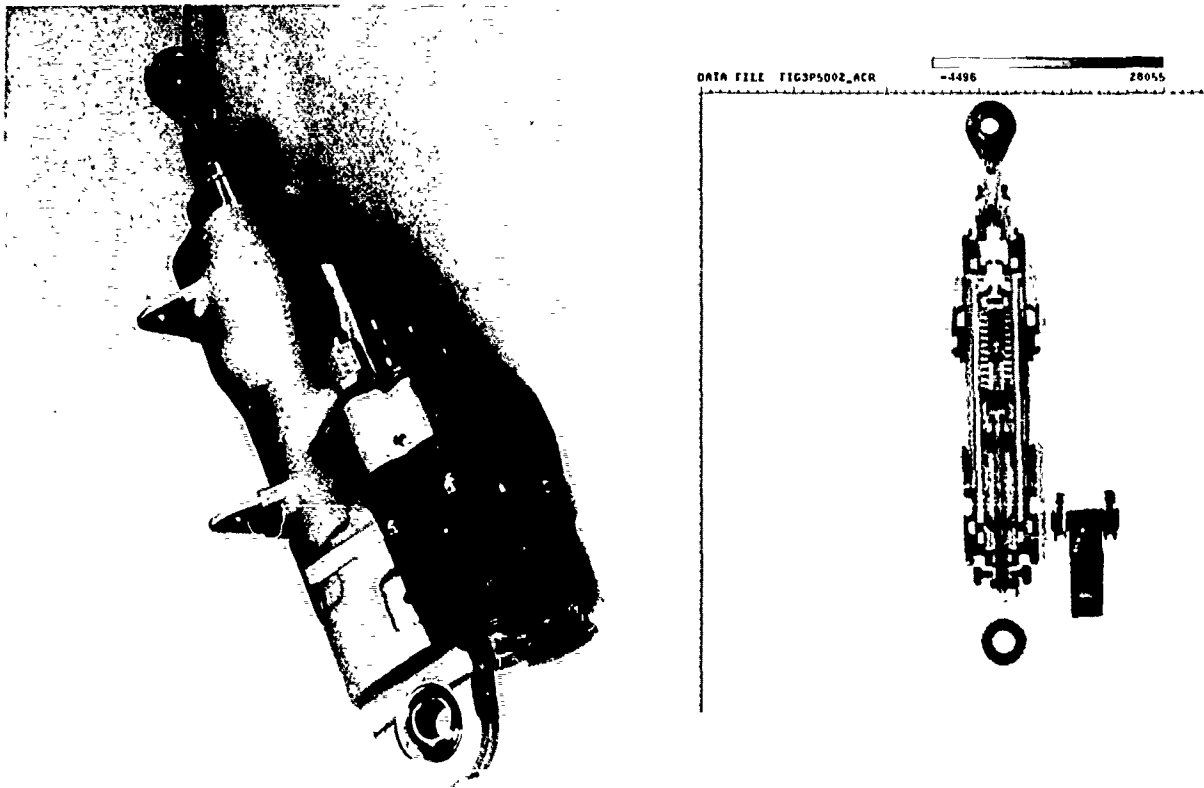


FIGURE 7. AIRCRAFT HYDRAULIC SLAT ACTUATOR (LEFT) AND LONGITUDINAL CT IMAGE (RIGHT)

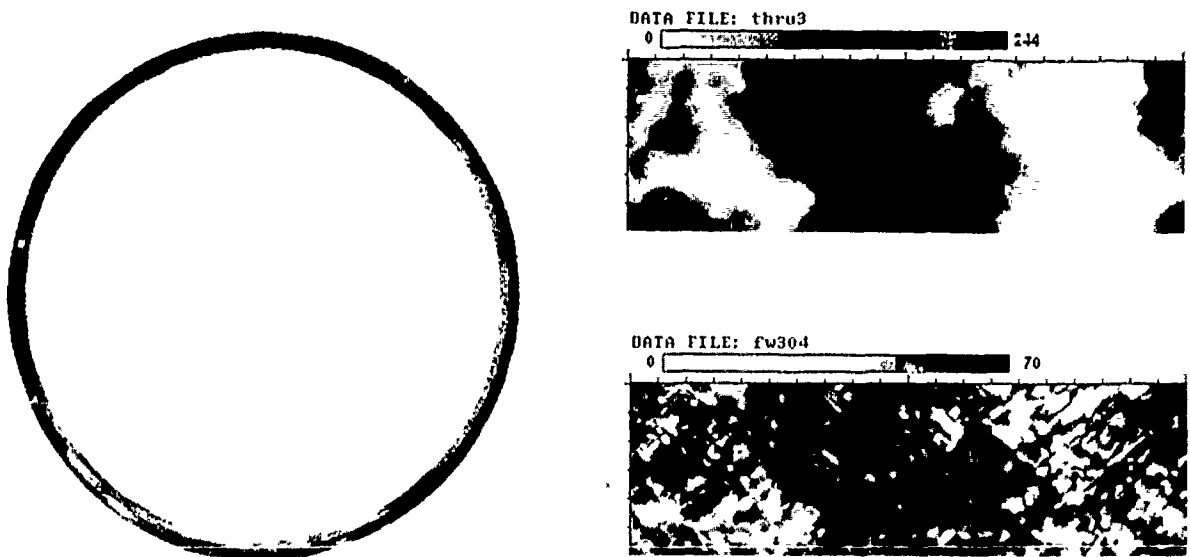


FIGURE 8. CT IMAGE OF FILAMENT WOUND GLASS MATRIX/CARBON FIBER CERAMIC TUBE (LEFT IMAGE). THE LOW DENSITY AREAS ARE SHOWN AS THE LIGHTER SHADES. THESE AREAS FOUND IN THE CT IMAGES WERE FOUND TO CORRELATE WELL WITH THE HIGH ATTENUATION AREAS FOUND ULTRASONICALLY IN THRU TRANSMISSION (LIGHT AREAS IN UPPER RIGHT IMAGE) AND STRONG REFLECTORS IN THE BACK SCATTER MODE (LIGHT AREAS IN LOWER RIGHT IMAGE).

DATA FILE: SCRW9_CO
SCALING FACTOR = 2

-302 2303

DATA FILE: SCRW9_MO_AL
SCALING FACTOR = 2

0 3000



FIGURE 9. CHEMICAL SEPARATION USING DUAL-ENERGY RADIOGRAPHY. DIGITAL RADIOGRAPH OF BEAKER OF STEEL AND ALUMINUM SCREWS (LEFT IMAGE). IMAGE PROCESSED TO ELIMINATE ALUMINUM SHOWING ONLY THE FOUR STEEL SCREWS (RIGHT IMAGE).

DATA FILE: AL_PVC_CO -009 27402

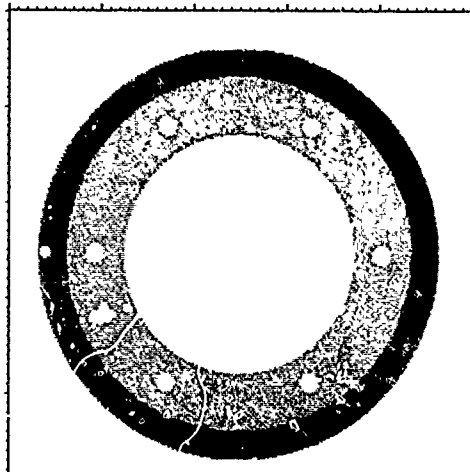


FIGURE 10. DUAL ENERGY CT IMAGE OF CONCENTRIC ALUMINUM AND PVC RINGS WITH TWO STEEL PINS (BLACK CIRCLES IN OUTER RING) PROCESSED TO GIVE ACCURATE DENSITY INFORMATION.

DATA FILE: PAND124RL 6894 28982



DATA FILE: PAND126RL -32330 32700

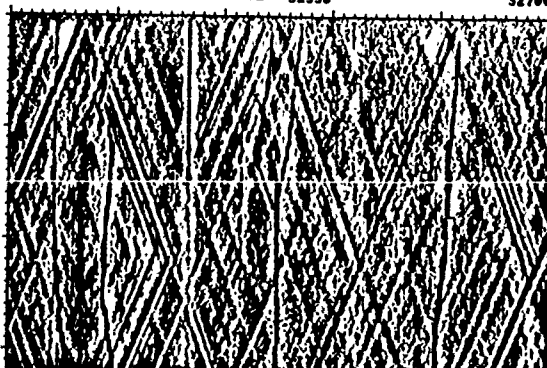


FIGURE 11. LAMINOGRAPHS OF FILAMENT WOUND COMPOSITE CYLINDER. VERTICAL AXIS IS AXIAL DIRECTION ALONG CYLINDER, HORIZONTAL IS 360 DEGREE UNWRAP OF LAYER AT A DIAMETER OF 124mm (LEFT IMAGE) AND 126mm (RIGHT IMAGE).

APPLICATION DE LA THERMOGRAPHIE INFRAROUGE AU CONTRÔLE NON DESTRUCTIF DES MATÉRIEAUX COMPOSITES

Hervé TRETOUT, Jean-Yves MARIN, René DE MOL
AVIONS MARCEL DASSAULT-BREGUET AVIATION
78, Quai Marcel Dassault
92214 - Saint-Cloud -
FRANCE

RESUME :

La fabrication de pièces structurales en matériaux composites par les avionneurs, oblige ceux-ci à se doter de moyens de contrôle importants, afin d'assurer la qualité du produit fini. Ce contrôle doit s'effectuer avant le montage sur l'avion et dans le temps sur le terrain ou après démontage à l'usine. Différentes méthodes de contrôle non destructif, tels les contrôles par ultrasons et par radioscopie X sont déjà largement utilisées. Cependant le besoin d'une plus grande rapidité de contrôle et d'une plus grande facilité de mise en oeuvre, nous a conduit à développer la thermographie infrarouge stimulée.

1° - INTRODUCTION

Le contrôle par thermographie infrarouge stimulée (TIS) fait appel à la méthode passive qui consiste à soumettre la pièce à contrôler à un flux thermique bref dit impulsif, à l'aide d'une source de chaleur. Un système de détection infrarouge analyse alors sur l'une ou les deux faces de la pièce, le rayonnement lié à la distribution spatiale et temporelle des températures dans le matériau. Les anomalies observées sur le thermogramme traduisent la présence de corps étrangers ou de défauts dans le matériau.

Une technique originale a été développée pour contrôler une grande surface tout en obtenant un chauffage de type impulsif. La pièce est déplacée rapidement devant un système de chauffage linéique, puis devant l'analyseur thermique utilisé en balayage ligne (1). Un système de contrôle transportable avec une source de chaleur surfacique a aussi été développé pour le contrôle sur site (2).

La définition du domaine d'application de cette méthode de contrôle s'appuie sur deux aspects essentiels :

- La caractérisation des matériels et des matériaux afin d'assurer la reproductibilité des mesures et d'optimiser les caractéristiques nécessaires à un système industriel.
- La modélisation des phénomènes thermiques pour faciliter les développements qui doivent faire face à l'arrivée constante de nouvelles fibres et résines, éléments constitutifs des matériaux composites.

Des essais ont été effectués avec des pièces en matériaux composites représentatives de notre fabrication, notamment des panneaux autoraidis à raidisseurs rapportés et des plaques dans lesquelles sont insérés, à différentes profondeurs, des défauts simulés par des films de téflon de dimensions variables.

2° - LES METHODES

Le principe du contrôle non destructif par thermographie infrarouge consiste à stimuler thermiquement la pièce à contrôler, et à observer avec un analyseur thermique infrarouge la distribution spatiale et temporelle des températures à la surface du matériau.

Dans ce cas, l'observation ne peut se faire qu'en régime transitoire, qui met en évidence des variations dans la diffusion du flux thermique à l'intérieur du matériau. Lorsque l'équilibre en température est atteint, ces contrastes thermiques disparaissent. Ces considérations montrent la nécessité de donner un caractère impulsif au chauffage de la pièce à contrôler; les inhomogénéités sur les thermogrammes indiquent alors la présence de défauts.

La stimulation thermique est réalisée soit par un chauffage surfacique soit par un chauffage linéique (Figures 1 et 2). L'observation peut être faite sur la face chauffée (analyse face avant) ou sur la face opposée (analyse face arrière). Les pièces les plus épaisses sont contrôlées successivement sur les deux faces, en analyse face avant avec retournement de la pièce.

- Méthodes passives ou avec stimulation thermique :

- . Chauffage surfacique (figure 1) :

La zone contrôlée ou la totalité de la surface dans le cas de petites pièces est soumise à un instant donné, à une impulsion uniforme de chaleur de courte durée. Cette impulsion est produite par des tubes à éclairs ou des tubes infrarouges avec un obturateur mécanique. La surface homogène actuellement contrôlée est de 300x300mm. L'analyseur thermique est ici utilisé en mode trame.

. Chauffage linéique (figure 2) :

La pièce à contrôler est déplacée à une vitesse constante successivement devant une source de chaleur linéique (tube infrarouge, source laser avec dispositif de balayage ou d'étalement de faisceau) et un analyseur thermique utilisé en mode ligne. La ligne d'analyse est parallèle à celle de chauffage. La distance entre les deux lignes est choisie pour détecter les défauts au temps de contraste maximum qui est fonction de leurs profondeurs dans le matériau.

- Comparaison des méthodes de chauffage

Par opposition à la méthode de chauffage linéique qui permet une détection rapide des défauts (30 à 70m²/heure), la méthode de chauffage surfacique permet une détection plus lente (20m²/heure) mais une analyse quantitative. En effet, la pièce restant immobile, l'évolution des températures dans le temps peut être observée et enregistrée. Pour un défaut donné, la mesure de la valeur maximum de contraste en température obtenue entre une zone saine et une zone défectueuse, et du temps écoulé à partir de l'impulsion du chauffage permettent son identification, son positionnement en profondeur et son dimensionnement. La méthode de chauffage linéique ne peut être envisagée que sur une installation à poste fixe en laboratoire ou en usine, alors que la méthode de chauffage surfacique peut en plus être utilisée sur site.

3° - CARACTERISATION

3.1 Caractérisation du matériel

La caractérisation des matériels de chauffage et d'analyse est un aspect essentiel de la mise en oeuvre des méthodes de Contrôle Non Destructif par Thermographie Infrarouge. En effet seule une bonne connaissance de tous les paramètres entrant en jeu lors d'un contrôle peut assurer la reproductibilité des mesures et autorise l'utilisation des modèles thermiques.

Des procédures d'étalonnage ont été définies pour les différents moyens de chauffage.

Elles permettent la détermination de l'énergie de stimulation reçue par les pièces contrôlées.

La caractérisation des analyseurs infrarouges est effectuée selon les procédures définies par les normes expérimentales AFNOR A09420 et A09421.

3.2 CARACTERISATION DES MATERIAUX

L'utilisation des modèles théoriques pour l'aide au développement du contrôle non destructif par Thermographie Infrarouge suppose la connaissance d'un certain nombre de grandeurs physiques qui sont :

- la conductivité thermique
- la diffusivité thermique
- la capacité thermique massique
- l'émissivité

L'introduction relativement récente des matériaux composites, leur évolution constante et rapide et leurs propriétés particulières notamment d'anisotropie, font qu'il n'y a pas ou peu de données disponibles. Des méthodes spécifiques ont dû être développées. (3).

4° - MODELISATION

- Homogénéisation :

Les travaux d'Amazouz et Degiovanni (4,5) ont montré que, bien qu'inhomogènes et anisotropes, les matériaux composites pouvaient être traités du point de vue thermique comme des matériaux homogènes à condition que le nombre de plis soit assez élevé. Nous pouvons alors définir des conductivités thermiques axiale (suivant l'épaisseur) et radiale (dans le plan des fibres), et les diffusivités correspondantes.

- Modélisation des défauts

Les comparaisons entre modèle trilicouche et modèle bicouche avec une résistance de contact ont montré que les défauts du type, décollement ou inclusion isolante mince peuvent-être représentés par leur résistance thermique. Les inclusions épaisses ou constituées d'un matériau plus conducteur que le matériau composite, peuvent être étudiées en prenant en compte leur épaisseur et leur capacité thermique massique.

- Le chauffage

Les deux méthodes de chauffage envisagées pour le contrôle par TIS (thermographie infrarouge stimulée) ont été étudiées et comparées. Le calcul des températures dans le matériau est simple dans le cas du chauffage surfacique, mais présente des difficultés pour le chauffage linéique.

Nous avons cependant pu montrer que pour des vitesses élevées, les courbes de température en fonction du temps, en surface sont identiques à celles obtenues pour le chauffage surfacique.

Ceci est vrai si :

$$\frac{vb}{2a} \gg 10 \quad \text{et} \quad \frac{ve}{2a} \gg 10$$

avec : v - vitesse de déplacement de la pièce à contrôler
 b - demi largeur de la ligne de chauffage
 a - diffusivité thermique
 e - épaisseur du matériau

Une modélisation avec une source surfacique est donc suffisante pour l'étude de tous les phénomènes thermiques rencontrés lors d'un contrôle.

- Etude des contrastes

Des modèles unidimensionnel bi ou tridimensionnel ont été développés par le LEMTA pour l'étude des contrastes en fonction du temps, de la résistance thermique, de la profondeur et éventuellement de la dimension des défauts. (5) Le modèle unidimensionnel suffit pour mettre en évidence la plupart des phénomènes thermiques liés à la présence d'un défaut. Il a permis de mettre en évidence l'existence pour chaque défaut de deux paramètres caractéristiques : T_m , contraste maximum correspondant à l'écart maximum de température entre une zone saine et une zone défectueuse, et t_m , temps nécessaire pour obtenir T_m (Figure 3). Pour un même défaut, T_m et t_m ont des valeurs différentes suivant que l'observation ait lieu en face avant ou en face arrière. Ces valeurs dépendent non seulement des caractéristiques du défaut, mais aussi du matériau et de l'énergie de chauffage.

Le modèle unidimensionnel ne permet pas l'étude du contraste des défauts de petite dimension, ou plus précisément des défauts pour lesquels le rapport D/l (plus petite dimension sur profondeur par rapport à la face avant) est petit. Il faut alors utiliser un modèle tridimensionnel, analytique ou numérique. Le modèle analytique tridimensionnel du LEMTA est applicable aux défauts circulaires ou rectangulaires et tient compte de l'anisotropie éventuelle du matériau. Les résultats obtenus sont très satisfaisants et on été corrélés avec des calculs par éléments finis effectués aux AMD-BA avec le logiciel ELFINI. (6)

- Evolution de T_m et t_m en fonction de la profondeur du défaut

En face avant le contraste maximum diminue avec la profondeur alors que le temps de contraste maximum augmente.

En face arrière, il existe pour T_m et t_m une symétrie par rapport à la mi-épaisseur, profondeur à laquelle les contrastes et temps de contraste sont les plus élevés.

- Evolution de T_m et t_m avec la résistance thermique du défaut

En face avant comme en face arrière le contraste maximum est une fonction croissante de la résistance thermique ; en première approximation on peut considérer qu'il y a proportionnalité.

Le temps de contraste maximum augmente légèrement avec la résistance thermique.

- Amélioration du contraste

Les différents modèles ont mis en évidence un phénomène particulièrement intéressant : le contraste maximum en face avant de défauts profonds est sensiblement amélioré par une augmentation des échanges thermiques à travers la face arrière (Figure 4).

Cette amélioration du contraste s'accompagne d'un allongement important des temps de contraste maximum.

Deux logiciels TIRANA et TIREX, ont été développés aux AMD-BA à partir du modèle unidirectionnel.

Le premier est un logiciel d'aide à l'analyse qui permet :

- la caractérisation d'un défaut à partir des contrastes mesurés sur les thermogrammes
- la simulation du contraste d'un défaut à partir de ses caractéristiques.

Le second est un logiciel d'aide au contrôle. Il a été conçu pour déterminer les conditions de contrôle permettant la meilleure détection des défauts dans une pièce en matériau composite. A partir des caractéristiques des matériels de chauffage et d'analyse et de la pièce à contrôler, le logiciel calcule tous les paramètres de réglage de l'installation et indique la méthode d'observation qui doit être employée. Les deux logiciels sont applicables au chauffage linéique et au chauffage surfacique.

5°- SYSTEMES DE DEVELOPPEMENT

Banc expérimental d'analyse linéique (Fig.5)

Le banc expérimental a été développé par les Avions Marcel Dassault - Bréguet Aviation pour appliquer la méthode d'analyse linéique.

Le banc assure un déplacement longitudinal de la pièce à contrôler qui passe successivement devant le système de chauffage linéique puis devant un ou plusieurs analyseurs thermiques. La scène thermique est ainsi analysée suivant une ligne perpendiculaire au sens du déplacement. La surface contrôlée en un passage de la pièce analysée est décrite par la combinaison de son déplacement et du champ optique de l'analyseur thermique. La totalité de la pièce est contrôlée par balayages successifs et déplacements verticaux d'un incrément compatible avec le champ de l'analyseur et la surface de recouvrement désirée. Un axe motorisé assure le positionnement parallèle de l'analyseur thermique à une distance précise du système de chauffage.

Les exigences de cette méthode imposent de minimiser les variations de distance entre :

- le système de chauffage et la surface de la pièce afin de préserver l'uniformité de flux ;
- l'analyseur thermique et la surface de la pièce afin de conserver la mise au point et la longueur de la ligne d'analyse constantes.

Ceci est notamment le cas pour des pièces de forme complexe, dont la courbure dans une direction au moins est relativement faible. Pour ce faire, une commande numérique NUM 760 assure une interpolation linéaire entre les déplacements longitudinaux de la pièce et latéraux de l'analyseur et du chauffage, sur le profil moyen de chaque zone à contrôler. Ce profil moyen est déterminé par apprentissage préalable à l'aide d'un capteur de type "Renishaw" ou par le module informatique de CFAO.

Système de chauffage linéique.

Une ou deux lampes sont pilotées par la commande numérique.

- gamme de puissance unitaire : 500 W/m à 8000 W/m
- longueur utile de chauffage : 100 à 300 mm pour une variation d'uniformité inférieure à 5 %
- obturation mécanique et refroidissement à eau piloté par l'automate de la commande numérique.
- Le banc est tout à fait compatible avec un système d'analyse surfacique. Dans ce cas, le déplacement de la pièce est incrémental dans ses deux directions.

Une configuration idéale qui éviterait les phénomènes parasites de convection, et qui faciliterait, le chargement/déchargement des pièces et le fonctionnement des émetteurs Infrarouges, serait :

- . pièce horizontale et incrémentation latérale,
- . système de détection et de chauffage verticaux.

Système d'Acquisition et de Prétraitement d'Images InfraRouges-SAPIR

Le SAPIR est un système de traitement et de restitution d'images, il assure la numérisation sur 12 bits (512 points par ligne) des signaux reçus des analyseurs ligne ou image, simultanément sur 2 voies synchrones ou indépendantes. Les lignes ou les images formées sont ensuite moyennées ou accumulées et des opérations arithmétiques d'une voie à l'autre sont effectuées. Les images ou les lignes peuvent être visualisées ou stockées en temps réel avant ou après le traitement. Le SAPIR est commandé et configuré par l'utilisateur au moyen d'un terminal de dialogue, et est pourvu d'une liaison rapide spécialisée pour le transfert vers un ordinateur hôte, des informations stockées en temps réel. Le SAPIR est particulièrement adapté aux différentes configurations de contrôle non destructif par thermographie infrarouge :

- analyse ligne en face avant et/ou face arrière avec un ou deux analyseurs lignes,
- analyse trame en face avant et/ou face arrière avec un ou deux analyseurs trames.
- contrôle de zones d'accès difficiles ou particulières,
- contrôle de pièces en matériaux très isolants.

Illuminateur à tubes à éclair : Système à quatre tubes en silice dopée remplie de Xénon, disposés en carré. Énergie maximale par tube pour une tension de charge des condensateurs de 1000 V et pour une durée d'éclair de 10 ms : 5 KJ

Illuminateur à tubes Infrarouges : Système à quatre tubes disposés en carré, chaque élément est composé d'un filament de Tungstène sous atmosphère Argon dans un tube en quartz. Puissance 2 KW à la tension nominale d'alimentation de 240 V.

Un obturateur électromécanique assure des durées d'impulsions de 0,1 à plusieurs secondes.

Stations de traitement d'image (Figure 5) : Deux systèmes VINIX, l'un dédié à l'acquisition et l'autre à l'exploitation assurent l'analyse des images acquises. Ces stations spécialisées effectuent tous les traitements nécessaires pour assurer la détection d'anomalies, l'identification des défauts et leur dimensionnement. L'intégration en cours d'intelligence artificielle fournira un diagnostic automatique sur la qualité des pièces contrôlées. Les traitements utilisés et développés font appel aux processeurs spécialisés des systèmes qui effectuent en temps réel convoiutions, segmentations et morphologie mathématique.

- Système d'analyse surfacique de contrôle non destructif par thermographie Infrarouge - MECIR

Le système MECIR a été développé en collaboration avec le SUE - Université de Reims et les Sociétés SECA et MECICA (5).

Le système d'analyse surfacique MECIR est un ensemble portable de contrôle non destructif par thermographie Infrarouge. Le système permet d'appliquer l'analyse surfacique en contrôle sur site, en usine et/ou en laboratoire, à des pièces en matériaux composites et métalliques, aux assemblages collés, soudés ou brasés et aux revêtements minces.

Différents ensembles constituent ce système (Fig.7) :

- un appareillage de thermographie Infrarouge,
- un illuminateur,
- une unité informatique.

Deux illuminateurs sont disponibles en fonction du matériau et de l'environnement (Fig.8) : à tubes à éclairs, à tubes Infrarouges.

Les illuminateurs sont optimisés pour chauffer d'une manière homogène une surface de 300 x 300 mm, ce qui les rend portables et permet leur maintien par une seule personne, leur installation sur un robot (Fig.1) ou leur montage sur un banc de contrôle. Les applications possibles sont multiples :

- En production : - retour sur défaut détecté en analyse linéique pour le caractériser,
- contrôle de pièces de petites dimensions (300 x 300),
- Sur site : - détection d'impacts sur les matériaux composites,
- suivis d'endommagements.

En laboratoire : - suivi d'essais mécaniques.

6°- PROGICIEL "IRAQ"

Ce progiciel, écrit en langage C, est capable de gérer l'examen non destructif de pièces en matériaux composites par les différentes méthodes de thermographie Infrarouge (chauffage ligne ou surfacique, analyse face avant ou face arrière). Décomposé en modules spécifiques, il peut ainsi être adapté aux différents matériels utilisés.

Une base de données centralise les informations sur les pièces, les matériaux, les systèmes de chauffage, les analyseurs thermiques, la machine de déplacements. Chaque module s'enquiert auprès de cette base des informations qui lui sont nécessaires pour fonctionner, et fournit à cette base ses résultats.

Ce progiciel est constitué des modules suivants; CFAO, robotique, métrologie, modélisation thermique, acquisition et exploitation.

Ce progiciel facilement adaptable à d'autres types de matériaux va s'enrichir de nouveaux modules spécialisés, par exemple un module d'intelligence artificielle.

7° - DISCUSSIONS

Les résultats expérimentaux obtenus sur des pièces représentatives sont en très bon accord avec ceux donnés par les modèles mathématiques. Les avantages et inconvénients de la thermographie Infrarouge stimulée sont maintenant bien mis en évidence. C'est une méthode :

- qualitative assurant la détection de beaucoup de défauts
- quantitative assurant l'identification et le dimensionnement des mêmes défauts.
- rapide, jusqu'à 20 fois les temps de contrôle par ultrasons
- facile à mettre en oeuvre, pas de couplant.
- applicable sur site
- applicable à tous les matériaux, des très conducteurs aux très isolants.

Cependant la méthode :

- est peu sensible aux défauts de faible résistance thermique (porosité) situés au delà de la mi-épaisseur dans un matériau. Une lame d'air de 10 μm (résistance thermique : 0,0004 Km^2/W) située avant le dernier pli engendre en contrôle face avant un contraste thermique maximum de 0,02° au temps (tm) de 2,15 s pour une densité d'énergie de 25 000 J/m^2 dans un CFRP T300/914 de 2 mm d'épaisseur, ce qui est pratiquement indétectable aujourd'hui.
- est limité au contrôle de matériaux de faibles épaisseurs, quelques mm pour les composites.
- est difficilement interprétable, variations d'émissivité, effets de bord, de forme, d'épaisseur et d'assemblages qui s'ajoutent aux gradients thermiques liés aux défauts.

8° - CONCLUSION

Les développements entrepris pour déterminer le domaine d'application de la thermographie Infrarouge stimulée au contrôle des matériaux composites font appel à de nombreuses techniques, optronique, électronique, robotique, traitement du signal et de l'image, intelligence artificielle. Ces développements nécessaires pour industrialiser les deux méthodes mises en oeuvre, analyse ligne et surfacique, ont été facilités par l'utilisation de modèles mathématiques analytiques et la caractérisation des matériels et des matériaux.

Des travaux sont encore nécessaires pour améliorer la détectivité et faciliter l'interprétation des thermogrammes tels que :

- l'amélioration de la sensibilité de détection
- l'augmentation de la densité d'énergie déposée
- le traitement d'images
- l'intelligence artificielle.

9° - REFERENCES

- (1) J.Y. MARIN et H. TRETOUT, "Transient Thermal Technique for Infrared Non Destructive Testing of Composite Materials", Proceedings S.P.I.E., vol. 590, 1985, pp. 227-292
- (2) P. EGEE, E. MERIENNE, J.L. BEAUDOIN, R. DANJOUX, H. TRETOUT, "Dispositif de détection automatique de défauts pour matériaux minces par thermographie photothermique", Opto, n°51, Juillet-Août 1989, pp. 26-30
- (3) M. LACHI, D. LEGRAND, A. DEGIOVANNI, "Mesure de la diffusivité thermique de matériaux composites en plaques minces", Eurotherm 4, Nancy, 1988.
- (4) M. AMAZOUZ, Thèse de Docteur-Ingénieur, INPL, Nancy 1987.
- (5) A.S. LAMINE, D. MAILLET, A. DEGIOVANNI, "Modélisation et détection thermique d'un défaut limité dans un matériau composite", Eurotherm 4, Nancy 1988.
- (6) H. TRETOUT, "Infrared Thermography development for composite material evaluation" Proceedings S.P.I.E., vol. 918, 1988, pp. 12-22.

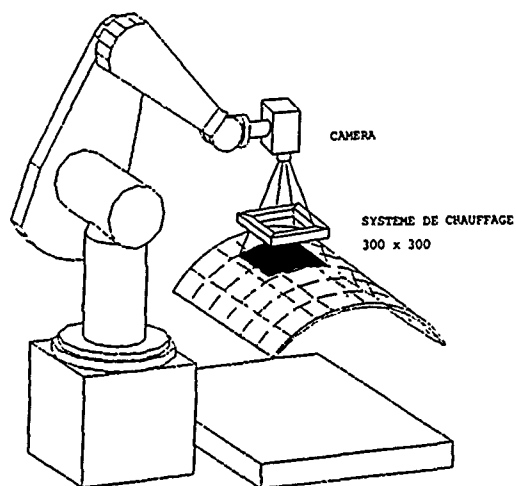


Fig.1 Système de contrôle par thermographie infrarouge avec chauffage surfacique

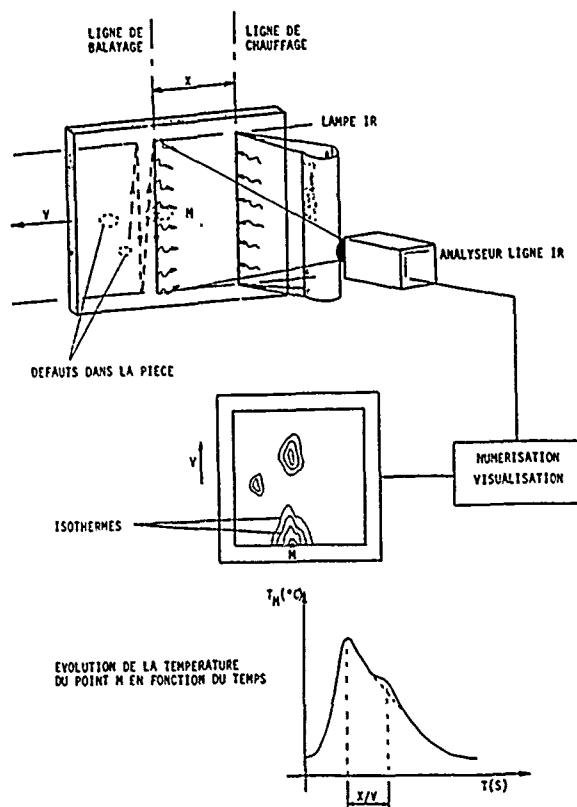


Fig.2 Analyse thermique face avant avec chauffage linéique

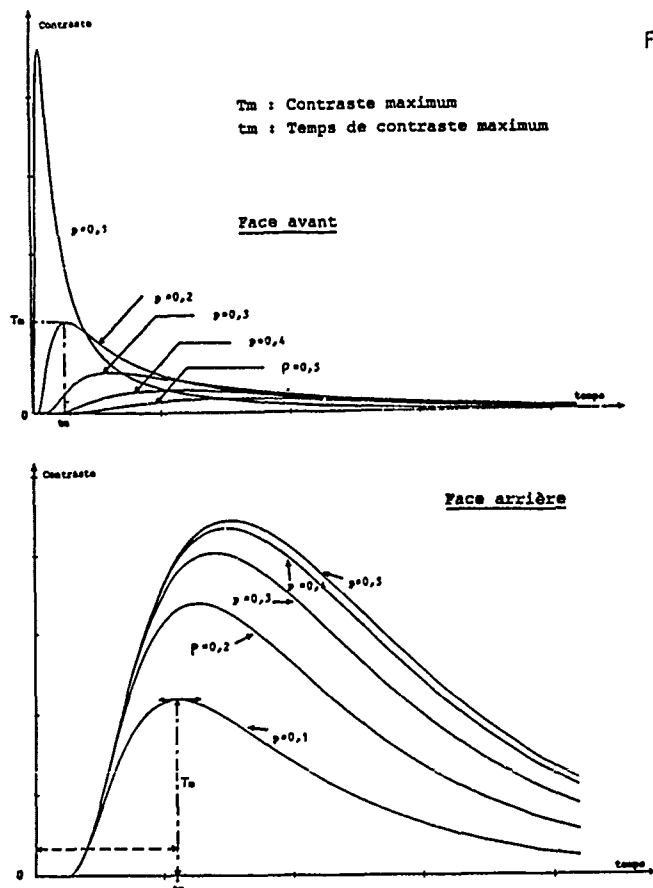


Fig.3 Courbes de contraste en fonction du temps pour un défaut à différentes profondeurs

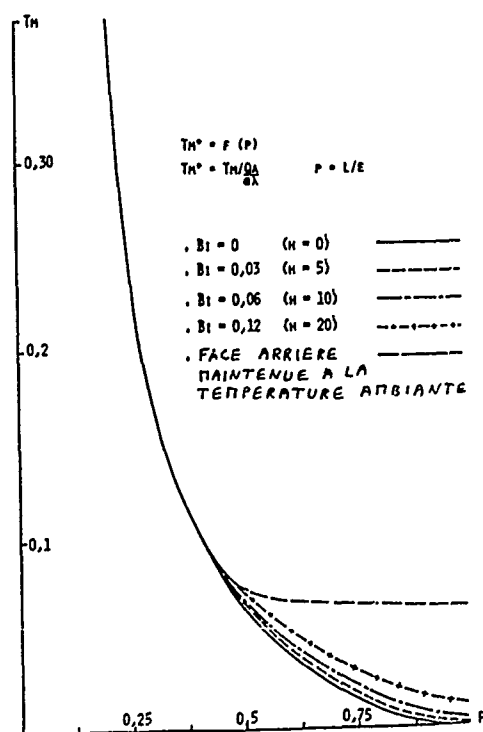


Fig.4 Contraste maximum en fonction de la profondeur d'un défaut de résistance thermique fixée ($R^* = 6.7 \cdot 10^{-2}$)

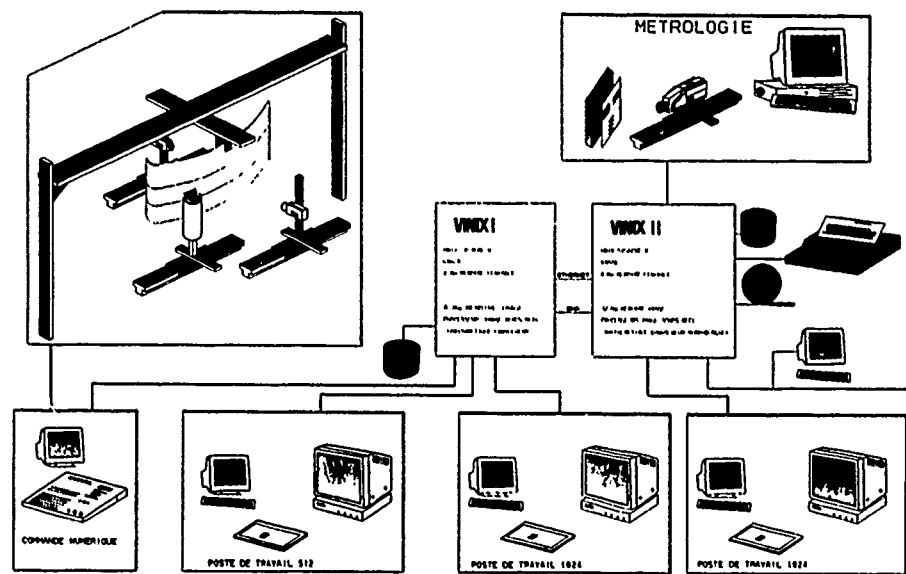


Fig.5 Installation de développement de thermographie infrarouge.

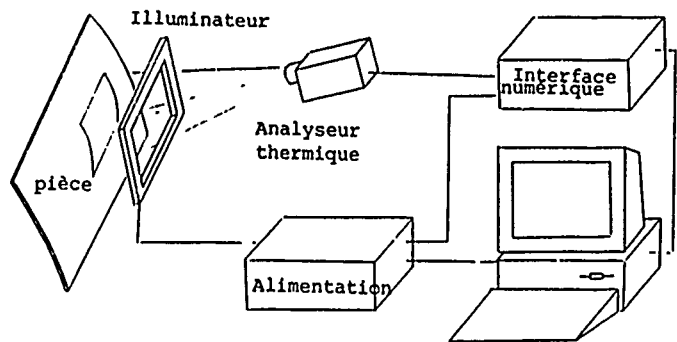


Fig.6 Système d'analyse surfacique

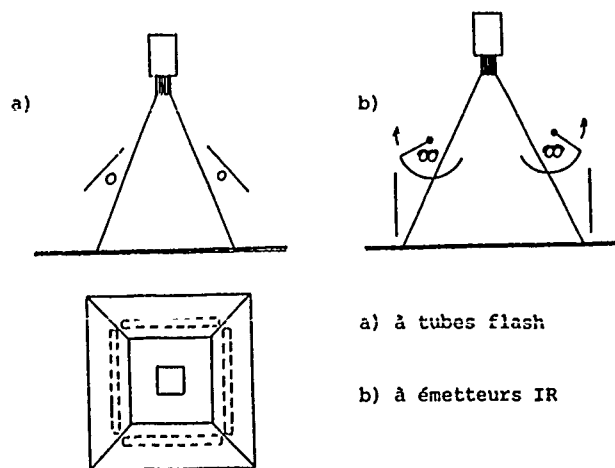


Fig.7 Dispositifs de chauffage surfacique

NEW ASPECTS IN AIRCRAFT INSPECTION USING EDDY CURRENT METHODS

Dr. Manfred Tietze
INSTITUT DR. FÜRSTER, D-7410 Reutlingen

1. INTRODUCTION

High demands in safety at highest possible load of aircraft structures cause increasing expenditure in development of testing procedures for production, maintenance and overhaul. Aircraft structural parts which are generally designed to achieve minimum weight as well as high mechanical stability unfortunately very often have the disadvantages of low corrosion resistance and high susceptibility to crack formation and propagation. Consequently the latitude for tolerable flaw sizes is very small. Therefore, reliable, documented inspection is of increasingly vital importance.

Eddy current testing is one of the most effective tools to detect open or concealed corrosion and to assess damage caused by fatigue or corrosion cracking. In respect of the different sources of corrosion and possible crack formation, to enable identification, evaluation and location it is necessary to have appropriate eddy current units and sensors optimized to the expected inspection program. The following describes the use of a meter type instrument (fig. 1) for inspection of surface defects and a new impedance plane instrument (fig. 2) that allows static and dynamic applications for detection of metal thinning due to corrosion, metal spacing, subsurface cracks etc. and for very quick fastener hole inspection. Finally new signal processing techniques for displaying flaw dimensions through imaging procedures are discussed. All units described herein are portable and battery operated.

2. INSPECTION WITH METER TYPE EQUIPMENT

One of the most common meter type instruments is the well known DEFECTOMETER 2.835 (fig. 1), a micro-processor controlled unit with automatic lift-off and zero compensation. The main field of application is the detection of near surface cracks, such as in turbine blades or bladed wheels for instance and of stress cracks or surface roughness caused by corrosion respectively. By using the lift-off compensation defects can also be detected when located underneath protective coatings up to approx. 300 μm thick. This instrument is very well suited for testing materials with low electrical conductivity because of its high test frequency of approx. 2 MHz (NFe) or 4 MHz (Fe, Aust) respectively.

Using two fixed test frequencies results in an outstanding surface flaw sensitivity where under good conditions minimum detectable flaw depths of approx. 20 μm can be achieved, because probes can be fitted best possible to the resonant circuitry of the instrument. In addition only a minimum of adjustment keys is necessary for an easy set-up and simple operation.

Fig. 1 shows a selection of new probes with a novel lay-out and special shieldings to stabilize and to improve the possible flaw resolution. The special shielding decreases edge, wobble or tilt effects and improves the lift-off compensation. Corresponding to the selected shield material (non-ferrous, ferrous, austenitic) the influence of walls or other disturbing parts can be suppressed when inspecting lobes, ribs, mounting supports, metal fittings etc. Sometimes when inspecting points where access is difficult it is useful to connect a storage oscilloscope to the DEFECTOMETER analog output. This overcomes the problems of moving the sensor on the surface and watching the meter display at the same time. In some cases it is necessary to have tailor made sensors for very specific inspection tasks. Thereby the optimum function is maintained if the impedance of the probe core is fitted to the resonant circuitry of the DEFECTOMETER, otherwise overall sensitivity losses might occur. Therefore a large variety of probe-kits is available to prevent damping of the signals when using metal housings (see fig. 1 to the right).

The meter type instrument DEFECTOMETER is easy to set-up and to operate with simple "go/no go" decisions and therefore is very often used to perform routine inspections. Meter type instruments can only detect changes in impedance but no phase shifts. Hence in test situations where different variables such as lift-off, dimensions, corrosion and flaws e.g. are mixed it is necessary to have phase-analysis instruments.

3. INSPECTION WITH IMPEDANCE PLANE INSTRUMENT

As mentioned above impedance plane instruments have among others the advantage of distinct separation between flaw response and lift-off response. There is the new DEFECTOSCOP SD (fig. 2) for static and dynamic applications that unites the functions of its predecessors S and D. It has a wide frequency range of 100 Hz to 10 MHz (static) or 30 kHz to 3 MHz (dynamic) using signal conditioning filters (LP, HP) to maintain a large bandwidth for both applications. Test frequencies can be varied continuously to optimize the setting relative to the specific flaw problem or material to be tested. Further benefits are given by the digital store for holding flaw signals permanently or continuously within holding times of up to 32 sec. The operator does not need to continuously monitor the screen and can concentrate on probe manipulation.

As a consequence that very often probes from various suppliers are to be kept in stock when replacing old equipments for further use all kind of foreign probes available for flying dot instruments can be connected to the DEFECTOSCOP SD and D.

One tough problem is the detection of concealed corrosion in multi-layer structures as indicated in fig. 3. Normally low frequency absolute hand-guided scanning coils are used. Fig. 4 shows test results obtained from two 3 mm thick Aluminium plates ($f = 1,8 \text{ kHz}$) where phase shift was varied until lift-off was horizontal with nearly 90 degree phase angle to the corrosion signals. These signal

amplitudes are given in fig. 5 as a function of thickness reduction at constant spacing where they show a slightly parabolic behaviour. From fig. 4 can be seen, that all effects except corrosion signals point to the left side of the CRT and therefore movements can be interpreted in an easy way relative to their last position. "Short" means electrical contact between two adjacent layers for example.

Another application is the inspection of rivet rows where probes slide along the row and detect cracks caused by corrosion for instance on the outer and internal skin. Fig. 6 shows crack locations and propagation directions in an airplane structure. For the inspection of the internal skin a frequency of 1,8 kHz is used and for the external skin the frequency is 12 kHz. Experimental results have shown that cracks with lengths from 4 mm onwards can be detected (fig. 7).

In regard of the wide frequency of 100 Hz to 10 MHz, the DEFECTOSCOP SD can be applied for detection of surface cracks using DEFECTOMETER probes and adjusting the test frequency exactly to their optimum sensitivity when phase analysis is required. Fig. 8 shows, for example, the inspection of a cabin at a military aircraft using a DEFECTOMETER dental probe shown in fig. 1.

The inspection of individual fastener holes using hand-held rotating heads (180 rpm, 800 rpm and 1500 rpm) is the fastest and most sensitive method in crack detection (fig. 9). A very complex structure is shown in fig. 10 with corresponding defect indications using high sensitive differential coils.

4. DISPLAYING FLAW DIMENSIONS

In the last few years for example bolt hole testing has become a more and more common test procedure and further increasing expenditure in inspection and documentation of test results can be expected. In regard to this tendency in obtaining more detailed information about defects a new generation of impedance plane instruments is under development. The essential innovation will be the application of imaging procedures for improved flaw signal evaluation. Pattern recognition techniques are already in use in the testing of semi-finished products.

Some arguments for automated image processing are the recognition of interrelated structures, the distinction between different flaw types, the determination of defect size and orientation and therefore improved documentation and the possible tracking of flaw evolution by storing the whole test information.

Two stages of a two-dimensional analysis of the measurement signals are available and that is first a C-scan method to indicate flaws and second based on this detailed calculations of flaw parameters. Fig. 11 shows experimental details in the case of bolt hole inspection using rotor scanner with implemented indexer. The response of the surface layer in the bore corresponding to the penetration depth of the eddy currents is then recorded track by track, where the inner circumference of the bore is "unwinded" to a linear representation. The result of the C-scan is shown on the right hand side of fig. 11. The flow-chart of the corresponding test arrangement can be seen from fig. 12. When moving the scanning probe into the bore, a personal computer (PC) records the EC-signals generated by the tester DEFECTOSCOP, the distance z and the phase angle ϕ generated by the indexer and the rotor scanner respectively using multiplexer (MUX) and analog to digital converter (ADC). All the data can be stored, printed-out and displayed. During the test each track of the growing C-scan is displayed in a gray-value representation (see fig. 13) where the actual recorded circumference is marked by a pointer and in addition the running EC-signal is traced below. This visualisation aid gives a rough assignment in flaw location (depth, circumference) to the inspector and some hints to flaw extension and orientation.

Detailed defect informations can be received by computer driven evaluation of measurement signals. Fig. 14 shows in principle the assessment procedure using pattern recognition technics. Two thresholds generated on both sides of the signal zero line named defect trigger level and defect tracing level are used where the first is situated just above the noise level and the latter is set to the noise level. Threshold crossings result in trigger events or in tracing events respectively relative to the sampling pulses of the system (fig. 14). For defect size calculations only trigger events start a certain search program for closed areas in the surroundings where trigger events occurred (defect tracing). Solely occurring defect tracing events are neglected (see left hand bottom side of fig. 14). After determination of the defect area, calculation of defect shape lines is accomplished (right hand bottom side of fig. 14). Finally, the calculated defect characteristics are mean and maximum flaw amplitude (A_{mit} , A_{max}), mean and maximum flaw width (b_{mit} , b_{max}), center point coordinates referred to a reference point (x_m , y_m), flaw length (l) and orientation angle (α) with respect to feed axis. If several defective areas were detected each defect is calculated and documented separately. The subsequent evaluation steps from the beginning C-scan to the final result are demonstrated in fig. 15 with (from top to bottom) C-scan, C-scan in gray-values, defect trigger area, overall defect area, calculated shape lines and defect contours and finally print-out of calculated flaw parameters.

With the above results improved crack growth predictions are conceivable when comparing previous data with now measured results regarding any changes in flaw parameters like crack extension, length, width and orientation. The relative signal height (A_{mit} , A_{max}), for example, works as an indication in crack depth changes. In addition flaw patterns give information about structural alterations when for example several single cracks have been documented earlier and now a coalescence to a long unique crack is detected.

5. CONCLUSIONS

Eddy current inspection procedures are going to obtain more and more importance because they are faster, no coupling media are required and test results are much more reproducible than other methods.

In order to optimize the inspection programs versatile eddy current equipment, which can adapt all kind of probes, is a basic requirement. Imaging procedures will become an important tool for improved flaw characterisation and documentation.

The best way for accomplishing a successful development of new equipments, probes and new inspection procedures is discussion and co-operation between equipment manufacturer and user of the instruments.

The INSTITUT DR. FÜRSTER is well prepared for intensive partnerships because of its worldwide representation and its wide production range for probes, equipments and systems applicable in aerospace industries. For testing tasks like crack detection, material mix detection, conductivity measurements in the field, lab and production facility the capabilities come up from hand held units (DEFECTOMETER, DEFECTOSCOPE, SIGMA TEST) to complete system equipments for automatic applications (STATOGRAPH S, MAGNATEST S).

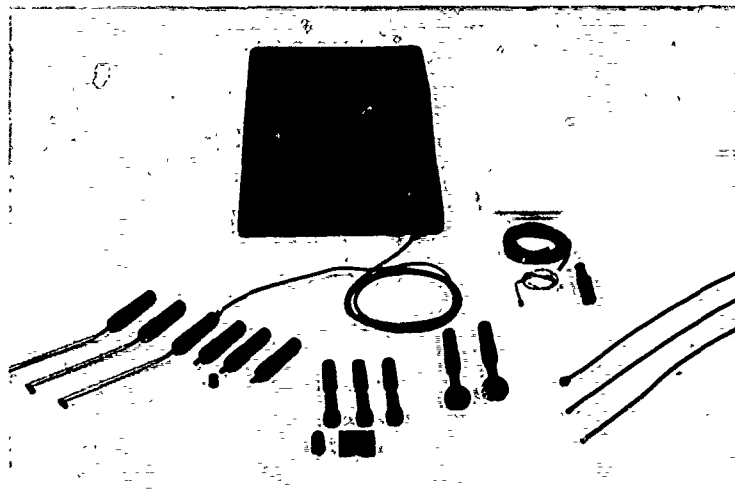


Fig. 1: Förster DEFECTOMETER H 2.835 new shielded probes (left), probe-kits (right)

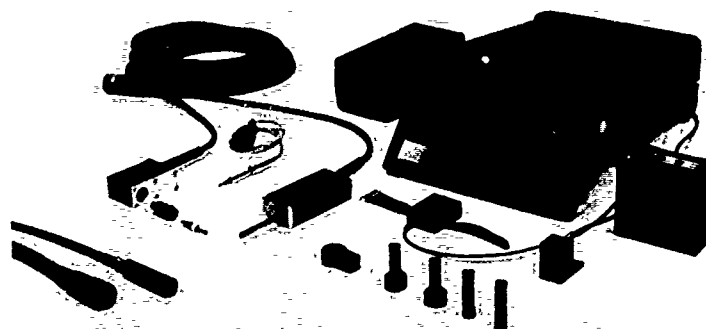


Fig. 2: Impedance plane instrument Förster DEFECTOSCOPE SD 2.832 with a selection of rotating probes, hand-held scanning probes (absolute, differential) and through-type coil. All DEFECTOMETER probes and all current foreign probes are connectable.

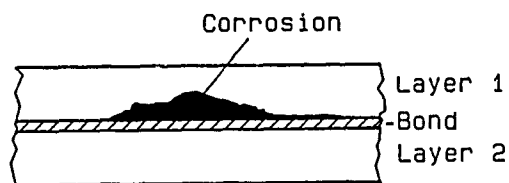
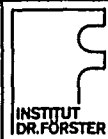


Fig. 3:

	Corrosion in multi-layer skins	2.832/006
---	--------------------------------	-----------

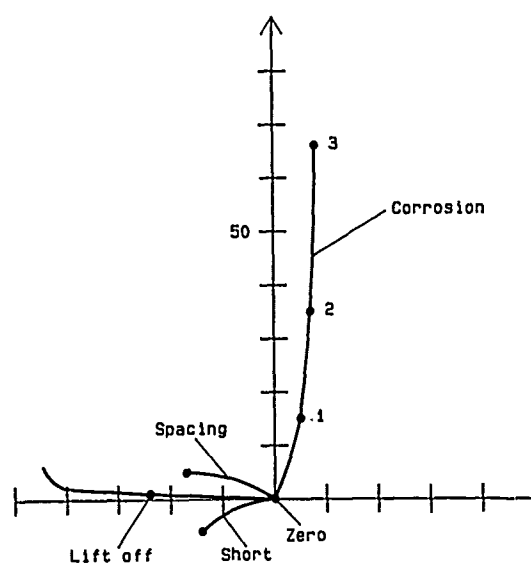



Fig. 4:

	Detection of corrosion using absolute scanning coils	2.832/007
---	--	-----------

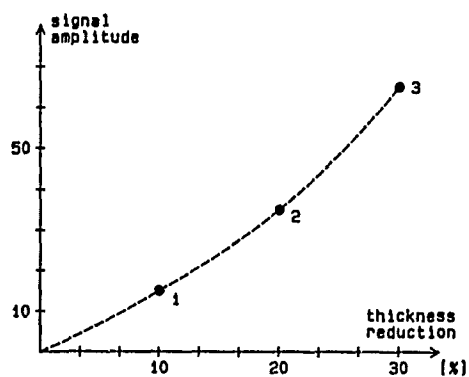
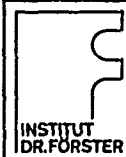


Fig. 5:

	Corrosion - thinning simulated at a 3mm thick Al - plate	2.832/008
---	--	-----------

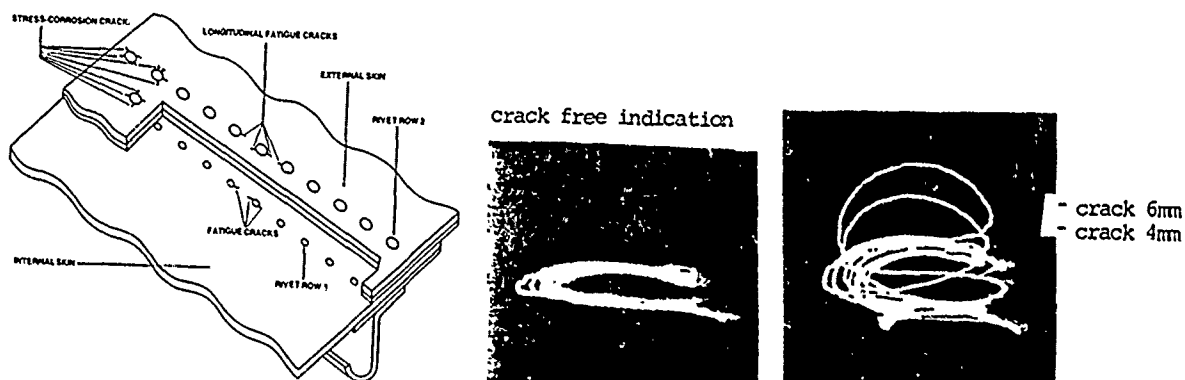


Fig. 6: Crack locations and propagation directions in airplane structure

Fig. 7: Signals from eddy current inspection of a rivet row with sliding probe



Fig. 8: Surface crack detection using DEFECTOSCOP SD and DEFECTOMETER probe



Fig. 9: Inspection of individual fastener holes with hand-held rotating head

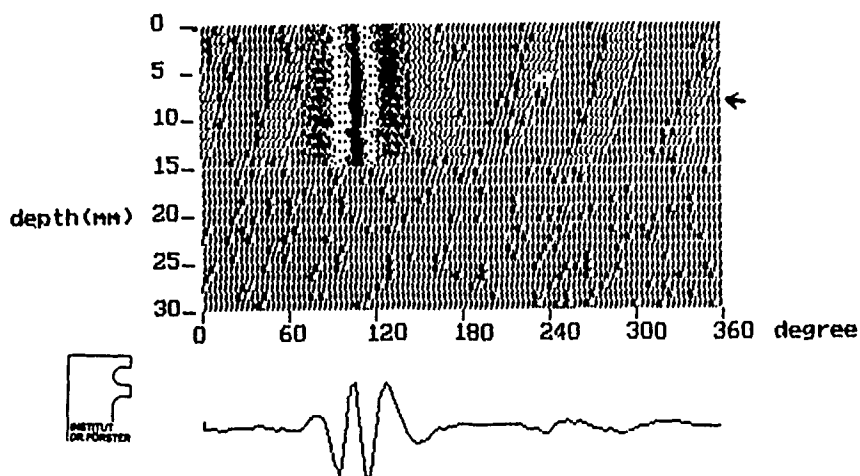


Fig. 13: C-scan in gray-value representation. The right hand pointer shows last probe position and corresponding EC-signal.

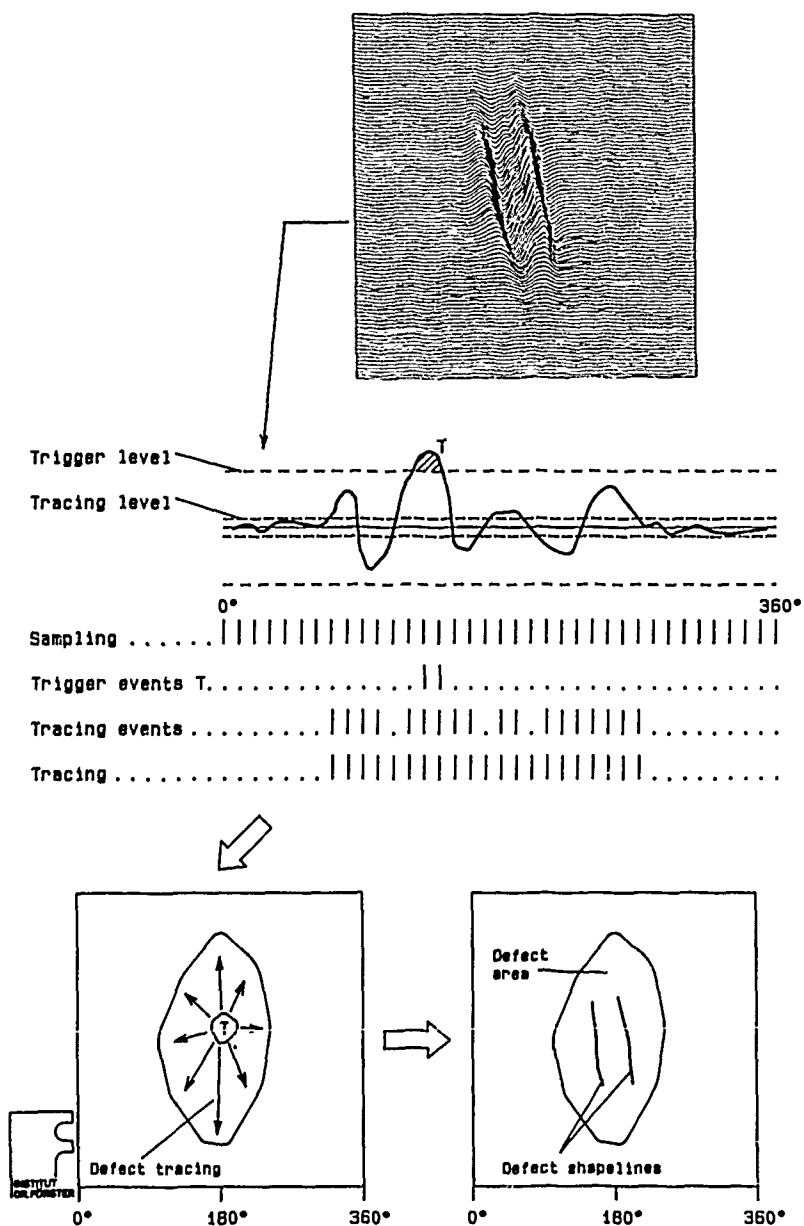
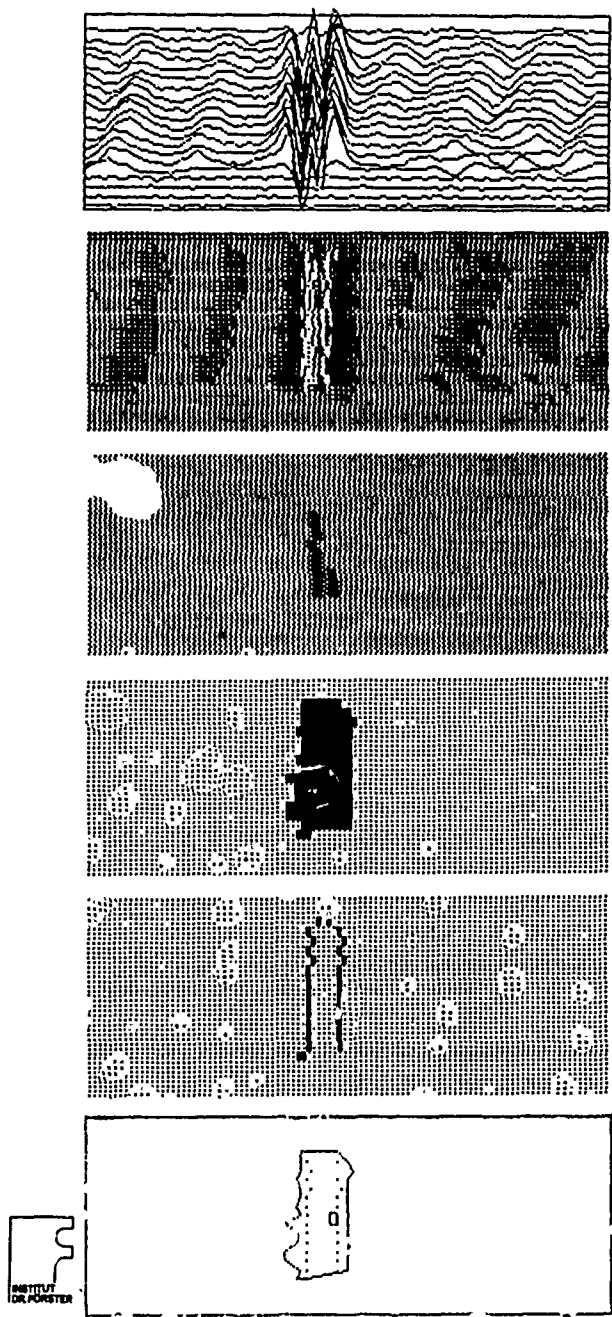


Fig. 14: Evaluation steps for pattern recognition method (for explanations see text).



File: test1 Pruefung Nr.1
Typ Nr amit amax bmit(cm) bmax(cm) xm (grad) ym (cm) l (cm) alpha
Riss 0 : 95.60 : 109.00 : 0.16 : 0.16 : 162.00 : 1.10 : 1.50 : -7.45 :

Fig. 15: Subsequent evaluation steps from the beginning C-scan to the final result (for explanations see text).

STENOPIC RADIOGRAPHY: A NON DESTRUCTIVE TEST WITHOUT CONTACT

Gabriel Delojo, José M. de los Ríos and José Miguel.
 INSTITUTO NACIONAL DE TÉCNICA AEROSPAIAL (INTA)
 STRUCTURES AND MATERIALS DIVISION
 Torrejón de Ardoz, 28850 Madrid, Spain

Summary

The Non Destructive Testing Laboratory of INTA, is working now in experiences about the practical applications of Stenope principle to obtain radiographic images from diffuse Compton Radiation.

Our experiments, until this moment, have showed that it is possible to have a photographic register from an object by its difused Radiation when it is "illuminated" with a very intense 400 KV, X-ray beam.

So we can obtain information about nature differences and/or subsurfacial discontinuities from one only side of the sample.

The first experiences have been made with a fine grain radiographic film and a high velocity salt screens. Next experiences will be carried out with a high sensibility electronic image intensifier assembled with a T.V. circuit, and, different energies radiation. Results obtained will be exposed and discussed.

0. Introduction

The understanding of the systems quality state and its tolerance to damage, while in service conditions, establishes new demands to the Non Destructive Testing. In some cases these demands gather to not allow the material contact with the tested object, as it happens with the space technology, this excludes the application of certain methods obliging to the modification of their applicable techniques. In some occasions they are real new problems needing new testing methods. The Non Destructive Testing Laboratory of the National Institute of Aerospace Technique, Spanish Research Centre of the Defence Ministry, has initiated the development of a new testing method allowing the application of X-ray in a different way to that of the conventional radiography, in order to acquire information about discontinuities and irregularities existing in materials and structural assemblies. This paper presents the method basis performed that demonstrates the feasibility and potential utilization as detection of honeycomb cavities or subsurfacial inclusions, or under protective coatings, as well as for the humidity detection in honeycomb structures or similar.

Naturally, the obtention of an operative system, will require electronic units for bright intensification and high power radiation generators.

1. Method Fundamental

The stenopic radiography allows the obtention of X-ray images by a technique, basically similar to the photographic one. So, while conventional radiography is the "shadow" of an object projected on a radiographic film with gamma or X radiation, a "stenoradiography" is an image projected by a stenopic objective with X radiation propagated from the object "illuminated" with an intense radiation beam.

This allows to obtain information on nature and discontinuities existing under the object surface until a deepness depending on the radiation energy used. This information (and this is the most important thing) is obtained from the radiated surface; opposite than in the ordinary radiographic technique, what requires to locate the film on the opposite side. Also the thickness of the object is, obviously, irrelevant.

2. Image Geometry

Electromagnetic radiation, propagates in space in straight line. Consequently, a point, or point image, projected on a screen by a radiation source, punctual also, is another point, or "shadow". If the radiation source is large, each point of the source shall project the opaque point in different position of the screen, being motive of a source dark image. These images are called "antistenenopic".

If the projected point is substituted by a pin hole perforated in an opaque material, the described process reverses, and the projected image of extense radiation point is now luminous. This is known as an "stenopic" image, and the pin hole as a "stenope".

Though theoretically the stenopic and antistenenopic images are equivalent (though with values of reciprocal light), in fact, the latter are negatively influenced by the luminous field surrounding them. The stenopic instead project themselves strongly over the dark field of the shadow projected by the material in which the stenope is open.

In the practice this effect is improved creating a closed ambit or "dark chamber" that avoids all light not coming from the hole.

An ideal stenope, that is to say, without dimensions, is unrealizable. So, a real stenope is always a circular hole of a determined radius: r . When this radius is small enough when traversed by radiation, is created image perturbing phenomena, due to diffraction. According to the distance at which is located the emitting radiation object, the diffraction shall be conducted according to Fresnel or Frauhoffer's equations, and its importance will be affected basically by the lengthwave (λ) of the radiation. When it is very small, as in X rays, the hole diameter that would cause diffraction perturbations is technically unrealizable. At the same time the need to obtain a radiation dosis big enough for the achievement of the image requires much bigger diameters than the minimum determined by the radiation lengthwave.

Actually the equation of conjugated focus for the stenope is:

$$\frac{1}{D} + \frac{1}{d} = \frac{2\lambda}{r^2} \quad (1)$$

being D and d , respectively, the distances of the radiant object and the screen to the stenope. By analogy with a thin lens, the focal distance, f , of the stenope is:

$$f = \frac{r^2}{2\lambda} \quad (2)$$

For a distance D , big enough ($D \rightarrow \infty$), of (1) equation is deduced that:

$$r = \sqrt{2d\lambda} \quad (3)$$

Applying this formula to radiation X of $\lambda = 0.1 \text{ \AA}$ has a value of $r = 1.4 \times 10^{-10} \text{ cm}$, for $d = 10 \text{ cm}$. It is evident that, the available diameter are very high regarding those that will produce diffraction perturbations.

Another question to have in mind is that an object-point image is projected as a small circle whose diameter is:

$$\varnothing = \frac{2r(D+d)}{D} \quad (4)$$

Naturally for $D \gg d$, $\varnothing \rightarrow 2r$, that represents the maximum geometrical definition attainable in practice.

Theoretically, $r_m = r = 0.1 \text{ mm}$, and $\lambda = 0.1 \text{ \AA}$, the focal distance, according with (2) will be:

$$f = \frac{0.1^2}{2 \times 10^{-8}} \approx 500 \text{ m.}$$

The short wavelength of the X-rays show that the optimum "focal" distance is unrealistic, but instead, real stenopes are far to present any diffraction problems in the images.

3. Diffuse Radiation

As it has been indicated, the object strongly irradiated by primary X-rays beam, is changed into a secondary emitter, whose image is focused by the stenope on a sensitive material or on a photomultiplier device.

To know the diffusion is indispensable in order to understand the possibilities and limitations of the method.

Diffusion is a secondary effect of the radiation absorption. In both cases, if it is a $\frac{dx}{dl}$ material thickness element; interposed to a radiation beam of I intensity, dI intensity that goes through dx is proportional to I and μ_l or attenuation lineal coefficient.

$$dI = -I \mu_l dx$$

$$I = I_0 e^{-\mu_l x} = I_0 e^{-\mu \times \varphi} \quad (5)$$

being μ the masic attenuation coefficient and φ the material's density.

As μ changes with λ , (5) is valid only for monochromatic photon beams. If its individual energy is, according to Planck equation:

$$E = h\nu = hc/\lambda \quad (6)$$

for $I_0 = nh\nu$ the energy loss will be

$$-\Delta E = h\nu(I_0 - I) \quad (7)$$

that has to be somewhere.

The misspended energy changes into scattered radiation and, finally in heat, basically by four mechanisms:

- a) By Rayleigh Effect or coherent scattering, produced while the photon goes through the negative electromagnetic field formed by electronic cloud surrounding the material atoms.
- b) Photoelectric Effect for photon energies in the range of those bonding the electrons to its energetic level, in the material atoms.

In this case:

$$h\nu = \varepsilon$$

If it is bigger, the gone out electron gets the difference in energy.

$$h\nu - \varepsilon = \frac{1}{2} m_e v^2 \quad (8)$$

In which m_e is the electron rest mass and v the acquired velocity.

Secondarily, the hole left by the electron is occupied by another one of bigger energetic level with the emission of a characteristic X-ray, whose energy and wavelength are given by:

$$\varepsilon_1 - \varepsilon_2 = h\nu = hc/\lambda$$

$$\lambda = \frac{hc}{\varepsilon_1 - \varepsilon_2} \quad (9)$$

- c) By Compton Effect in which the high energy photons interaction the electron, giving relativistic velocities on them, consequently the photon loses the corresponding energy in form of wavelength movements. It is deduced by Compton's examinations that according to the scattering angle the increasing of the wavelength $\Delta\lambda$ is:

$$\Delta\lambda = \lambda - \lambda_0 = \frac{h}{m_e c} (1 - \cos\varphi) \quad (10)$$

being φ the scattering angle and m_e the mass in rest of the electron, as we have said. This equation shows that the scattered photon will always have lesser wavelength and that the difference of wavelength will be as bigger as φ have been.

- d) By Production of Pairs (e^-, e^+) which we do not consider since it happens when the radiation has higher energies than 1.022 Mev., that is, much more high than those used in our work.

4. The Real Scattering

The effects considered in (3) interinduce themselves. So, a Compton photon can be re-scattered by photoelectric effect (the opposite is less probable) or by Rayleigh effect. This way, the photoelectric photons proportion coming from processes of superior range is increased, what explains, in fact, the abnormalities observed in the scattering at low energies which will be commented afterwards.

Anyway, the scattering of a monochromatic radiations beam produces a scattering spectrum including in diverse proportions photons of some wavelength lower than the primary. Logically a complex spectrum or a continuous spectrum as the one used in our tests produces an anisotropic scattering of incalculable composition, theoretically. In anycase, experience shows that scattered radiation intensity, is not undifferent to relative positions of the primary radiation source and stenopic chamber.

For energies in the range of 1 Mev., or higher, in which Compton effect is convenient, even for higher range processes, the scattering intensity is proportional to the atomic number (Z), since the Compton interaction probability is given by the absorption coefficient due to this effect: μ_c

$$\mu_c = \varphi N \frac{Z}{A} \sigma_e \quad (11)$$

where N is the Avogadro number and σ_e the cross-section of the link for interaction.

However, at low energies, the main radiation percentage of photoelectric origin, coming mainly from interactions of higher ranges of Compton photons, combined with autoabsorption phenomena, as it is showed in papers from F. Wachsman, H. Tiefel and E. Berger, to an intensities distribution really anarchical. So, the hydrogenated composites provided scattering radiation sources much more intense than metals, and among these, not always are better scatters those of bigger atomic number.

5. The Stenopic Chamber

Basically it is a cylindrical chamber radiationtight, whose demountable parts fit themselves avoiding radiation to penetrate through the slots. Figure 1 shows the aspect and construction details of the chamber whose walls are made of lead of 25 mm., thickness.

Essential part of the chamber is the "stenope" or pin hole that is used as "objective" of the chamber. Ideally, must be moved on a thin plate, but the need to stop radiation makes necessary to give the plate a considerable thickness. A good stenope shall be made by perforating with laser the bottom of a mechanized cone in a metal of high atomic number and hard enough (what excludes lead or bismuth). For accurate beams of less than 350 KV can be made of tungsten or in a gold-platinum alloy. In order not to make the device expensive and to be able of changing its diameter, the stenope can be on a little screen that fits in a container located on the front surface of the chamber. To avoid the lap of optical image of the object, the stenope is wrapped-up in a piece of black photographic paper. However, sometimes, the above mentioned lap may be useful in order to link the inner radiographic image with the object aspect, in such case, the paper can be removed once finished the exposure to X rays illuminating the object during some minutes with a strong light.

We must indicate that the described chamber is a prototype whose aim, already achieved, is to show the feasibility and usefulness of the method. At present, we are developing a chamber in which the radiographic film is substituted by photomultiplicable electronic devices which we hope will reduce the exposure times to operative levels.

6. The Exposure

The exposure times depend on:

- a) The stenope diameter. So the exposure time is inversely proportional to its radius squares.
- b) The film. It is convenient to use films of the fast type (II or III) since the scattering produced by the stenope diameter is, up to the moment, more important, than the emulsion grain.
- c) Intensifying screens. In order to avoid long time of exposure, it is indispensable to achieve image intensifier screen system. In tests already performed, high definition calcium-wolframite screens have been used.

Now we are working in the regulations of a reliable substance for previous examination calculations.

A semiempiric process that allows to economize a good deal of time consists in the performance of a quick exposure with a big diameter stenope that provides an image quite diffuse but allowing to evaluate the definitive exposure because of the law of radius squares relation.

7. Examples of Experiences Achieved

Figures 4, 5, 6, and 9 show the results of the experiences that we consider illustrative of our previous exposition.

Figure 4 is very demonstrative of the different behavior of four materials, Uranium, Lead, Copper and Paraffine, chosen by their dissimilar densities and atomic numbers of their elements. Considering that the reproduction has the photographic density values reversed, obviously diffusion is more important in light materials than in the thick ones. Figure 5 shows a lead cylinder in which four drills of 4 mm., 3mm., 2 mm. and 1 mm., diameter have been mechanized. The surface hidden by an aluminium sheet and white paint, the stenopic image shows with accuracy, besides the part's contour, the relative location and size of the drills through the coating.

Owing to the remarkable diffusiveness showed by the paraffine, we verified if water (as it can be expected) showed also this property. Figure 6 shows the stenoradiography of a halved bear can. There exists the possibility of using the stenope for the obtention of a photography of the object. For this purpose, it is sufficient to take out the opaque disc illuminating for some minutes the object by means of a powerful light.

Finally, Figure 9 shows a practical application of these tests. It is a stenoradiography performed to detect water in a honeycomb structure.

8. Future Developments

Our main interest, at present, is the design of an operative system allowing real time inspections or, at least, in a short time. With this purpose our actual works intend to obtain the adaptation of an image intensifier system of elevated cost chamber and T.V. as well as digital system and image analyzer.

Also, the possibility to employ radiographic flash equipment of cold discharge, lighter than the conventional hot cathode one, and even isotopic sources.

Parallely, the behaviour of diverse materials must be studied as well as the informative "deepness" of the method on them.

9. Conclusions

In view of all the exposed herein, can be said that Stenopic Radiography is a new method for nondestructive testing, without contact, basically different from the conventional radiography. So, this one gets its images (radiographic) by projection of the object's "shadow" on a film or screen. On the contrary, the stenoradiography works as a real photography made with X-ray, what allows to investigate from one of the sides of the object its structure up to a certain deepness. Thus, the stenoradiography does not provide the same information than the conventional radiography, consequently, can not be used to solve the same problems. Now we are learning really, which are the new problems that can be studied by this test method.

However, we hope to find applications that allow a more accurate acknowledgement of the aeronautical materials and structures operative state, as well as other of a more general character in the industry.

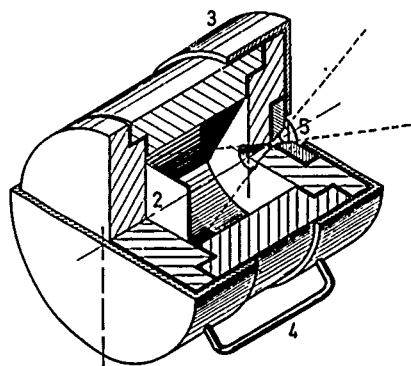


Fig.1- Section view of the stenope camera.



Fig.2- External aspect of the camera.

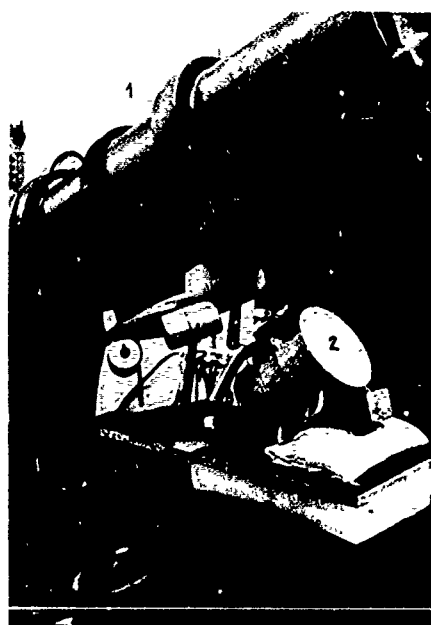


Fig.3- Elements disposition to make a stenope radiography.

- (1) X-ray source
- (2) Camera
- (3) Object

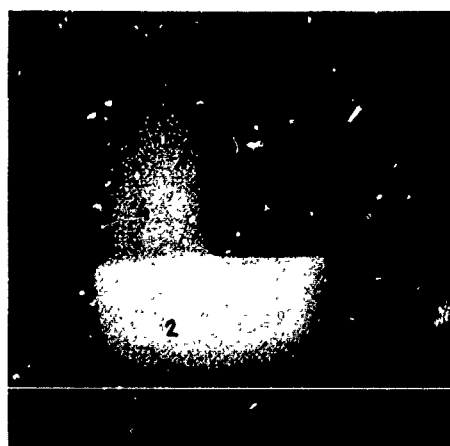


Fig.4- Stenope response for different materials.

- (1) Uranium
- (2) Paraffine
- (3) Lead
- (4) Copper

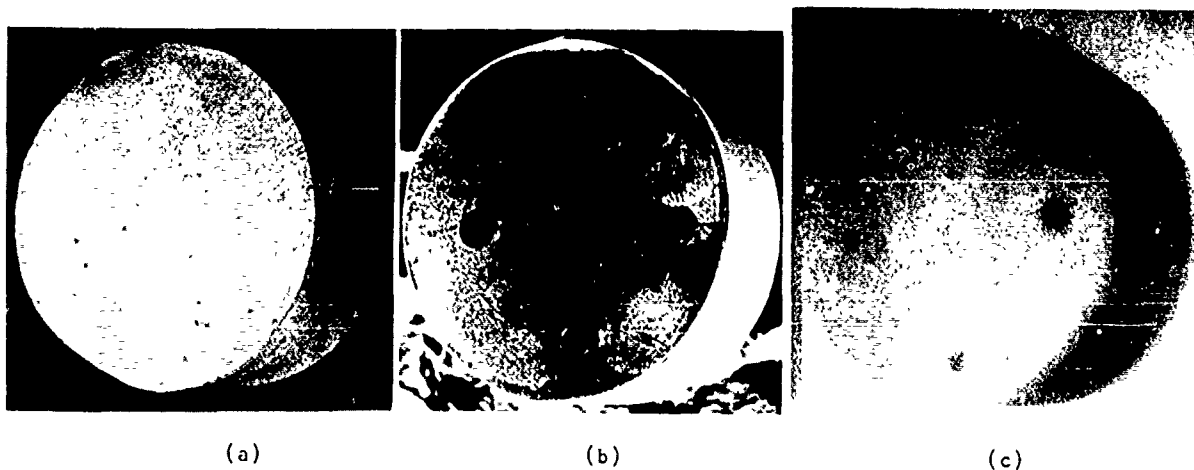


Fig.5-

- (a) Lead cylinder with Al cover foil and paint
- (b) The same one without Al foil
- (c) Stenoradiography through Al foil

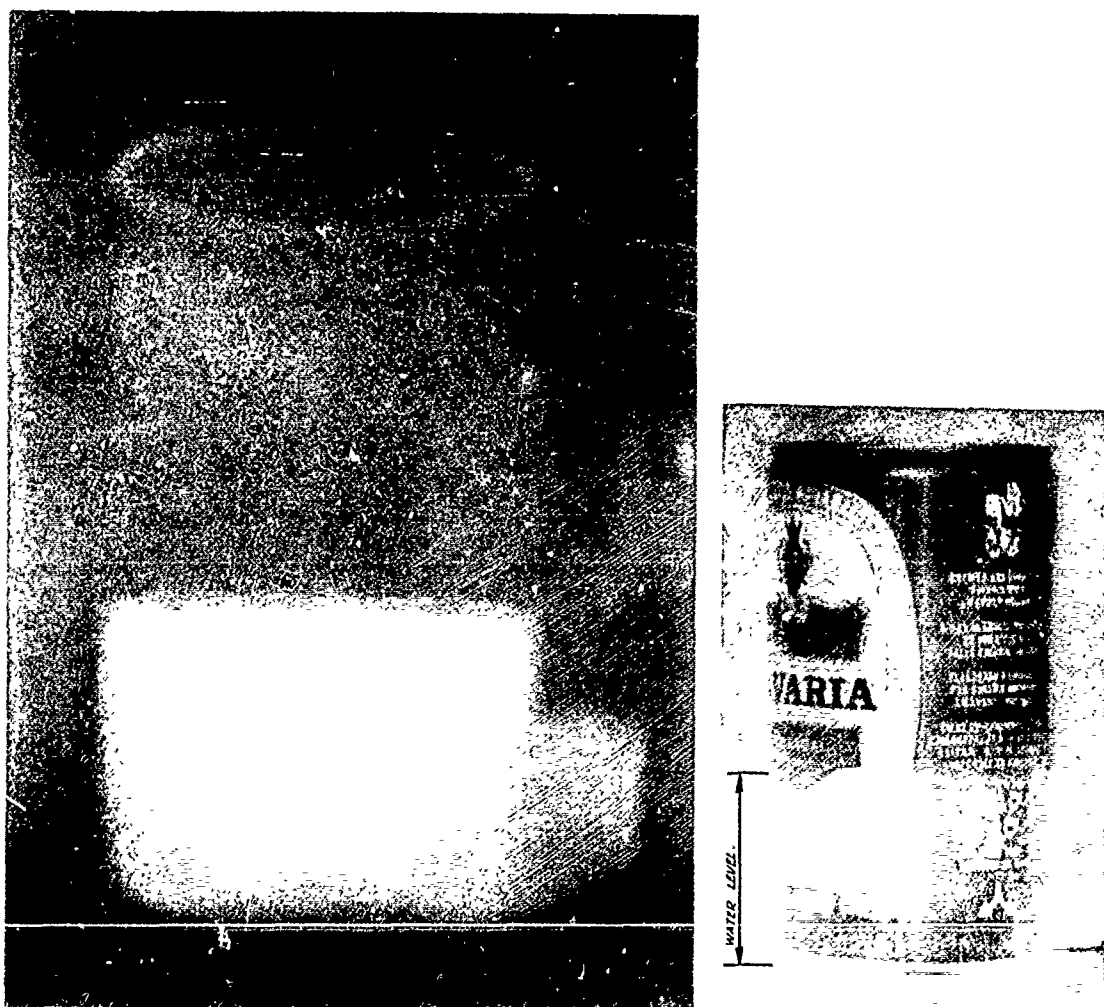


Fig.6- Stenoradiographic image of a halved bear can. It is possible appreciate the liquid level (white part). On the right the same one with optical stenopic image superimposed.



Fig.7- Photography of honeycomb structure with water contamination inside.

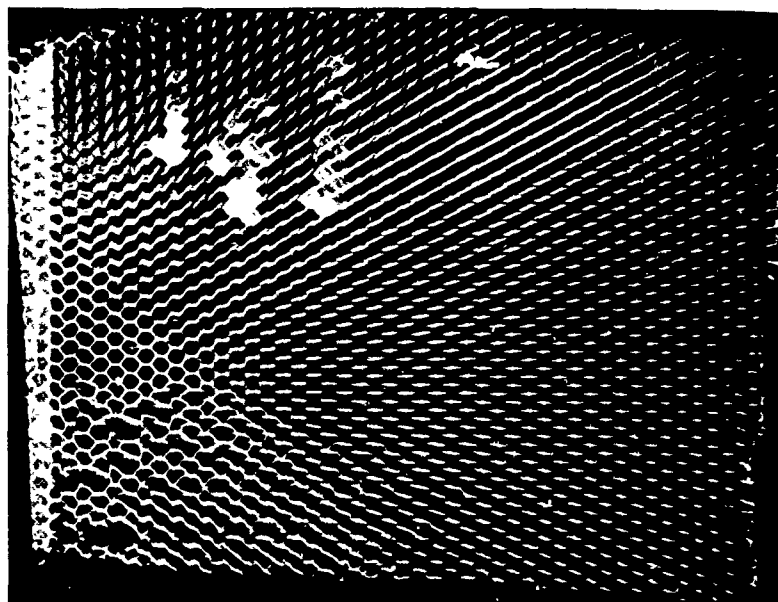


Fig.8- Radiography of specimen in Fig. 7 showing traces of water contamination (white part).

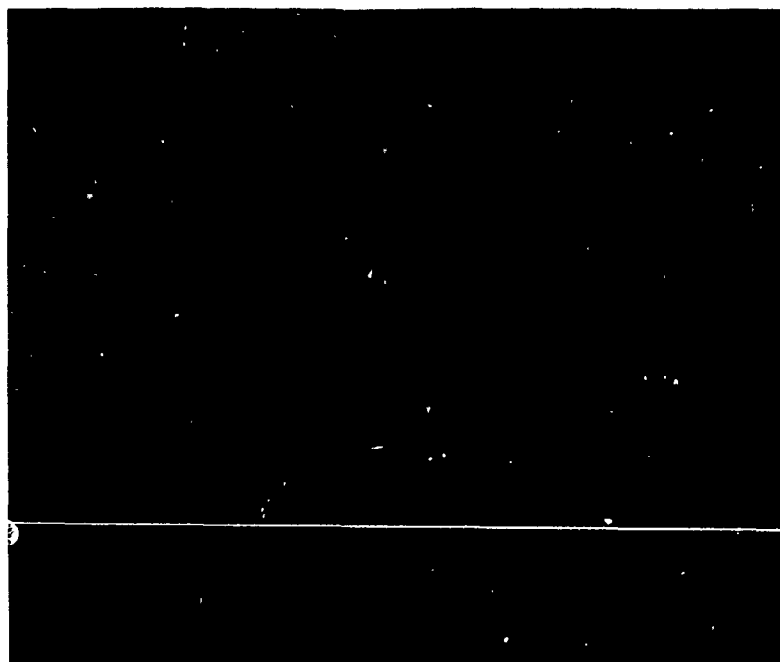


Fig.9- Stenoradiography of specimen in Fig.7. Note as parts containing water are clearly visible and are the same as in above radiography.

Noncontact Laser Thermomechanical Nondestructive Evaluation for Advanced Coatings

by

H. I. Ringermacher

Nondestructive Evaluation and Diagnostics Research

United Technologies Research Center

Silver Lane

East Hartford, Connecticut 06108

USA

SUMMARY

Unique photoacoustic microscopy techniques have been developed that permit the evaluation and visualization of thermomechanical properties of advanced coating systems including evaluation of attachment to various substrates, coating in-plane modulus, thickness variation as well as variation in thermal properties. The technique involves scanning a component surface with a modulated laser beam while monitoring the induced vibration with a laser Doppler heterodyne interferometer. The induced vibration level is strongly dependent on the near surface thermomechanical coupling, thus making coatings an ideal application. Thermomechanical images of coatings along with physical modeling will be described. Applications include silicon nitride and zirconia coatings for thermal barrier and oxide protection.

INTRODUCTION

Thermal imaging for the nondestructive evaluation (NDE) of materials appears to be of ever increasing importance for industrial applications. The development of new materials, both metallic and ceramic, as thermal and oxide barrier coatings present new challenges to inspection techniques. Thermal imaging methods seem ideally suited for such applications, being particularly sensitive to surface and near-surface material thermal inhomogeneities that may be defect-related. However, these same sophisticated materials can pose rather severe requirements upon the efficacy of any particular type of thermal imaging. Typical problems encountered include rough, optically scattering surfaces, surfaces ranging from highly reflective to absorptive, complex surface geometry and microscopic to very macroscopic (practical components) imaging requirements.

Thermal techniques include both photo-thermal and photoacoustic imaging. Infrared camera methods can image subsurface defects in both metal and insulating coatings and have the advantage that large areas can be covered quickly (1, 2). These methods, however, fail to provide any indication of the mechanical coupling of the coating to its substrate. Even a fully disbonded coating in good touch contact with its substrate will appear bonded thermally since the thermal resistance at such an interface is very low.

For the reasons cited above, it is desirable to use noncontacting laser photoacoustic methods to evaluate the mechanical bonding of coatings. The laser photoacoustic methods generally involve scanning a laser beam over the surface of a component in order to generate sound either in the air above the surface or in the component itself. The sound is then monitored with a microphone, a transducer attached to the component or a noncontacting laser interferometer used for vibration sensing.

Photoacoustics using noncontact laser interferometric sensing will be discussed in the present work.

Photoacoustics

Photoacoustics research is a new and still evolving area of NDE. UTRC is among the first to bring photoacoustics from a basic laboratory environment into an industrial one. Photoacoustics is a technique wherein a chopped laser beam striking an absorbing surface is converted to heat, which, via thermal expansion, is subsequently converted into sound at the chopping frequency. The sound is detected by a laser Doppler heterodyne interferometer which senses the velocity of the vibrating surface. The technique is fundamentally sensitive to changes in material thermal and mechanical properties arising from the presence of subsurface voids, inclusions, defects and impurity concentrations at micron resolution levels.

Thermomechanical Imaging

Recently, a new contrast mechanism, thermomechanical imaging, was developed at UTRC. This provides, for the first time, the ability to visualize the mechanical properties of an interface and thus has application to coating adherence and bonding of thin sheets and plates to substrates. Thermomechanical imaging can display a graded image of coating adherence from good bond to total disbond. The method works by thermally stressing the surface with the input laser beam and monitoring the resultant sound transmission, via mechanical coupling to the substrate, with the laser interferometer. A weak acoustic response is representative of a poor mechanical coupling at the interface. Successful applications include evaluation of ceramic coatings on metal substrates, aluminide coatings on metals, ceramic coatings on carbon/carbon composites, subsurface defect detection in both metals and ceramics and thermomechanical evaluation of electronic materials and components.

PHOTOACOUSTIC SYSTEM

Figure 1 shows the experimental arrangement of the laser heating source together with the Doppler heterodyne interferometer detection and computer control system. A typical power level is 200–500 mW to the target from the argon laser. The beam is modulated at the desired photoacoustic frequency up to 100 kHz. The modulated beam is then raster scanned over the specimen with galvanometer mirrors at a rate of up to 10 mm/sec. A typical image coverage would be a 25 mm x 25 mm area with 50 micron resolution in approximately 10 minutes. Finer resolutions are achievable at the cost of increased scanning time. As a rule, the resolution of thermomechanical imaging is approximately equal to the depth of the imaged defect below the surface. For example, a 100 μm wide defect located 200 μm below the surface will appear at least 200 μm wide in the image. Thus, it is most efficient to scan at a rate providing this minimum resolution.

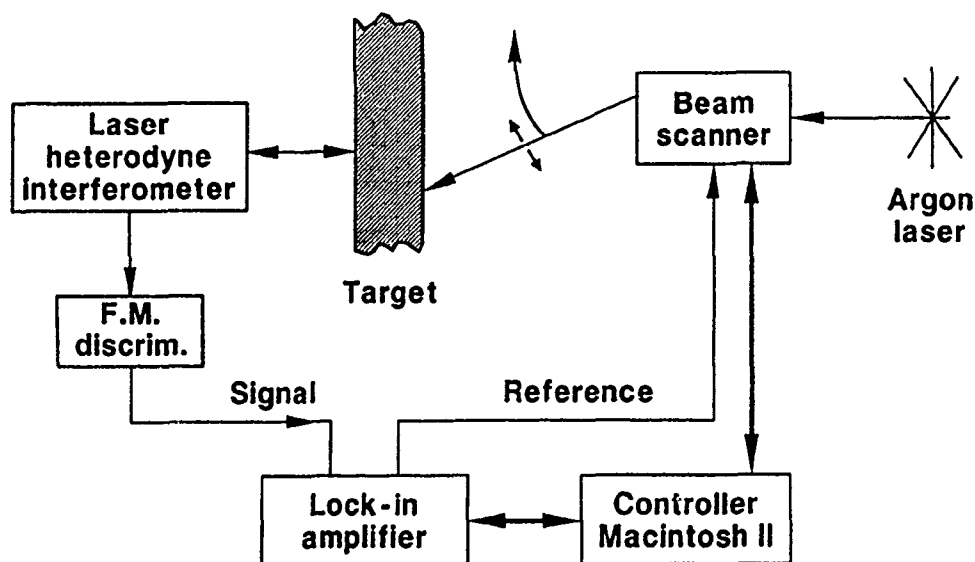


Figure 1. Block diagram of photoacoustic laser scanning and interferometer detection system.

Beam modulation can be either intensity or coordinate modulation. Intensity modulation is the standard technique. Coordinate modulation involves dithering the beam slightly in the direction of the scan. This has the effect of producing a spatial signal-difference image. Its advantage is an improvement of image contrast and signal/noise ratio. Coordinate modulation is discussed more extensively in Refs. (3, 4). Both techniques have been used in the present work.

During examination, the specimen is held at the edges so as to obtain, as closely as possible, a simply supported boundary condition. The interferometer can be focused almost anywhere on the back or front side of the specimen except too close to support points. The interferometer is discussed in Ref. (5).

THEORETICAL MODELING

The thermomechanical mechanism has been observed (6) and verified both experimentally and using finite element modeling with excellent agreement (7). Recently, analytic modeling has also been completed and compared with observation on plate bonding applications such as examples shown in this work. Figure 2 shows the model used to evaluate the thermomechanical response of a bonded coating platelet to a substrate. Some coatings on stable substrates tend to fracture naturally. This model simulates such a response. A laser is scanned from one edge of the platelet to the other. This heats a small spot on the surface which provides a time dependent thermal load to the platelet at the modulation frequency. The platelet is modeled as being perfectly attached to an elastic foundation, here approximated as a beam. The thermal load then bends the beam and this deflection is monitored by a laser interferometer producing the observed image as the spot is rastered over the surface. The frequency is kept below any fundamental modes of the sample and the resultant response is phase-coherently detected so that a static elastic model is adequate. The theory predicts a known deflection response for a perfectly attached coating with known thermoelastic properties (8). This is then compared to the observed response in a real specimen. A disbond or weak bond will show as a deviation from the predicted scan response. Figure 3 shows the modeling results for a single scan line across a platelet. The stiffness constant K includes the known mechanical properties of both the coating and substrate with $K = 100$ corresponding to a very stiff system and $K = 1$ corresponding to a very compliant system. The $K = 10$ response corresponds to the sample evaluated in this work, namely a perfectly attached silicon nitride coating on a carbon/carbon substrate. According to the assumptions of the model, a perfect silicon nitride coating response to the laser beam scan would be the $K = 10$ response while a poorly attached coating would respond more like the $K = 1$ case.

APPLICATION AND RESULTS

Figure 4a shows a scanning electron microscope (SEM) image of typical silicon nitride platelets on a carbon/carbon substrate. Figures 4a–4d show the results of a single laser beam line scan through the large central platelet. Figure 4b is a

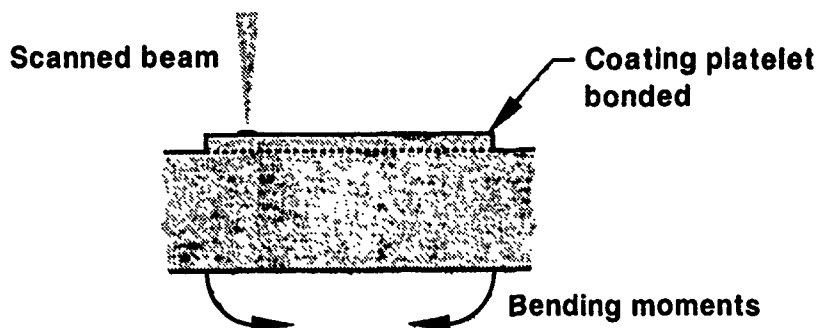


Figure 2. Thermomechanical model of a coating platelet attached to an elastic foundation.

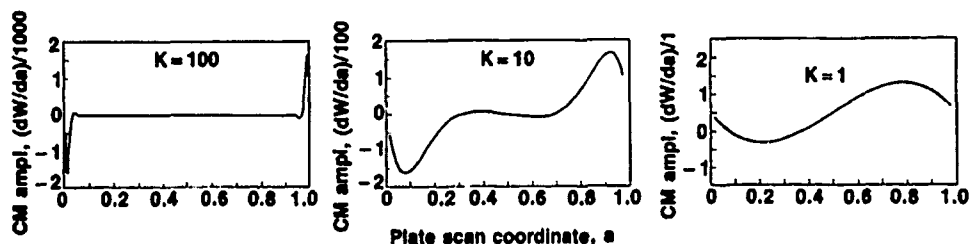


Figure 3. Thermomechanical modeling results showing the deflection responses of the substrate to a single scan line over the coating.

laser thermomechanical image of the nitride platelets with a single white line superimposed where the single scan line data was taken. This image is reversed left to right from Figure 4a. The experimental scan response from left to right on the large platelet (Fig. 4c) compares favorably with the $K = 10$ theory case (Fig. 4d) indicating a good bond and valid thermomechanical modeling. Coordinate modulation (CM) was used in this example.

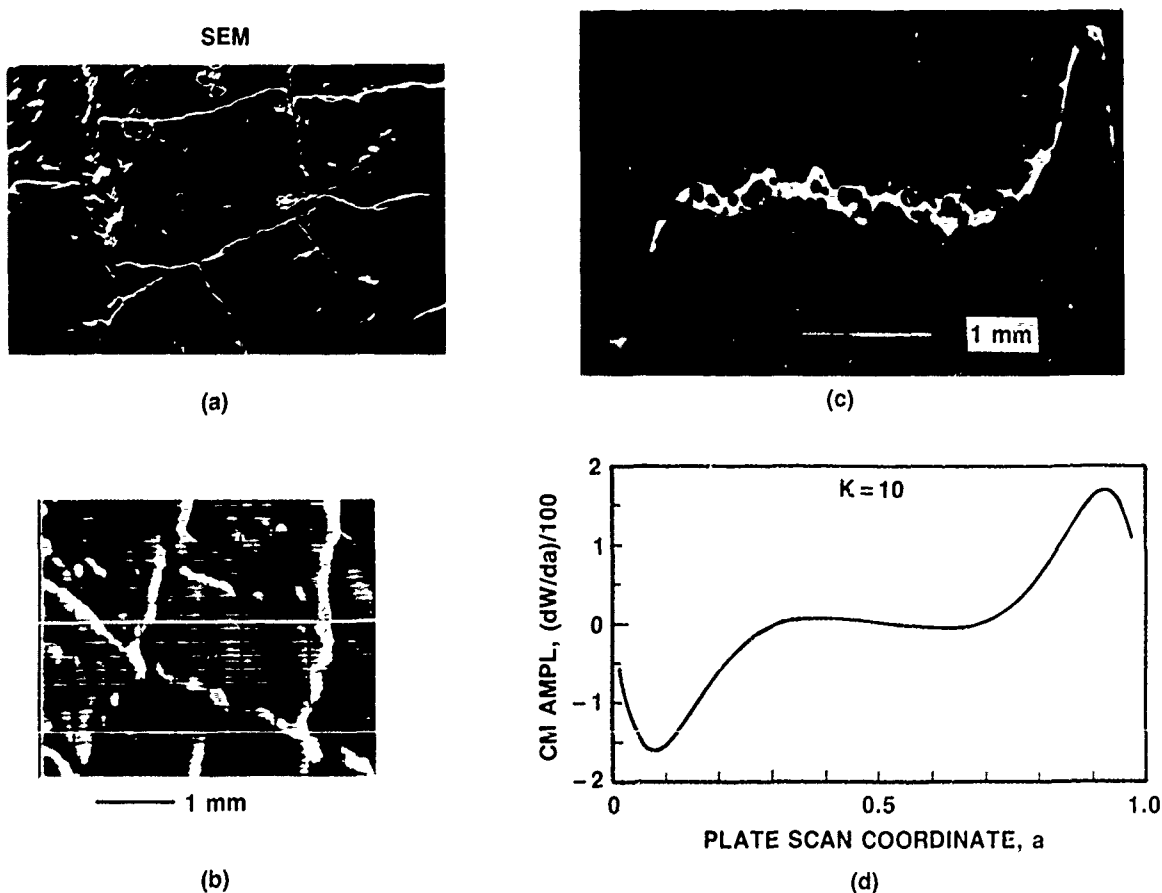


Figure 4. Comparison of experiment and theory for the thermomechanical response of silicon nitride on C/C.

A more recent application is to zirconia thermal barrier coatings on nickel alloy substrates for aircraft engine blades. Shown in Fig. 5a is such a coating approximately 0.01 inches thick on a one-half inch rod specimen which has been subjected to a high temperature burn resulting in ablation and partial disbonding in places. The purpose of the thermomechanical evaluation was to determine the extent of disbonding beyond the ablated regions and to follow the progress of disbonding as the burn continued. The thermomechanical image of the same region obtained with the above noncontact laser technique is shown in Fig. 5b. The ablated, bare metal black areas (A) and totally disbonded white areas (B) are clearly seen. In addition, it is evident that at least two other regions stand out: areas (C) are well bonded and remained intact during the burn while areas (D) show partial disbonding, indicated by white blotchy zones. These areas are of greatest interest since, apparently, this is where disbonding initiates. The image clearly shows bond compliance variation everywhere and thus can be useful in interpreting bond strength.

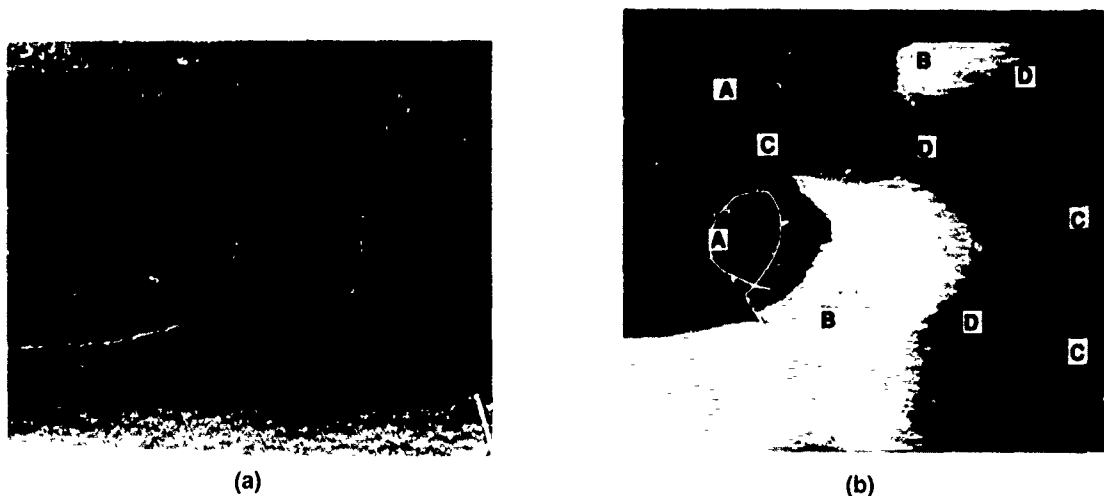


Figure 5. Thermomechanical imaging of a zirconia coating on a nickel alloy rod substrate.

SUMMARY

Noncontact laser thermomechanical NDE provides a visual image of bondline mechanical properties. The observed variation in bond compliance can be correlated to bond strength if the bonding failure mechanism is understood but at the very least can provide a continuous indication of bond integrity from total disbond to perfect attachment. Thermomechanical images generated by this method can be readily understood and interpreted since the supporting theoretical modeling has been confirmed experimentally several ways. Recent applications are primarily to ceramic coatings for oxidation and thermal barrier protection in aircraft engines.

REFERENCES

1. P. K. Kuo, Z. J. Feng, T. Ahmed, L. D. Favro, R. L. Thomas: *Springer Series in Optical Sciences*, Vol. 58, pp. 415-418, Photoacoustic and Photothermal Phenomena, Editors: P. Hess and J. Pelzl, Springer-Verlag Berlin Heidelberg (1988).
2. L. J. Inglehart, E. H. LeGal-LaSalle: *Photothermal Characterization of Ceramics by Mirage Effect*, Conference on NDT of High-Performance Ceramics, Boston, MA, USA, August 25-27 (1987).
3. H. I. Ringermacher: *Coordinate Modulation Photoacoustics with Piezoelectric Detection*, IEEE Ultrasonics Symposium, IEEE Cat. #82CH1823-4, Vol. 2, p. 576 (1982).
4. H. I. Ringermacher and C. A. Kittredge: *Photoacoustic Microscopy of Ceramics Using Laser Heterodyne Detection*, Review of Progress in Quantitative Nondestructive Evaluation, Vol. 6B, pp. 1231-1240 (1987).
5. H. I. Ringermacher: *Laser Doppler Heterodyne Interferometer for Photoacoustic Applications*, Ultrasonics International 87 Conference Proceedings, p. 165 (1987).
6. H. I. Ringermacher and L. Jackman: *Deep Thermoacoustic Imaging Using Scanning Electron Acoustic Microscopy*, Review of Progress in Quantitative Nondestructive Evaluation, Vol. 5A, pp. 567-574 (1986).
7. H. I. Ringermacher and M. Bak: *Thermomechanical Contrast Mechanism in Thermoacoustic Imaging for NDE*, Review of Progress in Quantitative Nondestructive Evaluation, Vol. 7A, p. 238 (1988).

ADVANCED NDE TECHNIQUES FOR QUANTITATIVE CHARACTERIZATION OF AIRCRAFT

by

Joseph S. Heyman and William P. Winfree
NASA, Langley Research Center, MS-231
Hampton, Virginia
23665-5225
USA

SUMMARY

This paper reviews recent advances in NDE at NASA, Langley Research Center and their application that have resulted in quantitative assessment of material properties based on thermal and ultrasonic measurements. Specific applications include ultrasonic determination of bolt tension, ultrasonic and thermal characterization of bonded layered structures, characterization of composite materials, and disbands in aircraft skins.

INTRODUCTION

Traditional Nondestructive Evaluation (NDE) emphasizes finding and sizing flaws. To that end, it has been very successfully applied to improving the safety and reliability of aircraft structures. As the technology matured in the early 50's, new instrumentation provided relatively easy access to the internal geometry of materials. This insight launched NDE as a profession and created much of the infrastructure present in the technology today. Today NDE is on the threshold of another renaissance, that of quantitative measurement science combined with materials science. Metamorphosis is normal in most technologies, but has been accelerated in NDE by the advent of fast computers, robotics, digitizers, and of most importance, scientific analysis.

As we moved from isotropic, homogeneous planer structures, to anisotropic, inhomogeneous, layered structures, NDE found new challenges that required re-analysis. For example, are the same instruments developed for simple metals appropriate for composites? A more important question raised focuses on the fundamental process of NDE: are we only looking for flaws?

For many cases, the answer is still yes. Of importance to the aircraft industry, however, NDE is growing up to the challenge of assessing the condition of materials providing information critical to evaluating structural performance. To that end, NDE is becoming a quantitative science, based on physical measurements of real material properties. In this paper, we discuss the use of physical models for NDE analysis with broad applications for aircraft materials characterization based on thermography and ultrasonics.

Thermal NDE, for example, has been practiced for many years with great success, yet has not achieved its full potential. The early use of thermal NDE involved detecting "defects" by viewing an IR image generated after application of heat to the sample. For the defects to be detected for this case, the subsurface heat flow needs to be impeded by the defect in such a way to give a surface temperature contrast of at least $.3^{\circ}\text{C}$.

Currently high speed digital systems are in use for real time enhancements such as averaging of the IR digital images. When properly used, these tend to increase the probability of defect detection and lower the minimal amount of contrast required. Often, however, such measurements enhance other artifacts such as uneven heating and emissivity variations which hide the presence of defects or can be confused as defects. Therefore, to optimize the use of these new systems, physical models of heat diffusion are required for interpretation of these IR images and their time evolution.

Such physical models have been developed for NDE which describe the interaction of thermal, ultrasonic, and magnetic energy with structures to permit inversion of the data to give quantitative structural information. By using analysis based on physical models it has been possible to optimize the NDE measurements and determine how to best reduce the data to maximize specificity, resolution and contrast.

Examples will be presented of recent applications of quantitative thermal and ultrasonic NDE for diverse applications including layered thermal control structures, composite materials, and aircraft skin disbands.

PHYSICAL MODELS

In the past, the most common approach to using NDE has been to "try it out". For example, to determine if ultrasonics can detect a certain condition such as an unbond, one would place a transducer on the object in question, connect the transducer to a commercial

ultrasonic device, and look at the display to see if the condition expressed itself. The results were subjective, and did not necessarily exercise all the capabilities of ultrasonics.

Today, if simple approaches are unsuccessful, one may model the part being tested and examine the interaction of the probing energy with the part to more fully explore possible NDE methodologies. This is parallel to the philosophy of using modeling to design new structures; where it is cost effective to use models to explore the efficiency of different designs before proceeding with construction of the structure. In NDE, it is proving true that modeling not only saves money by focusing the NDE technology to the task at hand, but it also improves the resolution and quantitative analysis capability.

For example, in one class of tests, thermal NDE was initially ruled out because it could not detect a specific built-in flaw. This decision was based on many hours of measurement which proved unsuccessful in detecting a fabricated disbond in a layered structure. The scientists involved felt that it would be appropriate to develop a model of the disbanded part, and use the model as a test-bed for assessing the technology. After careful construction of a thermal model, a different computational method for reducing the same thermal data was easily able to characterize the defective condition.

The success of many such tests have established a methodology for NDE that enhances the technology and its effective application to well defined problems.

THERMAL NDE

There are two major classes of radiometric thermal NDE, passive and active. In passive thermal NDE, some condition of the examined part is at a different temperature because of its geometry, heat capacity or thermal environment. For example, a thinned part will equilibrate to its environment faster than a thick part thus differentiating it from its surroundings. Therefore, if the object is processed through an oven such as might be done for some painted parts, a passive thermal NDE test would involve a measurement of the change in temperature as the part enters/emerges from the oven.

In active thermal NDE, a prescribed amount of energy is injected into the part causing a change in temperature with respect to time. The dynamic thermal state of heating up as well as cooling down can be monitored.

ULTRASONICS NDE

Ultrasonics as a field has developed along two lines, NDE and physics. In NDE, most applications are related to geometry effects such as finding cracks, delaminations, and thicknesses. In physics, however, the use of ultrasonics is very broad including applications such as electron-phonon interactions, spin interactions with nuclei, and nonlinear absorption. Recently, many labs are bridging the two fields introducing a new era for NDE.

As a result of such work, problems that were intractable for NDE are now possible. For example, the development of theory and models of acoustic propagation in stressed materials has resulted in a major advance [1] in understanding the nonlinearity of materials. Practical applications of this work have resulted in the ability to measure the stress profile of a loaded member, the stress in critical fasteners, and residual stress in the bulk of some materials.

CRITICAL FASTENER PRELOADING

The conventional approach of tightening bolts using torque to control preload has proven to be unacceptable when bolt accuracy of better than about 20% is required. In such critical bolting situations, numerous solutions have been offered such as instrumenting bolts with strain gauges, and measuring bolt elongation using micrometers. These approaches can give acceptable accuracy but are cumbersome.

In recent years, ultrasonics has solved some of these and other stress problems with success. One such approach, developed at NASA Langley Research Center in 1980 [2,3,4,5], is an ultrasonic phase measurement technique. Other ultrasonic techniques such as time of flight are in use but are not addressed herein.

To measure the change in length that accompanies tensioning in a fastener, ultrasonic waves are caused to propagate along the axis of the bolt and to reflect off the end. The phase measurement technique when locked, forces the ultrasonic phase to be constant by changing the instrument's output frequency. Therefore, as the bolt is tightened, an exact frequency shift proportional to the change in bolt load results. This frequency change is due to load-induced changes in acoustic pathlength and sound velocity.

In practical use, the bolt monitor must be calibrated on the tested bolt or on a material with the same properties. Figure 1 shows a typical calibration system in which the bolt is placed in a load cell. The ultrasonic transducer is bonded to the bolt and the ultrasonic

as well as the load cell data are read by a computer as the bolt is tightened. In figure 2, the slope of the load vs. normalized frequency shift curve is determined and is used as the calibration factor. Bolt load is then determined in the actual field joint by measuring the frequency shift and applying the calibration factor.

Figure 3 illustrates the ability of ultrasonic bolt monitor systems to measure load independently of friction. A right wheel bolt was tightened in a load cell using several different lubricants, each resulting in a different coefficient of friction. Torque and ultrasonic data were recorded while tensioning the bolt. The effect of frictional variations is clearly shown on preload for torque and ultrasonic tension monitoring systems.

Ultrasonic techniques provide an excellent means to achieve accurate bolt preload and the reliability of ultrasonic systems has been demonstrated through numerous critical applications. The success of these systems demonstrates the evolution of NDE from qualitative to quantitative information. The full utility of this technology is built on the development of instrumentation as well as theoretical models of the propagation of acoustics in stressed material.

LAYERED BONDED STRUCTURES

A conventional application of ultrasonics to NDE involves the use of broadband pulse-echo excitation to insonify the tested material. Normal analysis of the returning signals consists of establishing a time gate to include the sample region of interest and a signal threshold level established from test parts containing characteristic defects. Such tests were made on samples simulating bonded layered complex material geometries such as are typical in aerospace applications [6]. Defects such as disbands between materials were easily found for first layer flaws. However, it was not possible to detect deep internal disbands between layers of absorbing materials cased in metal. Multiple ringing of the ultrasonic pulse in the low-loss metal case obscures energy coming from disbands buried behind more absorbing materials.

An ultrasonic computational model of the complex structure was developed to evaluate the performance of unconventional approaches required by the complexity of the material. The model insonified the structure with a long tone burst plane wave normal to the metal surface. A transmission line impedance was calculated including the effects of each reflecting interface in the structure. The resulting reflected wave consists of the superposition of all reflected waves and was examined as a function of frequency.

Figure 4 shows the calculated spectral response of the layered sample viewed from the metal side as a function of frequency. The two curves represent a numerical evaluation of a good bond and an unbond, between an internal surface of the layered geometry. The figure shows small differences between the two bond conditions with the average difference decreasing with frequency. The decrease is caused by the high attenuation of the absorbing internal material preventing ultrasonic energy from penetrating into the deeper structures. The difference between the two curves depends strongly on frequency, with maximum contrast (difference between the bond and unbond condition) occurring at resonance peaks.

The difficulty in examining the deeper bondline with pulse-echo is now clear. Pulse-echo uses a narrow pulse which comprises many frequencies. Only those frequencies which lie in the narrow range of a mechanical resonance contribute to the measurement of the disbond. The other frequencies represent background noise through which the weaker bondline signals must be discriminated.

The results of the numerical calculations point to the benefit of using a narrow band of ultrasonic frequencies near the composite resonance of the structure involved. To verify the model, a sample was built consisting of a flat metal plate with multiple layers of absorbing materials simulating the needed test geometry.

A block diagram of the experimental test is shown in fig. 5 with a spectrum analyzer used to measure the response of the sample [7]. The output from a tracking generator in the spectrum analyzer is gated and amplified to drive the insonifying transducer coupled to the sample through a water delay line. The spectral response of a reflected wave time gated into the spectrum analyzer is shown in fig. 6, in excellent agreement with the calculated response of fig. 4.

A realistic layered sample was fabricated by the industrial manufacturer of the part using the same materials, processes and thickness as are used in production. The sample was 30.5 cm. (12 in.) square with a brass wedge shaped shim cured into the sample at the bond interface layer in question. The wedge extended from the sample and was pulled after curing to create a disbond in the desired location. The shape of the sample is shown in fig. 7.

An image of the sample is shown in fig. 8 obtained using the spectrum analyzer system to scan the sample with a coarse step size of 0.2 cm. over the image area of 8 x 12 cm. A similar scan was made using a conventional pulse-echo system gating the signal for the inner bond interface using peak detection and various threshold levels. The conventional scan could not resolve the disbond above background variations in the signal. The image obtained with the tone burst system clearly resolved the wedge delamination

shown in fig. 7. The improved ultrasonic signal to noise was made possible by using information obtained from the physical model calculations. Such tests are providing the basis of practical solutions to NDE problems in complex bonded joints.

Although ultrasonics is a logical approach to examining bonded structures, different, complimentary techniques add significant reliability factors to the inspection. In particular, thermal NDE also provides significant cost benefits for large area rapid scanning. Traditional thermal NDE consists of surface heating while measuring the temperature radiometrically with an IR camera. A near surface disbond would appear as a transient hot spot.

LaRC has developed OPTITHERMS (OPTical THERmal Infrared Measurement System) [8], a thermal NDE system composed of a scanned modulated laser, an IR camera, an image frame grabber, and most important, a thermal model. Similar to ultrasonics, the model is used to interpret the data and to point the way to improved signal-to-noise measurements.

The thermal dynamics are simulated using a computational diffusion (thermal impedance) model [9]. The different layers of the sample are represented by proper model elements with values determined to map the thermal diffusion physics into the equivalent model analogues.

The results of the analysis show that the best signal-to-noise one can achieve is equal to the highest contrast, defined as the maximum difference in temperature, for the sample with and without a flaw. A more complex analysis of the thermal system involves the determination of equivalent thermal sources and sinks that effect the flow of thermal energy. An example of the power of this approach is shown in fig. 9a where the image shows one time increment of the temperature of the surface of the layered sample of fig. 7. Note that the main visible feature in this figure is the effect of uneven heating of the surface of the sample. The wedge delamination is hidden.

Figure 9b, on the other hand, was obtained from analysis results of the model using the same data base as fig. 9a. to extract thermal sources. The wedge shaped delamination clearly stands out from the background. By imaging and processing data using the physical model as a driver, we are able to differentiate delaminations from other processes in the sample thus improving our ability to interpret the image.

CURE MONITORING AND NDE OF COMPOSITES

An important problem facing practical use of composite materials for aerospace is cost. Costs are driven by the raw material, labor intensive fabrication, and by poor yield. The use of QNDE can reduce costs by permitting automation of processes based on reliable sensors and by increasing yields through process control feedback in autoclaves for curing composites.

The autoclave process for curing composites first raises the temperature of the uncured part causing a decrease in the matrix resin viscosity. Any excess resin is removed by bleeder cloths surrounding the part. Further into the cure cycle, the viscosity begins to increase as the molecular length of the polymer chains increases. At this point, the pressure is increased in the autoclave to insure compaction of the composite, to eliminate gas volatiles and reduce the size of any porosity. As the process continues, the viscosity further increases until the polymerization is complete.

Usually, monitoring is accomplished by measuring the autoclave temperature and pressure by placing sensors on the part itself. Such monitoring procedures only measure the environment in which the part sits. It is more quantitative to measure properties of importance, in the part itself, such as viscosity or degree of cure. There are physical relationships between the degree of cure and ultrasonic parameters of the resin. These are possible inputs for feedback control of autoclaves improving the reliability, yield, and cost effectiveness of composites.

The longitudinal velocity is related to the degree of cure using the principle of additive moduli, which relates the bulk moduli of an organic liquid to a sum of contributions from its constitutive molecular groups. The concept was first found for liquids by Rao[10], then expanded on by Van Krevelin[11] and has been shown to be applicable for solids[12]. The analytical expression for relating the moduli (K) to the contributions of different molecular groups is given by the expression:

$$K(t) = \rho (\sum C_i(t) R_i / (\sum C_i(t) V_i))^6 \quad (1)$$

where C_i are the concentrations, R_i is the Rao function and V_i is the molecular volume for each molecular group and the sum is over all molecular groups. From this expression, the velocity as a function of degree of cure can be shown to be[13]:

$$V(t) = [(\sum S_2 + \alpha(t) \sum S_3)^6 (1 + 4/3 A) - 4/3 A \sum S_2^6]^{1/2} \quad (2),$$

where $\sum S_2$ and $\sum S_3$ are sums of Rao functions, A is an experimentally determined constant, and $\alpha(t)$ is the degree of cure.

An experimental approach was developed to verify the theoretical ultrasonic model of a curing composite. The experimental configuration consisted of a parallel plate curing cell with a 20 Mhz transducer bonded to one of the outside faces. An oven surrounds the cell to control the temperature of the resin during the cure reaction. Resin and curing agents are mixed, introduced into the cell, and raw data is obtained from digitized pulse-echo ultrasonic signals.

The data is processed to improve the signal-to-noise and to remove the effects of the transducer/cell from the measurements of the propagation in the resin. The signal processing is based on a physical model of the test cell, which adjusts the acoustic propagation parameters of the model to determine a best estimate of the velocity, the attenuation, and the frequency dependence of the attenuation. Based on a criteria of least squares error, the processing uses all the data rather than just the leading edges or peak amplitudes, as is usually done in simple time-of-flight measurements. This approach significantly improves the resolution and accuracy of the data. Velocity as a function of cure time found for a typical run and the degree of cure as calculated by equation (2) is shown in figure 10.

The development of quantitative physical models was essential to the successful application of ultrasonics to monitoring autoclave curing of composites. The models not only identified what parameters needed to be measured, but also resulted in process insight such as the ability to determine reaction rates, their temperature functionality, and activation energies for cure of aliphatic and aromatic amines/epoxy systems.

NDE of composites after fabrication is a complex and often misunderstood process. Simple delamination detection is typically the only test performed leaving many questions unanswered. For example, the assessment of fiber condition is a critical parameter to insuring performance of the composite. One technique of examination is based on quantitative thermal diffusion measurements. An example of this approach is shown in fig. 11. This figure represents a vector diffusivity map as a function of fiber angle in the part. From this information, one can determine the uniformity of fiber direction and fiber condition.

Analysis based on these measurements has been used to detect broken fibers. For example, fig. 12 shows a thermal diffusivity scan across a composite material containing fibers that were damaged prior to matrix curing. The change in diffusivity accompanying the fiber damage is clearly visible.

NDE OF AIRCRAFT SKINS

The recent emphasis on NDE for mature aircraft has highlighted the need for detection and analysis of degraded conditions of bonded lap-joints. Both ultrasonics and thermal technologies have been applied to characterizing that geometry. In particular, thermal NDE has the attributes of being non-contact, remote, and able to image large areas. Bonded lap-joints were obtained to evaluate the direct application of thermal measurement techniques to the aircraft configurations.

The samples were constructed for NDE evaluation and contained built-in disbonds between the skin and the hidden stiffeners. A simple heating protocol was used to provide a necessary heating pulse calculated to inject energy per unit time required to detect the condition of the bonded interface. This was achieved with quartz lamps driven by a computer determined heating profile.

The temperature of the surface of the sample was measured radiometrically with an infrared camera video frame grabbed directly to an image processor also under computer control. Signal averaging, processing, and analysis were done, for the most part on line, providing direct imaging feedback to the user.

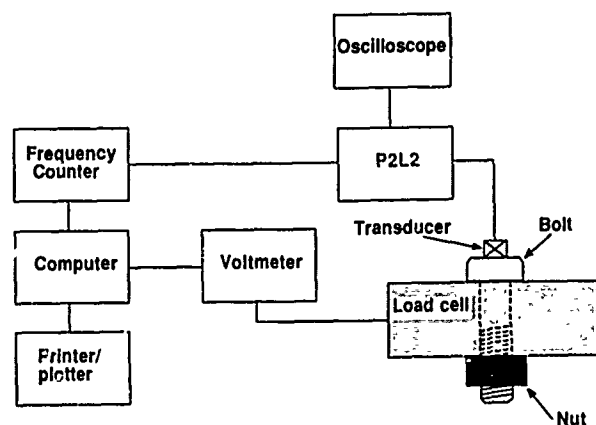
Fig. 13a shows the processed thermal image of the skin over the bonded section. The stiffeners clearly show up as thermal sinks and are uniformly bonded as determined from the diffusivity uniformity of the data. In contrast, Fig. 13b shows the region of the panel with the disbonded stiffener. The thermal image differentiates the degraded condition from the background. At present, an optimum inversion process of the thermal data is underway for generic application to these bonded geometries. The inversion process is based on such parameters as the physical models of the geometry, the materials involved, the material properties and their anticipated variations. Such advanced signal processing insures that spurious effects such as variations in heating, thermal absorption, and emissivity can be minimized so as to produce images that can be quantitatively interpreted.

CONCLUDING REMARKS

The technology and science of NDE is in a rapid state of flux. The traditional roles played by NDE people are expanding to include capabilities of providing quantitative information for analysis. The development of physical models, theories, and computational techniques to simulate NDE are the backbone of these advances. The applications shown are broad and include recent successes in NDE of bolt stress, space propulsion, composites, and aircraft.

REFERENCES

- 1.) Cantrell, J.H., Jr, "Anharmonic Properties of Solids from Measurements of the Stress Acoustic Constant," *Journal of Testing and Evaluation*, Vol. 10, No. 5, Sept. 1982, pp. 223-229.
- 2.) Heyman, J. S., "Pulsed Phase Locked Loop Strain Monitor", *United States Patent 4,363,242*, Dec. 14, 1982.
- 3.) Heyman, J. S. and Chern, E. J. "Ultrasonic Measurement of Axial Stress", *Journal of Testing and Evaluation*. Vol. 10, No. 5, Sept. 1982, pp. 202-211.
- 4.) Allison, S. G. and Heyman, J. S., "Nondestructive Ultrasonic Measurement of Bolt Preload Using the Pulsed Phase Locked Loop Interferometer", *The Second Symposium on Welding, Bonding and Fastening*. NASA Langley Research Center, Hampton, Va., October 23-25, 1984.
- 5.) Heyman, J. S. and Issler, W. "Ultrasonic Mapping of Internal Stresses", *1982 IEEE Ultrasonic Symposium Proceedings*. Oct. 27-29, 1982. 6.) Madaras, Eric I., Winfree, William P., Smith, B. T. and Heyman, Joseph S., "Detection of Bondline Delaminations in Multilayer Structures with Lossy Components," *1987 IEEE Ultrasonics Symposium Proceedings*, 87CH2492-7, pp. 1047-1052 (1987).
- 7.) Cantrell, John H.; Heyman, Joseph S.: "Ultrasonic Spectrum Analysis Using Frequency-Tracked Gated RF Pulses," *Acoust. Soc. Am.* 67, 1623-1628 (1980).
- 8.) Heath, D. M., Welch, C. S., Winfree, W. P., Heyman, J. S. and Miller, W. E., "Quantitative Thermal Diffusivity Measurements of Composites," *Review of Progress in Quantitative Nondestructive Evaluation*, Vol 5B, D. O. Thompson and Dale E. Chimenti, eds, pp 1125-1132 (1986).
- 9.) Welch, C. S. "Contrast Enhancement Through Source Impedance Control In Thermal NDE", *Review of Progress in Quantitative Nondestructive Evaluation*, Vol 7A, D. O. Thompson and Dale E. Chimenti, eds, pp. 279-285, (1987).
- 10.) R. Rao, *J. Chem. Phys.* 9, 682 (1941).
- 11.) D. W. Van Krevelen, *Properties of Polymers, Correlations with Chemical Structure*, (Elsevier, Amsterdam, 1972).
- 12.) B. Hartman and G. F Lee, *J. Appl. Phys.* 51, 5140 (1980).
- 13.) W. P. Winfree, F.R. Parker, *Review Of Progress In Quantitative Nondestructive Evaluation*, 5B, ed D. O. Thompson and D. E. Chimenti, 105b, (Plenum, New York, 1986).



Calibration measurement system

Figure 1 Calibration measurement system block diagram.

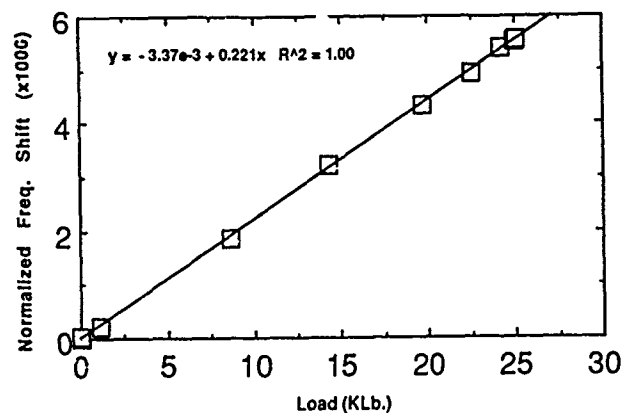


Figure 2 Flight bolt ultrasonic calibration data.

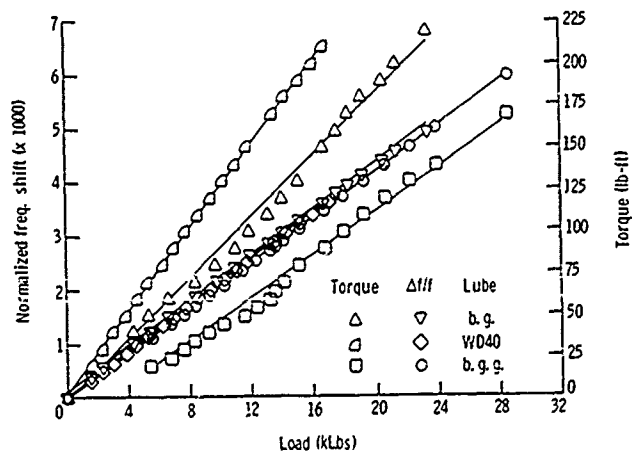


Figure 3 Friction variations on ultrasonic and torque-load relationships.

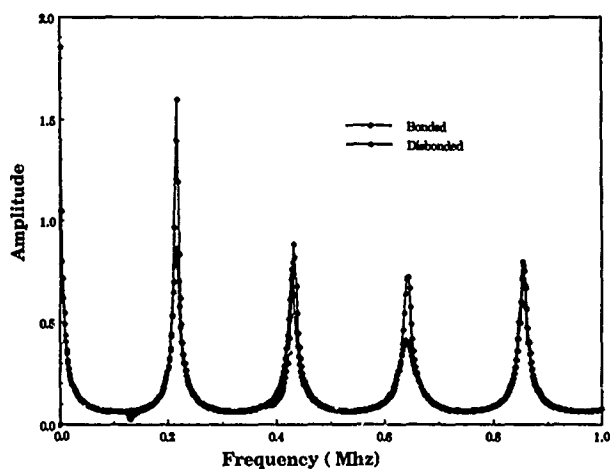


Figure 4. Calculated spectral response of the layered geometry for two conditions representing good bond and lack of internal bond.

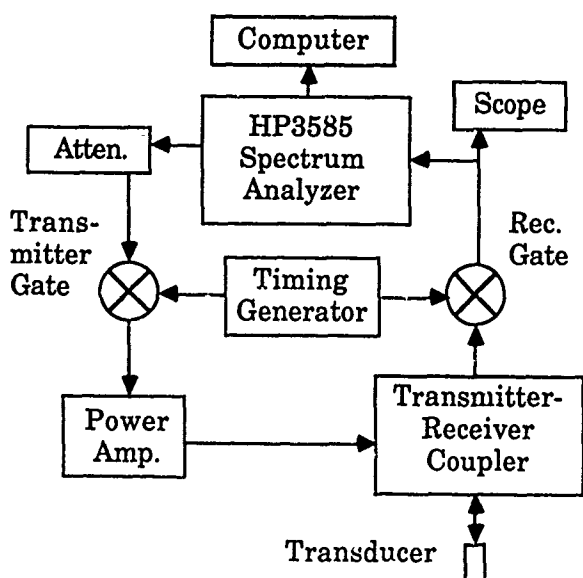


Figure 5. Block diagram of the ultrasonic experimental test set-up.

Solid Rocket Motor's Frequency Response

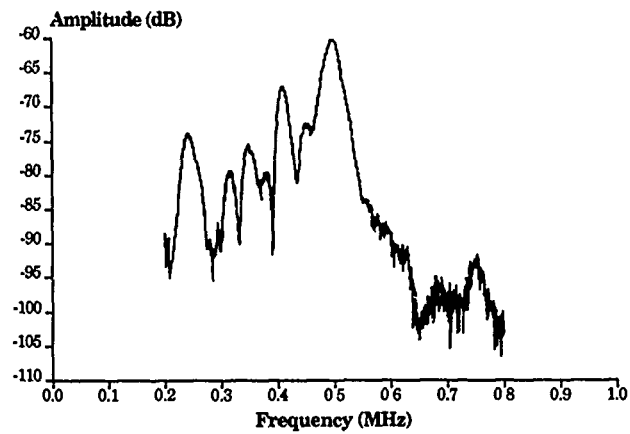


Figure 6. Spectral response of the layered metal sample showing the computation model resonance peaks. Detection of internal disbands is optimized using ultrasonic frequencies corresponding to the high contrast predicted by the computational model in fig. 4.

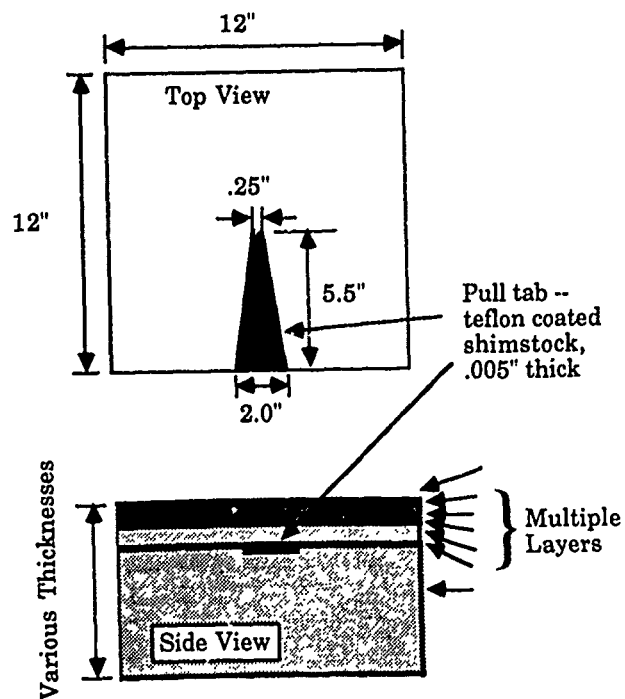


Figure 7. Layered samples with built-in disbands to simulate possible manufacturing defects. Disbands were placed in various bondlines to evaluate their detection.

MORTON THIOKOL SAMPLE 6
AMPLITUDE MEASUREMENT AT 250 KHZ

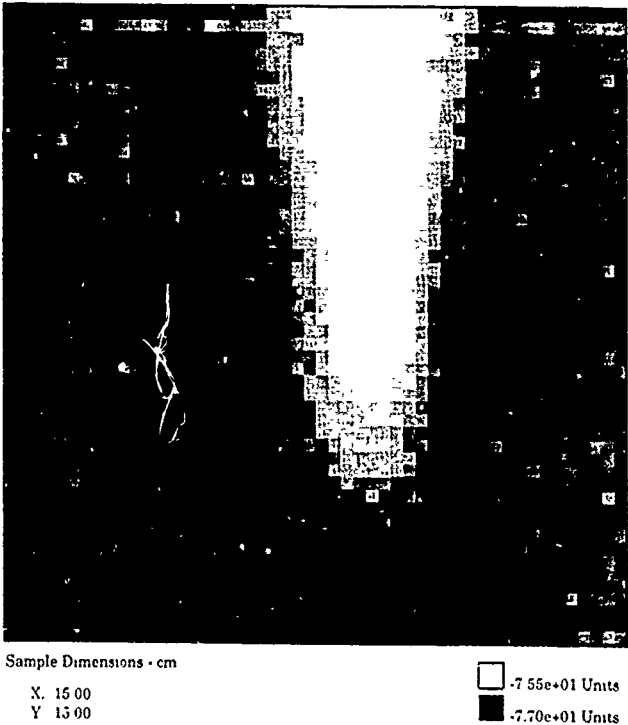


Figure 8. Grey scale ultrasonic image of reflection amplitude at the resonance frequency of the layered sample. Image clearly shows the wedge disbond in the internal bonded layer.

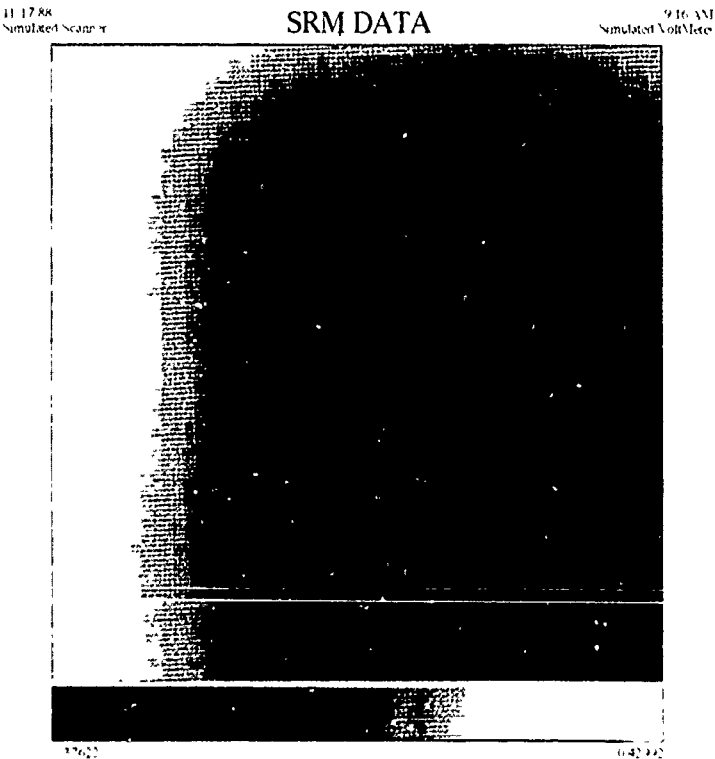


Figure 9a. Surface temperature profile of the layered sample after uniform surface heating followed by a cooling time period.

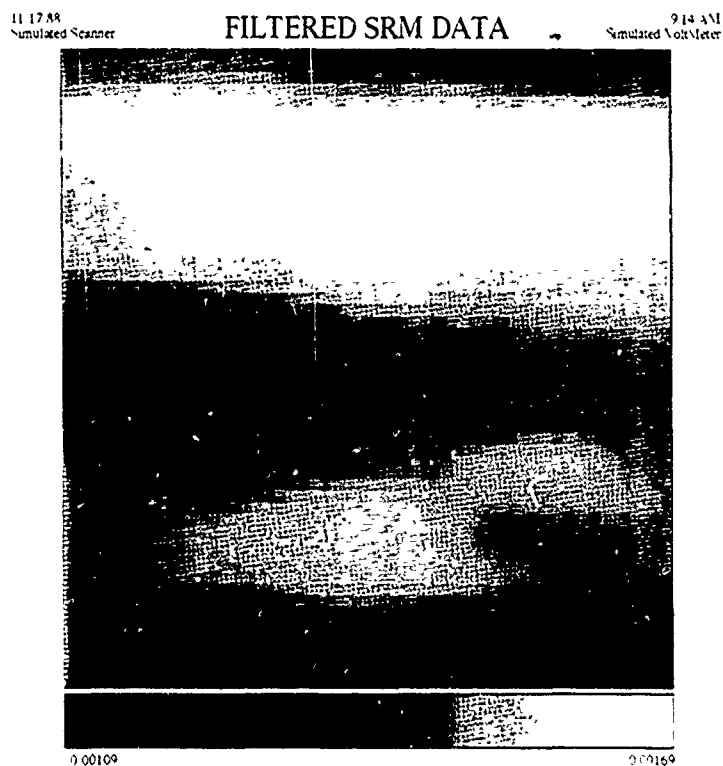


Figure 9b. Thermal NDE image showing the wedge disbond. The image is derived from an inversion of the data combined with the physical model of the sample geometry.

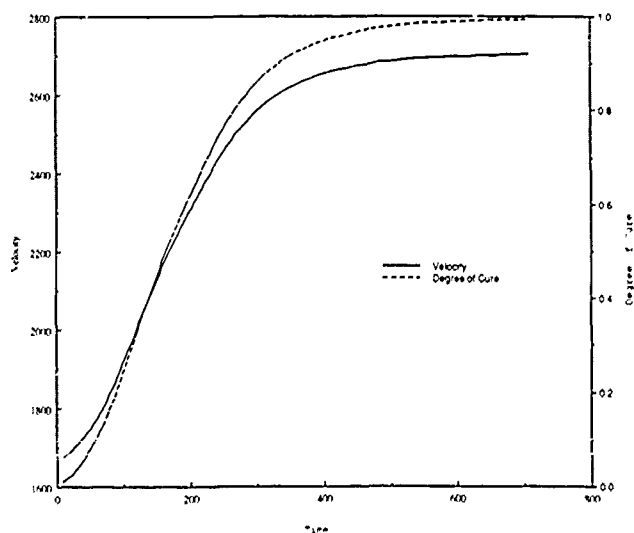


Figure 10. Longitudinal velocity measured during cure of a two part resin system with the degree of cure calculated from the velocity using equation (2).

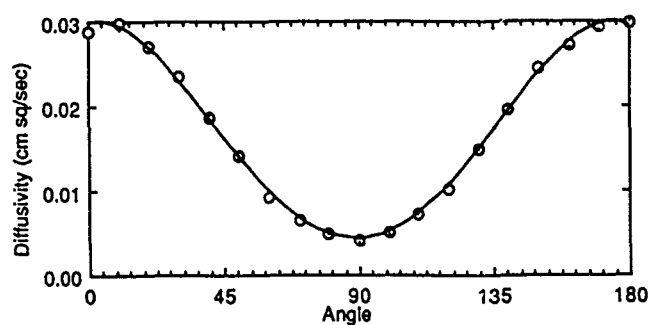


Figure 11. Vector thermal diffusivity for a unidirectional fiber composite as a function of angle.

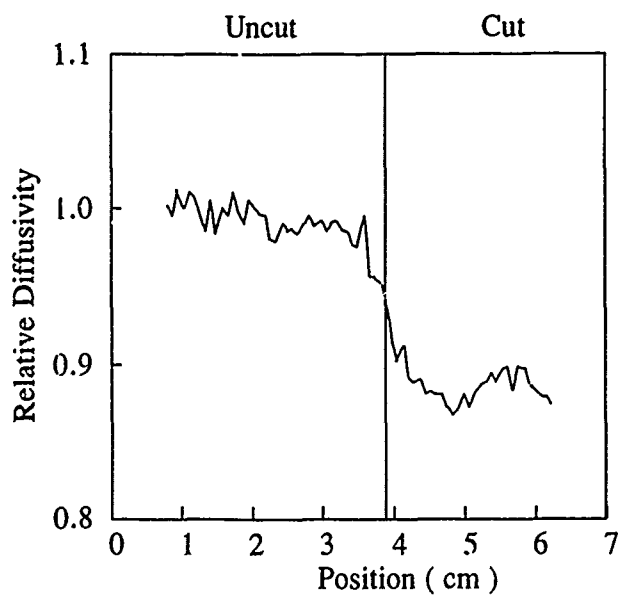


Figure 12. Quantitative thermal diffusivity measured across a composite containing broken fiber damage.

11589

SAMPLE WITH NO DISBOND

147PM

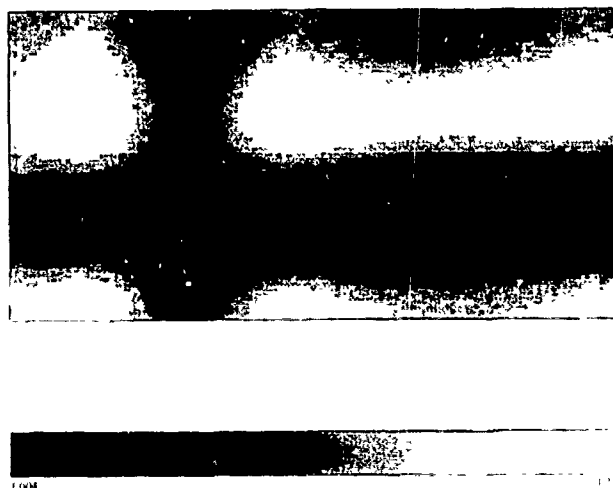


Figure 13a. Thermal NDE image of an aircraft skin showing a good skin stiffener bond.

11589

SAMPLE WITH DISBOND

147PM

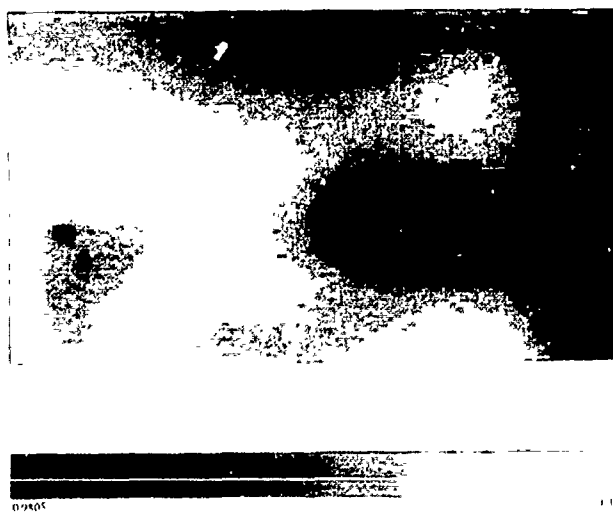


Figure 13b. Thermal NDE image of an aircraft skin showing a skin stiffener disbond.

ACOUSTIC EMISSION FROM A GROWING CRACK

L.J. Jacobs*, W.R. Scott, D.M. Granata, and M.J. Ryan

Naval Air Development Center
Advanced Metallic and Ceramic Materials Branch
Warminster, PA 18974
USA

* Engineering Science and Mechanics Program
Georgia Institute of Technology
Atlanta, GA 30332
USA

SUMMARY

A dynamic crack growth event is modeled using an integral equation method to develop an analytical expression for an acoustic emission waveform at any point in front of a crack propagation source. An experimental procedure is under development for investigating the important characteristics using a simple precracked compact tension specimen. A laser interferometric apparatus is used to measure displacements and velocities normal to the specimen surface. Crack propagation gages are used to determine the crack velocity. These experimental results are then used to verify the analytical model.

INTRODUCTION

Separation of crack growth signals is of fundamental importance for detecting, locating, and determining the significance of an internal flaw. The difficulty associated with modeling acoustic emission is not only in providing an accurate representation of the source mechanism, but also in determining the effect of the specimen geometry and the sensor on the acoustic emission signal.

An influence function is used to develop an integral equation to model the near tip dynamic stress due to a prescribed crack growth event. The propagation of the crack greatly influences the stress field in the vicinity of the crack tip, causing stress waves to radiate into the body and on the crack surface; it is the displacement caused by these stress waves that is being modeled. Acoustic emission testing detects stress waves at the body's surface and relates these back to crack propagation events. An advantage of the analysis presented is that the source for the acoustic emission signature is an actual crack propagation event and not a simple point source model.

The velocity of the moving crack tip and the time dependent displacement due to the crack growth event are measured using a crack propagation gage and an interferometric displacement/velocity sensor respectively. The displacements being measured are acoustic emissions from the dynamic crack growth. These displacements are the benchmark comparison to the analytical model. The velocity measurements are input parameters for the analytical model.

In the next section, the analytical method is developed and discussed. Then the experimental procedure is explained, and these results are compared with the analytical model in the last section.

ANALYTICAL METHOD

First, the dynamic Mode I stress caused by a semi-infinite crack propagating with a prescribed velocity is determined, and then the displacements at any point are calculated. The method for determination of the stresses, summarized in [1], uses an influence function (or Green's function) method to formulate an integral equation in two variables, a spatial coordinate (x) and time (t). The influence function $U_{yy}(x-x', t-t')$, obtained in closed form using the Cagniard-de Hoop method, is the vertical displacement of an elastic half-space subjected to a unit concentrated impulse acting at a point normal to its edge.

Assume that a crack exists at time $t=0$ with its tip located at $x=a(0)$ and $y=0$. For time $t>0$, the crack tip moves from $x=a(0)$ to $x=a(t)$. The two relevant boundary conditions are that the newly formed crack faces are stress free and that the vertical displacement in front of the moving crack tip is zero. These boundary conditions are satisfied by:

- Removing the existing known static stress, $\sigma_{yy} = P(x)$, and assuring that a new unknown time-dependent stress, $\sigma_{yy} = F(x, t)$, develops.
- Requiring that this new stress distribution be developed such that there is vertical displacement continuity in front of the moving crack tip.

The continuity boundary condition can now be expressed in terms of the influence function, $U_{yy}(x-x', t-t')$ as:

$$\begin{aligned}
& - \int_0^t \int_{-\infty}^{\infty} P(x') U_{yy}(x-x', t-t') dx' dt' \\
& + \int_0^t \int_{-\infty}^{\infty} F(x', t') U_{yy}(x-x', t-t') dx' dt' = 0
\end{aligned} \quad (1)$$

The above expression is a Volterra integral equation of the first kind in the variables x and t . To provide a simple solution of this integral equation, assume some spatial form of the unknown stress distribution, $F(x', t')$, that contains a square root singularity at its tip location, $a(t')$. This unknown stress in front of the moving crack tip is assumed to have the spatial form of a static crack with its tip located at $a(t')$, multiplied by some unknown time function, $K(t')$:

$$F(x', t') = K(t') / \sqrt{2\pi} \sqrt{x' - a(t')} \quad (2)$$

It should be noted that the assumed spatial stress distribution exists instantaneously for all values of $x' > a(t')$ for any time, t' .

For the steady state case of a crack propagating with a constant velocity, the calculated value of $K(t')$ is a constant that is only a function of the crack tip velocity. As the crack tip speed increases, the corresponding constant value of $K(t')$ decreases. The results for the case of a crack that suddenly stops after propagating is that the calculated value of $K(t')$ discontinuously jumps to the value of the corresponding static stress; there is no transition zone and the stress never increases above the value of an equivalent static crack. The dynamic stress results computed here compare well with those calculated using the Wiener-Hopf Technique (Freund [2] and Rose [3]).

The displacement at any point in the infinite body is determined using the above dynamic stress, $F(x', t')$, and the influence functions, $U_{xy}(x-x', y, t-t')$ and $U_{yy}(x-x', y, t-t')$. These influence functions represent the displacement u_x and u_y at any point (x, y) in an elastic half-space. The solution for these influence functions is again accomplished using integral transform techniques. Using the previously calculated dynamic stress distribution, convolution integrals can be written to calculate the vertical and horizontal displacement as a function of time for any point (x, y) within the body. For numerical simplicity, the displacement is determined at a point, x , in the plane of the crack ($y=0$). At any point on this plane, the displacements are given by:

$$u_y(x, t) = 0 \quad (\text{because of symmetry}) \quad (3)$$

$$\begin{aligned}
u_x(x, t) = & - \int_0^t \int_{-\infty}^{\infty} P(x') U_{xy}(x-x', y=0, t-t') dx' dt' \\
& + \int_0^t \int_{-\infty}^{\infty} F(x', t') U_{yy}(x-x', y=0, t-t') dx' dt'
\end{aligned} \quad (4)$$

The proposed solution procedure is illustrated for the case of a crack tip that instantaneously reaches a constant velocity, c_A , propagates for a length of time, t_A , and instantaneously stops. Figure 1 illustrates the time dependent displacement at a point, x , caused by a crack that propagates at a velocity of approximately 20% of the Rayleigh wave velocity (c_R) for a short time duration. The effect of the arrival of the longitudinal wave fronts from the starting and stopping phases of the crack propagation (t_{start} and t_{stop}) is clearly seen. After the arrival of the transverse wave from the stopping event (t_{stop}), the displacement reaches a quasi-static value larger than the original static value. The small non-zero displacement prior to the arrival time of the fastest wave from the initial crack tip (t_{start}) is due to the assumed spatial stress distribution of Eqn. (2). This assumption implies the physically unrealistic case that an instantaneous stress exists in front of the moving crack tip. The stress distribution assumed in Eqn. (2) contains a square root singularity at the moving crack tip which dominates the dynamic stress field while the stress values away from the moving crack tip are negligible in comparison. Except for this discrepancy in arrival times, the assumed stress distribution accurately models the actual dynamic stresses. Figure 2 shows the change in displacement due to variations in crack velocity while Figure 3 illustrates the effect of the duration of crack propagation. The results indicate that the maximum displacement increases for increasing values of constant velocity or duration of propagation and that the displacement gradients increase for increasing values of constant velocity.

EXPERIMENTAL PROCEDURE

The experimental procedure examined the incremental propagation of an existing crack in a modified compact tension specimen. Polymethyl methacrylate (PMMA) material was used to fabricate one-half inch thick specimens that have varying length and width dimensions. The material's low fracture toughness and nearly brittle failure mode allowed cracks to be easily propagated. Optical transparency permitted the size, geometry and location of cracks to be readily determined. The crack propagation gages were located at the initial crack tip to measure crack tip velocities. A high sensitivity heterodyne interferometer was used to detect acoustic events resulting from crack growth in the specimen. A schematic of the instrumentation is shown in Figure 4. The device used in these studies permits high fidelity localized measurement of displacements resulting from acoustic emission events arriving at various locations on the

sample surface. Since this type of measurement does not acoustically load the sample, the event being observed is undisturbed by the measurement process.

The polished face of the specimen, opposite the crack, serves as one mirror of the interferometer. The beam striking this face is approximately 1.5 mm in diameter and samples the average displacement over this region, which is much smaller than the wavelength of the acoustic events being observed. The sample is designed so that initial acoustic emission events leaving the crack tip will arrive at this face prior to reflection from other faces of the specimen.

It should be noted that the analytical procedure being developed describes events prior to the arrival of stress waves reflected from the test specimen's boundary and is invalid for the time period after the fastest reflected waves interfere with the direct signal from the crack propagation event.

The operation of the heterodyne interferometer is similar to that described elsewhere [4]. Briefly, single frequency laser light is split into two components using an acousto-optic modulator. These two components, which are separated in frequency by 40 MHz, are sent along two arms of an interferometer one of which contains the sample to be monitored. The beams are recombined on the surface of a photodetector producing a beat frequency of 40 MHz. Phase shifts in the light reflected from the sample surface result in proportional phase shifts in the beat signal. As a result the 40MHz signal acts as a carrier that can be demodulated to determine the time dependent displacement occurring at the sample surface. The signal from the photodetector was demodulated in real time using an FM discriminator with a bandwidth of 10MHz. The demodulated output signal is proportional to the normal surface velocity of the specimen and can be integrated to determine its time dependent displacement.

The initial crack velocity is determined by measuring the change in resistance of the crack gage as a function of time. Both the acoustic emission waveform and the crack velocity profile are acquired on a pretriggered dual channel, digital oscilloscope. The time difference between the start of the crack growth event and the arrival of its signal at the observation point is easily determined with the pretriggering feature of the scope.

DISCUSSION AND CONCLUSIONS

A characteristic crack emission is shown in Figure 5. Here, a delay of 11.4 μ sec exists between the start of the gage and acoustic emission signal, which compares well with a calculated time lag of 11.2 sec. The first reflected wave from the specimen boundary is calculated to arrive 10.4 μ sec after the arrival of the initial signal. By using an estimated velocity profile for the final stage of growth, the last transverse wave should arrive approximately 70 μ sec after the arrival of the starting event. The velocity profile, curve fitted from the crack propagation gage data, is shown in Figure 6, while the integrated acoustic emission signal is shown in Figure 7. This integrated signal represents the measured displacement at the observation point, x, due to the actual crack propagation event. This displacement curve is needed to verify the analytical results being developed. In the early time period, Figures 1 and 7 show fairly good qualitative agreement between the analytically predicted and experimentally measured displacements. The two curves begin to deviate from each other at later times as the finite specimen geometry dominates the experimentally obtained signal.

Anomalies in the fracture behavior of the specimen included out of plane growth and crack tunneling. Tunneling was caused by the stress gradient through the specimen thickness. In some cases crack growth as initiated on the surface opposite the propagation gage and there was a reduced time lag between the start of propagation and the arrival of its signal. More experimental development is necessary to reduce the influence of the specimen geometry on the measured acoustic emission waveforms. The analytical model must also be refined to diminish the effect of the assumed spatial stress distribution.

REFERENCES

1. L.J. Jacobs and M.P. Bieniek, "An Integral Equation Method for Dynamic Crack Growth Problems," International Journal of Fracture, in press.
2. L.B. Freund, "Crack Propagation in an Elastic Solid Subjected to General Loading," Journal of the Mechanics and Physics of Solids, Vol. 20 pp. 129-152, 1972.
3. L.R.F. Rose, "The Stress-Wave Radiation from Growing Cracks," International Journal of Fracture, Vol. 17 pp. 45-60, 1981.
4. L.J. Jacobs, W.R. Scott, D.M. Granata and M.J. Ryan "Acoustic Emission from a Crack Growth Event," Review of Progress in Quantitative Nondestructive Evaluation, Vol. 8B, pp. 1811-1818, 1988.

ACKNOWLEDGEMENT

This work was performed while the first author was a participant in the Navy/ASEE Summer Faculty Research Program.

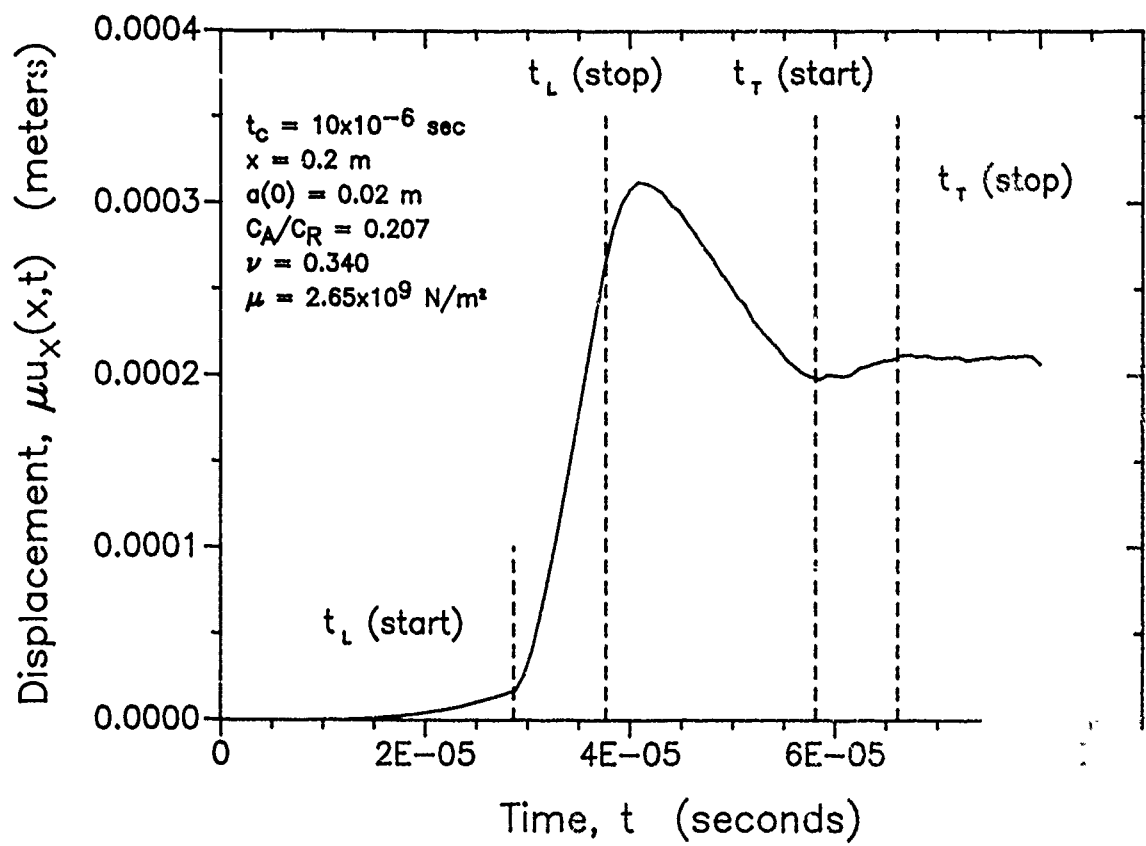


Figure 1: Displacement in Solid Due to Abrupt Crack Extension

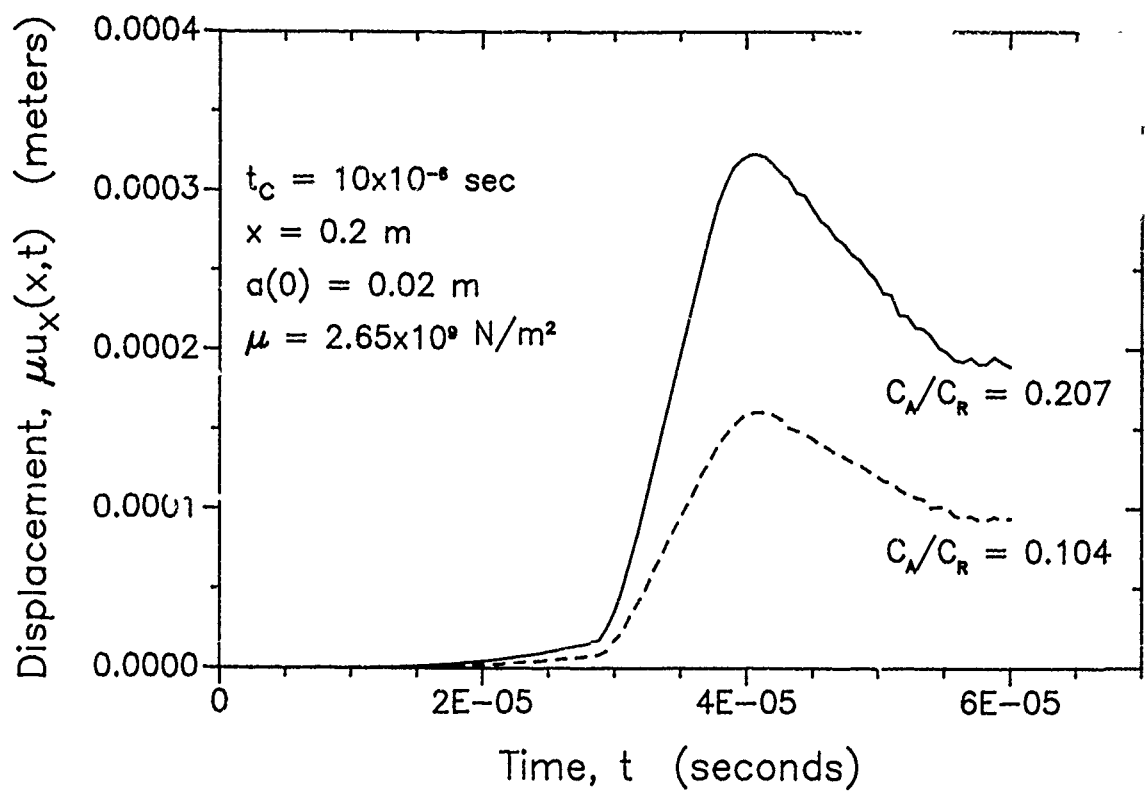


Figure 2: Variation of Displacement with Crack Velocity (C_A)

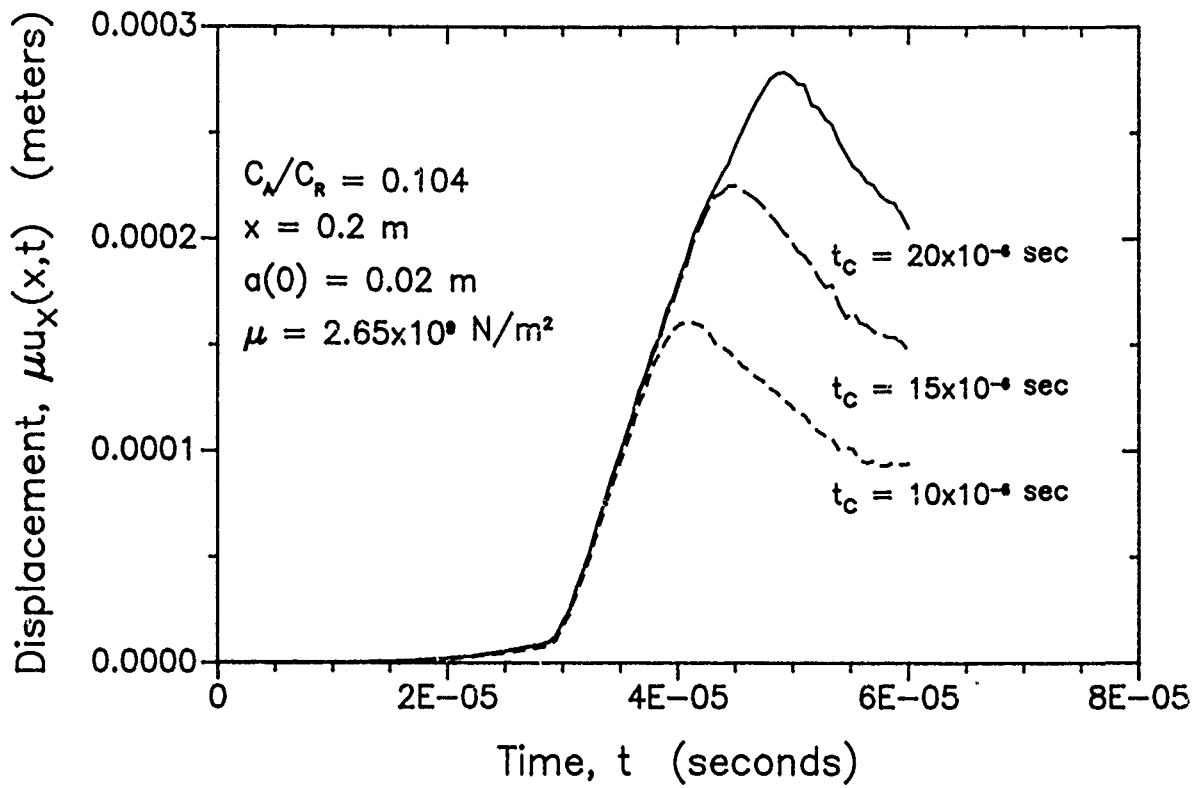


Figure 3: Variation of Displacement with Duration of Crack Propagation (t_c)

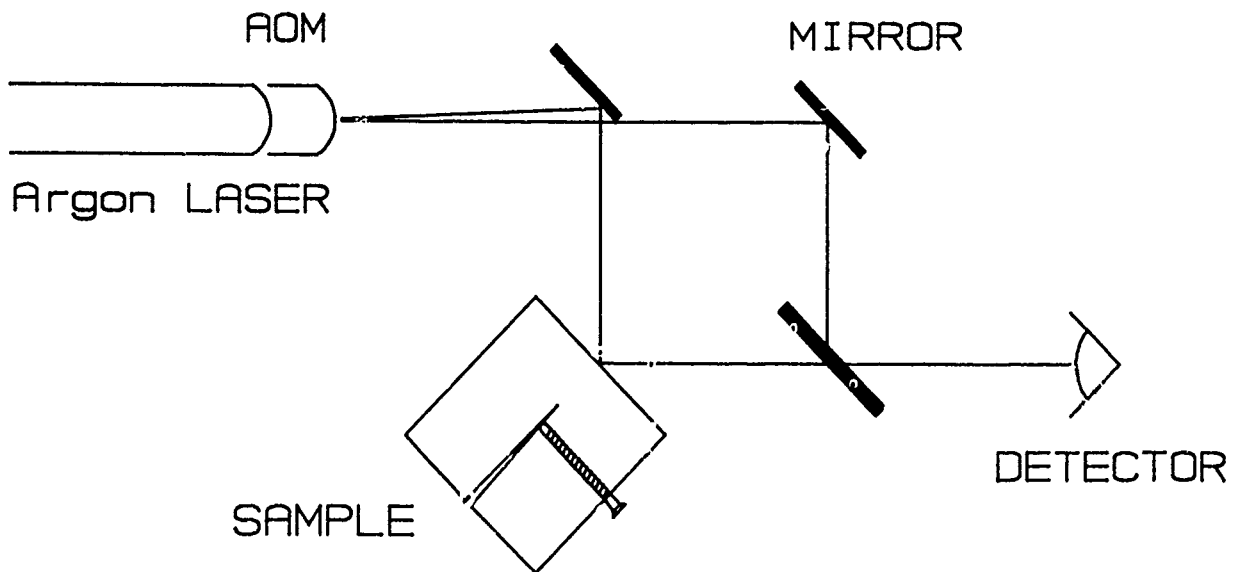


Figure 4: Interferometer Schematic

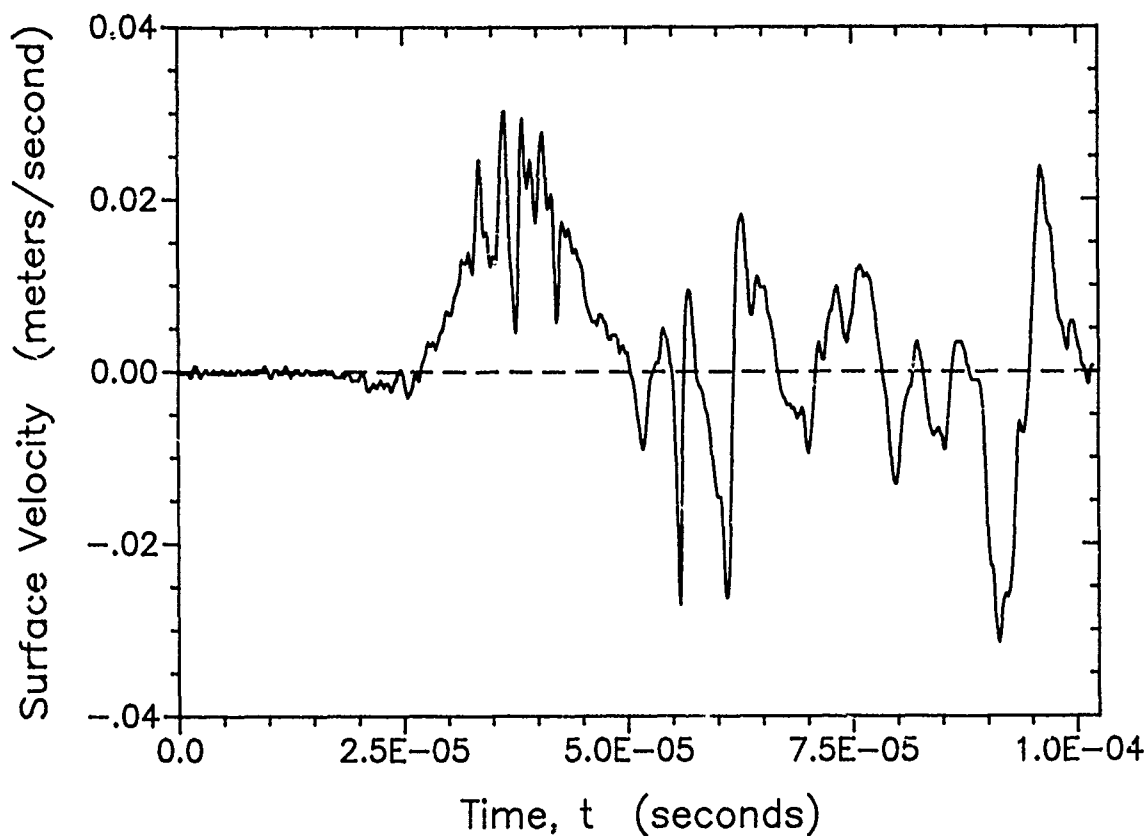


Figure 5: Characteristic Surface Velocity from a Crack Emission

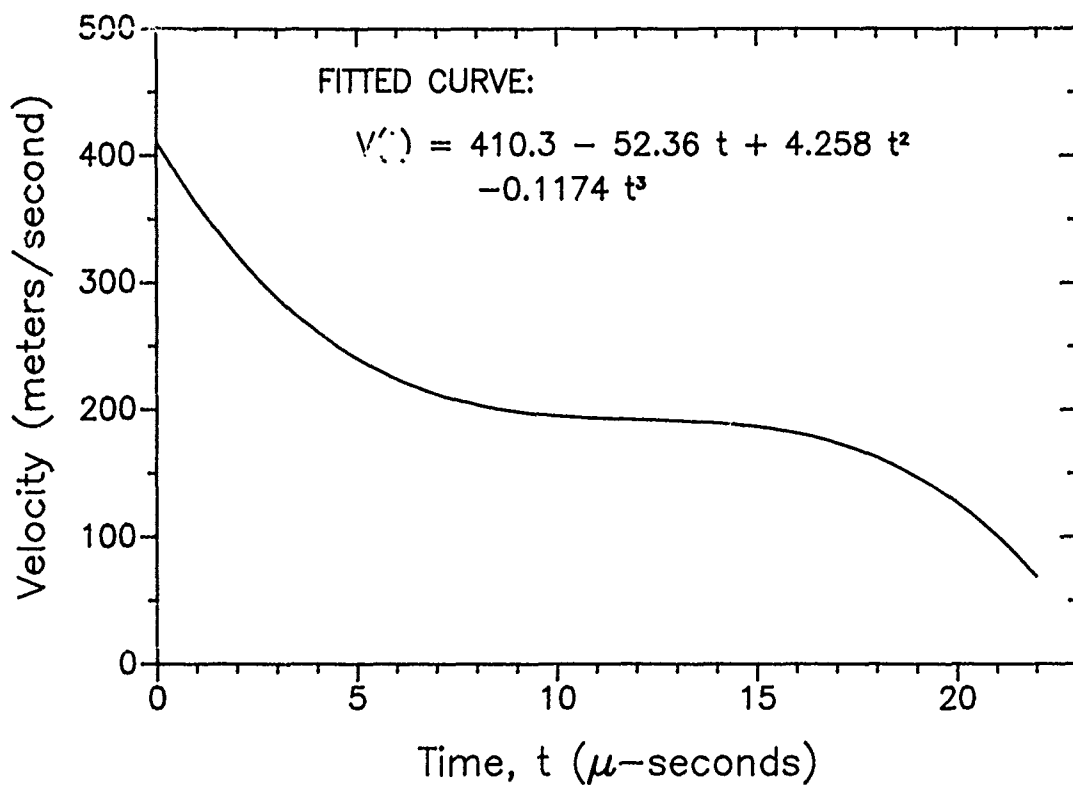


Figure 6: Crack Tip Velocity Through Crack Gage (Initial time, $t=0$, occurs when the first gage wire is broken.)

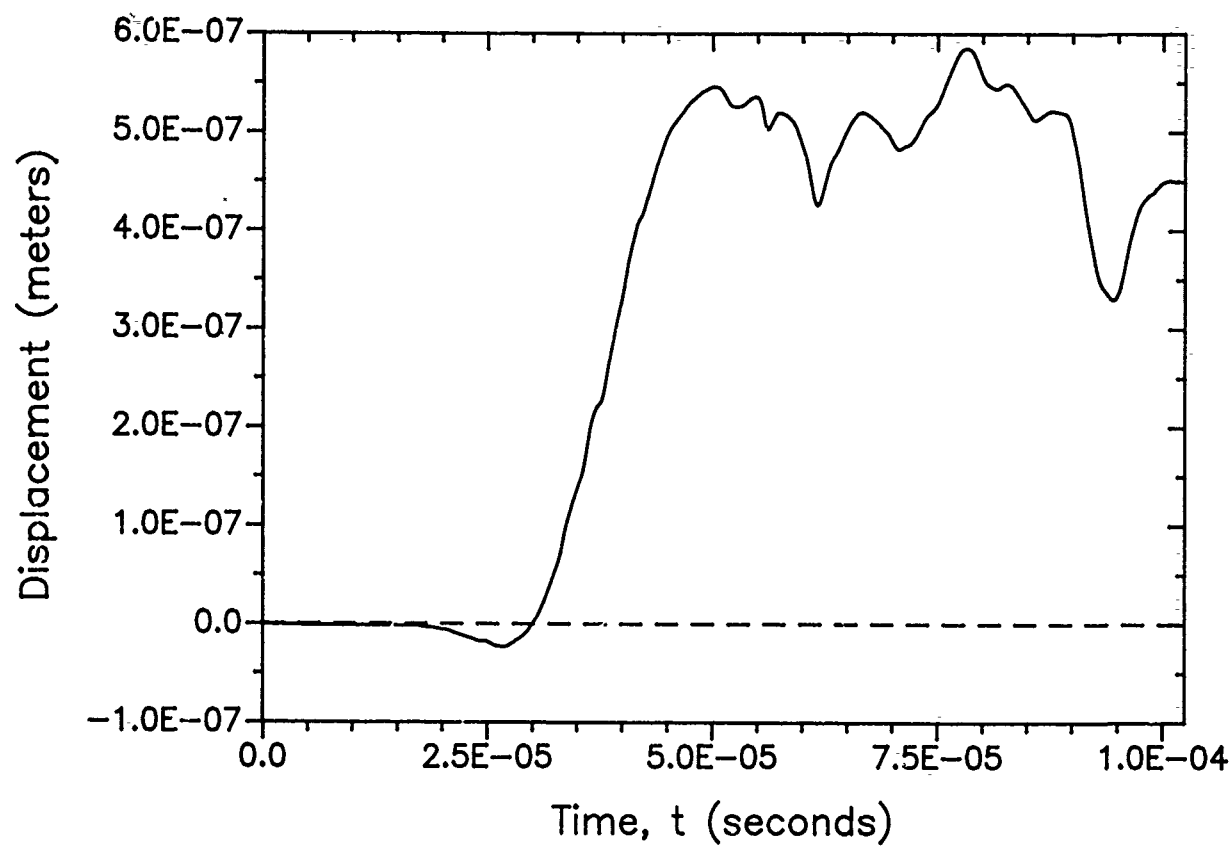


Figure 7: Displacement at Surface
Perpendicular to Crack Path

STUDY OF FAILURE PROCESSES IN FIBER REINFORCED COMPOSITES USING ACOUSTIC EMISSION TECHNIQUES

by

C. Roy, A. Maslouhi and M. El Ghorba
Department of Mechanical Engineering
Université de Sherbrooke
Sherbrooke, Québec - Canada
J1K 2R1

SUMMARY

Static and fatigue failures of composite materials are dominated by the initiation, growth and propagation of typical damages, up to some catastrophic condition. NDE techniques are used to detect and monitor the progressive development of damage and therefore they contribute profoundly to furthering the understanding of damage growth and its effect on the material response. With few exceptions, most of the presently used non-destructive evaluation do not possess a real-time, in situ capability. Fortunately, acoustic emission (A.E.) techniques show promise for monitoring structures in service and to assess damage at various stages in the life of a composite structure.

This paper describes new directions in the study of damage growth in composite specimens subjected to cyclic loading. A part of the paper assesses changes in the rate of damage accumulation in GFRP during cyclic Mode II loading using traditional A.E. techniques. Typical damage growth patterns are identified and represented on a S-N fatigue curve highly significant to the composite designer.

The other part of the paper attempts to identify the microfailures in CFRP during uniaxial fatigue testing by applying advanced signal processing techniques on the actual event waveforms coupled with pattern recognition analysis. The data analysis procedure has evolved from our earlier work analyzing acoustic emissions from the discrete components of a CFRP laminate. Pattern recognition analysis using the reduced waveform features on independent groupings of the data and training sets resulted in discriminating between A.E. and noise signals and in distinguishing signal classes from damage related sources.

INTRODUCTION

Ideally, the understanding of the damage capability of a composite system comprises, first that changes in the condition of the material that influence the structure's mechanical performance can be assessed non destructively and, second that the major damage modes in the composite under load can be identified. Due to the complexity and variety of defects and failure mechanisms in composites, conventional inspection methods have shown severe limitations with respect to monitor the growth of a region of damage arising from impact or manufacturing flaws, to warn of potential failures of structural components or possibly to identify poor design or installation. Therefore to ensure fuller utilization of life cycle capability of composites an economical NDE method of detecting, locating and assessing damage and its effects on the composite response is necessary.

Fortunately, acoustic emission (A.E.) techniques show promise for monitoring structures in service and to assess the damage at various stages in the life of a composite structure. Advanced A.E. signal analyses can be used to extract detailed information on the mode and state of damage present in a composite in real time thereby potentially providing continuous monitoring of the health of a structure.

In this paper, the approach to implement this capability is described. The first part of the paper is concerned with Mode II delamination analyzed in glass fiber/epoxy "DCB" specimens subjected to cyclic loading. The understanding of this failure mechanism lends itself to an evaluation of the damage tolerance of the composite and to the identification of the microfailure modes causing it. The second part of the paper is concerned with the identification of microfailures in a carbon fiber/epoxy laminate subjected to uniaxial fatigue loading using signal processing techniques of the actual event waveforms collected during the test rather than monitoring the numbers of events and their ring down properties. When combined, the data can be used to evaluate the damage tolerance properties such as delamination fracture toughness of a composite, and to obtain a one to one correlation between the microfailures and the detected A.E. signal sources.

METHODOLOGY

The overall concept of the work in progress can be represented by the flow chart shown in Figure 1. On the left hand side, an acoustic emission scenario unabling to depict the occurrence of damage in glass fiber/epoxy subjected to cyclic loading and to quantify the life cycle capability of a composite system up to delamination is summarized. On the right hand side of the chart, new directions in the field of acoustic emission testing and analyses are outlined to provide greater understanding on the nature of the defects developing in CFRP during fatigue loading.

The Delamination Problem in GFRP Composite.

Knowing the brittle nature of the current epoxy matrices, delamination constitutes a major damage in composite structure since it reduces the stiffness, strength and the fatigue life of the structure. Interlaminar stresses develop between layers of different fiber orientation due to high anisotropies of the laminae and these can lead to interlaminar fractures or delamination at free edges, holes or existing defects in the laminate. Therefore the composite designer not only has to contend with the computation of the stress distribution in his composite structure but with key damage tolerance properties of his composite such as the delamination fracture toughness.

The interlaminar toughness of composites is commonly characterized by the so-called Mode I tension test and Mode II shear test. Energy release rates G_I and G_{II} obtained from these tests provide the designer with a valuable measure of the interlaminar fracture energy for his composite laminate but this is only a minor part of the story of a major interlaminar fracture problem.

Generally, G_I and G_{II} values are determined with double cantilever beam (DCB) specimens containing an artificial delamination therefore generating a fracture energy value for stable and unstable crack growth conditions. In fact the most important initiation stage (matrix microcracking, fiber disbond,...) leading to delamination is neglected although the extend of this period can represent the most significant time interval of a component useful life.

In the present study, the emphasis is placed on distinguishing the various stages of fatigue life damage: initiation, progression, and delamination. S-N fatigue curves and residual life prediction are derived entirely by the A.E. signatures recorded during fatigue testing.

Identification of Failure Modes in CFRP.

Composites materials can fail in some different modes depending on their fabrication and mechanical loading history. The failure modes consist of an accumulation of many microfailures (matrix, fiber, interface debonding) before a catastrophic failure occurs. Therefore it is most important to know which type of microfailure is about to begin. So far it has been difficult to use A.E. data to discriminate efficiently between signals associated with different microfailure mechanisms. In principle, because the A.E. signals are originated by microfailure process which convert a portion of their elastic strain energy into waveforms, the shape of a propagating pulse must depend on the particular microfailure mode, the physical properties of the composite material and the response of the piezoelectric sensor. Therefore the A.E. signals which originate from different sources must differ also in their time characteristics and frequency content [1]. Since the signals detected by a sensor include the effects from the propagating composite medium and the A.E. sources themselves, it is imperative to eliminate the contribution of these effects on detected waveforms so that A.E. source can be identified.

Recent advances in computing power now makes complex signal analysis possible thereby enabling the extraction of much more information about the A.E. signals previously not available particularly in real or near-real time. In recent studies [2-5], signal processing coupled with pattern recognition techniques have been successfully applied to the problem of classifying several types of non-destructive evaluation data including A.E. waveforms. The transient digitizers and fast microcomputers used can only collect subsets of the total number of emissions thus at this point in time prohibiting real-time processing of all NDE data for on-line monitoring applications. This can be attributed to the fact that descriptors that characterize the signals are important in the recognition process and these have to be calculated in the time domain and frequency domain via transforms such as the fast Fourier Transform (FFT) [6]. However with the modern techniques based on data modeling procedures such as the autoregressive (AR) [7] and the autoregressive moving - average (ARMA) [7], spectral analyses can achieve increased spectral resolution [8], particularly for short data records. Representative AR and ARMA coefficients are evaluated and then employed as the features in the pattern recognition analysis.

The second part of this paper deals with: i) the analytical procedures to which the A.E. signals, collected during fatigue loading of CFRP, were subjected in order to extract the waveform features that are related to the microfailure mechanisms, ii) the pattern recognition techniques that exploited the above signal features to classify and recognize A.E. signals from damage related sources and spurious A.E. sources present during fatigue testing [9].

A schematic of the A.E. analytical process utilized in our laboratory is shown in Figure 2. The pattern recognition algorithms used here were created from the software "STATISTICAL ANALYSIS SYSTEM" (SAS) [10]. The main objective of pattern recognition is to classify a pattern, in our case the digitized waveform, into one of several possible signal classes. A second objective is to obtain possibly certain discrimination of the A.E. data. A key problem in pattern recognition is the feature extraction, i.e. the determination of the best features that can discriminate A.E. data from different classes of physical phenomena and to correctly identify samples from the same classes.

Generation of a feature file

The A.E. signal features are measurable scalar quantities extracted from the time domain and the frequency domain for each waveform. Previous studies on discrete components of a composite material system i.e. neat epoxy, carbon fibers, and delamination (DCB test) of simple laminate [5] have been used to correlate repetitive spectral characteristics to damage mechanisms which are known to be working within a CFRP composite during selected experiments. Therefore the reference waveform features generated from A.E. signals collected during these experiments provide an excellent base of A.E. sources since they relate closely to the microfailure mechanisms operating in the composite. The method of measurement of the waveform features utilized is illustrated schematically in Figure 3. Each set of features constitutes one variable X in a multidimensional space. Considering the values of the combined features for a specific A.E. signal, one can represent the signal with a point or a vector in the multidimensional space called pattern space.

The pattern recognition analysis

A pattern recognition routine includes (Figure 4) first of all, a learning stage (from the training samples for feature selection and classification) whereby a set of decision rules is assembled and second, an automatic classification of unknown signals collected during a fatigue test. Essentially it allows:

- dimensionality reduction, i.e. it searches for the optimal subspace of a given feature space;
- cluster analysis, i.e. for unknown classes of signals it consists in finding natural groupings of set of data by searching the similarity between their vector representation;
- discriminant analysis, i.e. it separates one class of signals from another in the feature space following certain classification processes such as the quadratic discriminant function and the K-nearest neighbors;
- classification, i.e. it sorts out new unknown signals based on the relative discriminatory power of the variables used, and following supervised classification rules.

TESTING PROGRAM

The Composite Materials

The delamination study was carried out on S-glass fiber/epoxy (CE 9000-9) developed by Ferro Corporation. The laminated panels which were fabricated by Bell-Helicopter Textron Canada consisted of 26 plies [± 45 , 04, ± 45 , 04, ± 45 , 04, ± 45 , 04, ± 45] giving a thickness of 5mm. The DCB specimens (295 mm long by 20 mm wide) were cut from the panels.

The actual event waveforms were collected from standard tensile specimens cut from (± 45)_{2S} carbon/epoxy (Hercules AS4/3501) panels 1.1 mm thick. These were fabricated by Fleet Industries, a division of Fleet Aerospace Corporation.

The two types of composites were C-scanned and found to be free of detectable defects.

Fatigue Loading and Acoustic Emission Monitoring

The details of the experimental procedures and the dimensions of the GFRP specimens for shear loading were reported earlier [11]. Summarily, the double cantilever beam specimen was subjected to cyclic Mode II forward shear as shown in the loading configuration (Figure 5). An AET-5000 B computerized system in conjunction with three resonant piezoelectric transducers mounted on the DCB specimen was used to detect and locate the acoustic signals originating from either of the two shear zones.

The fatigue loading of the CFRP tensile specimens was performed on a closed loop servo hydraulic testing machine under load controlled mode. Spurious acoustic emission noise due to hydraulic loading was eliminated using a polyurea (Delrin) insulating material between the specimen and the loading grips. The A.E. waveforms were detected by a broadband piezoelectric sensor (B & K 8312) mounted onto the tensile specimen. This sensor had a built-in preamplifier (40 dB gain) and was characterized by a nearly flat frequency response over the range 0.1 to 0.8 MHz [12]. The A.E. signals were digitized and processed in a self-contained system (Data Precision-6000). Software routines have been developed to facilitate rapid transfer from the digital storage of the Data-6000 to a PC/AT. In addition, precautions were taken to mitigate any adverse consequences of the signal distortions introduced by the detecting system [12]. This was achieved by identifying the inherent problems in the system causing the distortion of the signal and secondly by devising a methodology allowing us to eliminate the defective components of the distorted signal.

The fatigue loading characteristics for the two types of experiments are summarized in Figure 6.

RESULTS AND DISCUSSION

Cyclic Mode II Loading of GFRP Specimens.

The results of the static Mode II tests to determine the interlaminar shear strength, τ_u , for this material have been reported previously [11]. Seven identical specimens were tested to yield an average interlaminar fracture stress of 56.6 MPa. The results of the fatigue tests realized at different stress amplitudes are summarized in Table 1. In terms of A.E. activity, the data clearly differentiates three stages of the fatigue life identified as:

Stage 1 defined as the number of fatigue cycles below which there is no A.E. activity in the composite. It represents, for a given level of cyclic stress, a threshold leading to irreversible damage in the material.

Stage II corresponding to the progressive growth of A.E. activity during a fatigue test. The extent of this period (i.e. the number of fatigue cycles) is strongly dependent on the stress amplitude or the rate of damage generated by the cyclic loading.

Stage III corresponding to a sudden burst of A.E. activity in the material and analogous to the very large count rate of events recorded at the instant that the delamination occurs during a static test.

A typical histogram showing the distribution of A.E. events with increasing the number of fatigue cycles in the two shear zones of a specimen is shown in Figure 7. As the test progressed higher A.E. activity appeared first in zone 1 (left of center) then in zone 2 (right of center). Nevertheless the delamination occurred finally in zone 2 at cycle number 1667 as indicated by a sudden outburst of A.E. events, which was also confirmed by a microscopy analysis performed on the damaged specimens [13]. Figure 8 is an example displaying how the damage progression monitored through acoustic emission in the composite during fatigue loading can be represented graphically by a conventional S-N curve. This unique method of analysis enables us to estimate the period of the damage growth preceding the delamination process as a function of the fatigue stress amplitude, up to the fatigue limit of the composite (i.e. $0.4 \tau_u$ for an endurance limit corresponding to $1.5 \cdot 10^6$ cycles).

From a practical point of view, a knowledge of the damage evolution in a composite subjected to cyclic loading is highly valued to assess its damage tolerance capability. Since the A.E. activity measured during a fatigue test allows us to follow the material degradation as:

$$N_a + N_p = N_f$$

where

- N_a = number of fatigue cycles to initiate the damage in the composite (Stage 1)
- N_p = number of fatigue cycles to propagate the damage in the composite (Stage II)
- N_f = number of fatigue cycles leading to delamination (Stage III)

it is highly significant to quantify the relative importance of the two periods of the fatigue life, (initiation and growth of damage) with respect to the entire life of the composite and the effect of the stress amplitude. For this composite subjected to the present conditions of cyclic loading, it may be concluded (see Table 1) that at high fatigue stress the period of damage initiation (Stage 1) accounts for a small proportion (~ 8%) of the fatigue life whereas at low cycling stress amplitude (around the fatigue limit) the period of the damage initiation can reach up to 45% of the fatigue life. In line with this methodology, it is possible to measure the residual static shear strength of the composite at any life fraction, $\beta = N_i/N_f$ (N_i = the number of fatigue cycles registered), on the S-N curve.

The analysis of the internal microfailures relating to damage progression in the composite was of particular significance in this study since the C-scan images failed to reveal any microstructural changes in the composite until delamination had set in the shear zones of the specimen. The damage features in the composites and their relationship with the cracking mechanisms were reported earlier [11]. One of the major damage modes was matrix microcracking: shear failure showing propagation from one to an adjacent 45° or 0° ply and coupling, interlaminar cracking and cyclic cleavage striations.

Classification of Acoustic Emission Sources in CFRP

A very large number of A.E. waveforms are acquired during a fatigue test and as it was mentioned earlier the transient digitizer can only collect subsets of the total number of emissions. However the acquisition of the signals accounted for a small but representative fraction of the total number of acoustic events emitted during the entire test. Furthermore, it must be recognized that the rate of acoustic emissions varies not only according to the damage progression generated in the composite but also can be due to fretting amongst fracture surfaces that are created in the composite during fatigue loading [9].

To facilitate the analysis of the fatigue data, the test was divided in stages corresponding to time of A.E. event occurrence and position on the load cycle where each event was emitted. Table 2 presents a typical record of a fatigue test. Early in the test (~ 1300 cycles) the specimen emitted few A.E. signals, but after the 3360th fatigue cycle the acoustic emission was characterized by a large number of high energy signals thus suggesting rapid growth of damage in the composite. Later in the test, repetitive low amplitude waveforms appeared amongst the many signals recorded. These odd signals were attributed to friction and were eliminated from further analysis by adjusting the threshold setting on the trigger in the DATA 6000 A acquisition module. Typical waveforms collected at various stages of the fatigue test are presented in Figure 9. Visually, these waveforms exhibit distinct features (amplitude, frequency, duration, etc) yet it is impossible to link these to any damage mechanisms in the composite until the signals are processed and analyzed using advanced analytical techniques. Indeed analysis of the classical A.E. parameters (counts, events, energy and peak amplitude) can only provide qualitative information about the damage evolution in a fatigued specimen. An example of the characterization of the damage in the composite at various stages of the fatigue test using the energy parameter is shown in Figure 10. The energy distribution envelope exhibits three stages of defect avalanches possibly reflecting the nature of the main modes of damage progression in the specimen. In fact, this type of representation provides only a qualitative information and a trend in the damage evolution in the composite under fatigue loading.

The results reported so far relate to global analysis of the A.E. activity in the composite. To take into account the distinct features of the individual A.E. waveforms, pattern recognition techniques were applied to the experimental data in order to assign the A.E. signals to appropriate microfailure sets. However the performance of the discriminant rule is dependent on the quality of the feature sets used in the training process, thus much attention must be given to deciding which set of features should be used. The discriminatory power of the four most relevant features selected from the frequency domain have been calculated in a previous study [3].

The reference signals from the discrete components of CFRP were discriminated through these features using the STEPDISC procedure of SAS [10]. Figure 11 displays the separability power of the selected features to distinguish signal classes. The canonical variables spanning the subspace in which class separability is maximized were calculated enabling the training data to be projected in a plane. The same classification rules have been applied to the A.E. fatigue data displayed in Figure 12 together with the reference signals from the discrete components of the composite. The fatigue pattern appears to exhibit three separate data groups that compare favorably to the classes obtained from the discrete components of the composite. It is known that during fatigue loading, most of the emissions seem to be generated by microfailures and fretting between fracture surfaces. However to distinguish emission due to fretting from the actual emissions generated by the damage progression, a new set of features extracted in the frequency domain (see Figure 3) improves the recognition rate. The first feature, S_1 , is

related with the shape of a peak in each zone of the spectrum, the second, RF_i , to the ratio of the frequency difference in each zone selected and the third features, RA_i , to the ratio of the area in each zone to total area of the spectrum. Figure 13 displays the results of the classification in the feature space. It shows that these new features increase the degree of separability of the classes of A.E. Sources. Thus it appears that a characterization of different damage processes CFRP is possible, but obviously further experimental work is necessary for this to be firmly assessed.

CONCLUSIONS

The complex damage formation that develops during fatigue loading of composite materials, the sensitivity of the A.E. techniques in depicting the occurrence of damage and in identifying microfailures, the need for establishing appropriate testing procedures and data analysis, all make the investigation into the applicability of acoustic emission extremely challenging.

This study comprises two parts both of which are related to damage accumulation in composite materials. In the first part, emphasis was placed on distinguishing the various stages of fatigue damage in GFRP; initiation, progression and delamination. A S-N curve was constructed entirely on the A.E. signatures recorded during fatigue testing enabling the damage tolerance capability of the composite to be evaluated.

In the second part, advanced signal processing of A.E. waveforms were coupled to pattern recognition techniques to identify the microfailures in CFRP during fatigue loading. A methodology was proposed to classify the recorded waveforms so that feature extraction and classifier development could proceed. The current approach shows promise for A.E. waveform analysis to determine the type of emission source and could be extended for use "in real time, in situ non-destructive evaluation of composite structure".

ACKNOWLEDGEMENT

The authors would like to acknowledge the contribution of Bell Helicopter Textron Canada and Fleet Industries for contributing the composite panels used in this study. Support from the Natural Sciences and Engineering Research Council of Canada, the National Research Council of Canada and the Canadian Space Agency, Ottawa is greatly appreciated.

REFERENCES

1. Rotem, A., "Acoustic Emission Signature of Failure Modes". SPI-CARP, 2nd Int. Symp. Montreal, pp. 134-140 (1986).
2. Hay, R.D., Chan, R. W.Y., Sharp, D. and Siddiqui, K.J. "Classification of Acoustic Emission Signals from Deformation Mechanisms in Aluminium Alloys" J. of Acoustic Emission, Vol. 3, No. 3, pp. 118-129 (1984).
3. Roy, C., Maslouhi, A., Gaucher, D. and Piasta, Z. "Classification of Acoustic Emission Sources in CFRP Assisted by Pattern Recognition Analysis", Can. Aero. Sp. J. Vol. 34, No. 4, pp. 224-232 (1988).
4. Belchamber, R.M., Betteridge, D., Chow, Y.T., Lilley, T., Cudby, M.E.A. and Wood, D.G.M. "Evaluation of Pattern Recognition Analysis of Acoustic Emission from Stressed Polymers and Composites", J. of Acoustic Emission Vol. 4, No. 4, pp. 71-83 (1985).
5. Maslouhi, A., Roy, C., Proulx, D., Cherfaoui, M. and Zimcik D.G. "Statistical Analysis of Acoustic Emission Signals Associated with Fatigue Damage in CFRP Composites", AECM-3 Paris, pp. 250-258 (1989).
6. Melton, R.B., Doctor P.G. and Daly, D.S. "Pattern Recognition Analysis of Acoustic Emission Waveforms from Simulated Joint Specimens" presented at the AF/DARPA Review of Progress in Quantitative NDE, University of California at San Diego, August (1982).
7. Box, G.E.P. and Jenkins G.M. "Time Series Analysis: Forecasting and Control", Holden-Day, San Francisco (1976).

8. Chen. C.H. "Digital waveform processing and recognition", CRC Press, pp. 23-58 (1982).
9. Awerbuch, J. and Chaffari, S. "Monitoring Progression of Matrix Splitting during Fatigue Loading through Acoustic Emission in Notched Unidirectional Graphite/Epoxy Composite", SPI-CARP, 2nd Int. Symp. Montreal, pp. 51-58 (1986).
10. SAS User's Guide - Statistics, Version 5 Edition, SAS Institute Inc. Cary 1985.
11. Roy, C. and El Ghorba, M., "Monitoring Progression of Mode II Delamination During Fatigue Loading Through Acoustic Emission in Laminated Glass Fiber Composite" Polymer Composites Vol. 9, No. 5, pp. 352-357 (1987).
12. Maslouhi, A., Roy, C. and Proulx, D. "Characterization of Acoustic Emission Signals Generated in Carbon/Epoxy Composites" SPI-CARP, 2nd Int. Symp. Montreal pp. 112-116 (1986).
13. Roy, C. and El Ghorba, M. "Identification of Fatigue Threshold and Limit of Glass Fiber/Epoxy Composite by Acoustic Emission" ATMAM-89 paper 26, Montreal (1989).

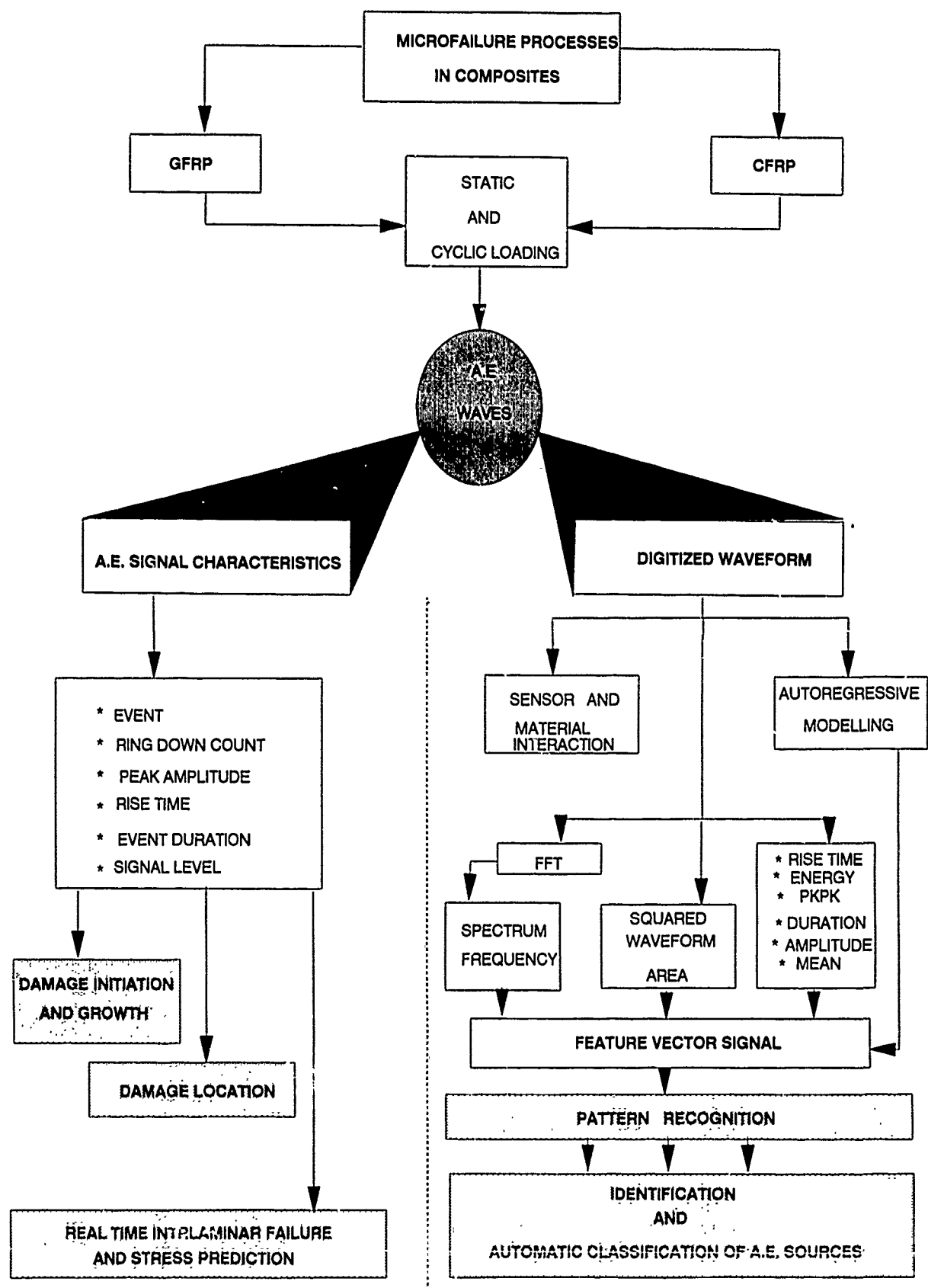


Fig. 1 Schematic diagram of A.E. data acquisition and signal analysis

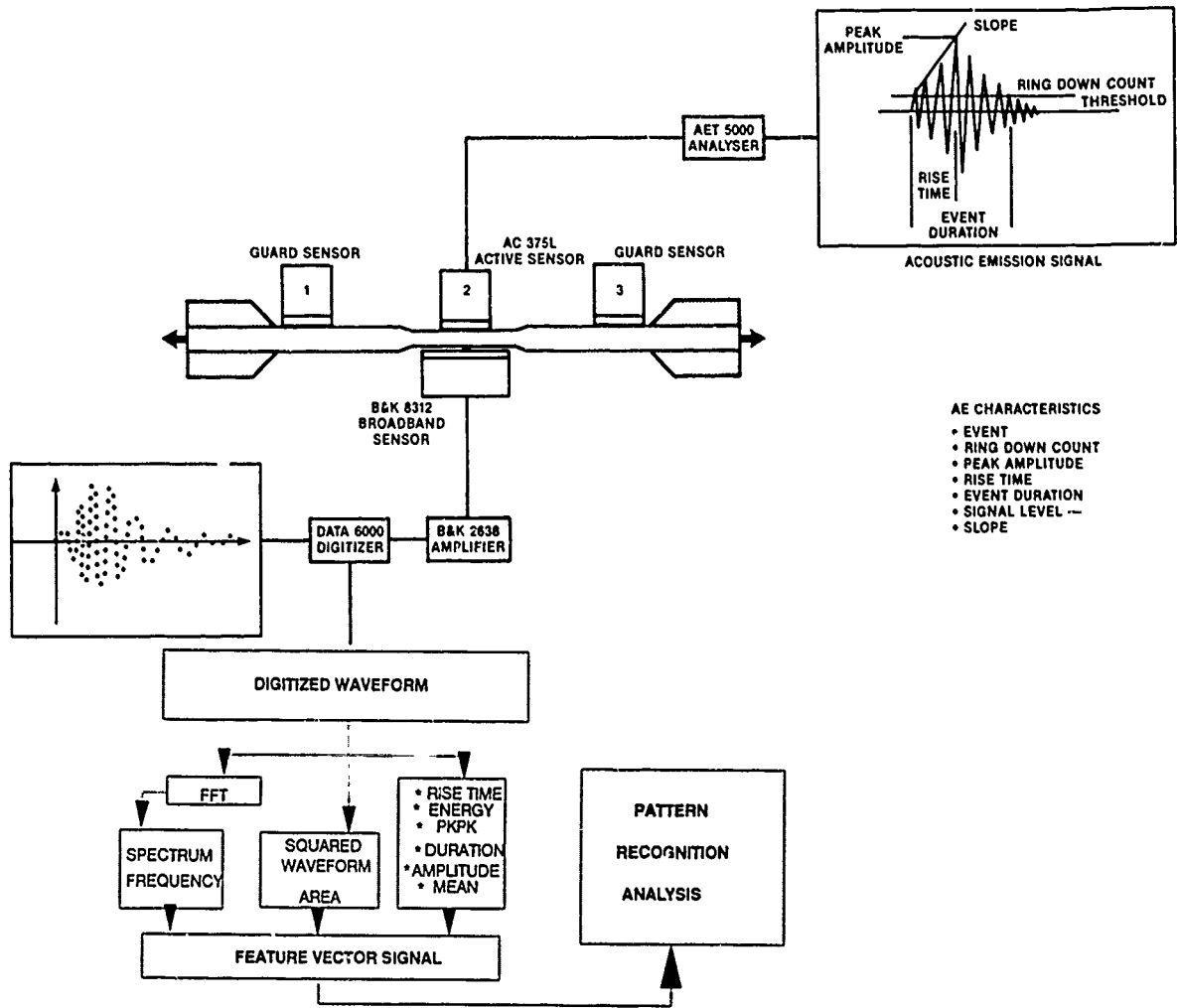


Fig. 2 Schematic diagram of the instrumentation setup

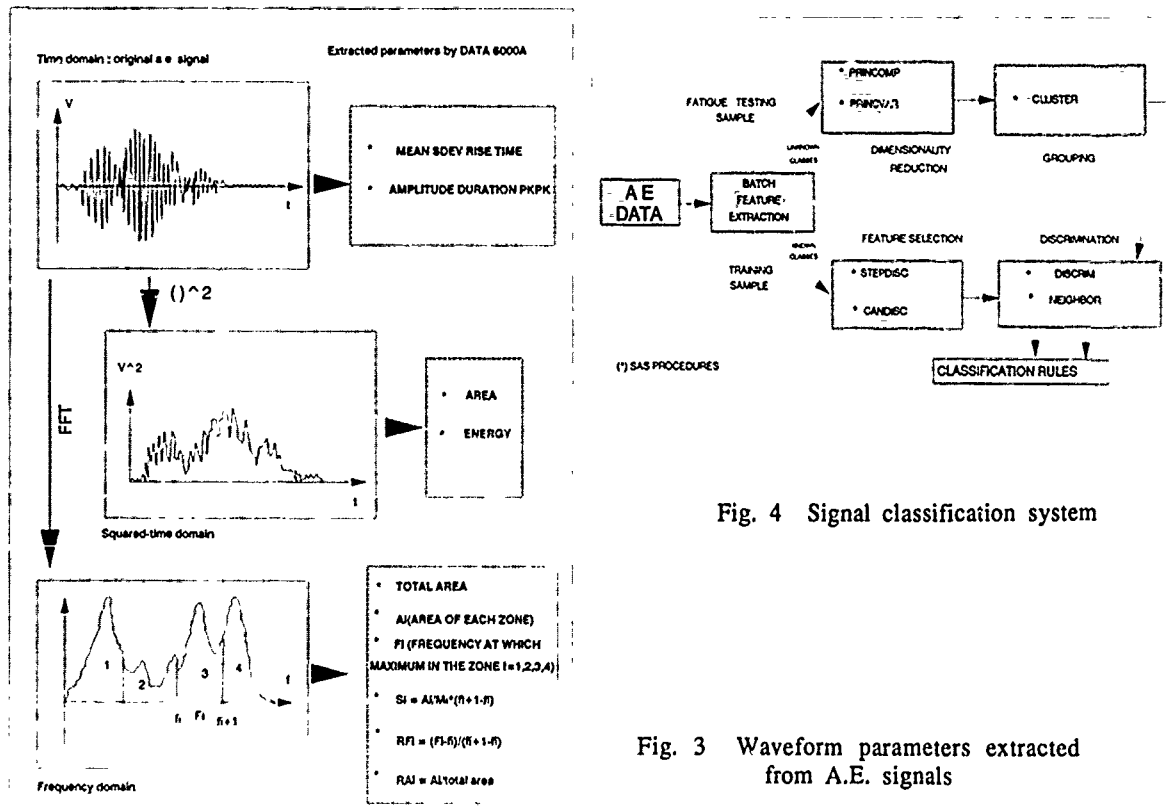


Fig. 4 Signal classification system

Fig. 3 Waveform parameters extracted from A.E. signals

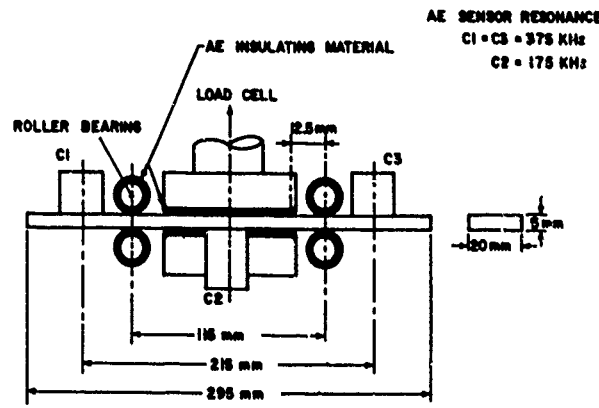


Fig. 5 Mode II loading configuration

	GFRP SPECIMEN (+45,0/-45,0/+45)	CFRP SPECIMEN (+45)2s
CYCLIC FREQUENCY (Hz)	5	25
R	-1, 0.1, 0.4	0.2
Pmax/Pu (%)	75, 70, 62, 50, 45, 40, 30	Pmax/Pu (%) 70
SHEAR STRESS Pu (MPa)	8.36	STATIC Pu (MPa) 6
CYCLIC LOADING	FORWARD SHEAR (MODE II)	TENSION-TENSION

Fig. 6 Fatigue loading characteristics employed for the two composite materials

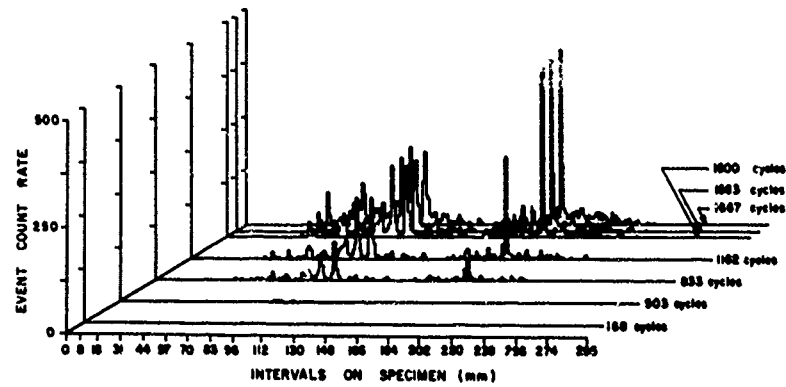


Fig. 7 Distribution of A.E. events in the two shear zones of a GFRP specimen during the fatigue test

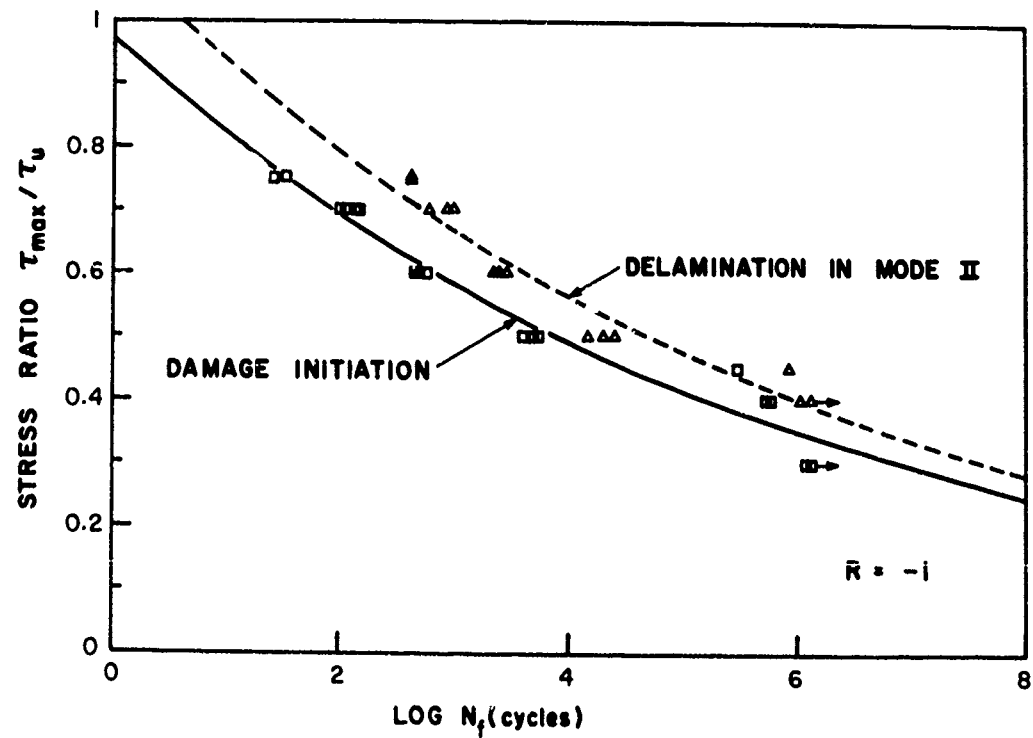


Fig. 8 S-N fatigue curve (Mode II) derived by A.E. analysis of damage initiation and growth in the GFRP composite

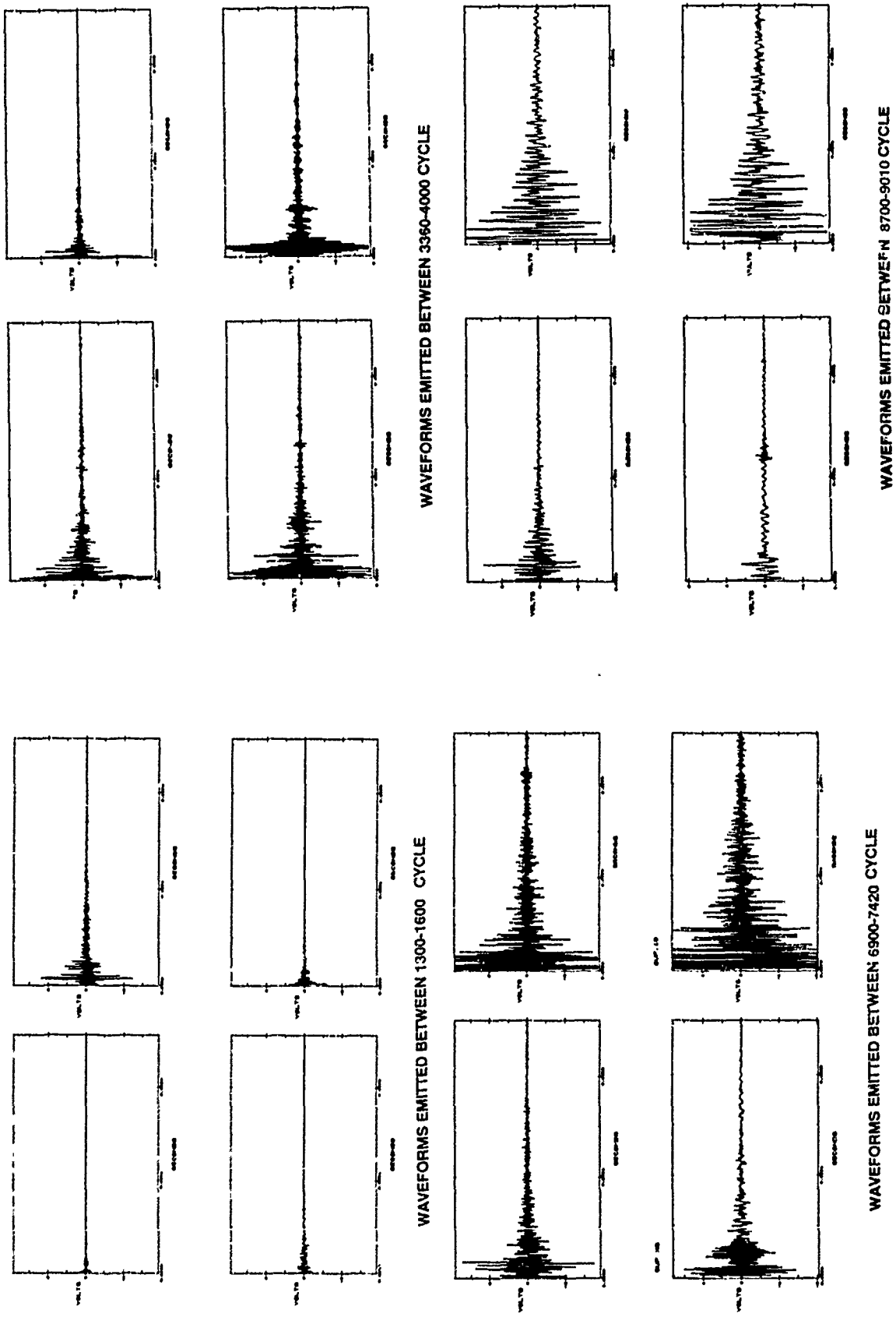


Fig. 9 Progression of A.E. waveforms during a fatigue test with a CFRP specimen

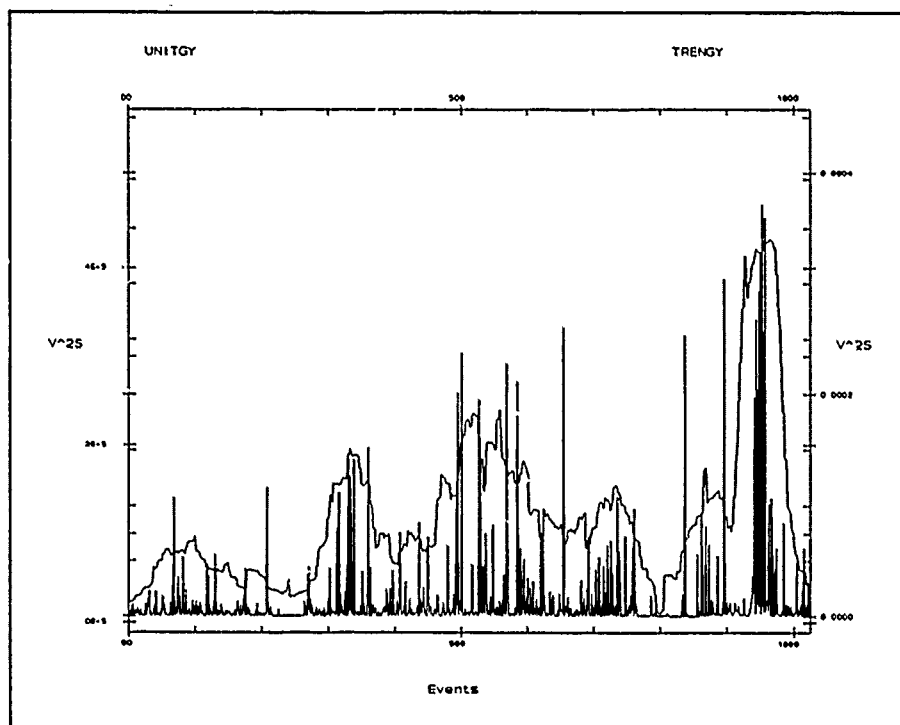


Fig. 10 Energy distribution of the A.E. signals collected during a fatigue test with a CFRP specimen

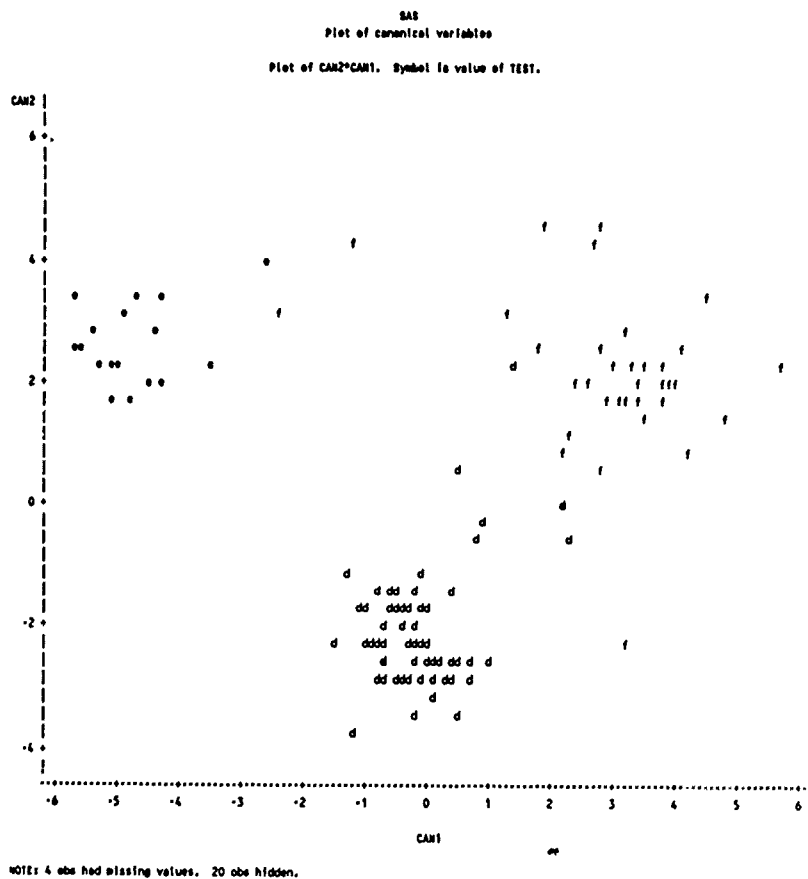


Fig. 11 Canonical variables projections using 4 signal features applied to reference A.E. signals

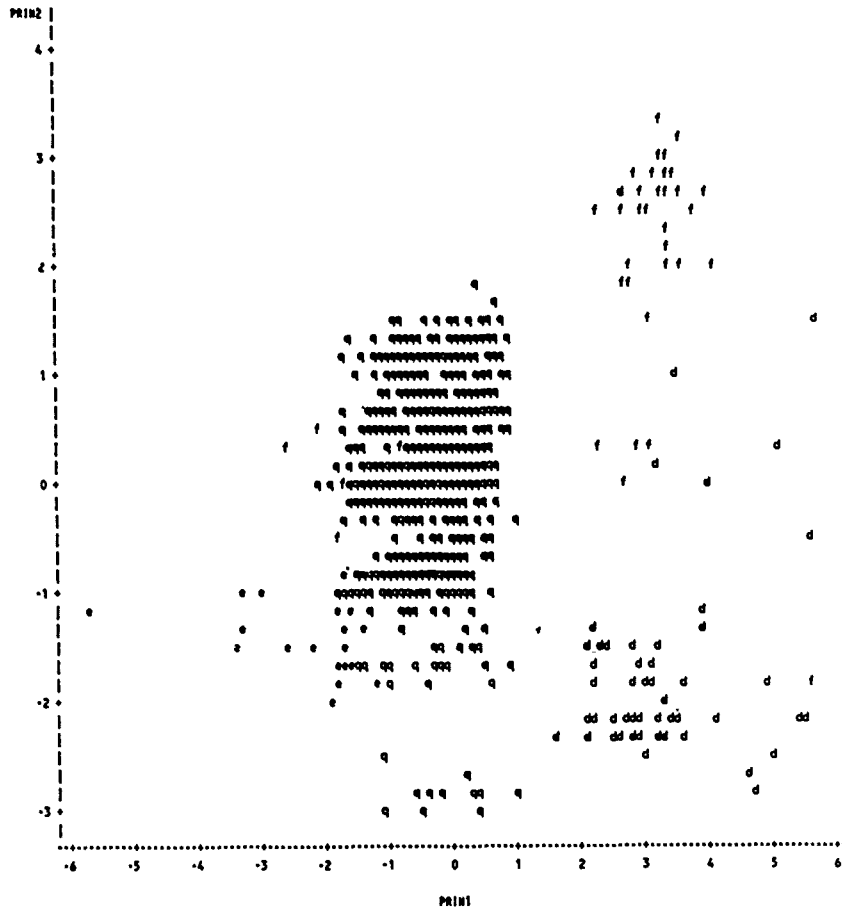


Fig. 12 Classification of A.E. signals collected during the fatigue test of a CFRP specimen by superposition onto the classes of reference signals in Fig. 11

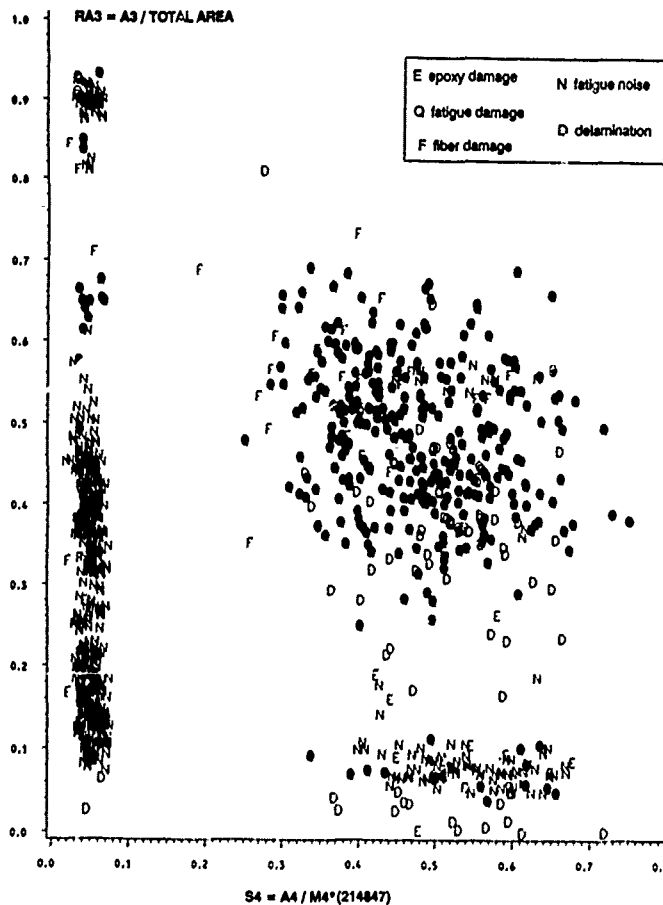


Fig. 13 Improved recognition rate of A.E. noise and damage related signals during fatigue test by more discriminatory features selection

TABLE I - FATIGUE DATA FOR MODE II LOADING OF DCB SPECIMENS. R = -1

Specimen No.	τ_{max}/τ_u (%)	No of fatigue cycles to		N_a/N_f (%)	N_p/N_f (%)
		Damage initiation N_a	Delamination N_f		
F 17900	75	34	415	8	92
F 18900	75	27	436	6	94
F 19900	70	109	600	18	82
F 20900	70	145	873	17	83
F 28900	70	102	614	17	83
F 32900	70	136	1 000	14	86
F 21900	60	511	2 898	18	82
F 30900	60	455	2 500	18	82
F 31900	60	511	2 273	23	77
F 36900	60	545	2 932	19	81
F 22900	50	5 114	20 455	25	75
F 29900	50	5 682	25 568	22	78
F 33900	50	3 977	15 000	27	73
F 35900	45	306 818	852 273	36	64
F 34900	40	527 271	1 072 727	49	51
F 26900	40	590 909	1 312 500	45	55
F 24900	30	1 345 670		
F 25900	30	1 283 730		

TABLE II - TYPICAL FATIGUE DATA WITH A CFRP SPECIMEN

DISK.	FATIGUE CYCLE	RECORDED SIGNALS	OBSERVATIONS	
1	1300	47		
	2160	94	Low rate of AE emission	
	2640	141		
	3080	154		
	3360	201	Emission of increasing energy AE signals	
2	3660	248		
	3960	295		
	4200	302	High proportion of repetitive AE signals (Adjustment of threshold setting)	
3	4570	355		
	4830	402		
	5110	449		
4	5380	462		
	5610	509		
	5930	556		
5	5930	556	High Rate of AE Emissions	Low amplitude AE signals Saturated AE signals of low frequency
	6190	603		
	6450	650		
	6700	663		
	6900	710		
6	7170	757		
	7420	804		
	7660	817		
7	7900	864		
	8080	911		
	8320	958		
	8500	971		
	8700	1018		
	9010	1065		

INSPECTION SYSTEM FOR IN-SITU INSPECTION OF AIRCRAFT COMPOSITE STRUCTURES

par
P. BLONDET - I. MOLINERO
AEROSPATIALE - CENTRAL LABORATORY
LOUIS BLERIOT JOINT RESEARCH CENTER
12, rue Pasteur
92152 SURESNES France

1. INTRODUCTION

The intensive use of composite materials in aircraft primary structures has led to the setting up of special inspection systems for the detection of any defects which may be produced during the life of the aircraft. The main defects which are investigated during maintenance are, in general, delamination defects produced by various types of impact (stones, lightning, effects of maintenance tools being dropped).

Until more global techniques (thermography, holography) are developed, the most suitable method for this type of inspection is ultrasonics. The problem involves application of these inspection procedures to an aircraft under maintenance conditions while scanning the areas to be inspected and obtaining a real time diagnosis.

The SIAM R-theta system has been especially designed to meet the requirements of this type of inspection. It is capable of both assessing the damage after detection of the defect (visually, for example), and detecting defects within the framework of general inspection.

2. GENERAL DESCRIPTION

The SIAM R-theta system can be broken down into four parts (see figure 1) as follows :

- 1) The ultrasonic probe and probe holder especially designed by Aerospatiale's Central laboratory for the inspection of composite materials.
- 2) The mechanical device locating the position of the sensor in the inspection plane.
- 3) The computer unit (hardware and software) comprising ultrasonic transmitter/receiver cards and digitizing cards. Control, management and display software has been especially developed for the inspection of composite materials.
- 4) Ancillary equipment.

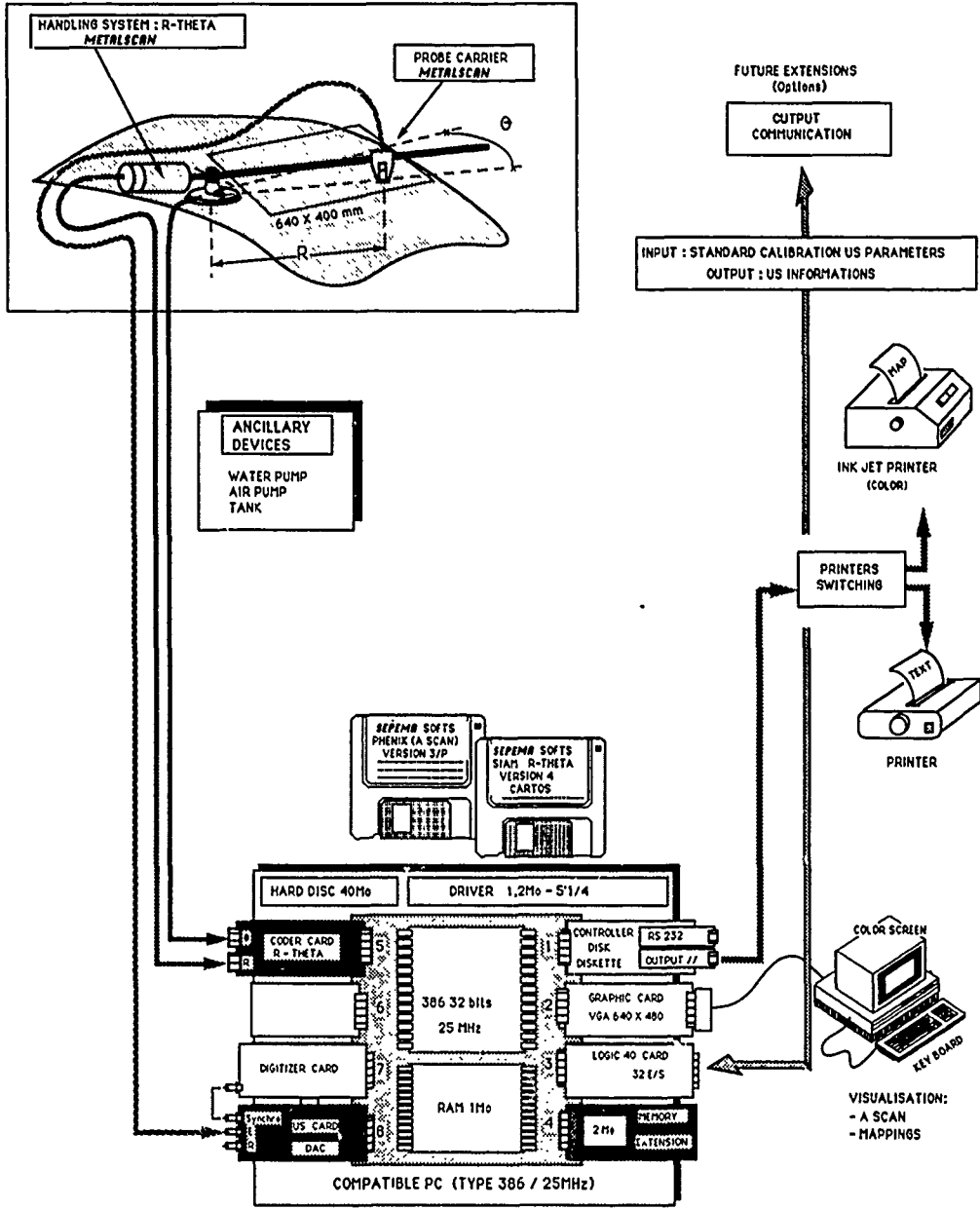


Figure 1 : SIAM R-Theta architecture

(a) Ultrasonic probe

A 9 MHz center frequency wideband relay-type ultrasonic sensor is used. Figure 2 shows the echo response on the relay/air interface with the characteristics of the electrical excitation pulse. The thickness of the relay allows up to 128 plies of composite to be inspected.

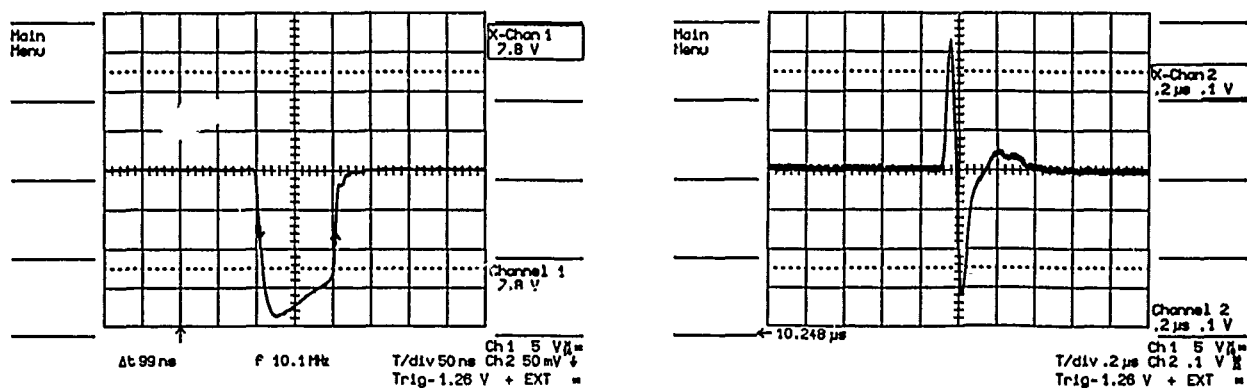


Figure 2a : Sensor excitation signal (50 ohms) Figure 2b : Relay echo ultrasonic signal

The sensor is installed in a support providing local coupling by a film of water (the sensor is not in direct contact with the part) which allows initiation of measurements and inspection of a perfect coupling. Water is fed by means of a valve which opens when it is applied to the part to be inspected.

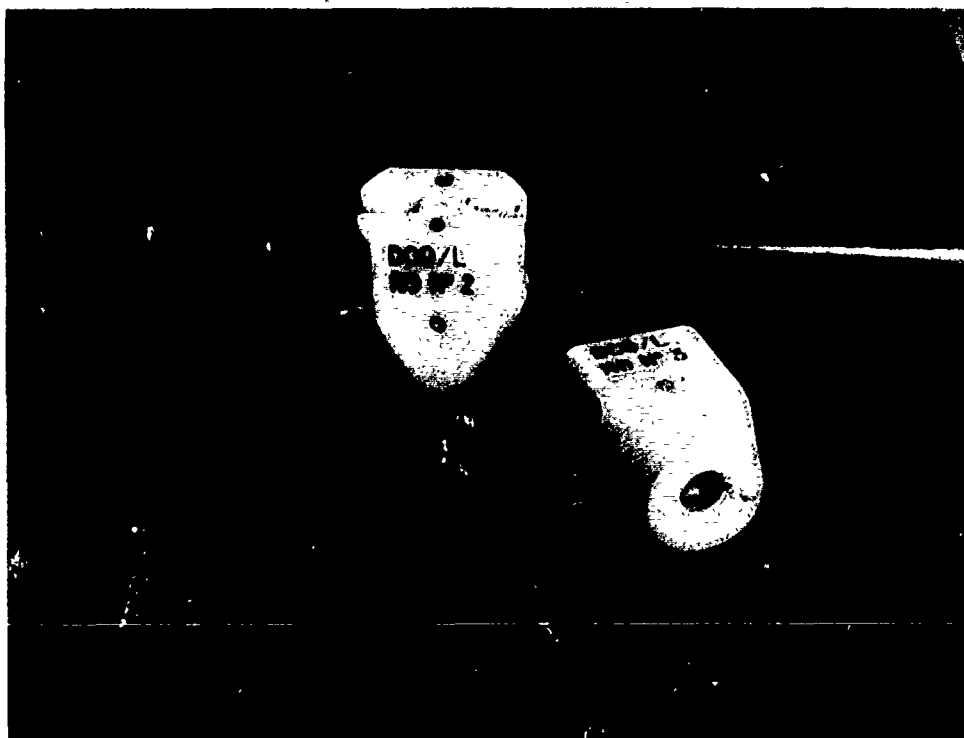


Figure 3 : Sensor and sensor holder

(b) The mechanical device (figure 4)

The mechanical device provides sensor position in polar coordinates (hence the name R-theta) using two sensors :

- an angle sensor (accuracy : 1 milliradian)
- an incremental sensor based on the magnetostriction phenomena : torsional deformation undergone by a magnetic material when subjected to an abrupt magnetic field variation (magnets are in the tactile sensor holder).

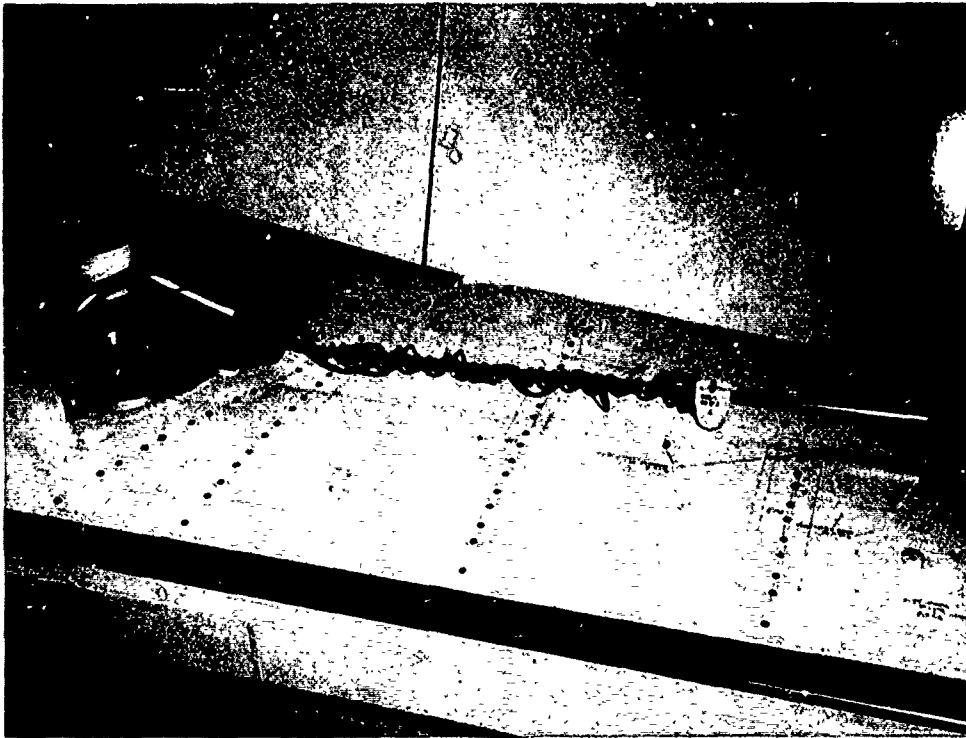


Figure 4 : Mechanical device for locating the sensor position in polar coordinates

This position sensor operates up to displacement speeds of 50 m/sec and provides an accuracy of 1/10 of a millimeter. The assembly is installed on a pivot which also provides vertical displacement of the order of 20 degrees. A vacuum suction cup enables the device to be secured in a vertical, horizontal or oblique position. The total weight of the assembly is about 4 kg. The scanned area is 640 x 400 mm which corresponds to a maximum definition of 1 x 1 mm for one screen pixel. The advantage of such a system is that it provides a guide permitting more methodical scanning, and thus time saving in the mapping as compared to contactless sensor type devices (acoustic triangulation).

(c) Ancillary equipment

Housed in the same rack is the 40 litre water tank, the water pumps and the vacuum pumps for the attaching suction cup.

(d) Hardware section (figure 5)

The characteristics of the transmitter-receiver-preamplifier card are as follows :

- excitation pulse width adjustable from 30 to 640 msec in steps of 5 msec,
- fall time : 6 msec,
- voltage adjustable from 30 to 250 V/30 V,
- receiver passband : 0.5 to 100 MHz,
- general gain from 0 to 40 dB.

A signal processing card (variable gain) provides in addition a total dynamic range of 45 dB. These are 4096 gain segments with a duration of 100 msec. These curves are stored in memory from measurements on standard parts.



Figure 5 : Upper part : microprocessor and screen
Lower part : ancillary equipment

Finally, the digitizing card which operates according to two principles.

- Sampling is initiated by the maximum levels of the input signals which permits the characteristic values of the echoes (amplitude and time) to be stored in memory and used for map representation. The maximum sampling frequency is 34 MHz.
- Sampling is initiated by a shifted time base permitting an A-scan display up to a virtual frequency of 200 MHz (basic frequency 25 MHz) over 256 points.

(e) Software

The software makes use of a linked menu screen presentation. A main menu provides access to sub-menus enabling the various parameters required for mapping to be programmed.

Mapping is accomplished using the distances or amplitudes acquired and results in an eight colour representation of the various thicknesses (or amplitudes) measured. A depth zone is assigned to each colour (for example : 8 plies = red, 12 plies = green).

Each depth zone of this scale of colours can be expanded or compressed to produce a zoom effect. A flashing cursor indicates the position of the ultrasonic sensor in the area explored. A coupling error (or incorrect measurement) does not affect the mapping or measurement file.

Changing over from the distance representation to that of amplitude and vice versa is accomplished by simply pressing a key. During a mapping operation, the operator at any time has the possibility of displaying an A-scan representation (oscilloscope) in order to check the validity of measurements.

All the acquired data are stored in a measurement file in a read/write memory.

It is possible to store this file on a hard disk and recall it subsequently for processing.

One pixel displayed on the screen represents an area of 1 x 1 mm. The maximum area which can be inspected has been set to 640 x 400 mm.

It is possible to change the vertical or horizontal dimensions of the acquisition zone (1, 3, 5, 7 mm) in order to locate a defect in the part to be inspected, by a rapid 7 x 7 mm scan. Once the defect is located, it is possible to detect its shape more accurately by selecting a 1 x 1 mm resolution.

3. RESULTS

Figure 6a, 6b shows A-scan representations of an ultrasonic sequence performed on a sound composite consisting of 33 and 66 plies using the DAC curve.

Figure 7 shows distance mapping of a self-stiffened standard part with a thickness varying between 16 and 65 plies and having porosities or delaminations at various depths.

The time required to obtain this mapping is of the order of 10 minutes, at a screen resolution of 3 x 3 mm.

Processing software is then used to perform a ply-by-ply analysis in order to visualize the exact position of the defects in the part.

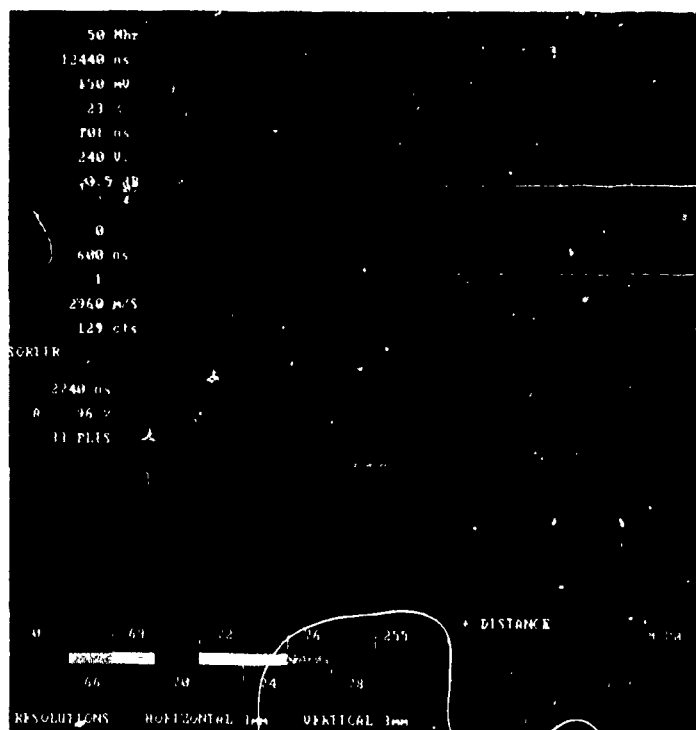


Figure 6a : A-scan representation on a 33 ply composite material

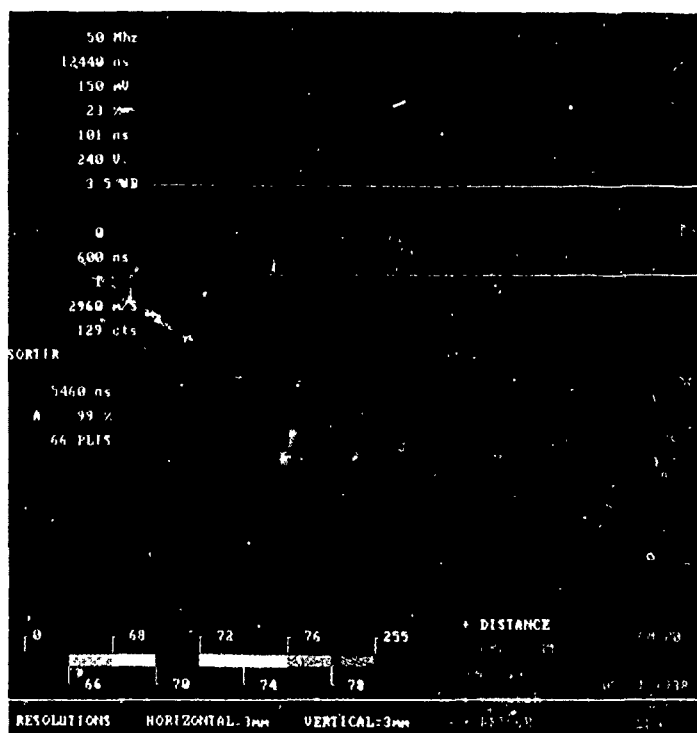


Figure 6b : A-scan representation on a 66 ply composite material



Figure 7 : Distance mapping on a standard part

4. CONCLUSIONS

The prototype system proved entirely satisfactory from the ultrasonics and utilization point of view. It was thus possible to inspect composite components (wings, fins, tailplanes).

The simultaneous amplitude-distance operating capability makes it possible to overcome to a large extent the problems posed by variable thicknesses (reinforcements - stiffeners).

The most serious problems now concern exact knowledge of the manufacturing drawings of parts and possible exceptions which make it necessary to provide interconnections of the R-theta inspection system with manufacturing test files obtained from computer-aided design and manufacture.

A SIAM system dedicated to inspection during manufacture already operates according to this principle. Diagnostics are then performed by comparing the measurements with the standard files of sound or theoretical parts. This configuration provides for great rapidity and ease of operation in areas which are sometimes complex.

The SIAM R-theta system will therefore evolve with this end in view.

USE OF ACOUSTIC EMISSION FOR CONTINUOUS SURVEILLANCE OF AIRCRAFT STRUCTURES

by

M. Nabil Bassim, Professor of Mechanical Engineering
University of Manitoba, Winnipeg, Manitoba
Canada, R3T 2N2

SUMMARY

Since its inception as a technique of nondestructive evaluation, acoustic emission has held great promise for its ability to provide monitoring of structures on a continuing basis. Equipment development, however, has emphasized periodic testing and a lack of adaptation to the specific conditions of a given structure, such as aircraft, in terms of operating conditions, noise, vibration....etc. Because of these factors, the use of acoustic emission for continuous monitoring of aircraft structures has been lacking. Recently, the author of the present paper has approached the problem from two angles. Firstly, he has developed a predictive approach for using acoustic emission to monitor fracture and fatigue of materials. In this approach, the relationship between acoustic emission and fatigue life (expressed as stress intensity factor or the number of cycles to failure) is defined both theoretically and experimentally. It is then possible, using techniques of dynamic pattern recognition, to obtain the status of a structure with respect to its remaining life. Acoustic emission maps for different materials failing by fatigue are produced. Secondly, he has patented a new acoustic emission system which relies on using intelligence and expert system software, as well as "rules" for defining fatigue damage. The combination of these two approaches produces a significant development in using acoustic emission for continuous monitoring of aircraft and other structures and fulfills the promise held by AE in that direction.

INTRODUCTION

Acoustic emission, which describes the method of detection of propagating stress waves in a material or a structure due to application of a load, has gained importance in the past two decades as a method of nondestructive evaluation. The occurrence of acoustic emission is due to the release of elastic energy when the material undergoes plastic deformation or when a crack is initiated or propagates in the material.

The present state of knowledge in acoustic emission parallels that what was experienced with ultrasonic testing when it started over fifty years ago. Thus, research in understanding the phenomenon has concentrated on three major topics (I) understanding the microscopic (and atomic) nature of the source, (II) determining the role of structure geometry on the propagation of the emission from the source to the transducer and (III) investigating the effect that the transducer and the electronic equipment has on the final observed signal.

Together with these studies, relationships on the behavior of different materials subjected to loadings varying from monotonic tensile loadings to fracture and fatigue loading of precracked specimens have been established. A summary of these studies is included in Reference 1.

What distinguishes acoustic emission from other nondestructive testing techniques and establishes its potential for use as the physical phenomena which can be monitored in continuous surveillance systems is the fact that it is passive. Thus, when a loading causes the emissions to occur, they propagate to a transducer (sensor) located at a fixed position on the structure. Compared to ultrasonics, there is no need for scanning the structure with a transducer to detect the defects present. The transducer can be left for a long time in a particular location and it would wait for the events to occur. Furthermore, because of this characteristic property of acoustic emission, several transducers can be positioned on the structure and the different times of arrival to these various transducers used to locate the source of the emission [2, 3].

The conventional acoustic emission system, shown pictorially in Fig. 1, can operate in the time and/or frequency domain to determine characteristic signal parameters such as total count, count rate, peak amplitude, risetime, pulse duration, root mean square of the amplitude (rms), energy....etc. in the time domain. In the frequency domain, the system can effect a Fourier transform to determine the power and frequency spectra. Further post test analysis include auto and cross correlation and triangulation to determine the location of the emitting source.

The conventional system can be equipped with a microprocessor (computer) for data acquisition and analysis. Also, for storage of signals, analog recorders were used and presently, storage on diskettes using a digital oscilloscope is performed.

The conventional acoustic emission system, as with all other NDE devices, relies heavily on the presence of a skilled operator for setting up and running the test. More importantly than other NDE methods, this operator is required to make judgements in interpretation of the data (on-line or post test analysis). This is a major consideration in the success of acoustic emission as a means of evaluation of the performance of structures on a continuous basis. Another consideration is the limited capacity of the equipment to handle large amounts of data making the use of acoustic emission periodic in nature.

APPLICATION OF ARTIFICIAL INTELLIGENCE TO ACOUSTIC EMISSION

The trend in computer technology is presently towards using the computer to replace human intelligence in solving problems where decisions have to be made. The definition of artificial intelligence (AI) is [4]: "An area of computer science that uses models of human reasoning to solve problems. The problems have enough elements of uncertainty to preclude use of specific algorithms". While the whole area of research in AI is at a young stage, it lends itself to the field of acoustic emission testing.

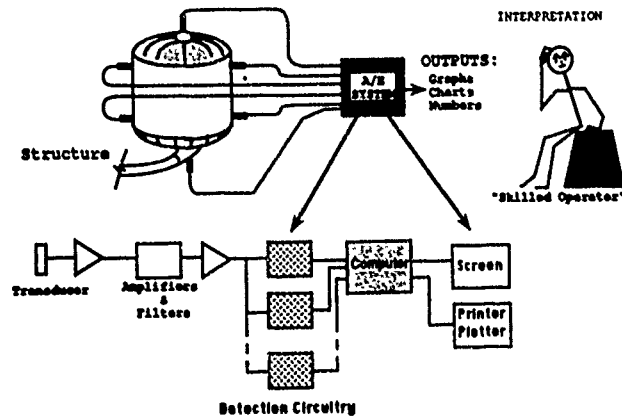


Fig. 1. Representation of a conventional system.

Referring to the skilled operator in Fig. 1, his (her) knowledge of acoustic emission allows him/her in the first instance to interpret what he sees on the screen of an oscilloscope and to determine that what he is seeing appears like acoustic emission signals.

For an operator who has no knowledge of acoustic emission, the series of signals shown in Fig. 2 have no particular significance. He would not be able to determine that the signals in line (e) look like acoustic emission signals compared to lines a (sine wave), b (triangular wave), c (square) and d (white noise).

The first skill of the operator is then to identify that signals like those in line (e) are important (they look like acoustic emission signals: fast risetime, almost sinusoidal decay, peak amplitude...etc.). He would know that they are AE signals because he may have seen them before in a controlled laboratory experiment or from a book or a paper.

The role of the skilled operator is not limited to just identifying AE signals from other dissimilar signals (even though this is his most important role), he has to relate what he sees on the screen to what the electronic equipment at his disposal "reads" as far as characteristics such as counts, events,etc. Also, he is required to distinguish between various shapes of emissions which are present in a complex test, including background noise, machine noise, artifacts such as shown in a fatigue test in Fig. 3. The measured results, using the electronic instrumentation, is meaningless if the skilled operator is not able to interpret his observations or if he cannot distinguish between real acoustic emissions from either signal-like emissions and background noise.

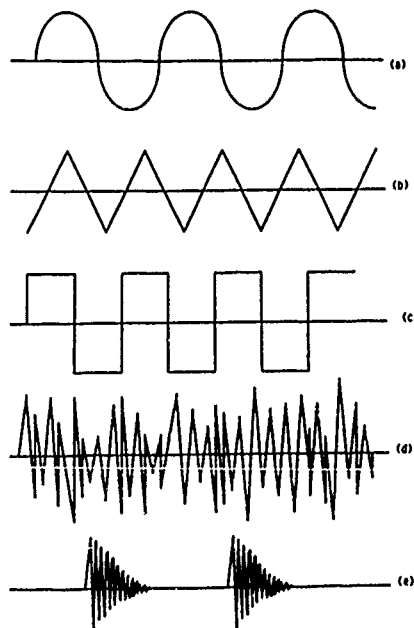


Fig. 2. Different types of signals (a) sine wave (b) triangular (c) square (d) white noise and (e) typical acoustic emission signal.

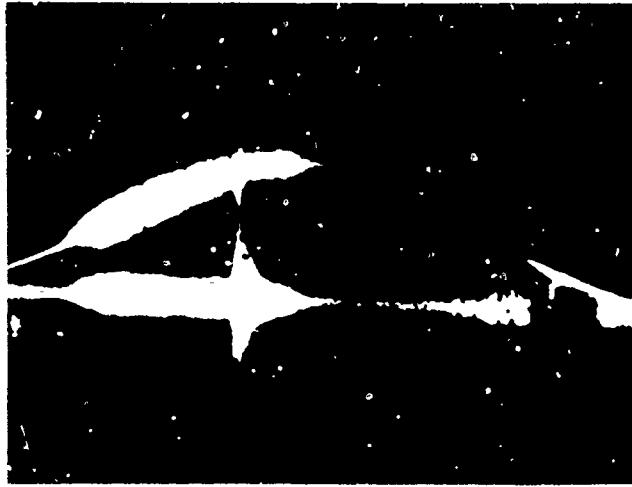


Fig. 3. Real acoustic emission obtained in the ascending part of a fatigue cycle.

It is interesting to note the following: (I) that a skilled operator relies exclusively on his human sense of vision (sight) to effect this analysis (discrimination). (II) in normal conditions in a test, he is allowed to make minor mistakes or errors of judgement in interpretation of the signals from a periodic test, (III) the human brain of the operator does not process the signal which he sees numerically, but that a natural logic is applied intuitively to identify the signals and make decisions and. (IV) counting and analyzing the signals with electronic instrumentation is a step which follows the identifying process which the operator applies mentally.

The development of a system which does not rely on the presence of a human skilled operator and thus is able to perform continuously the monitoring of acoustic emission in structures has thus to take into consideration the above arguments. The most difficult of these arguments is that replacing a skilled operator by a computer requires, firstly, processing the signals logically while computers are geared for numerical processing, and secondly, requires the elimination of the human vision sense so that the computer "sees" the signal and processes it logically. After this, counting and trending, which is performed by conventional systems, will be implemented.

The problem then is to represent an acoustic emission signal to the computer. The first step is to describe acoustic emission signals to the computer in a language which it understands (and does not use vision to see). The approach used here is of "windows" where the composite picture of the signals is given in terms of limits that parameters should have to describe a valid signal. The parameter windows are basically the risetime, the peak amplitude (adjusted for gain), the total duration of the signal, and the energy or RMS of the envelope of the signals. These limits are shown in Fig. 4 (which does not resemble a signal as we know it). Any signal which will agree with these limits will be a good signal (accepted) and any signal which does not agree with these limits is a bad signal (rejected). The limits are adjusted using a calibration procedure (basically, they fit the decisions of the skilled operator). Accepted signals are next counted and analyzed to detect whatever trends which are required in a specific situation (fatigue, corrosion, leaks...etc.). The algorithms of the computer in this part are implemented using the specific cases of the structure (geometry, material, crack length).

THE NEW ACOUSTIC EMISSION SYSTEM

The new acoustic emission system, has been patented by the author of this presentation (U.S. Patent 4609994 and Canadian Patent 1224867). It addresses the analysis described earlier and thus takes acoustic emission into the realm of use for continuous monitoring of large structures. The details of the system have been described earlier [5,6] and will be further discussed here briefly.

The configuration of the system is shown in Fig. 5. It consists of surveillance units which, in effect, are smart sensors equipped with a microprocessor and which are software operated. These surveillance units are positioned on the structure and accept all the signals (and noise and signal-like emissions). They analyze the signals logically by extracting relevant parameters and comparing these parameters within the windows previously established. Further, they analyze the signals to detect patterns of behavior which have been established as signs for failure.

The surveillance units are linked to a central Control Unit which is basically a dedicated computer capable of monitoring the performance of each of the surveillance units, programming each individual surveillance unit, trend analysis, diagnostic checking of the surveillance units, analyzing the data to obtain "Performance vs Time" information about the structure, and finally, communication and networking of all the surveillance and control units.

The new system is programmed for a given structure (aircraft, bridges, pipelines, offshore rigs, nuclear reactors, pressure vessels, . . . etc.) and can handle the data on a continuous basis. The system, as it is configured in a distributed-tiered approach, allows continuous monitoring of structures without the need of a skilled operator. A pictorial drawing of the new system is shown in Fig. 6.

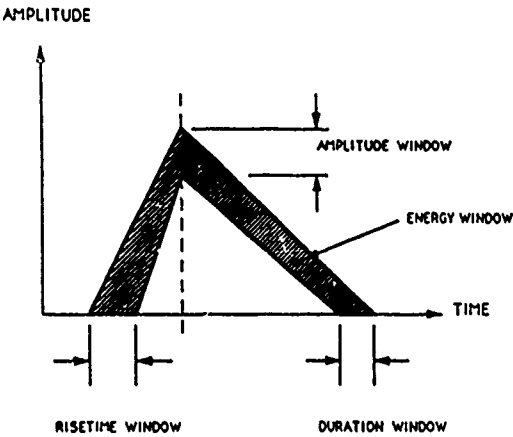


Fig. 4. Artificial intelligence approach to identification of acoustic emission signal.

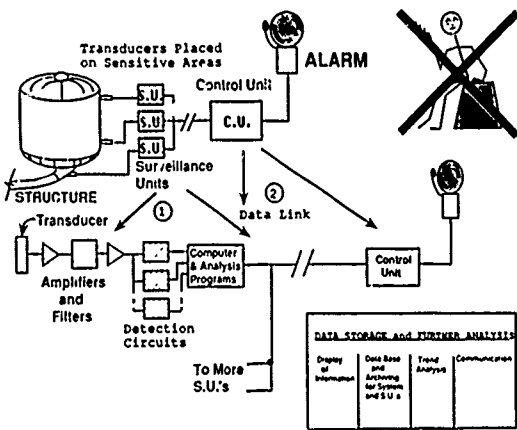


Fig. 5. Configuration of the new distributed system.

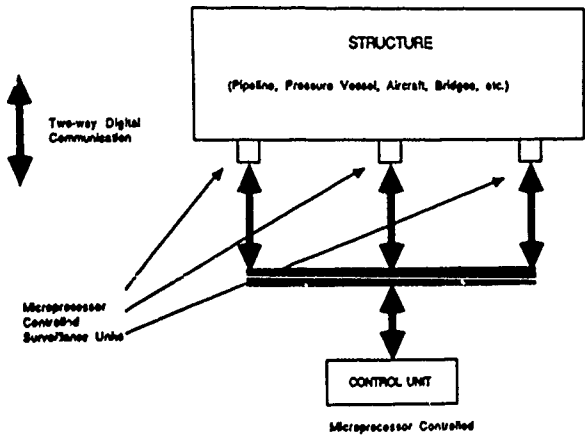


Fig. 6. Representation of the distributed system.

EXAMPLE OF APPLICATION: FATIGUE

Fatigue, which claims over 90% of the failure of structures in service, is a suitable candidate for demonstration of the AI approach. While numerous studies have been performed on characterization of AE from materials subjected to fatigue loading, the transportation of these results to large structures has generally been lacking.

Fatigue studies are generally classified in terms of crack initiation or crack propagation. If we concentrate on crack propagation, we notice that a crack with subcritical crack length grows to reach a length such that the remaining ligament of material cannot withstand the applied stress. This leads to final fracture.

Plot of the rate of progress of a crack as a function of time (or number of cycles) $\frac{da}{dN}$ versus the stress intensity factor $\Delta k = -\Delta\sigma\sqrt{\pi a}$ where $\Delta\sigma$ is the applied stress gives a curve characterized by three stages, the most important of which is Stage II which is linear, when $\frac{da}{dN}$ and k are on a logarithmic scale. This is Paris Law of fatigue crack growth and is given as

$$\frac{da}{dN} = A (\Delta K)^\alpha \quad (1)$$

where A and α are constants and characterize the behavior of materials or alloys such as steels or aluminum alloys generally varies between 2 and 6 for most materials.

In numerous studies [7], it was found that a similar relationship exists between an acoustic emission parameter, namely, count rate N' and ΔK :

$$N' = B (\Delta K)^\beta \quad (2)$$

Furthermore, there are direct relationships between α and β [8], such that β may only be equal to α or $\alpha + 2$ depending on the material and on the type of fatigue loading imposed (tension-compression or tension-tension). Thus, it is possible to develop a predictive approach to determine quantitatively the extent of fatigue damage, and the remaining life of the structure, using acoustic emission monitoring.

The general representation of the variation of any acoustic emission parameter as a function of time, material, stress, and structure geometry is shown in Fig. 7 and can be expressed mathematically as

$$P(N) = (t, \sigma, \text{material, geometry}).$$

For a given material and geometry (e.g. aluminum alloy in the shape of an aircraft wing), this equation reduces to Equation 2.

It is noticed in Fig. 7 that, with acoustic emission, there is a certain element of randomness in the parameter $P(N)$ at a given t . Thus, to establish and follow Equations 2 or 3, it is required to average out the behavior at time t_1 , and at subsequent t_2, t_3, \dots . This is the equivalent of applying dynamic pattern recognition techniques [9].

This process, now performed in the surveillance of signals which have been accepted using AI concepts allows accurate, quantitative determination of fatigue in large structures from trending of acoustic emission parameters. This confirms the scope of the approach to use acoustic emission as a passive technique for monitoring.

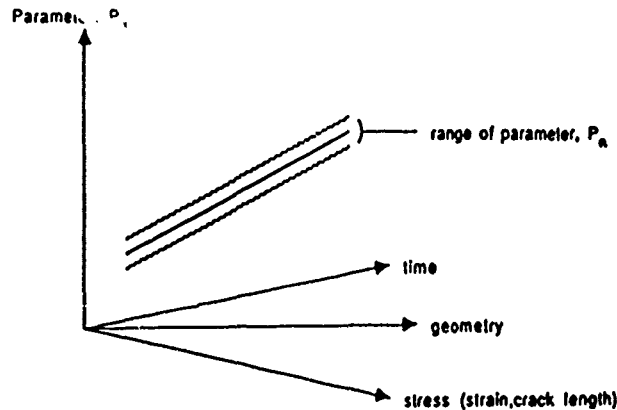


Fig. 7. Variation of a signal parameters $P[N]$ with time, material, geometry and stress in a fatigue curve.

ACKNOWLEDGEMENT

This project has been in progress since 1981. Several sponsors including Petro Canada, Ontario Hydro, Viatex Resources, the Canadian Natural Sciences and Engineering Research Council, the University of Manitoba, and more recently, the National Research Council of Canada through an IRAP program are responsible for this development.

REFERENCES

- 1) Handbook of Nondestructive Testing: Acoustic Emission, ASNT (1988).
- 2) N. Chretien, Bulletin d'Informations Scientifiques et Techniques, Commissariat a l'Energie Atomique, No. 211, 85 (1976).
- 3) B.F. Cron and C.H. Sherman, J. Acoustical Soc. Am., 34, 1732 (1962).
- 4) "Artificial Intelligence, A Personal, Commonsense Journey" by W.R. Arnold and J.S. Bowie, Prentice-Hall, (1986).
- 5) M.N. Bassim, in Proceedings of 10th World Conference on Nondestructive Testing, Las Vegas (1985) pp. 91-99.
- 6) M.N. Bassim, Materials Evaluation, Feb. (1988) pp. 49-51.
- 7) M.N. Bassim, in Handbook of Nondestructive Testing: Acoustic Emission, ASNT (1988).
- 8) M.N. Bassim, Journal of Acoustic Emission (1985) S224-S228.
- 9) M.N. Bassim and W.J. Pedrycz, Journal of Acoustic Emission (1988) submitted for publication.

Specialist Comments
Applied Point of View

Thomas D. Cooper
Chief, Materials Integrity Branch
Systems Support Division
Materials Laboratory
Wright Research and Development Center
Wright-Patterson AFB, Ohio 45433-6533
USA

Thank you, Mr Chairman. It is indeed a pleasure and a distinct honor to have been invited to serve as a Rapporteur for this Specialist's Meeting. It was, of course, necessary for me to establish clearly in my own mind just exactly what was expected of me in my official role as Rapporteur. The only help I was able to obtain was from my Webster's New Collegiate Dictionary, which defines a Rapporteur (Fig. 1) as one that "gives reports (as at a meeting of a learned society)." The latter part of that definition certainly is appropriate for this distinguished gathering. I must admit, however, that I may stray somewhat from the traditional role of a reporter, who normally only reports the facts as presented, because I will surely start presenting some of my own opinions mixed in with the facts.

The discussion I have planned (Fig. 2) will include some introductory comments, and then a presentation of what I consider to be the most important issues that have appeared as a result of the papers prepared and the presentations given during the course of the meeting. I will then end my report with a summary and concluding remarks.

I would like to begin (Fig. 3) by thanking the Organizing Group of the Structures and Materials Panel of AGARD for recognizing the growing importance of the NDE area and allowing this meeting to occur. Dr Bill Wallace from Canada is particularly to be acknowledged for all his efforts in working the many details necessary to bring us together.

Professor Bond and I have agreed that we will divide the technical content of the meeting into the applied or near term applications aspects, which I will cover and the fundamental or longer term research aspects, which he will address. We agreed to this at a brief strategy meeting held in London in May of this year, but since we have not had the opportunity to meet since then, I think that it is fair to assume that there will likely be some overlap in our comments. We hope that our overlaps do not turn out to be disagreements, however.

Sometimes it is interesting at the outset to take a step back and look at the overall content of a technical program. Assuming that the selection of presentations made by the organizing committee basically reflects the total efforts underway in the various NATO countries, such a breakdown can be informative as to what are recognized as the current major problems or areas of concern and where the important opportunities are seen to exist. Figure 4 reflects such an analysis which I made, along with some assistance from my staff. Recognizing that some perhaps arbitrary decisions were made and that some papers fit into more than one category, it is seen that of the 25 papers that discussed specific techniques or methods, they were fairly evenly divided between conventional techniques and advanced techniques, which I consider to be a very healthy and well balanced program. The one type of material that obviously attracted the most attention was composite materials (13 papers). Ten papers addressed in-service inspection of hardware, five made at least some reference to the reliability of the inspection methods, which I thought was disappointingly low, as was the apparent lack of interest in the inspection of gas turbine engine components. I will have more to say on some of these topics later.

In reviewing the papers that were available prior to the meeting and listening to the presentations, there were five major issues that attracted my attention from the applied point of view. These are listed in Fig. 5. While there were many interesting aspects of applied NDE brought out in the conference and I would like to acknowledge all the excellent points made by the authors, I am forced by the limited time available to focus my comments on these topics, admittedly arbitrarily selected.

Composite Materials Inspection. There was obviously a very high level of interest in composite materials inspection (Fig. 6) since fully half of the papers addressed that subject in one way or another. It reflects the fact that most new major systems are incorporating these materials in their design and construction. After reading the papers and listening to the presentations, however, I feel that the NDE communities in other countries are reacting in a manner similar to the US community in that inspection methods are being developed under pressure from the users to detect certain types of flaws with little or no guidance concerning the sizes of the particular defect that must be detected in order to protect the safety of the structure. Generally, specific quantitative inspection criteria were not mentioned in the papers and I assume that the criteria actually in use are

workmanship in nature, i.e. how well can the materials be fabricated as opposed to how well must they be fabricated. Ultrasonic inspection was the favored method being developed with significant progress being demonstrated in systems that will allow on-aircraft inspection to be conducted. The ARIS system in the US, the system being developed by DREP in Canada and the Aerospatiale system in France have already been demonstrated on aircraft in a hanger environment while prototype systems being developed by CASA in Spain and Aeritalia in Italy have been applied to composite structural components. Although there are some differences in the systems, particularly in the method being used to determine the spatial location of the transducer, it would seem that development of additional systems intended to provide a field-generated C-scan of composite components will result in unnecessary proliferation of equipment at a time when the resources could be better utilized elsewhere. Other similar systems are being developed that were not reported upon at this conference. Therefore, those who feel the necessity of having such a system would be well advised to shop in the marketplace before undertaking costly development programs. In fact, the ARIS system, as described by Tracy, Hardy and Fechek may well provide Lt Stoermer of the German Air Force, with most of the demanding capabilities that he described. Infrared thermography was presented in the paper by Tretout and Marin as a method suitable for use both in manufacturing inspection and for in-service inspection. While the approach apparently offers some significant potential for easy application and rapid scanning, the data presented raises questions about the sensitivity of the method. Finally, the paper by Roy, Maslouhi and El Ghorba proposed acoustic emission, combined with artificial intelligence technology, as a method for monitoring a structure. However, based on the information presented, it would seem to be a topic better addressed by Professor Bond.

Another very important aspect of composite materials technology that received attention was the question of the detection of impact damage, primarily because of the insidious nature of this mode, where little or no outward evidence of damage may be visible. Once again, there seems to be a difference of opinion as to whether non-visible or barely visible damage can endanger the integrity of the structure. A very interesting and unique optical approach is proposed by Komorowski, Gould and Pastorius that can detect the "barely visible" type of impact, if such detection is necessary. That is a system that may well merit additional evaluation. Ultrasonic methods were also proposed for this problem.

While several of the papers discussed the applicability of their method for use in the field, essentially all of the examples, with perhaps three exceptions, (US, Canada and France), were for demonstration purposes only. This strongly suggests that while there is significant momentum to develop such methods, little actual field use is being made of the systems. This means that either conventional inspection methods, which are accepted as being woefully inadequate, are being applied to those composite structures which are already in the field, or that no field inspection is currently being conducted.

Damage Tolerant Design. One of the major differences between the various countries that has emerged very clearly as a result of this conference (Fig. 7) is the extent to which damage tolerant design is being used. This was also apparent from the earlier workshop. While the NDE community in itself may have little or no control or influence over the decision to use such an approach, the impact once it is invoked is dramatic. It results not only in greatly increased pressure to develop more sensitive inspection methods to limit the size of flaw that can go undetected during a manufacturing or depot inspection, but requires that the reliability of the methods be clearly established. During the course of the Specialist's Meeting, very few presentations addressed the subjects of damage tolerant design or demonstrating inspection reliability on a statistical basis, and those were from the US and the UK, including one collaborative paper dealing with qualification of engine components. As noted in the paper by Taylor, Cooper and Vukelich, in the US, damage tolerant design is one of the key elements of the Structural Integrity Programs that the US Air Force has adopted as the keystone for increasing the reliability and safety of its systems. It has been incorporated in the design of airframes since the early 70's and has been applied to gas turbine engines for the past ten years. Aircraft and engines that were not designed to these requirements have all had after-the-fact analyses completed to allow them to be maintained in a similar manner. Application of this technology has not occurred in the European countries yet. Consequently, the development of the NDE technology required to support this approach has not been undertaken. Future activities in the US may impact that, however, since, as Mr Taylor reported, the Federal Aviation Administration (FAA) in the US is considering establishing a Commercial Aircraft Structural Integrity Program in response to the aging airliner problem that is now facing the commercial aviation community of the world. That, of course, would effect all countries as well.

As these new requirements evolve and as more joint efforts are developed between US and European engine and aircraft companies, the time will surely come when everyone will have to satisfy some form of structural integrity program requirements. It, therefore, seems prudent to start jointly developing the inspection procedures and demonstration protocols that will be required. The paper by Rummel provides an excellent overview of the considerations involved in assessing and demonstrating

inspection capabilities, while the paper by Taylor, Cooper and Vukelich recommends that a common AGARD approach be considered at least for the analytical methodology, based upon a draft Military Standard being prepared by the US Air Force. That would be one very positive action that could result from this meeting.

Engine Component Inspection. One of the surprising and perhaps disappointing aspects of the Meeting (Fig. 8) was relatively the little attention that was given in the Specialist's Meeting to the application of NDE to gas turbine engine components. The critical nature of many of these parts, particularly because of the catastrophic results of a failure, demands that the best NDE technology be applied to their manufacturing and service inspection. Moreover, since many of the shapes lend themselves to rotational inspection, they are ideally suited for automated inspection techniques that allow the development of inspection systems that can be made essentially independent of operator influence, greatly increasing the reliability of the inspection. The paper by Rasmussen, Pohlenz and Hoeffel illustrated that point very effectively. It has to be assumed that much more technology is being developed for these applications than was reflected by the content of the meeting. For reasons previously mentioned, the application of damage tolerance design and structural integrity life management will certainly put more pressure on the development of appropriate inspection technology for this area.

As was pointed out in the RAF overview paper by Dalziel, new materials are being introduced for advanced engine applications that will further challenge the inspection community. Such materials as thermal barrier coatings to help handle high heat flux on blades, advanced ceramic materials which border on being absolutely brittle in behavior and therefore intolerant of even the smallest flaws, carbon/carbon composites, powder metallurgy components, intermetallics and ceramic fiber/inter-metallic matrix composites are all on the horizon for application in advanced engines. Some of the new inspection technology reported upon during the meeting will undoubtedly be useful for these inspection requirements and hopefully will be reported upon during the next Specialist's Meeting.

Application of New/Improved Methods (Fig 9). Computed Tomography (CT) - The outstanding advances being made in CT technology were presented by Moran. This new technique has been implemented into both production and service use, with a large boost from the medical technology field. It is an excellent example of a method that is complementary to existing methods as well as one that is quantitative.

Acoustic Emission (AE) - AE is still struggling for implementation as a monitor for in-service aircraft structures. In spite of many efforts over many years, this method continues to fall into the regime of requiring still additional long-range fundamental efforts if it is to overcome its shortcomings for real in-service monitoring of critical structural elements in aerospace hardware. These shortcomings include extremely low amplitude signals from crack extensions and a low quantity of signals from the "safe" or stable crack growth portion of a structure's life. A number of papers were presented on work in this area. I am sure that Professor Bond will consider this work and its status.

Eddy Current (EC) - A highly sophisticated and fully automated application of this technique was presented by Rasmussen, Pohlenz and Hoeffel. The program described in the paper has conducted a full scale assault on the signal-to-noise ratio problem with impressive victories as a result. The paper by Tietze outlined advances in instrumentation with a wide range of illustrative applications to demonstrate the continuing potential of this mature but very versatile technique. Harrison's progress at RAE in developing the Eddy Scan system for detecting cracks under installed fasteners continues to show promise. Many are looking forward to being able to obtain an engineered system by an equipment manufacturer based upon his work to determine its effectiveness.

Radiography - Neutron radiography. This is another technique that has become an applied and relied upon NDE tool. The paper by Mast and Schutz discussed both potential applications and a potential solution to the major hindrance to this method - the low flux levels of thermal neutrons from most currently available neutron sources.

Stenoptic radiography - If you think neutron radiography has a problem with low flux levels at the detector, consider this technique! Obviously this technique of imaging with back-scattered radiation is still in the stage of long-range fundamental efforts and it will be some time before practical applications are seen. I will leave further observations to Prof Bond.

Real-time Radiography - Although this technique (with x-ray radiation) was only mentioned in passing in one paper, it has become a standard technique in both the manufacturing and in-service inspection arenas. While it has yet to demonstrate either the spatial resolution or the contrast sensitivity routinely available with film radiography, the versatility of the technique coupled with applications where high spatial resolution or contrast is not a requirement has made this a widely used tool, both in the US and Europe. I am somewhat surprised that it did not receive more attention.

Infrared - Tretout and Marin presented a completed package on thermal inspection as applied to composites, starting with the basics, a model of the physical process, and then specific applications. Heyman and Winfree continue this approach in their paper. Infrared, once touted about 25 years ago as the greatest development of mankind's since sliced bread, finally is being successfully introduced, although somewhat cautiously, in both production and in-service usage. The technique discussed by Ringermacher can be viewed at least partially as a thermal technique and is an excellent example of what advances in this area hold as a promise. It is another area, however, that needs additional longer range research.

Optical - The only serious discussion is the paper by Komorowski, Gould and Pastorius for the detection of surface deformation (i.e. impact sites). Noticeably absent is discussion of holographic techniques of any nature. Perhaps the glamour has worn off in the light of practical realities.

Artificial Intelligence (AI) - This was discussed in several papers, almost as a panacea for advancing the usability of a technique such as acoustic emission in the absence of a sound theoretical base. Obviously, this is a tool for the future, and of uncertain potential usefulness. Once again, I am sure that Prof Bond will have much more to say on this topic.

Adhesive Bond Inspection (Fig 10). The old problem of evaluating the adequacy of bond strength, either adhesive or cohesive, is still with us and has yet to yield to a solution via nondestructive evaluation methods. Only the paper by Fahr and Tanary confined itself to this subject and it certainly does not offer promise of an effective solution in the near future. There certainly is no argument that areas of zero bond strength (disbonds) can be readily detected with a variety of methods. It is those areas with strength between zero and that which is required that pose the challenge. This problem has been in existence for so long that one starts to wonder if a solution is necessary.

SUMMARY AND CONCLUSIONS (Fig 11). Considering the Applications side of the Meeting, the following comments are offered:

- There was a very strong emphasis in the meeting on the inspection of composite materials, still with only a bare minimum of clearly defined, quantitative inspection requirements.

- Efforts to support Structural Integrity are limited to the US. We heard early in the week, the alternative approach - "process control" - which is a somewhat vague phrase not defined in quantitative terms. It requires heavy emphasis on NDE at the outset, followed by careful control of all processes that could lead to the introduction of flaws. The biggest question is whether such an approach can be made sufficiently reliable for critical parts.

- Quantitative NDE is a firm requirement for the application of Structural Integrity in design or even for the use of damage tolerance. An opportunity was identified for a cooperative effort under AGARD to all countries to participate in the development of a consensus document that would define standard procedures and analytical methods to be used for qualifying inspection processes on a quantitative basis.

- Engine component inspection was given relatively little attention during the meeting. There are many new complex and high temperature materials being developed that will require concerted effort for the development of acceptable, reliable inspection methods.

- Of the new techniques discussed during the meeting, CT is the only one that stands out as being sufficiently mature to be used in real applications. Other new ones show promise, but are not yet ready to be applied.

- The measurement of adhesive bond strength by nondestructive methods still has not been achieved. It should continue to be a research objective.

Finally, I would judge this Specialist Meeting to have been an outstanding success. It is not possible to measure success just by the number of papers included or the elegance of their presentation. What also counts greatly is the personal contact that occurs during the breaks and at lunch time. The interesting mix of representatives from government and industry from such a significant number of countries is further evidence that the subject of the meeting is of great importance. I know that we will all take home not just new information, new thoughts and new ideas, but many new friendships as well.

LIST OF FIGURES

- Figure 1 : RAPPORTEUR - One that gives Reports (as at a Meeting of a Learned Society)
- Figure 2 : DISCUSSION - I. Introduction/Background
 II. Discussion of Issues
 III. Summary of Discussions
- Figure 3 : INTRODUCTION/BACKGROUND
- Acknowledgements
- Plan for Session
- Emphasis of Meeting
- Issues
- Figure 4 : EMPHASIS OF MEETING - Subject
- | | <u>Nr of Papers</u> |
|-----------------------------|---------------------|
| NDE Techniques | 25 |
| - Conventional | 15 |
| - Advanced | 19 |
| Composite Inspection | 13 |
| In-Service NDE | 10 |
| NDE Reliability | 5 |
| Engine Component Inspection | 5 |
| Artificial Intelligence | 4 |
- Figure 5 : ISSUES
- Composite Materials Inspection
- Damage Tolerant Design
- Engine Component Inspection
- Application of New/Improved Methods
- Adhesive Bond Inspection
- Figure 6 : COMPOSITE MATERIALS INSPECTION
- High Level of Interest
- Inspection Criteria
- Equipment Proliferation
- Impact Damage
- Service Experience

LIST OF FIGURES (Continued)Figure 7 : DAMAGE TOLERANT DESIGN (STRUCTURAL INTEGRITY)

- Future Directions?
- Quantitative Inspection Capability
- Application to Non-Metallic Materials
- Need for Coordinated Approach

Figure 8 : ENGINE COMPONENT INSPECTION

- Very Little Coverage
- Role of Automation
- Future Emphasis?

Figure 9 : APPLICATION OF NEW/IMPROVED METHODS

- Computer Tomography (CT)
- Acoustic Emission
- Eddy Current
- Radiography
 - . Neutron Radiography
 - . Stenopic Radiography
 - . Real Time Radiography
- Infrared
- Optical
- Artificial Intelligence

Figure 10 : ADHESIVE BOND INSPECTION

- Current Problem in Aging Aircraft
- Little Emphasis in Meeting
- Flaws vs Strength

Figure 11 : SUMMARY AND CONCLUSIONS

- Strong Emphasis on Composite Materials
- Structural Integrity Efforts Limited to US
- Quantitative NDE Must Receive More Attention
- Engine Component Inspection Inadequately Addressed
- CT Only "New" Technology Being Applied
- Bond Strength Measurement Still a Challenge
- Very Successful Conference.

IMPACT OF NDE-NDI METHODS ON AIRCRAFT DESIGN, MANUFACTURE AND MAINTENANCE, FROM THE FUNDAMENTAL POINT OF VIEW.

Leonard J. BOND

NDE Centre,
Department of Mechanical Engineering
University College London
Torrington Place
LONDON, WC1E 7JE
United Kingdom

SUMMARY.

This paper presents a rapporteurs comments on the impact of emerging NDE-NDI methods on aircraft design, manufacture and maintenance. In particular fundamental aspects of recent developments are considered, together with current trends and future prospects. The meetings presentations and discussion are reviewed in terms of the philosophy, the physics, and the technology involved. NDE-NDI is shown to require to be considered as an integral part of the design, manufacturing and operational condition monitoring process, for all parts of an aircraft. Various areas of NDE are highlighted and these include the importance of high performance quantitative NDE, the impact of new materials (e.g. composites), changes in manufacturing processes (e.g. diffusion bonding) and the importance of mathematical modelling for inspection optimisation and also for the identification of novel NDE inspection techniques. Automation of the implementation of NDT and both the recording and the display of the resulting data is seen to be necessary in many cases to achieve the required sensitivity and level of reliability of inspection. Global inspection techniques are being sought which highlight suspect zones that can then be investigated using other techniques, to provide detailed local examinations.

1. Introduction

My co-rapporteur Dr Cooper has provided a detailed summary of the scope and contents of the 25 papers presented at this meeting, including a review of the current state of implementation for various NDT techniques. It now falls to me to try and look at the more fundamental aspects of the topic of this meeting; the impact of emerging NDE-NDI methods on aircraft design, manufacture and maintenance and especially to try and look towards the future. Such predictions and extrapolations are always risky: NDT is driven by economics and problems which relate to safety, so that if the industry faces a problem which is serious enough, the pace of innovation and development in any of several areas could then well be faster than current trends indicate.

In reviewing the material presented the contents of each paper was considered in relation to its impact on design, manufacture and maintenance or some combination of these areas. However before turning to consider the fundamentals and future developments in NDE some basic background information is given. This is followed by a review of the field in terms of the contributions made to the three areas of the philosophy, the physics and the technology of NDE-NDI.

2. Background

Given the current mix of aircraft in service with NATO countries, inspectors are faced with a wide diversity of designs, materials and inspection requirements. For any structural element or component its life can be estimated by considering the combination of the operational parameters (temperature and stress), material properties (fracture toughness) and defect population (flaw size) all combined in the context of a suitable failure model. Such life estimation concepts are at the heart of Damage Tolerance and Retirement-for-Cause (RFC) [1].

In any aircraft in service structural degradation may be due to wear, corrosion, impact damage or fatigue [2]. An aircraft may also experience changes to its typical mission profile after its introduction into operational use, which can also result in modifications to loadings such as through the introduction of new weapons or instrumentation systems. These factors all combine to influence the remaining life of an aircraft and these effects all require evaluation.

If the remaining life of an aircraft is to be estimated it is necessary to provide detailed data with regard to its current condition. For most aircraft fleet operators the inspection situation is a classic case of, "If you are looking for the place to start; don't start from here!" Older aircraft were designed to safe-life codes, they used mostly metals and conventional jointing technology, they were not designed for testability and now, in many cases, operators are required to seek life extension. The capital investment in aircraft is quite simply such that older types of aircraft can be expected to remain in service for many more years and this complicates the requirements for inspection technology as each type of aircraft presents its own particular problems.

Modern aircraft, such as the EAP demonstrator, McDonnell Douglas/Bae AV-8B (Harrier) and Airbus A320 are all being considered in terms of new design philosophies and they are also using increasing quantities of new materials including composites. The growing interest in composites and its inspection was reflected in many of the papers presented at this meeting. There is also a growing interest in advanced jointing techniques using adhesive bonding and various forms of solid-state bonding.

When one looks further into the future, subsequent generations of aircraft can be expected to use a wide range of different materials and manufacturing techniques, including new composites, ceramics and ceramic coatings, metal-matrix composites, powder metals, diffusion bonding and also smart structures, with their own integral condition monitoring systems. Such trends will present many new NDT requirements, some of which cannot be expected to be met using current conventional NDT technology.

The current capability of NDT was considered recently [3] and it was also discussed extensively in various papers at this conference. The causes of the limitations on NDT performance have been identified as being due to [4];

- i. The physics of the fundamental interactions.
- ii. The instrumentation which is used.
- iii. The inspection techniques employed, including human factors.
- iv. The defect population; its range of types and sizes, base material properties and the component geometry.

From an engineering point of view the problems associated with current NDT technology have been summarised as [5];

- i. Lack of NDT considerations at the design stage.
- ii. Inadequate 'engineering' of the NDT techniques.
- iii. Defect detection requirements which are often too close to the detection threshold.
- iv. Human factors in the inspection cycle.

The various causes of limitation on NDT capability, however they are expressed, have important implications for the main subject of this meeting; the impact of NDE-NDI on design manufacture and maintenance and also implications for future trends in the development of the field. For example reliable inspections cannot be expected to be performed to levels that are close to, or better than, the limits set by the physics of the phenomena employed. The effect of flaws on the structure and necessary inspection requirements must be considered at the design stage of a project if realistic inspection levels are to be set. The implementation of the inspection goals should then be achieved using the best available technology, and trained staff, which can then be expected to give systems with a quantifiable level of performance.

3. Philosophy

A range of lifeing philosophies are now well established. The traditional concept of 'Safe Life' is still important and it will remain so in many areas. There is however now an increasing use of Damage Tolerance and Retirement-for-Cause (RFC) [1]. An integrated design and life cycle engineering approach, Unified Life Cycle Engineering, (ULCE) has also been proposed and this has many useful features to guide designers thinking [6]. NDE and the various life models in all their features are by the very nature of the situation statistical and this must be taken into account in the design/life estimation process. From an NDE point of view when considering NDT capability the critical aspect of component life is the population of flaws and the critical flaw size, the inspection detection threshold and the probability-of-detection (POD) in a particular part.

It is however all well and good to have an adequate design/life philosophy, but it is then necessary to ensure that it is implemented. The whole area of RFC/ENSIP and process control and the drive for a new NDI reliability standard was considered at this meeting by Taylor et al [7]. There are interesting contrasts between the European and US approaches, but whichever was considered it is seen that there is a need to have high quality quantitative NDT, which can either be a part of process control or form a final inspection.

In summary the necessary philosophy to ensure NDT requirements, limitations and capability are considered as an integral part of design and its subsequent implications for manufacturing quality control (QC), component life and maintenance are available [1,6,7]. In this area a common AGARD approach is strongly recommended, particularly for the analytical methodology employed [7]. The implementation of codes which ensure such a design approach is then a customer and a management responsibility. In some NATO countries NDT is already having a significant impact on component design and life decisions and new codes and standards are currently being prepared.

4. Physics

It is the fundamental physics of each particular inspection technology which in almost all cases sets the ultimate limits for the best achievable performance for NDT detection capability in the laboratory [4,8]. A summary of the limits for detection capability for various NDT technologies is given as Table 1 [4,8]. Such a single number, the detection limit, is not however an adequate parameter for the characterisation of the performance of an inspection technology; a series of probability of detection curve is better as this can take into account many more inspection parameters and gives a better guide to probable detection performance [4]. When the data given in Table 1 is considered there are important differences to be seen between the best performance that is achieved in the laboratory and that in manufacture or in maintenance. The causes of the failure to achieve laboratory level performance in manufacture and maintenance are many, but they are not usually due to the physics (See section 2). The data given in Table 1 may be considered to be somewhat old (1974) but since it was collected it is probably only in eddy currents that there has been a significant improvement in field inspection capability [4].

The physics of NDT is of particular importance to the understanding of system performance. Modelling is now central to many studies to optimise inspection and in the determination of performance limitations and many examples of studies which included modelling were to be seen in the research papers presented at this meeting. The selection of the basic NDT phenomena to be employed must give a method which is suitable and which can be optimised in the laboratory before it is automated, if expensive modifications or re-design of the final inspection system is to be avoided.

NDT remains a technology which is seeking to give the data needed to solve illposed inverse problems: to provide material and flaw characteristics, which can then be used in a suitable failure model to determine the components remaining life. One of the weak links which remain in the NDE and RFC process is providing data from NDT flaw characterisations which is in a form such that it can be used directly in fracture mechanics calculations. Inversion schemes are required to extract defect characteristics and this then requires bridge-building, at a fundamental level, to draw together NDT and fracture mechanics

to give compatibility of the data that one field provides for the other. An agreed degree of flaw characterisation is required, for example is it adequate to give a flaw's location, its type, dimensions and orientation to some level of accuracy?

5. Technology

With the aging aircraft fleet both civil and military operators are faced with many problems due to corrosion and fatigue. Current NDT inspection practice has been stated as not being adequate to meet all these needs [2]. However techniques do exist in the laboratory [3] and in prototype systems such as those reported at this meeting to meet many of the current range of new inspection requirements.

I do not wish to repeat here comments about the detailed contents of the various papers made by Dr Cooper in his review of the current state of NDT technology, so I will restrict myself to saying that various NDT technologies were considered at the meeting and a range of systems demonstrated that are available today. These systems included an optical global inspection scheme "D-sight" [9], as well as a range of ultrasonic and eddy current systems; the RFC NDE System (US Kelly AF Base) [10] for disc inspection, the US system ARIS and prototype systems from DREP (Canada) and Italy for on-wing C-scans. Various eddy current developments and systems were reported including a UK system for detection of cracks under fasteners in wing skins. Powerful neutron radiography systems are also now available for use on aircraft systems which can detect some forms of corrosion, as well as a range of conventional radiography developments including CT, microfocus and real time displays that are being used in the laboratory and which will no doubt receive much more attention [13]. There are also a range of thermography systems available for composite inspection, one of which was discussed. Performance, in the medium term in a maintenance environment, is unlikely to be improved significantly on that achieved by the various systems reported at this meeting.

Several good papers considering fundamental aspects of acoustic emission (AE) were presented. AE was shown to have a useful role to monitor parts in the laboratory and restricted sections of aircraft structure in flight tests. I consider that although progress is being made acoustic emission has yet to be demonstrated to be a technology capable of being the global aircraft structural monitoring tool that some appear to hope it will be.

It has been shown at this meeting that NDE is starting to have an impact on the design of both engines and airframe [7] and this is in turn being related back to NDT capability and its quantification. Much has been done to start to measure NDT performance with the POD and reliability of characterisation (ROC) curves [11]. However, more work is required to expand the data base for quantified NDT performance. In Europe the EFA presents new challenges and there is a need to prepare the inspection capability that will need to be available for its introduction into service in the next decade [12]. It is important to recognise that the development of modern high performance NDT capability requires high grade staff and it can be expensive to establish, as in many cases the automation of NDT will be required if the desired levels of sensitivity and reliability of performance are to be achieved.

When the longer term future for NDT is considered several technologies can be identified as being of potential importance, but little was said about these at this meeting. For non-contact ultrasonic inspection EMAT's and laser ultrasonics will be considered. For detailed material characterisation studies various forms of acoustic microscopy have considerable potential. There are also inspection schemes which employ non-conventional wave modes such as leaky Rayleigh waves, leaky Lamb waves and interface waves. In radiography - in particular CT, thermography and eddy currents, sensor and instrumentation further developments can all be expected [4]. Within the field of technology further progress in the use of automation and robotics, signal processing, automated data recording and improved displays, defect characterisation using inversion schemes and AI can all be expected to grow. In all technologies employed in NDE there remains considerable scope for research and for many there are significant areas of potential application that should be investigated. Areas in several of the topics listed here can be considered to be to a large extent technology transfer as much of the necessary capability is already available in other fields of study.

6. Discussion and Conclusions

The integration of NDE-NDI into the complete life cycle of a part and system is crucial if the full technological and economic benefit is to be made of the available range of NDT technologies. There can be expected to be a move to integrate NDT into process control and to see it being used to monitor and characterise material properties [14] as well as locate and characterise isolated flaws or groups of flaws. As NDT capability is upgraded flaw characterisation will move to be more quantitative. In relation to this if the same flaw is found several times the manufacturing process can be expected to be changed to seek to minimise the possibility that it is produced again. The result will be that in many areas of routine aero-space production, such as for engine discs, NDT will be considering only "random" flaws and the statistics are such that when a process is under control only a small numbers of significant NDT indications will be detected.

For the condition monitoring of structures in service there can be expected to be increasing interest in the use of optical systems, such as D-sight, thermal methods for composites and the introduction of smart structures using optical fibres to monitor a wide variety of parameters.

To give a balanced picture of current NDT capability and recent trends it is necessary to look outside the scope of this meeting and into the wider literature. The field of acoustic microscopy, which can give material characterisation and inspection in both the laboratory and in the production facilities, is now available as a routine tool [15]. New bonding methods, including both adhesive and solid state bonding technologies are topics of considerable research interest [16,17]. For some years eddy current theory in NDT has received much less attention than the theory for ultrasonics, but recently more attention has been focused on eddy currents with encouraging developments to be seen in the necessary theory [18]. Central to many developments in quantitative NDE is mathematical modelling which can be used to consider both forward and inverse problems [19,20], and the role of modelling in NDE research

can be expected to grow as conventional NDT techniques are no longer able to meet new inspection requirements. One final area is that of signal processing and data display which is building on the enhanced computing capability that is now so readily available. This area is a topic in its own right and it can be expected to have a continuing major impact on developments in NDE [21]. If one source of information is sought which will give an overview of trends and developments in quantitative NDE over the past 10-15 years, with particular reference to the aero-space industry, then this is the series of volumes "Review of Progress in Quantitative NDE" [22].

One of the most significant and encouraging developments at this meeting was to have the economics of NDE being considered. The USAF RFC system was reported to have given savings of approximately \$80 million to date, with over 8,000 F-100 engine discs inspected between October 1986 and July 1989 [11]. Such data can only serve to highlight the impact that NDE can have on aircraft design, manufacture and maintenance.

NDE-NDI requires to be considered as an integral part of the design, manufacturing and operational condition monitoring process for all parts of an aircraft. In the area of fundamental design/life philosophy a common AGARD approach is strongly recommended, particularly for the analytical methodology employed. A common AGARD approach to NDT system performance evaluation, standards and clear presentation of the statistics used to determine parameters such as probability of detection would greatly ease problems currently encountered in performance comparisons. Increased information exchange on NDE topics, as encouraged through this meeting, and within AGARD can only be to the benefit of all groups involved.

7. References

1. AGARD. (1985) Damage Tolerance Concepts for Critical Engine Components. AGARD Conference Proceedings No 393.
2. Bobo S (1989) The aging aircraft fleet, a challenge for NDI. In "Review of Progress in Quantitative NDE, Vol 9." Ed D O Thompson and D Chimenti. Plenum (New York) (In Press)
3. AGARD. (1988) AGARD/SMP Review Damage Tolerance Concepts for Critical Engine Structures 1. Non-Destructive Evaluation. AGARD Report No 768.
4. Bond L J (1988) Review of existing NDT technologies and their capabilities. In AGARD/SMP Review Damage Tolerance Concepts for Critical Engine Structures. 1. Non-Destructive Evaluation. AGARD Report No 768.
5. Taylor R G (1985) Limitations of manual NDT systems and the 'No Eyes' concept. In "Damage Tolerance Concepts for Critical Engine Components". AGARD Conference Proceedings No 393. Paper 5.
6. Burte H M and Chimenti D E (1987) Unified Life Cycle Engineering: An Emerging Design Concept. Review of Progress in quantitative NDE, Vol 6B. Ed D O Thompson and D Chimenti. Plenum (New York) pp 1797-1809.
7. Taylor R G, Cooper T and Vukelich S (1989) The role of NDI in the certification of turbine engine components. Paper 2. These Proceedings.
8. Pettit D E and Krupp W E (1974) The role of NDI in fracture mechanics applications, In" ASM 3 Fracture Prevention and Control. American Society of Metals.
9. Stoermer M (1989) NDI- concept for composites in future aircraft. Paper 2. These Proceedings.
10. Rummel W D (1989) Assessment and demonstration of the capabilities of NDI processes, equipment and personnel. Paper 4. These Proceedings.
11. Rasmussen et al (1989) Critical inspection of high performance turbine engine components - the concept and development of the retirement for cause (RFC) NDE System. Paper 6. These Proceedings.
12. Komorowski J P and Gould R (1989) A technique for rapid inspection of composite aircraft structures for impact damage. Paper 11. These Proceedings.
13. Sheppard L M (1987) Detecting material defects in real time. Advanced Materials & Processes inc Metal Progress. 11/87 pp 53-60.
14. Bhardwaj M C (1989) Modern ultrasonic concepts of NDC. Advanced Materials & Processes. 5/89 pp 53-59.
15. Gilmore R S, Tam K C, Young J D and Howard D R (1986) Acoustic microscopy from 10 to 100 MHz for industrial applications. In "Novel techniques of non-destructive examination" Ed E A Ash and C B Scruby, The Royal Society, (LONDON) pp 55-75.
16. Thompson D O and Chimenti D (1989) Solid State Bonding session In "Review of Progress in quantitative NDE, Vol 9." Ed D O Thompson and D Chimenti. Plenum (New York) (In Press)
17. Thompson R B [Editor] (1988) Special Issue on NDE of Solid-State Bonds. Journal of NonDestructive Evaluation. Vol 7 (3/4) pp121-235.
18. Moulder J C [Editor] (1988) Special Issue on Eddy-Current Modelling. Journal of NonDestructive Evaluation. Vol 7 (1/2) pp 1-120.
19. Datta S K et al (1989) Proceedings IUTAM Symposium on Elastic Wave Propagation and Ultrasonic Non-Destructive Evaluation. Ed. S K Datta, J D Achenbach and Y D S Rajapakse. Elsevier Science Publishers (Amsterdam). (In Press)

20. Blakenore M and Georgiou G A (Editors) (1988) "Mathematical Modelling in NDT," Clarendon Press (Oxford).
21. Chen C (Editor) (1987) "Signal Processing and Pattern Recognition in NDE of Materials," NATO ASI Series Vol F44, Springer Verlag.
22. Thompson D O and Chimenti D [Editors] (1980-1989) "Review of Progress in Quantitative NDE, Vols 1-9 (Annual). Plenum (New York)

ACKNOWLEDGMENTS

My thanks are due to the authors who provided pre-prints for the of papers presented at this meeting.

TABLE 1. Estimated variations in flaw detection limits by type of inspection. (Flaw size in mm; Pettit and Krupp [8]).

NDT Technique	Surface cracks		Internal flaws	
	Processing	Fatigue	Voids	Cracks
Test specimens, laboratory inspection				
Visual†	1.25	0.75	+	+
Ultrasonic	0.12	0.12	0.35	2.0
Magnetic particle	0.75	0.75	7.5	7.5
Penetrant	0.25	0.5	+	+
Radiography	0.5	0.5	0.25	0.75
Eddy current	0.25	0.25	+	+
Production parts, production inspection				
Visual	2.5	6.0	+	+
Ultrasonic	3.0	3.0	5.0	3.0
Magnetic particle	2.5	4.0	+	+
Penetrant	1.5	1.5	+	+
Radiography	5.0	*	1.25	*
Eddy current	2.5	5.0	+	+
Cleaned structures, service inspection				
Visual	6.0	12.0	+	+
Ultrasonic	5.0	5.0	4.0	5.0
Magnetic particle	6.0	10.0	+	+
Penetrant	1.25	1.25	+	+
Radiography	12.0	*	4.0	*
Eddy current	5.0	6.0	+	+

+ Not applicable. † Use with magnifier. * Not possible for tight cracks. (Based on 25-mm ferritic steel, surface 63 RMS.)

REPORT DOCUMENTATION PAGE			
1. Recipient's Reference	2. Originator's Reference	3. Further Reference	4. Security Classification of Document
	AGARD-CP-462	ISBN 92-835-0546-8	UNCLASSIFIED
5. Originator	Advisory Group for Aerospace Research and Development North Atlantic Treaty Organization 7 rue Ancelle, 92200 Neuilly sur Seine, France		
6. Title	IMPACT OF EMERGING NDE-NDI METHODS ON AIRCRAFT DESIGN MANUFACTURE AND MAINTENANCE		
7. Presented at	the 69th Meeting of the Structures and Materials Panel in Brussels, Belgium, 1st-6th October 1989.		
8. Author(s)/Editor(s)			9. Date
Various			March 1990
10. Author's/Editor's Address			11. Pages
Various			244
12. Distribution Statement	This document is distributed in accordance with AGARD policies and regulations, which are outlined on the Outside Back Covers of all AGARD publications.		
13. Keywords/Descriptors			
<div style="display: flex; justify-content: space-between;"> <div> <p>Non-destructive tests, Inspection, Maintenance, Aircraft engines,</p> </div> <div> <p>Airframes, Reliability, Design, Manufacturing, (SLD) NATO.</p> </div> </div>			
14. Abstract			
<p>At its sixty-ninth meeting the Structures and Materials Panel held a conference of Specialists, to review developments in NDE-NDI applicable to the major components and assemblies in airframes, engines and their sub-assemblies. Users' needs and priorities were discussed with emphasis on identification of the constraints that present-day NDE-NDI methods impose on the activities of aircraft designers/manufacturers, airworthiness authorities and aircraft operators. The methods available for the characterisation and control of materials and processes were examined and current developments in techniques for improved reliability and in-service inspection were assessed. In a final session, research studies in both physical and analytical methods were reviewed.</p> <p>This document contains the papers presented at the meeting and a summary of the key points discussed.</p> <p>Keywords.</p>			

<p>AGARD Conference Proceedings No.462 Advisory Group for Aerospace Research and Development, NATO IMPACT OF EMERGING NDE-NDI METHODS ON AIRCRAFT DESIGN MANUFACTURE AND MAINTENANCE Published March 1990 244 pages</p> <p>At its sixty-ninth meeting the Structures and Materials Panel held a conference of Specialists, to review developments in NDE-NDI applicable to the major components and assemblies in airframes, engines and their sub-assemblies. Users' needs and priorities were discussed with emphasis on identification of the constraints that present-day NDE-NDI methods impose on the activities</p> <p>P.T.O.</p>	<p>AGARD-CP-462</p> <p>Non-destructive tests Inspection Maintenance Aircraft engines Airframes Reliability Design Manufacturing</p>	<p>AGARD Conference Proceedings No.462 Advisory Group for Aerospace Research and Development, NATO IMPACT OF EMERGING NDE-NDI METHODS ON AIRCRAFT DESIGN MANUFACTURE AND MAINTENANCE Published March 1990 244 pages</p> <p>At its sixty-ninth meeting the Structures and Materials Panel held a conference of Specialists, to review developments in NDE-NDI applicable to the major components and assemblies in airframes, engines and their sub-assemblies. Users' needs and priorities were discussed with emphasis on identification of the constraints that present-day NDE-NDI methods impose on the activities</p> <p>P.T.O.</p>	<p>AGARD-CP-462</p> <p>Non-destructive tests Inspection Maintenance Aircraft engines Airframes Reliability Design Manufacturing</p>
<p>AGARD Conference Proceedings No.462 Advisory Group for Aerospace Research and Development, NATO IMPACT OF EMERGING NDE-NDI METHODS ON AIRCRAFT DESIGN MANUFACTURE AND MAINTENANCE Published March 1990 244 pages</p> <p>At its sixty-ninth meeting the Structures and Materials Panel held a conference of Specialists, to review developments in NDE-NDI applicable to the major components and assemblies in airframes, engines and their sub-assemblies. Users' needs and priorities were discussed with emphasis on identification of the constraints that present-day NDE-NDI methods impose on the activities</p> <p>P.T.O.</p>	<p>AGARD-CP-462</p> <p>Non-destructive tests Inspection Maintenance Aircraft engines Airframes Reliability Design Manufacturing</p>	<p>AGARD Conference Proceedings No.462 Advisory Group for Aerospace Research and Development, NATO IMPACT OF EMERGING NDE-NDI METHODS ON AIRCRAFT DESIGN MANUFACTURE AND MAINTENANCE Published March 1990 244 pages</p> <p>At its sixty-ninth meeting the Structures and Materials Panel held a conference of Specialists, to review developments in NDE-NDI applicable to the major components and assemblies in airframes, engines and their sub-assemblies. Users' needs and priorities were discussed with emphasis on identification of the constraints that present-day NDE-NDI methods impose on the activities</p> <p>P.T.O.</p>	<p>AGARD-CP-462</p> <p>Non-destructive tests Inspection Maintenance Aircraft engines Airframes Reliability Design Manufacturing</p>

<p>of aircraft designers/manufacturers, airworthiness authorities and aircraft operators. The methods available for the characterisation and control of materials and processes were examined and current developments in techniques for improved reliability and in-service inspection were assessed. In a final session, research studies in both physical and analytical methods were reviewed.</p> <p>This document contains the papers presented at the meeting and a summary of the key points discussed.</p> <p>ISBN 92-835-0546-8</p>	<p>of aircraft designers/manufacturers, airworthiness authorities and aircraft operators. The methods available for the characterisation and control of materials and processes were examined and current developments in techniques for improved reliability and in-service inspection were assessed. In a final session, research studies in both physical and analytical methods were reviewed.</p> <p>This document contains the papers presented at the meeting and a summary of the key points discussed.</p> <p>ISBN 92-835-0546-8</p>
<p>of aircraft designers/manufacturers, airworthiness authorities and aircraft operators. The methods available for the characterisation and control of materials and processes were examined and current developments in techniques for improved reliability and in-service inspection were assessed. In a final session, research studies in both physical and analytical methods were reviewed.</p> <p>This document contains the papers presented at the meeting and a summary of the key points discussed.</p> <p>ISBN 92-835-0546-8</p>	<p>of aircraft designers/manufacturers, airworthiness authorities and aircraft operators. The methods available for the characterisation and control of materials and processes were examined and current developments in techniques for improved reliability and in-service inspection were assessed. In a final session, research studies in both physical and analytical methods were reviewed.</p> <p>This document contains the papers presented at the meeting and a summary of the key points discussed.</p> <p>ISBN 92-835-0546-8</p>

AGARD

NATO  OTAN

7 rue Ancelle • 92200 NEUILLY-SUR-SEINE

FRANCE

Telephone (1)47.38.57.00 • Telex 610 176

**DISTRIBUTION OF UNCLASSIFIED
AGARD PUBLICATIONS**

AGARD does NOT hold stocks of AGARD publications at the above address for general distribution. Initial distribution of AGARD publications is made to AGARD Member Nations through the following National Distribution Centres. Further copies are sometimes available from these Centres, but if not may be purchased in Microfiche or Photocopy form from the Sales Agencies listed below.

NATIONAL DISTRIBUTION CENTRES

BELGIUM

Coordonnateur AGARD — VSL
Etat-Major de la Force Aérienne
Quartier Reine Elisabeth
Rue d'Evere, 1140 Bruxelles

CANADA

Director Scientific Information Services
Dept of National Defence
Ottawa, Ontario K1A 0K2

DENMARK

Danish Defence Research Board
Ved Idraetsparken 4
2100 Copenhagen Ø

FRANCE

O.N.E.R.A. (Direction)
29 Avenue de la Division Leclerc
92320 Châtillon

GERMANY

Fachinformationszentrum
Karlsruhe
D-7514 Eggenstein-Leopoldshafen 2

GREECE

Hellenic Air Force
Air War College
Scientific and Technical Library
Dekelia Air Force Base
Dekelia, Athens TGA 1010

ICELAND

Director of Aviation
c/o Flugrad
Reykjavik

ITALY

Aeronautica Militare
Ufficio del Delegato Nazionale all'AGARD
3 Piazzale Adenauer
00144 Roma/EUR

LUXEMBOURG

See Belgium

NETHERLANDS

Netherlands Delegation to AGARD
National Aerospace Laboratory, NLR
Kluuyverweg 1
2629 HS Delft

NORWAY

Norwegian Defence Research Establishment
Attn: Biblioteket
P.O. Box 25
N-2007 Kjeller

PORTUGAL

Portuguese National Coordinator to AGARD
Gabinete de Estudos e Programas
CLAFIA
Base de Alfragide
Alfragide
2700 Amadora

SPAIN

INTA (AGARD Publications)
Pintor Rosales 34
28008 Madrid

TURKEY

Milli Savunma Bakanlığı (MSB)
ARGE Daire Başkanlığı (ARGE)
Ankara

UNITED KINGDOM

Defence Research Information Centre
Kentigern House
65 Brown Street
Glasgow G2 8EX

UNITED STATES

National Aeronautics and Space Administration
Langley Research Center
M/S 180
Hampton, Virginia 23665

**THE UNITED STATES NATIONAL DISTRIBUTION CENTRE (NASA) DOES NOT HOLD
STOCKS OF AGARD PUBLICATIONS, AND APPLICATIONS FOR COPIES SHOULD BE MADE
DIRECT TO THE NATIONAL TECHNICAL INFORMATION SERVICE (NTIS) AT THE ADDRESS BELOW.**

SALES AGENCIES

National Technical
Information Service (NTIS)
5285 Port Royal Road
Springfield
Virginia 22161, USA

ESA/Information Retrieval Service
European Space Agency
10, rue Mario Nikis
75015 Paris, France

The British Library
Document Supply Centre
Boston Spa, Wetherby
West Yorkshire LS23 7BQ
England

Requests for microfiche or photocopies of AGARD documents should include the AGARD serial number, title, author or editor, and publication date. Requests to NTIS should include the NASA accession report number. Full bibliographical references and abstracts of AGARD publications are given in the following journals:

Scientific and Technical Aerospace Reports (STAR)
published by NASA Scientific and Technical
Information Branch
NASA Headquarters (NIT-40)
Washington D.C. 20546, USA

Government Reports Announcements (GRA)
published by the National Technical
Information Services, Springfield
Virginia 22161, USA



Printed by Specialised Printing Services Limited
40 Chigwell Lane, Loughton, Essex IG10 3TZ

ISBN 92-835-0546-8